

Developing A New Mammalian Cell-Based
Vaccine Manufacturing Platform and Novel
Antibodies for the Treatment of Dengue Fever

2023

Laura Dyball

A thesis submitted to the University of Kent for the
degree of Doctor of Philosophy

University of Kent
School of Biosciences

Declaration

No part of this thesis has been submitted in support of an application for any degree or other qualification of the University of Kent or any other university or institute of learning.

Laura Dyball

November 2023

Abstract

The development of biotherapeutics is an important field in the modern approach to treating and preventing current and emerging global health challenges. Vaccines and monoclonal antibodies are two biotherapeutic modalities that are particularly important in addressing the unmet need for the treatment or prevention of a wide range of diseases and conditions. Alongside the development of such biotherapeutics comes the need to be able to manufacture/produce these complex medicines at a quality and quantity suitable for treating the target population. Chinese hamster ovary (CHO) host cell lines are the gold-standard mammalian expression system used in bioprocessing for the expression of biotherapeutics due to their ability to produce high quality products with human-like post-translational modifications (particularly glycosylation) and a record of producing safe therapies at large scale. Due to these attributes and their ability to tolerate genetic engineering for manipulation of secretion and vesicular pathways, CHO cells are an excellent candidate for the development of a mammalian-cell based vaccine platform for manufacture of recombinant exosomes. Additionally, CHO cells are routinely used for the production of monoclonal antibodies (mAbs) and have been successfully used to produce difficult-to-express (DTE) antibodies. This thesis presents investigations into the development of (1) a 'plug & play' CHO cell-based system for the expression of engineered exosomes which could be adapted for rapid response to outbreaks, and (2) the enhanced expression of a DTE novel anti-dengue antibody (Den54) using the CHO cell expression system via antibody sequence engineering. CHO-S host cells were shown to be a suitable cell host for the production of engineered exosomes to which can be targeted proteins/antigens of interest when fused (tagged) with exosome-targeting proteins. Two exosome targeting strategies were explored, ubiquitin-tagging and tetraspanin-tagging, both of which resulted in the production of engineered exosomes bearing fluorescent reporter proteins GFP and mCherry. However, of the strategies, a CD81 tetraspanin-tagging method resulted in more consistent targeting of cargo (GFP/mCherry) into recombinant exosomes, possibly due to the higher abundance of CD81+ exosome populations found in native CHO-S exosome populations. Further investigation using different SARS-CoV-2 structural proteins to test strategies to target antigens of varied lengths and complexities showed that successful generation of engineered exosomes is also dependent on the antigen targeted to them, with the Spike subunit 2 (S2) being most successfully targeted to recombinant CHO-S cell exosomes. The CHO-S host cell line was also used to investigate enhanced expression of a novel anti-dengue mAb that was DTE. Hybridisation or grafting of the DTE antibody sequences, particularly the variable regions, onto the constant and framework regions of well-characterised mAbs known to express well in CHO cells, trastuzumab and nivolumab, resulted in a marked improvement of secreted anti-dengue antibody. The molecule produced at the greatest yield, Den2, was a hybrid which contained more of the Den54 native sequence than its counterpart, Den4. Further investigation of the expression of these molecules and localisation of the antibody chains within the cells to determine where bottlenecking may be occurring, highlighted a problem with the Fc region of the native molecule resulting in a lack of secretory expression. This may be due to the formation of intra-ER crystals and the absence of the native Den54 Fc in the hybridised molecules allowed for higher secreted mAb amounts to be observed. The combined data described in this thesis provides evidence that CHO-S cells can be a platform for manufacture of engineered exosomes containing target antigens that could be investigated as vaccines and shows that protein engineering of a model mAb can improve the secretory expression of an anti-dengue DTE mAb and identify limitations upon its expression.

Acknowledgments

I'd like to thank all of the people who have helped to support and encourage me throughout my PhD. It has certainly been both incredibly challenging and rewarding in many ways.

Firstly, a very special thank you to Prof. Mark Smales who has been an incredible supervisor with immense support and guidance throughout the entire project, believing in me even in times when I did not.

For their mentorship and patience, I would like to thank Dr Emi Nemoto-Smith, Dr Alex Jones, Dr Tanya Knight and particularly Dr James Budge. They always had time for me to discuss issues and to teach me the skills I needed to complete this project, for which I am incredibly grateful.

I would also like to thank all members of the Smales lab group, both past and present, for their support and input into scientific challenges but also for making me feel incredibly welcome and like part of a second family away from home.

Lastly, I would like to thank my family and friends who all had nothing but love and support to give throughout my PhD journey.

Table of Contents

DECLARATION	2
ABSTRACT.....	3
ACKNOWLEDGMENTS	4
TABLE OF CONTENTS	5
ABBREVIATIONS	10
LIST OF FIGURES.....	13
LIST OF TABLES.....	27
CHAPTER 1: INTRODUCTION.....	29
1.1 Current Vaccine Platforms.....	29
1.1.1 General Introduction.....	29
1.1.2 Traditional Vaccines	29
1.1.3 Next Generation Vaccines.....	31
1.2 Current Global Healthcare Challenges Which Warrant Innovative Research Approaches to Vaccine and Biotherapeutic Development	35
1.2.1 Dengue Fever	35
1.2.2 SARS-CoV-2.....	38
1.3 Exosomes as Antigen-Display Vehicles.....	44
1.3.1 Exosome Composition and Biogenesis.....	44
1.3.2 Exosomes: Cellular Messengers and Mediators.....	48
1.4 Exploring mAb Production and Development to Improve the Diversity and Availability of mAb Biotherapeutics.....	55
1.4.1 The Current Global Market	55
1.4.2 Antibody Discovery and Hybridoma Technology	55
1.4.3 Antibody Structure and Immunology.....	56
1.4.4 CHO Cells as a Platform for Optimised Monoclonal Antibody Production.....	57

1.5	Concluding Remarks	64
1.6	Aims of This Study.....	65
CHAPTER 2: MATERIALS & METHODS.....		66
2.1	Bacterial Cell Culture Techniques.....	66
2.1.1	Liquid Media Culture	66
2.1.2	Solid Media Culture	66
2.1.3	Antibiotic Selection	66
2.1.3	Competent Cells	66
2.1.4	Transformations	67
2.1.5	Glycerol Stocks	67
2.2	Molecular Cloning Techniques.....	67
2.2.1	RNA Extraction	67
2.2.2	cDNA Synthesis (Reverse Transcription)	67
2.2.3	Phusion™ PCR.....	68
2.2.4	Reverse-Transcription PCR	71
2.2.5	Colony PCR Screening.....	73
2.2.6	Agarose Gel Electrophoresis	74
2.2.7	Gel and PCR DNA Clean-up.....	74
2.2.8	Restriction Enzyme DNA Digests	74
2.2.9	Ligation Reactions	75
2.2.10	Plasmid DNA Purification.....	75
2.2.10	Plasmid DNA Sequencing.....	76
2.3	Mammalian Cell Culture	76
2.3.1	Revival of Cell Lines from Cryopreservation.....	76
2.3.2	Routine Cell Culture Passage.....	76
2.3.3	Cell Growth Curves.....	76
2.3.4	Transient Transfections	79
2.3.5	Stable Cell Line Construction.....	79
2.3.6	Cryopreservation of Cell Lines.....	80
2.3.7	Monoclonal Cell Line Lineage Development	81
2.3.8	Cell Culture Protein Analysis	81
2.4	Analysis & Purification Techniques	83
2.4.1	Western Blotting	83

2.4.2	Confocal Microscopy	86
2.4.3	Enzyme-Linked Immunosorbent Assay (ELISA)	87
2.5	Antibody Recovery & Purification	88
2.5.1	Fast Protein Liquid Chromatography.....	88
2.5.2	Product Concentration and Buffer Exchange	88
2.5.3	Exosome-Specific Protocols.....	89

CHAPTER 3: EXPLORING THE *IN VITRO* LOADING OF PROTEINS OF INTEREST INTO EXOSOMES AS A NOVEL CELL-BASED VACCINE PLATFORM IN CHINESE HAMSTER OVARY CELLS 90

3.1	Introduction	90
3.2	Results	92
3.2.1	Generation of Ubiquitin-fusion vectors.....	92
3.2.2	Expression Assessment of Ubiquitin-Fusion Vector Expression in CHO Cell Lines	94
3.2.3	Generation of Exosome Marker-Fluorescent Report Fusion Based Vectors	105
3.2.4	Expression Profiles of Exomarker-based Vector Cell Lines.....	108
3.3	Discussion	116
3.3.1	Transient Data	116
3.3.2	Stable Fusion Protein Expression	118
3.3.3	DLS Data	122
3.4	Conclusions	126

CHAPTER 4: INVESTIGATING EXOSOME-TARGETING STRATEGIES FOR THE DEVELOPMENT OF AN EXOSOME-BASED VACCINE PLATFORM FROM CHO CELLS USING SARS-COV-2 DISPLAY ANTIGENS 129

4.1	Introduction	129
4.2	Results	131
4.2.1	Generation of Ubiquitin-SARS-CoV-2 fusion sequences and constructs.....	131
4.2.2	Western Blot Analysis of Ubiquitin-SARS-CoV-2 Fusion Protein Expression in Stable CHO-S Cell Pools	135
4.2.3	DLS analysis of exosome preparations	138
4.2.4	Generation of Tetraspanin-fusion based vectors	142

4.2.5	Western Blot Analysis of Tetraspanin-SARS-CoV-2 Fusion Protein Expression in Stable CHO Cell Pools	144
4.2.6	DLS analysis of exosome preparations	148
4.3	Discussion	151
CHAPTER 5: OPTIMISATION, EXPRESSION AND PROFILING OF NOVEL MONOCLONAL ANTIBODIES FOR THE TREATMENT OF DENGUE FEVER		154
5.1	Introduction	154
5.2	Results	156
5.2.1	Generation of Den54-native vectors	156
5.2.2	Redesign and engineering of anti-dengue antibody, Den54, amino acid sequences to improve secretory expression	159
5.2.3	Generation of Den54(1-5) vectors.....	161
5.2.4	Expression Profiles of newly designed Den54 sequences: D1 – D5	163
5.2.5	Initial Development of Monoclonal Stable Cell Lines Expressing Anti-Dengue Molecules D1 – D5	169
5.2.6	Fed-batch production runs of D1 – D5 molecule expressing monoclonal cell lines.....	172
5.2.7	Second Round of Limiting Dilution Cloning for Generation of Monoclonal Stable Cell Lines Expressing Anti-Dengue Antibody Molecules D1 – D4	177
5.2.8	Investigating Potential Bottleneck Points in Protein Production of Den54-Derived Antibodies	201
5.3	Discussion	207
5.3.1	Re-design of Den54 sequences to incorporate elements of IgG molecules expressed well in CHO-S cultures to improve anti-dengue antibody production	207
5.3.2	Development and Scale-Up of Monoclonal Lineages of each Redesigned Anti-Dengue Molecule.....	210
5.3.3	Manipulation of Culture Conditions to Improve Anti-Dengue mAb Yields of Each Engineered Molecule and Cell Line.....	213
5.3.4	Investigation of Potential Bottlenecks in Antibody Production for the Different Anti-Dengue mAbs	217
5.4	Conclusions	218
CHAPTER 6: DISCUSSION		221

6.1	Exosome Targeting Proof-of-Concept CHO Cell Work	221
6.1.1	Orientation Effects of Ubiquitin Fusions	221
6.1.2	Differences are observed between GFP and mCherry ubiquitin fusions	222
6.1.3	Exosome cargo loading favours a CD81-fusion approach in CHO-S cells	223
6.2	Generation of Recombinant SARS-CoV-2 Antigen Containing Exosomes	224
6.2.1	Differences between host and recombinant cell line HIS tag presence suggests the successful targeting of fusion proteins to exosome populations	225
6.2.2	Spike Subunit 2 Is the Best Targeted Exosome Cargo of the SARS-Cov-2 Antigens	225
6.2.3	Approaches to Exosome Isolation and Characterisation for An Improved and More Robust Analysis in Future Work.....	226
6.3	Improvement of anti-dengue monoclonal antibody secretory expression from CHO-S cells	231
6.3.1	Sequence Hybridization of Den54 with Nivolumab Showed the Most Improvement in Expression.....	231
6.3.2	The Secretion Bottleneck of Den54 May Be Due to Fc Engineering Leading to Intra-ER Crystal Aggregate Formation.....	232
6.3.3	Future Approaches in Sequence Optimisation and Cell Line Development to Improve the Expression and Secretion of the anti-dengue mAb in CHO.	233
6.4	Conclusions	235
	REFERENCES	236
	APPENDIX	257
	Vector Maps	257
	Gene Sequences	300

Abbreviations

ACE2	angiotensin converting enzyme 2
ADE	antibody-dependant enhancement
APR	aggregation prone region
BSA	Bovine serum albumin
CDR	complementary determining region
cDNA	complementary DNA
CHO	Chinese hamster ovary
CMV	cytomegalovirus
Ct	cycle threshold
CV	column volume
DAPI	4',6-diamidino-2-phenylindole
DC	dendritic cell
DENV	dengue virus
DHF	dengue haemorrhagic fever
DHFR	dihydrofolate reductase
DLS	dynamic light scattering
DNA	deoxyribonucleic acid
DSS	dengue shock syndrome
DTE	difficult-to-express
DTT	dithiothreitol
ER	endoplasmic reticulum
ESCRT	endosomal sorting complex required for transport
EVs	extracellular vesicles
Fab	(antibody) antigen-binding fragment
FACS	fluorescence-associated cell sorting
Fc	(antibody) fragment crystallisable
Fcy	(antibody) fragment crystallisable gamma
FITC	Fluorescein isothiocyanate
FPLC	fast protein liquid chromatography
FR	framework region

GFP	green fluorescent protein
GS	glutamine synthetase
H5N1	avian influenza
HEK293	human embryonic kidney cell line 293
HER2	human epidermal growth factor 2
HC	heavy chain
HPLC	high performance liquid chromatography
HRP	horseradish peroxidase
Ig	immunoglobulin
IHN	infectious hematopoietic virus
ILV	intraluminal vesicle
IRES	internal ribosomal entry site
kDa	kilo-Dalton
LB	Luria-Bertani (medium)
LC	light chain
LMM	lipid metabolism modifying
mAb	monoclonal antibody
mCh	monomeric (fluorescent) cherry protein
MERS-CoV	middle-eastern respiratory syndrome coronavirus
MHC	multi-histocompatibility complex
mRNA	messenger RNA
miRNA	microRNA
MVB	multivesicular body
MWCO	molecular weight cut-off
NC	nucleocapsid
nSMase2	type II sphingomyelinase
NTP	nucleotide (N-)tri-phosphate
ORF	open reading frame
P5CS	pyroline-5-carboxylase synthetase
PAMP	pathogen-associated molecular pattern
PASP	pathogen-associated structural pattern
PCR	polymerase chain reaction

POI	protein-of-interest
prM	pre-membrane
PRRSV	porcine reproductive and respiratory virus
PTEN	phosphatase and tensin homologue
PTM	post-translational modification
PU	polyubiquitin
RBD	receptor binding domain
RFP	red fluorescent protein
RNA	Ribonucleic acid
RPM	revolutions per minute
RT-PCR	reverse transcription PCR
S1	spike subunit 1
S2	spike subunit 2
SARS-CoV	severe acute respiratory syndrome coronavirus
SARS-CoV-2	severe acute respiratory syndrome coronavirus (Covid-19)
SCD1	stearoyl coenzyme A desaturase 1
SDS-PAGE	sodium dodecyl sulphate polyacrylamide gel electrophoresis
siRNA	short interfering RNA
SNARE	soluble N-ethylmaleimide-sensitive fusion attachment protein receptor
SP	signal peptide
SREBF-1	sterol regulatory element binding factor 1
SV40	simian virus 40
TAA	tumour-associated antigen
tFLS	truncated full-length spike protein
TLR	toll-like receptor
TRITC	Tetramethylrhodamine
TSG101	tumour suppressor gene 101
Ubi	ubiquitin
UTR	untranslated region
VLP	virus-like particle
VSV	vesicular stomatitis virus
WNV	West Nile virus

List of Figures

Figure 1.1	Vaccination impact on case numbers for diseases targeted by national vaccination programmes in the UK.	30
Figure 1.2	DENV structure and the genomic organisation of structural and non-structural proteins within an open-reading frame (ORF) flanked by a 5' untranslated region (UTR) and 3' UTR. Structural proteins on the mature virion include the envelope (E) and membrane (M) proteins (derived from pre-membrane (pre-M) protein) and the capsid forming capsid protein (C).	36
Figure 1.3	The spread of COVID-19 across continents illustrated by confirmed case numbers as seven-day rolling averages. The start date of the COVID-19 pandemic, 11 th March 2020, is shown as an orange dashed line	39
Figure 1.4	(Bottom) SARS-CoV-2 virion structure with the viral RNA genome and structural proteins (nucleocapsid (N), membrane(M), envelope (E) and spike (S)). (Top) S protein cleavage by furin from the host-cell golgi apparatus results in two non-covalently associated S1 and S2 subunits on mature virions.	41
Figure 1.5	Schematic depicting exosome formation and release from cells. Cargo taken in by endocytosis is sorted at early endosomes which is then packaged into either lysosomes for degradation, or multivesicular bodies (MVB) containing intraluminal vesicles (ILV) formed by budding of late endosomal membranes. ILVs are then released as exosomes into the extracellular space when MVBs fuse with the plasma membrane	46
Figure 1.6	Vesicle formation via the ESCRT Pathway in which ubiquitinated proteins at the endosomal membrane are recognized by ESCRT-0 (i), which then binds with ESCRTI and -II to begin invagination of the endosomal membrane (ii). This process results in the budding of the endosomal membrane, encapsulating the ubiquitinated cargo which is then deubiquitinated (iii), and the vesicle is formed when the membrane opening of the developing bud is fused by ESCRT-III (iv). (B) Endosomal membrane budding for vesicle formation via the Ceramide Pathway in which conversion of	47

sphingomyelin (i) to ceramide within the membrane by nSMase2 (ii) results in clustering of ceramide to create the curvature of the membrane (iii) due to its more branched, unsaturated fatty acid tail structures.

Figure 1.7	Variations on the types of exosome-cargo loading (I-III) and their possible presentation strategies to the respective immune cells, dependent on cargo type, to illicit immune responses.	50
Figure 1.8	Ubiquitin-tagging gene constructs employed using eGFP as a fluorescent reporter to test if fusion with ubiquitin (Ub)/ modified ubiquitin (mUb) results in trafficking to exosomes in HEK293 cells.	53
Figure 1.9	(A) The mammalian expression vector used to express CD63-GFP fusion proteins and its configuration within the plasmid. (B) Schematic of engineered exosomes for surface display of proteins of interest via fusion with tetraspanin proteins. Proteins can be fused at the extracellular transmembrane loop domain for external display (red oval, RFP), while those at the C-terminus are found on the inner surface (green oval, GFP).	54
Figure 1.10	Schematic of the IgG antibody structure. Complementarity-determining regions (CDRs) are located in the variable heavy (V_H) and variable light (V_L) chains on each arm of the structure, together with the constant heavy chain-1 (C_{H1}) region they are referred to as a Fab (fragment antibody binding) region. The lower domains of the heavy chains, C_{H2} and C_{H3} , form the Fc (fragment crystallizable) region.	56
Figure 3.1	Vector map showing the 3.1 hygro plasmid backbone layout with the Ubi_GFP fusion protein gene sequence inserted at the multiple cloning site which is flanked by an enhanced CMV promoter and a bGH polyA terminator. The vector also includes ampicillin and hygromycin resistance genes for use in bacterial and mammalian systems respectively.	92
Figure 3.2	Schematic of the ubiquitin-based vector cassettes and respective control vector cassettes created and described throughout this chapter. Also shown are the restriction enzymes insertion sites	93

used to clone sequences into the 3.1 hygro plasmid backbone. The annotated name used for each construct is shown on the left of each schematic.

Figure 3.3	1% Agarose DNA gel analysis of test restriction digests from finalised cloned ubiquitin vectors with 1 kbp DNA markers (M). Restriction enzymes for each lane: GFP (HindIII, BamHI); mCh (BamHI, XhoI); Ubi_GFP and Ubi_mCh (HindIII, BamHI, XhoI); GFP_Ubi, mCh_Ubi, GFP_Polyubi, mCh_Polyubi (NheI, HindIII, BamHI).	93
Figure 3.4	Western blotting of cell pellet lysates collected from transient transfection of CHO-S cells with ubiquitin-based fusion sequence containing vectors. (A) Anti-mCherry probe, 10 second exposure, red arrow shows mCherry size, blue arrows show mCherry-fusion bands. (B) Anti-GFP probe, 90 second exposure, green arrows show GFP sizes, orange bands show GFP fusion bands. (C) Anti- β -actin probe, 10 second exposure, purple arrow shows β -actin band sizes.	95
Figure 3.5	Merged channel ZEISS confocal microscopy images for each ubiquitin-based GFP stable cell line, alongside positive (GFP) and negative (CHO-S) control cell lines, in triplicate, showing the co-localisation of the nucleus (blue) and GFP (green) at 63x magnification plus oil immersion.	98
Figure 3.6	Merged channel ZEISS confocal microscopy images for each ubiquitin-based mCherry stable cell line, alongside positive (mCherry) and negative (CHO-S) control cell lines, in triplicate, showing the co-localisation of the nucleus (blue) and mCherry (red) at 63x magnification plus oil immersion.	99
Figure 3.7	Western blots of cell pellet lysates (P), supernatants(S) and exosome suspensions (E) for each of the ubiquitin stable cell pools, each prepared with a DTT-reducing buffer and boiled prior to loading. (A) Anti-GFP probe, 10-minute exposure (B) Anti-mCherry probe, 1 minute exposure.	101
Figure 3.8	Particle size distributions of exosome preparations from the ubiquitin-based GFP stable cell pool exosome suspensions,	103

including (A) negative control (CHO-S), (B) positive control (GFP only), (C) Ubi_GFP, (D) GFP_Ubi, and (E) GFP_PolyUbi exosome suspensions. Each figure shows the average DLS measurement (n=10) for relative intensity frequency weight (%) vs. particle diameter (nm) with a log10 scale applied.

- Figure 3.9** Particle size distribution of exosome preparations from for the ubiquitin-based mCherry stable cell pool exosome suspensions, including (A) negative control (CHO-S), (B) positive control (mCherry only), (C) Ubi_mCh, (D) mCh_Ubi, and (E) mCh_Polyubi exosome suspensions. Each graph shows the average DLS measurements (n=10) for relative intensity frequency weight (%) vs. particle diameter (nm) with a log10 scale applied. **104**
- Figure 3.10** Schematic of the exosome marker-eGFP based vector cassettes and respective control vector cassette created and used throughout this chapter. Also shown are the restriction enzymes insertion sites used to clone sequences into the commercially available 3.1 hygro plasmid backbone. **105**
- Figure 3.11** Double-stranded DNA and amino acid view of the restriction site sequence inserted into both CD63 and CD81 to create a mid-gene cloning site. The sequence is comprised of restriction sites PteI (blue) and Bsp119I (orange) flanking a filler sequence (Gly, Lys, Gly, Val, Ala) and is inserted after Ala-136 and Ala-133 for CD63 and CD81, respectively. **106**
- Figure 3.12** 1% Agarose DNA gel analysis with 10 uL volumes of test restriction digests from finalised cloned exosome marker-based vectors with 1 kbp DNA markers (M). (A) CD63-only vector digest vs CD63-GFP fusion digests. (B) CD81-only vector digest vs CD81-GFP fusion digests. (C) Tsg101 full vector cassette digests **107**
- Figure 3.13** Western blot analysis of cell pellet lystates collected from transient transfection of CHO-S cells with exosome marker-based vectors. (Top) Anti-GFP probe, 3 minute exposure. (Bottom) Anti-β-actin probe, 10 second exposure. **109**

Figure 3.14	Merged channel ZEISS confocal microscopy images for each tetraspanin-based GFP stable cell line, alongside positive (GFP) and negative (CHO-S) control cell lines, in triplicate, showing the co-localisation of the nucleus (blue) and GFP (green) at 63x magnification plus oil immersion.	111
Figure 3.15	Western blots of cell pellet lysates (P), supernatants(S) and exosome suspensions (E) for each of the tetraspanin-based stable cell lines, each prepared with a DTT-reducing buffer and boiled prior to loading, blotted with an anti-GFP probe and exposed for 5 minutes.	113
Figure 3.16	Particle size distribution for the tetraspanin-based GFP stable cell line exosome suspensions, including (A) negative control (CHO-S), (B) positive control (GFP only), (C) CD63 _{MID} GFP, (D) CD81 _{TAG} GFP,(E) CD81 _{MID} GFP, and (F) CD81 _{TAG} GFP exosome suspensions. Each figure shows the average DLS measurements (n=10) for relative intensity frequency weight (%) vs. particle diameter (nm) with a log ₁₀ scale applied.	114
Figure 4.1	Vector map showing the 3.1 hygro plasmid backbone layout with the Ubi_RBD fusion protein gene sequence inserted at the multiple cloning site which is flanked by an enhanced CMV promoter and a bGH polyA terminator.	130
Figure 4.2	Vector map showing the 3.1 hygro plasmid backbone layout with the Ubi_RBD fusion protein gene sequence inserted at the multiple cloning site which is flanked by an enhanced CMV promoter and a bGH polyA terminator.	131
Figure 4.3	Schematic of the ubiquitin-SARS-CoV-2 vector cassettes and respective control vector cassettes created and described throughout this chapter. Also shown are the restriction enzymes insertion sites used to clone sequences into the 3.1 hygro plasmid backbone. The annotated name used for each construct is shown on the left of each schematic.	132
Figure 4.4	1% Agarose DNA gel analysis of test restriction digests from finalised cloned ubiquitin-covid vectors with 1 kbp DNA markers (M). (Left) N-terminal ubiquitin-tagged sequences, digested with	133

	HindIII, BamHI and XhoI. (Right) C-terminal ubiquitin-tagged sequences, digested with NheI, HindIII and BamHI.	
Figure 4.5	Western blot images of cell pellet lysates (P), supernatants (S) and exosome preps each taken from a CHO-S cell culture.(A) anti-CD63 probe (B) anti-CD81 probe and (C) anti-CD9 probe, 10 minute exposure.	134
Figure 4.6	Western blot images of cell pellet lysates (P), supernatants (S) and exosome preps taken from each of the cell pools expressing SARS-CoV-2-ubiquitin fusion proteins containing a His-tag, using an anti-His antibody probe (exposure time 4 minutes).	136
Figure 4.7	Western blot images of cell pellet lysates (P), supernatants (S) and exosome preps taken from each of the SARS-CoV-2-ubiquitin fusion protein expressing cell pools, using an anti-His antibody probe (exposure time 40 minutes).	137
Figure 4.8	Particle size distributions of exosome preparations from the C-terminally tagged ubiquitin-SARS-CoV-2 fusion protein expressing stable cell pool exosome suspensions, alongside negative control (CHO-S) exosome suspensions. Each figure shows the average DLS measurement (n=10) for relative intensity frequency weight (%) vs. particle diameter (nm) with a log ₁₀ scale applied.	139
Figure 4.9	Particle size distributions of exosome preparations from the N-terminally tagged ubiquitin-SARS-CoV-2 fusion protein expressing stable cell pool exosome suspensions, alongside negative control (CHO-S) exosome suspensions. Each figure shows the average DLS measurement (n=10) for relative intensity frequency weight (%) vs. particle diameter (nm) with a log ₁₀ scale applied.	140
Figure 4.10	Vector map showing the 3.1 hygro plasmid backbone layout with the CD63_RBD fusion protein gene sequence inserted at the multiple cloning site which is flanked by an enhanced CMV promoter and a bGH polyA terminator.	141
Figure 4.11	Vector map showing the 3.1 hygro plasmid backbone layout with the CD81_RBD fusion protein gene sequence inserted at the multiple cloning site which is flanked by an enhanced CMV promoter and a bGH polyA terminator.	142

Figure 4.12	1% Agarose DNA gel analysis of test restriction digests, using BamHI and XhoI, on intermediate and finalised cloned tetraspanin-SARS-CoV-2 vectors with 1 kbp DNA markers (M). (Left) CD63-based sequences. (Right) CD81-based sequences.	143
Figure 4.13	Western blot images of cell pellet lysates (P), supernatants (S) and exosome preps taken from each of the CD63-ubiquitin fusion protein expressing cell pools, using an anti-CD63 antibody probe (exposure time 30 minutes).	144
Figure 4.14	Western blot images of cell pellet lysates (P), supernatants (S) and exosome preps taken from each of the CD81-ubiquitin fusion protein expressing cell pools, using an anti-CD81 antibody probe (exposure time 40 minutes).	145
Figure 4.15	Western blot images of cell pellet lysates (P), supernatants (S) and exosome preps taken from each of the cell pools expressing tetraspanin-ubiquitin fusion proteins containing a His-tag, using an anti-His antibody probe (exposure time 4 minutes).	146
Figure 4.16	Particle size distributions of exosome preparations from the CD63-SARS-CoV-2 fusion protein expressing stable cell pool Exosome suspensions, alongside negative control (CHO-S) exosome suspensions. Each figure shows the average DLS measurement (n=10) for relative intensity frequency weight (%) vs. particle diameter (nm) with a log ₁₀ scale applied.	147
Figure 4.17	Particle size distributions of exosome preparations from the CD81-SARS-CoV-2 fusion protein expressing stable cell pool exosome suspensions, alongside negative control (CHO-S) exosome suspensions. Each figure shows the average DLS measurement (n=10) for relative intensity frequency weight (%) vs. particle diameter (nm) with a log ₁₀ scale applied.	149
Figure 5.1	Vector map for pcDNA 3.1 GS which has the Den54 light and heavy chain sequences cloned into the restriction sites XhoI/BamHI and KpnI/ApaI, respectively, flanked by T7 promoters and bGH polyA signals. This vector also contains the metabolic selection marker glutamine synthase (GS) gene and antibiotic selection marker ampicillin resistance (AmpR) gene for	155

	mammalian and bacterial use, respectively.	
Figure 5.2	1% agarose gel loaded with test digests (KpnI/ApaI) for GS-Trast + DenHC ligation. (B) 1% agarose gel loaded with test digests (KpnI/ApaI for (A) + DenLC ligation. (C) Supernatant samples from a transient expression for 72 h of the Trast and Dengue antibody constructs analysed by western blot after running samples on a 12% SDS gel prepared with non-reducing buffers boiled. Probed for Heavy Chain (Fc) region (Sigma) with 30 second exposure. Negative controls: Blank (TE buffer only) and an Empty GS vector. Positive Control: Trastuzumab vector (GS backbone).	156
Figure 5.3	Annotated schematic of an IgG antibody molecule, including the variable heavy (V_L), variable light (V_H) and constant heavy domains (C_{H1} , C_{H2} and C_{H3}). Complementarity-determining regions (CDRs) and framework regions are found in the antigen binding site in the Fab region. Constant heavy domains 2 and 3 form the crystallised fragment (Fc) region	157
Figure 5.4	Schematic diagram showing the re-engineered of the anti-dengue Den54 amino acid sequence designs (molecules D1 – D5), with colour coding to represent sequence origins of each antibody region. Blue: trastuzumab sequence; Gold: nivolumab sequence; Red: Den54 sequence; and Light Blue bars: Den54 CDRs. (Left) Icons representing fully assembled antibody. (Right) Individual light and heavy chain sequences for expression vectors.	158
Figure 5.5	Restriction enzyme digest analysis of dengue plasmids D1 – D5 (Figure 5.3) on 1% agarose gels with a 1 kb DNA ladder marker. (A) LC1/2 and LC5 double-digested with XhoI and ApaI, LC3 and LC4 digested with PstI. (B - D) All plasmids digested with BamHI.	160
Figure 5.6	Western blot of CHO-S cell culture supernatants collected from transient transfections of the D1 – D5 vectors in biological duplicate 72 h post-transfection. A 10% SDS-PAGE analysis was undertaken with an anti-HC (Fc) primary antibody probe and 10 second exposure.	161

Figure 5.7	Western blots of culture supernatants collected from stable cell line pools, created with the D1 – D5 vectors. Prepared using an 12% SDS gel for electrophoresis. (A) Anti-HC (Fc) primary antibody, 5-second exposure; (B) Anti-LC (λ), 30-second exposure; (C) Anti-LC (κ), 10-second exposure.	162
Figure 5.8	Western blot analysis of anti-dengue antibody present at harvest from the D1 – D5 stable cell pool 100 mL fed-batch production run. Samples were separated using a 10% SDS-PAGE and then probed with an anti-HC (Fc) primary antibody. (A) Cell culture supernatants, 1-second exposure; (B) Cell pellet lysates, 4-second exposure.	164
Figure 5.9	Western blot analysis of the harvested cell culture supernatants and the elutions, flowthroughs and washes collected during FPLC Protein A affinity chromatography purification of the secreted antibody from the supernatants harvested from 100 mL fed-batch productions runs of the D1- D4 stable cell pools. Prepared using a 10% SDS-PAGE gel for electrophoresis, probed with an anti-HC(Fc), 10-second exposure.	165
Figure 5.10	ELISA-determined concentration (ng/mL) of each of the purified anti-dengue antibodies produced from the respective stable pool cell lines D1 - D4.	166
Figure 5.11	Western dot blot using 100 μ L of the cell culture supernatants of specific D1 - D5 clonal cell lines, grown in 96-well plates post-limiting dilution. Blots probed with an anti-HC (Fc) primary antibody and 20-minute exposure. Clones from each cell line are grouped and colour-highlighted: (Top) Blue = D1; Orange = D2; Green = D3; (Bottom) Yellow = D4 and Purple = D5. Clones selected for further scale-up are highlighted further with dashed red circles.	167
Figure 5.12	Western blot analysis of D1 – D5 expressing clones after scaling to static T25 flasks with 10 mL culture volumes. Analysis undertaken using a 10% SDS-PAGE gel for electrophoresis, probed with an anti-HC (Fc) primary antibody, 10-minute exposure.	168
Figure 5.13	Western blot analysis of D1 – D5 clone cell culture supernatants	169

	after growing in suspension shaking incubation at 220 rpm in 50 mL falcon tubes in 10 mL culture volumes. Analysis undertaken using a 10% SDS-PAGE gel for electrophoresis, probed with an anti-HC (Fc) primary antibody, 30-second exposure.	
Figure 5.14	Western blot analysis of supernatant from D1 – D5 clones after growth at 140 rpm in 125 mL Erlenmeyer flasks in 20 mL culture volumes. Analysis undertaken using a 10% SDS-PAGE gel for electrophoresis, probed with an anti-HC (Fc) primary antibody, 30-second exposure.	170
Figure 5.15	100mL fed-batch production run sampling results from monoclonal lines D1A-16, D2B-1, D3A-13, D4B-21 and D5A-11. (A) Western blots of supernatants collected during culture sampling on feed and harvest days. Prepared using an 10% SDS gel for electrophoresis and probed with an anti-HC (Fc) primary antibody, 5-second exposure; (B) Viable cell counts of each culture over time (days); (C) Viability percentages of each culture over time (days).	172
Figure 5.16	Western blot analysis of the elutions, flowthroughs and washes collected during FPLC Protein A affinity chromatography runs for the supernatants harvested from fed-batch productions runs of D1A-16, D2B-1, D3A-13, D4B-21 and D5A-11. Analysis undertaken using a 10% SDS-PAGE gel for electrophoresis, probed with an anti-HC (Fc) primary antibody, 2-second exposure.	173
Figure 5.17	Coomassie blue-stained SDS-PAGE of the purified and concentrated monoclonal D1 – D5 antibody products in 1 uL and 5 uL volumes, alongside 5 uL volumes of commercially produced Trastuzumab in a standard concentration range.	174
Figure 5.18	Western blot (anti-HC probe, 2-second exposure) comparison of purified antibody material from monoclonals D1_8, D2_1 and D3_11 with standard concentration range of commercially produced trastuzumab.	175
Figure 5.19	Western blot analysis of anti-dengue mAb from the clones produced from lines D1A-16, D2B-1, D3A-13 and D4B-21 after scaling to shaking incubation at 220 rpm in 50 mL falcon tubes with 10 mL culture volumes. Analysis undertaken on a 10% SDS-	176

	PAGE gel for electrophoresis, probed with an anti-HC (Fc) primary antibody, 2-minute exposure.	
Figure 5.20	Western blots of the clones produced from lines D1A-16, D2B-1, D3A-13 and D4B-21 after scaling to shaking incubation at 140 RPM in 125 mL Erlenmeyer flasks with 20 mL volumes. Prepared using a 10% SDS gel for electrophoresis, probed with an anti-HC (Fc) primary antibody, 10-minute exposure	177
Figure 5.21	100 mL fed-batch production growth characteristics from clones derived from cell lines D1A-16, D2-1, D3A-13 and D4B-21. (Top) Viable cell concentrations of each culture over time (days). (Bottom) Culture viability of each culture over time (days).	178
Figure 5.22	Western blot analysis of supernatants collected during culture on feed and harvest days for the clones derived from cell lines D1A-16, D2-1, D3A-13 and D4B-21. Analysed on a 10% SDS-PAGE gel for electrophoresis and probed with an anti-HC (Fc) primary antibody, 1-second exposure.	179
Figure 5.23	Western blot analysis of the elutions, flowthroughs and washes collected during FPLC Protein A affinity chromatography purification of mAbs from the supernatants of cell culture harvest from clones derived from D1A-16, D2B-1, D3A-13 and D4B-21. Analysed using a 10% SDS-PAGE gel for electrophoresis, probed with an anti-HC(Fc), 1-second exposure.	181
Figure 5.24	Coomassie Blue-stained SDS-PAGE analysis of the purified and concentrated antibody products from further monoclonal development of the cell lines D1A-16, D2B-1, D3A-13, and D4B-21. Lanes are loaded with equal volumes (5 uL) alongside commercially produced Trastuzumab in a standard concentration range.	182
Figure 5.25	Daily cell growth, culture and size measurements of the small-scale temperature optimization experiment showing: (Top) Daily culture viabilities (%); (Middle) Daily Viable Cell Concentrations ($\times 10^6$); and (Bottom) Daily average cell diameters (μm).	184
Figure 5.26	Western blot analysis of supernatants collected from daily sampling of the small-scale temperature shift experiment, analysed using a 10% SDS-PAGE gel for electrophoresis and probed with an	185

	anti-HC (Fc) primary antibody, 10-second exposure. Lanes: Condition A (32°C throughout); Condition B (37°C until day 6, then 32°C); and Condition C (37°C throughout).	
Figure 5.27	Daily viable cell concentrations, culture viabilities and cell size data for the larger-scale temperature optimized production run of four replicate flask of clone D2_1, showing: (Top) Daily culture viabilities (%); (Middle) Daily Viable Cell Concentrations ($\times 10^6$); and (Bottom) Daily average cell diameters (μm).	187
Figure 5.28	Western blot analysis of supernatants collected daily from the larger-scale temperature-optimized production run of clone D2_1, analysed on a 10% SDS-PAGE gel for electrophoresis and probed with an anti-HC (Fc) primary antibody, 10-second exposure. Lanes "1", "2", "3" and "4" each represent the corresponding replicate flask cultures.	188
Figure 5.29	Western blot analysis of the flowthroughs, washes and elutions collected during FPLC Protein A affinity chromatography 1 Litre run of the supernatants harvested from the larger-scale temperature-optimized production run of clone D2_1. Analysed using a 10% SDS-PAGE gel for electrophoresis, probed with an anti-HC (Fc) primary antibody, 10-second exposure.	189
Figure 5.30	Western blot analysis of the flowthroughs, washes and elutions collected during FPLC Protein A affinity chromatography 200 mL run of the supernatant harvested from the larger-scale temperature-optimized production run. Analysed using a 10% SDS-PAGE gel for electrophoresis, probed with an anti-HC (Fc) primary antibody, 10-second exposure.	190
Figure 5.31	Growth measurements of cell lines grown under controlled ambr250 bioreactor conditions with reactor 1 and 2 growing cell lines D1A-16-8 and D2B-1 respectively. (Top) Culture viability (%) and (Bottom) Viable Cell Concentration ($\times 10^6$ viable cells/mL) across culture on a daily basis.	192
Figure 5.32	Combined trace graph produced in Sartorius' 'Results Viewer' software for bioreactor 1 (D1A-16-8 cells) which shows dissolved oxygen (DO%), foam sensor readings, pH, temperature ($^{\circ}\text{C}$),	194

	volume of base added (mL) and gas flow (mL/min) of the bioreactor vessel over the 9-day process.	
Figure 5.33	Combined trace graph produced in Sartorius' 'Results Viewer' software for bioreactor 2 (D2B-1 cells) which shows dissolved oxygen (DO%), foam sensor readings, pH, temperature (°C), volume of base added (mL) and gas flow (mL/min) of the bioreactor vessel over the 13-day process.	195
Figure 5.34	Western blot analysis of daily samples from the ambr250 bioreactors 1 and 2, growing cell lines D1A-16-8 and D2B-1 respectively. Analysis was undertaken on a 10% SDS-PAGE gel for electrophoresis, probed with an anti-HC (Fc) primary antibody, 30-second exposure.	196
Figure 5.35	Western blot analysis of samples taken from the elution fractions, flowthroughs and washes produced during the purification of the the supernatants harvested from ambr250 bioreactors 1 and 2, growing cell lines D1A-16-8 and D2B-1 respectively. Analysed using an 10% SDS-PAGE gel for electrophoresis, probed with an anti-HC (Fc) primary antibody, 30-second exposure.	196
Figure 5.36	Western blot (anti-HC probe, 2-second exposure) comparison of purified antibody material from various D2-expressing cells grown with a temperature shift at peak cell concentration alongside a range of standard concentrations of commercially produced trastuzumab.	197
Figure 5.37	Comparison of A_{280nm} measurements of purified antibody material from cell pools and lines along the various stages of cell line and process development to improve titres.	198
Figure 5.38	Western blots analysis comparing antibody intracellular or secretion levels from stable cell line pools D1A, D2B, D3A, D4B, D5A and D5B collected at harvest from the stable cell line 100 mL production run. Analysed on a 10% SDS-PAGE gel for electrophoresis and probed with an anti-HC (Fc) primary antibody. (A) Supernatants, 1-second exposure; (B) Cell pellet lysates, 4-second exposure.	199
Figure 5.39	mRNA expression fold changes for the light (LC) and heavy	200

(HC) chain of the different anti-dengue molecules determined from qPCR carried out on stable cell pools, using GAPDH as a housekeeping gene control.

- Figure 5.40** Images of the CHO-S native cell line and stable cell pools Den1, Den3 and Den5 after fixation and immunofluorescent staining collected by confocal microscopy at 63x magnification under oil immersion with a 10 μm scale bar. Immunofluorescence stains include anti-calnexin (orange, ER marker) and anti-heavy chain (green), with a DAPI nuclear stain (blue) and are presented as viewed with individual channels and a merged view of all three. **202**
- Figure 5.41** Enlarged confocal images of the immunofluorescent stained stable cell pools Den1 and Den5, comparing the anti-heavy chain localisation (top) with the merged view co-localisation of heavy chain, calnexin and DAPI (bottom) to show differences in heavy chain presence between the two cell pools. **203**

List of Tables

Table 1.1	List of COVID-19 vaccines which have been validated for use by WHO, or Emergency Use Listing (EUL) status, as of January 2022.	42
Table 2.1	Thermocycler program used for Phusion™ PCR reactions	68
Table 2.2	List of custom primers used to amplify gene sequences via PCR, including the restriction enzyme site encoded and melting temperature (T _m) of each oligo.	69
Table 2.3	List of components and volumes for each RT-PCR reaction for use with the QuantiNova™ SYBR Green RT-PCR Kit (Qiagen).	72
Table 2.4	Cycling Conditions for RT-PCR reactions using the QuantiNova™ SYBR Green RT-PCR Kit (Qiagen).	72
Table 2.5	List of custom primers used in RT-PCR reactions, including melting temperature (T _m) of each oligo.	73
Table 2.6	Thermocycler program for colony PCR reaction protocol	74
Table 2.7	FastDigest™ Restriction Enzyme double digest reaction compositions, both incubated at 37 °C for 1 hour.	75
Table 2.8	NEB® Restriction Enzyme double digest reaction composition, incubated at 37 °C for 1 hour.	75
Table 2.9	Feeding Schedules and Volumes (as percentages of total culture volume) for fed-batch style culture using Gibco™ CHO CD EfficientFeed™ B (as recommended by manufacturer).	77
Table 2.10	Process detailing the parameters and setpoints used for CHO-S cultures grown in the Sartorius ambr® 250 Modular system.	78
Table 2.11	Composition of the varying percentage of polyacrylamide gels used in SDS page. Each column represents volumes required to make 4 gels.	83
Table 2.12	List of primary and secondary antibodies (including product codes) and each of the corresponding recommended dilution factors and (when applicable) secondary antibody types for western blotting (WB) and Immunofluorescence (IF).	85
Table 4.1	A list of the approximate molecular weights for each of the	135

ubiquitin-SARS-CoV-2 fusion protein components expressed in this section.

Table 4.2	A list of the approximate molecular weights for each of the tetraspanin-SARS-CoV-2 fusion protein components expressed in this section.	144
------------------	-----------------------------------------------------------------------------------------------------------------------------------------	------------

Chapter 1: Introduction

1.1 Current Vaccine Platforms

1.1.1 General Introduction

Whilst every year treatments and drugs against infectious disease improve with greater innovations in medical and pharmaceutical science, the most effective defence against infections is a preventative strategy via immunisation programmes. This is evidenced by the extreme reduction in childhood deaths in countries which have high vaccine programme coverage (Pollard and Bijker, 2021) (Fig. 1.1). Vaccines introduce material into the body which mimics a pathogen/antigen in order to elicit an immune response and lead to immune memory, but is attenuated or unable to cause a disease state. There have been several generations of vaccine platforms designed, licensed and implemented to do this, each generation with a multitude of varied targets.

1.1.2 Traditional Vaccines

1.1.2.1 Discovery and Early Development

The first vaccines consisted of inactivated or weakened pathogens, which when introduced into a host produced an immune response and protective antibodies to reduce the severity or incidence of future infection. Edward Jenner is credited with pioneering the concept of immunisation in the West with his successful vaccine against smallpox using cowpox (*Vaccinia virus*) inoculations at the end of the 18th Century. Further understanding of bacterial pathogens in the 19th Century facilitated the development of vaccines for infections notorious for devastating populations, including anthrax (*Bacillus anthracis*), typhoid fever (*Salmonella enterica Typhi*), cholera (*Vibrio cholerae*), and bubonic plague (*Yersinia pestis*) (Plotkin, 2014). These vaccines provided the foundation of understanding for the scientific community and governments of the real potential impacts of vaccine technology on public health.

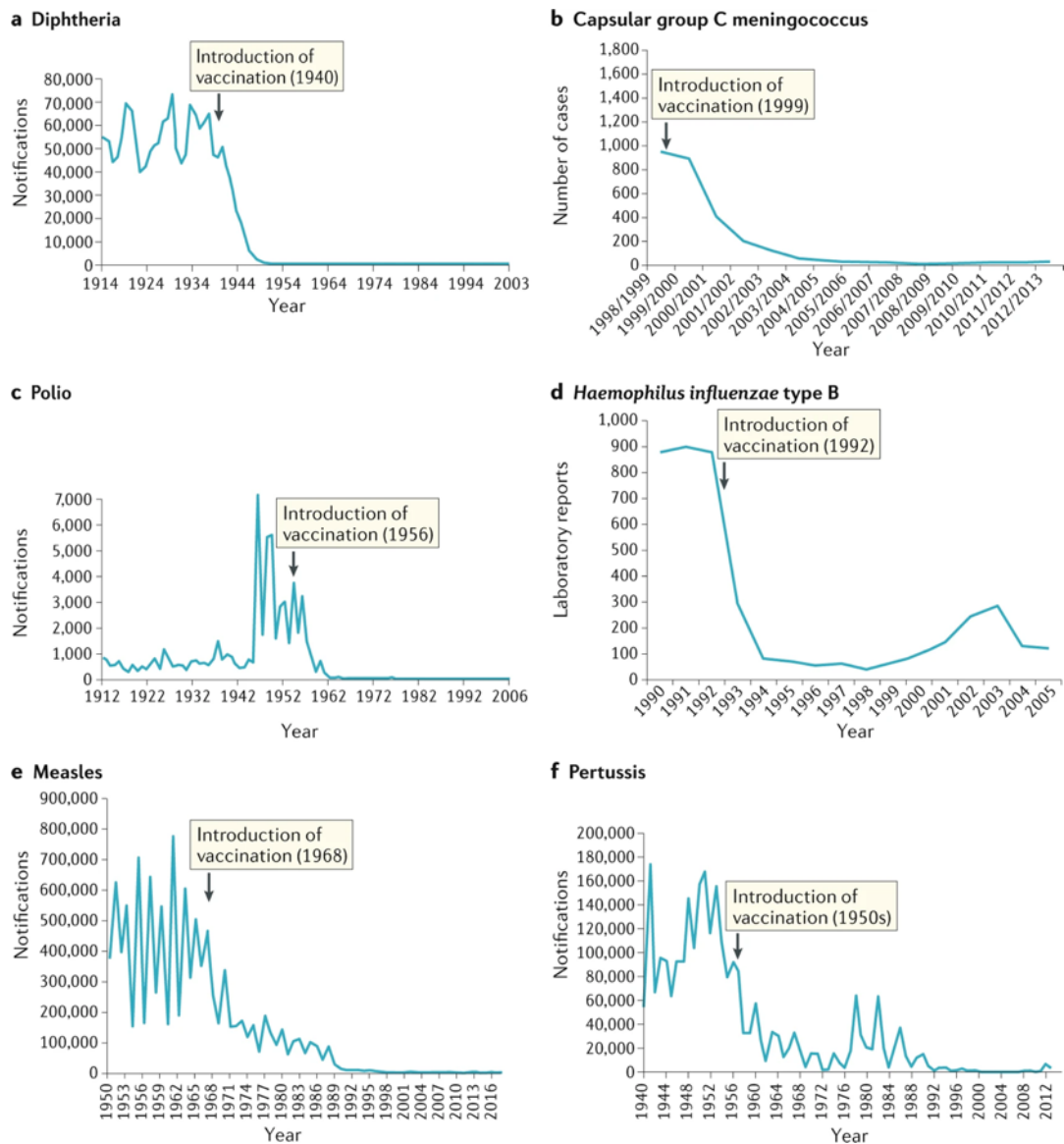


Figure 1.1: Vaccination impact on case numbers for diseases targeted by national vaccination programmes in the UK. (Pollard and Bijker 2021)

Live-attenuated and inactivated bacterial vaccines developed against tetanus (*Clostridium tetani*), diphtheria (*Corynebacterium diphtheriae*), whooping cough (*Bordetella pertussis*) and tuberculosis (*Mycobacterium tuberculosis*) were so successful they were eventually introduced as routine inoculations for children in the UK. Advancements in virology and viral tissue culture methods allowed for the development and manufacture of inactivated/live-attenuated viral vaccines and produced enormous global impacts on viral outbreaks, such as polio, measles, mumps and rubella. However, vaccines created in this way carry a risk of adverse side effects, most infamously the Cutter Laboratories incident (USA, 1955) in which polio vaccinees were infected with live viral material due to a defective inactivation process in the manufacturing process

(Nathanson and Langmuir, 1963). Even in vaccines which are produced correctly, adverse side effects are not uncommon and developing improved immunisations is key for tackling infectious disease and safeguarding public trust. Alternative approaches may offer advantages of cost of production, how rapidly they can be developed against new and emerging threats, and the ability to produce large (or very tailored small) amounts that can be introduced into the global supply chain.

1.1.2.3 Second Generation Vaccines

The rise of biotechnology and development of increasingly effective recombinant protein expression systems produced a new generation of vaccine platforms. Subunit, conjugate, polysaccharide and toxoid vaccines utilise proteins or, for the latter, a toxin associated with the targeted pathogen to illicit an immune response and memory which can protect against future infection by the target pathogen. Safer than their live-attenuated and inactivated predecessors, they do not introduce whole pathogens into the body and therefore eliminate risk of infection from the vaccine, demonstrated in comparing the whole-cell pertussis vaccine with the acellular pertussis vaccine (Podda *et al.*, 1994). These platforms do not require live virus cultivation of a pathogen, reducing the risk involved in the preparation of inoculations, and can often be produced/manufactured using low-cost bacterial expression systems. However, they are not as immunogenic and as such often require adjuvants and boosters to convey effective and long-lasting immunity.

1.1.3 Next Generation Vaccines

1.1.3.1 Virus-Like Particles

Virus-like particles (VLPs) are particles composed of the viral coat proteins presented in a 3D conformation which mimics virions in order to trigger the body's immune response but lacking the genetic replication machinery components within. The diameter of VLPs ranges from 20 – 200 nm and the repetitive surface structures form pathogen-associated structural patterns (PASP), providing a much greater immunogenicity than

their subunit vaccine predecessors (Mohsen *et al.*, 2017). These artificial nanostructures can be produced in prokaryotic and eukaryotic expression systems but the capacity for producing VLPs with complex post-translational modifications means mammalian-based expression systems are the expression system of choice as VLP producers that provide optimal immune responses (Fuenmayor, Godia and Cervera, 2017). Of the mammalian-based systems, Chinese hamster ovary (CHO) cell lines are often favoured due to the mitigated risk of contamination from human viruses as they are not human derived, the platform allows for transient transfection manufacturing processes which can produce small quantities of varying VLPs without issues of toxicity for the host - ideal for research settings or pathogens with high genetic drift, but troublesome for more stable, mass-produced processes where larger yields are required (Fuenmayor, Godia and Cervera, 2017).

VLPs can be used for antigen display as well as targeted cargo delivery in which drugs or viral vectors can be targeted and released into specific cells via receptor binding directed by the presence of particular surface antigens (Qian *et al.*, 2020). As a vaccine platform they have proven successful with vaccines against Hepatitis B, Hepatitis E and Human Papillomavirus currently licensed and marketed, and many more in pre-clinical and clinical trials (Qian *et al.*, 2020). Despite these approved products, the safety and large-scale production of VLPs imposes limitations on their overall success. The use of genetic material which originates in pathogenic agents raises serious safety concerns for producing human vaccines, whilst the production method itself suffers from low yields hindered further by the cytotoxicity of the product itself upon cell culture-based production (Federico, 2012).

1.1.3.2 Nucleic Acid-based Vaccines

First conceived in the 1990's, DNA based vaccines are a vaccine platform with a mechanism of action that introduces genetic material into host cells for endogenous antigen expression to elicit an immune response. Usually delivered as bacterial DNA plasmids encoding antigens via strong eukaryotic or viral promoters, these vaccines offer a cost- and speed-advantage with target flexibility due to the ease of rapid varied

nucleic acid synthesis and can be rapidly formulated, manufactured and isolated on a large scale into thermostable inoculations (Eusébio *et al.*, 2021). Currently five licensed DNA vaccines are available for veterinary use across multiple species including West Nile Virus (WNV) in horses (Davidson *et al.*, 2005); infectious haematopoietic necrosis (IHN) virus in salmon (Garver, LaPatra and Kurath, 2005); tyrosinase for reduced risk of melanoma in dogs (Bergman *et al.*, 2006); *Mycoplasma hyopneumoniae*/Porcine Reproductive and Respiratory Syndrome virus (PRRSV) in pigs (Thacker *et al.*, 2006); and avian flu (H5N1) in chickens (Jiang *et al.*, 2007). However, beyond pre-clinical trials, DNA vaccines candidates for use in human have been generally shown to exhibit low potency and immunogenicity in clinical trials (Liu, 2019). Proposed advances in the designs of DNA vaccines include: improved plasmid designs to boost antigen expression; suitable adjuvants; formulation and delivery methods for a high dose to low cost and invasiveness ratio; prime-boost combinations; and potential self-amplifying replicon systems (Eusébio *et al.*, 2021; Liu, 2019).

Alternatively, RNA vaccines deliver genetic material in the format of single-stranded messenger RNA (mRNA) for endogenous expression of antigenic proteins in order to induce an immune response. Although mRNA shares the highly adaptive synthesis and production advantages of DNA, the vaccines were initially overlooked in favour of DNA-based platforms due to mRNA instability, difficulties in delivery and triggering of inflammatory responses (Bloom, van den Berg and Arbuthnot, 2021; Pardi, Hogan and Weissman, 2020). Engineering of mRNA sequences to incorporate modified nucleotides (Karikó *et al.*, 2008), as well as improved purification techniques like HPLC (Karikó *et al.*, 2011) and cellulose adsorption (Baierdörfer *et al.*, 2019) for removal of double stranded RNA contaminants, have allowed for production of therapeutic mRNA which is highly translatable and can be delivered without creating inflammation responses (Pardi, Hogan and Weissman, 2020). The development of lipid nanoparticles (LNPs) as vehicles which can protect mRNA from degradation and can be taken up by host cells (Pardi *et al.*, 2015) facilitated meaningful advancement and approval of RNA-based vaccines BNT162b2 (Pfizer and BioNTech) (Lamb, 2021) and SpikeVax (Moderna) (Ledford, 2020).

The race to develop vaccines to tackle the novel coronavirus (SARS-CoV-2) pandemic declared in 2020, provides a lens to compare nucleic acid-based vaccines as products using these platforms to introduce the same antigenic target (SARS-CoV-2 spike protein) which were rapidly developed, trialled and licensed in response to the outbreaks. The ZyCoV-D vaccine (Zydus Cadilla), was the first licensed DNA vaccine for use in humans against SARS-CoV-2 received licensing in November 2021 under emergency authorization in response to Covid-19 in India. Interim results of a phase III trial published on the efficacy, safety, and immunogenicity of ZyCoV-D found the vaccine's efficacy to be 66.6% after two 3 mg doses, with no significant differences in the numbers of adverse side effects between treatment and placebo groups (Khobragade *et al.*, 2022). In contrast, initial trial data for the novel mRNA vaccine BNT162b2 (Corminaty®, Pfizer/BioNTech) encapsulated in lipid nanoparticles (LNP) and delivered as two 30 µg doses reported an efficacy of 95% (Polack *et al.*, 2020), with later data reporting 91.3% overall efficacy but 96.7% efficacy against severe disease (Thomas *et al.*, 2021). Data from both of these trials showed a favourable safety profile for the mRNA-based BNT162b2, though it did suffer from a gradual decline in efficacy over time (Thomas *et al.*, 2021). In light of the decline, trialling of a third dose of BNT162b2 was carried out and reported a relative vaccine efficacy of 95.3% compared to a two-dose regimen (Moreira *et al.*, 2022).

Additionally, viral vector vaccines are another option for nucleic acid-based vaccines and also introduce nucleic acids to host cells for endogenous antigen expression with delivery via viral vectors such as adenoviruses. The ChAdOx1, or AZD1222, (AstraZeneca/Oxford University) COVID-19 vaccine was developed and approved for clinical trials in a very similar timeframe to BNT162b2. Initial trial data showed that two standard doses (5×10^{10} viral particles) resulted in 62.1% vaccine efficacy, whilst efficacy from a lower half dose followed by a standard dose was 90% giving an overall efficacy of 70.4% across both groups (Voysey *et al.*, 2021). Data published later from phase III trials with a two standard dose regimen reported vaccine efficacy to be up to 74% (Falsey *et al.*, 2021) with 92.1% efficacy against severe disease (Sobieszczyk *et al.*, 2022) and low incidences of serious adverse side effects.

1.2 Current Global Healthcare Challenges Which Warrant Innovative Research Approaches to Vaccine and Biotherapeutic Development

1.2.1 Dengue Fever

1.2.1.1 Dengue Virus: A Major Cause for Concern

One of the growing major public health threats worldwide with very few vaccine and drug candidates is caused by the mosquito-borne (arboreal) Dengue virus, or DENV (Nanaware *et al.*, 2021). Introduction of dengue virus through a mosquito bite (primarily *Aedes aegypti*) can result in a mild infection, or in more severe cases, potentially fatal Dengue haemorrhagic fever (DHF) and/or Dengue shock syndrome (DSS). Dengue virus is estimated to result in approximately 390 million cases and 22,000 deaths annually (Roy and Bhattacharjee, 2021; Bhatt *et al.*, 2013). The virus is now endemic to more than 100 countries in predominantly tropical and sub-tropical areas, the most-seriously affected located in in the Americas, South-East Asia and Western Pacific regions, with around 70% of the global burden present in Asia (WHO, 2023). The outlook for controlling dengue outbreaks in South-East Asia has further declined since the coronavirus pandemic which began in 2020. Increased dengue cases have been attributed to multiple factors stemming from the coronavirus pandemic including the redirection of resources for coronavirus mitigation strategies, socioeconomic disruption, interruption of vector control programs and overburdening of healthcare systems (Alied *et al.*, 2023). However, other strong contributing factors such as the intensification of global warming effects on tropical and subtropical climates and reports of insecticide resistance in dengue vectors (Alied *et al.*, 2023) combined with the lack of targeted medical intervention available for this virus suggest the building of a perfect storm for substantial Dengue outbreaks in this region.

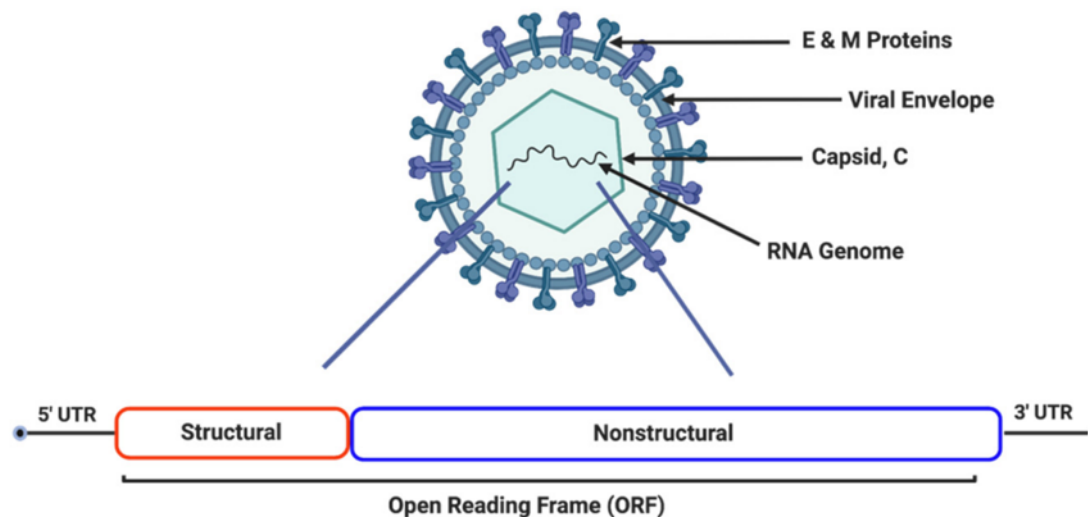


Figure 1.2: DENV structure and the genomic organisation of structural and non-structural proteins within an open-reading frame (ORF) flanked by a 5' untranslated region (UTR) and 3' UTR. Structural proteins on the mature virion include the envelope (E) and membrane (M) proteins (derived from pre-membrane (pre-M) protein) and the capsid forming capsid protein (C). (Obi, Gutiérrez-Barbosa et al. 2021)

Dengue virus is an enveloped single-stranded positive-sense RNA virus of the Flaviviridae family and has four antigenically distinct serotypes (DENV-1, -2, -3 and -4) (Roy and Bhattacharjee, 2021). The genome of this RNA virus is 11 kb long and includes an open reading frame (ORF) coding for 10 proteins flanked by a 5' untranslated region (UTR) and 3' UTR (Obi *et al.*, 2021). The ORF encodes a precursor polyprotein which is cleaved into 3 structural proteins (C (capsid), PrM (pre-membrane) and E (envelope)) and 7 non-structural proteins (NS1, NS2A, NS2B, NS3, NS4A, NS4B and NS5) (Obi *et al.*, 2021)(Fig. 1.2). The glycoprotein shell is formed of the E and prM proteins, of which the three discrete E protein domains (EDI, -II and -III) facilitate viral entry into host cells, whilst the PrM protein helps to prevent premature fusion and release of EDII's fusion loop during virus maturation (Shukla *et al.*, 2020).

1.2.1.2 Challenges in Dengue Vaccine & Biotherapeutic Development

During dengue infection, antibodies induced to recognise the structural proteins are often produced to combat and neutralize the initial infection. However, these same antibodies in any subsequent infection with a different dengue serotype will hinder the host's immune response and often leads to increased disease severity (Tsai *et al.*, 2015).

This is known as antibody-dependant enhancement (ADE) and is due to PrM- and fusion loop-targeting antibodies, induced during the initial dengue infection, facilitating binding of the new dengue serotype to monocytes and macrophages through Fc γ receptors and mediating entry of the virus into the cell and increased viral replication rather than neutralisation (Shukla *et al.*, 2020). Additionally, uptake of dengue into host cells via Fc γ receptors in ADE results in a ten-fold increase in comparison to entry of the virus through host-cell receptors (Halstead *et al.*, 2010), further contributing to the increased viral load and severity of infection in secondary infections.

Antibodies which demonstrate ADE through Fc γ receptor-mediated viral entry are most commonly elicited by the PrM protein (accounting for approximately 60% of antibody response (Dejnirattisai *et al.*, 2010)) and E protein fusion loop epitope (approximately 20-30% (Smith *et al.*, 2014)), have been reported to be highly cross-reactive and strong promoters of ADE (Shukla *et al.*, 2020). On-the-other-hand, antibodies which target serotype-specific, non-immunodominant epitopes, such as EDIII, show protection against dengue in a secondary heterotypic infection (Shukla *et al.*, 2020). Consideration of the intricacies in dengue ADE are therefore critical in the design of vaccine and immunotherapy drug candidates against the virus, to avoid worsening the severity of infections. One of the few vaccines developed against dengue and successfully licensed, tetravalent live-attenuated virus Dengvaxia[®] (Sanofi Pasteur), was the subject of great controversy when serious safety concerns were raised for children immunised with the vaccine in the Philippines. Data collected in a phase III trial, which included immunisation of 800,000 children, showed that individuals that had not been infected with dengue prior to immunisation had an increased risk of hospitalization from severe dengue when exposed to a subsequent natural infection (Torres-Flores, Reyes-Sandoval and Salazar, 2022). This outcome is thought to be the result of imbalanced immunogenicity in response to the tetravalent vaccine leading to ADE due to varied levels of antibodies to each serotype (Pintado Silva and Fernandez-Sesma, 2023) and highlights one of the major challenges in vaccine and biotherapeutic development for Dengue.

1.2.1.3 Current Approaches to Dengue mAb Development

Due to the difficulty in creating tetravalent vaccines which can confer immunogenicity to each serotype equally, it is critical to continue exploring potential biotherapeutics for treatment of dengue infections. One approach includes development of antibodies which are induced during infection but do not target the envelope or pre-membrane proteins, such as non-structural protein 1 (NS1), which do not contribute to ADE. However, although anti-NS1 antibodies show little involvement in ADE, they do exhibit cross-reactivity to host molecules and can mediate endothelial damage and platelet dysfunction (Sootichote *et al.*, 2023; Kowaboot *et al.*, 2022).

An alternative approach is to engineer Fc regions of antibodies which target the envelope proteins with the intention of reducing ADE activity whilst still retaining their neutralising power. This has been investigated using a human monoclonal IgG-1 anti-DENV envelope antibody which was engineered to have Fc regions of each of the other IgG subclasses (IgG-2, -3 or -4) and a N297A point mutation in the Fc region (Ramadhany *et al.*, 2015). This study found that the molecule which contained the IgG-1 Fc region with the N297A mutation showed decreased ADE activity without loss of neutralising power, compared to the wildtype antibody isolated from infected sera. Further investigation by this research group showed that another mAb which targets DENV-EDII with strong neutralising activity across all four dengue serotypes and ADE activity *in vitro* was able to retain its neutralising power after a point mutation (N297Q) to the Fc region (Injampa *et al.*, 2017). Supply of the Fc-mutated mAb in this study was generated via the creation of a stable-expressing CHO-K1 cell line and in light of its success in mouse models was reported as a potentially marketable platform for a future dengue biotherapeutic.

1.2.2 SARS-CoV-2

1.2.2.1 The COVID-19 Global Pandemic

On 31st December 2019, public health officials in Wuhan, China reported viral pneumonia-like outbreak in which a novel coronavirus (severe acute respiratory syndrome coronavirus 2, or SARS-CoV-2) was identified as the causative agent. Prior to this, several human coronaviruses were known and often implicated in mild upper respiratory tract infections and common colds with the exception of severe acute respiratory syndrome coronavirus (SARS-CoV) and Middle East respiratory syndrome coronavirus (MERS-CoV) strains, responsible for outbreaks with case-fatality rates of approximately 10 and 34% in 2002-03 and 2012-20, respectively (Yang and Rao, 2021).

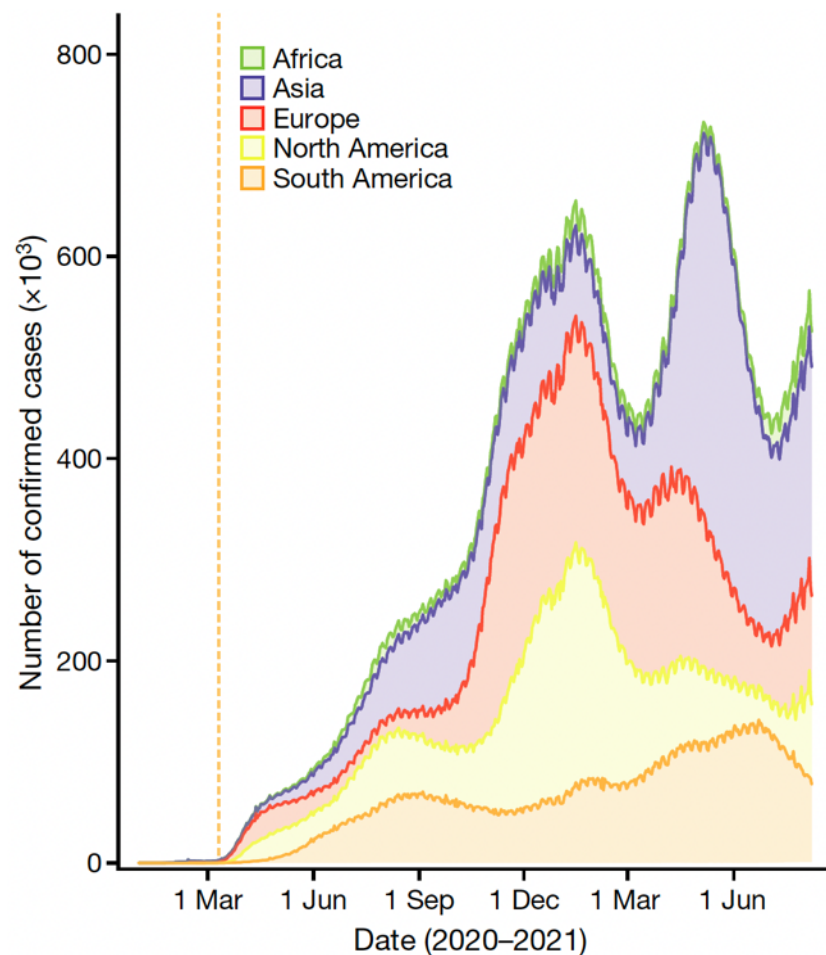


Figure 1.3: The spread of COVID-19 across continents illustrated by confirmed case numbers as seven-day rolling averages. The start date of the COVID-19 pandemic, 11th March 2020, is shown as an orange dashed line. (Li, Lai et al. 2021)

Outbreaks of SARS-CoV-2 infections, leading to a novel coronavirus disease eventually termed COVID-19, rapidly spread worldwide and an official global pandemic was declared by the World Health Organisation on 11th March 2020 (Hu et al., 2021).

Unfortunately, transmissions that occurred before the implementation of lockdowns in China in late-January 2020 meant that the virus had already begun to spread globally and new epicentres began forming across the globe (Li *et al.*, 2021)(Fig 1.3). By April 2020 global case numbers were reported as approximately 3 million with 200,000 deaths, which rose to over 25 million cases and 800,000 deaths by October 2020 (Salzberger *et al.*, 2021).

1.2.2.2 Structural Components and Potential Vaccine Targets of SARS-CoV-2

SARS-CoV-2 is an enveloped, positive-sense, single-stranded RNA virus which causes COVID-19. It's RNA viral genome is just under 30 kb with 14 ORFs which encode a total of 29 viral proteins, including 16 non-structural proteins and the four structural proteins: nucleocapsid (N), membrane (M), envelope (E) and spike (S) protein (Yang and Rao, 2021). The nucleocapsid protein is bound to the genome, whilst the other structural proteins form major components of the virion membrane, most notably the spike protein which gives the virus a crown-like appearance (Jackson *et al.*, 2022) (Fig 1.4)

During biosynthesis of SARS-CoV-2 virions within infected host-cells, spike protein is cleaved by furin from the Golgi apparatus into its two subunits, S1 and S2 (Jackson *et al.*, 2022). The spike protein exists as a trimer in a prefusion stable conformation until binding of the S1 subunit by a host cell receptor triggers the rearrangement into a post-fusion state. Fusion occurs when S1 binds via its receptor-binding domain (RBD) to host cell angiotensin converting enzyme 2 (ACE2) receptors, whilst S2 keeps the spike protein anchored to the viral membrane (Jackson *et al.*, 2022; Wrapp *et al.*, 2020). Due to its role in viral entry of SARS-CoV-2 into host cells and prominent display on the surface of the viral membrane, the spike protein was identified early in the pandemic as likely to be an ideal target for vaccines or antibody therapeutics (Wrapp *et al.*, 2020) and has been the therapeutic target for many since 2020.

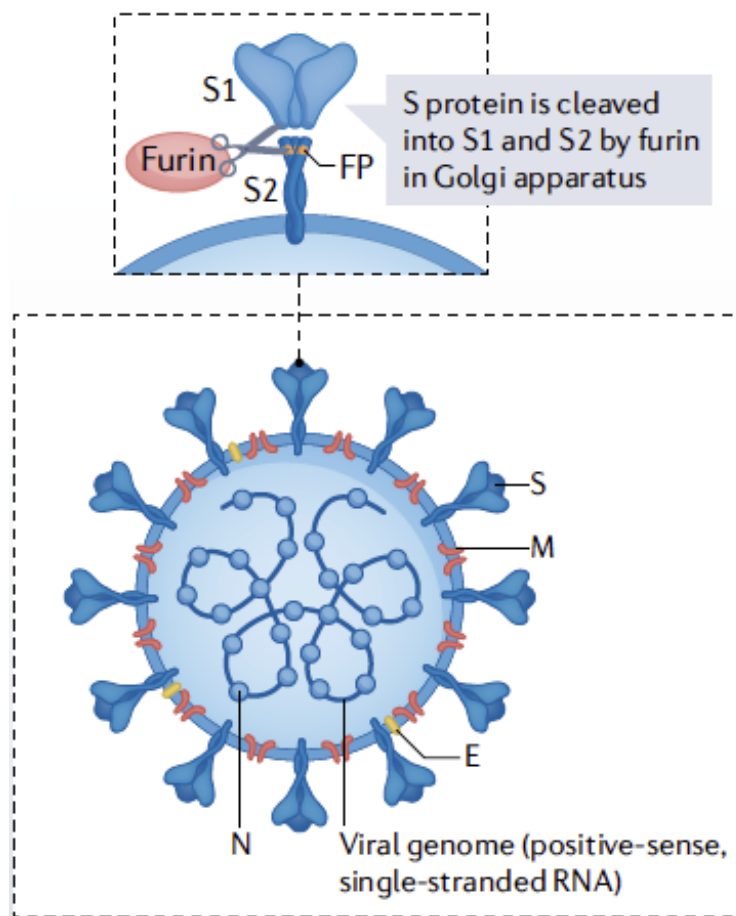


Figure 1.4: (Bottom) SARS-CoV-2 virion structure with the viral RNA genome and structural proteins (nucleocapsid (N), membrane(M), envelope (E) and spike (S)). (Top) S protein cleavage by furin from the host-cell Golgi apparatus results in two non-covalently associated S1 and S2 subunits on mature virions. (Jackson, Farzan et al. 2022)

Another target which is much more highly conserved than spike protein is the nucleocapsid which, due to its conserved sequence and abundance in infected cells, is an alternative vaccine target (Bai *et al.*, 2021). Sera from SARS-CoV and SARS-CoV-2 patients show high levels of IgG antibodies against nucleocapsid protein and it has also been reported to induce T-cell responses when used as the representative antigen in a vaccine for against the two infections (Bai *et al.*, 2021). An induced T-cell response is a highly desirable outcome in vaccine design as it can convey longevity of the vaccine's protection; patients who recovered from SARS-CoV in the 2003 outbreak have been shown to possess memory T-cells still reactive to nucleocapsid protein 17 years after infection (Bai *et al.*, 2021).

1.2.2.3 Strategies and Challenges to SARS-CoV-2 Vaccine Development

Since the initial outbreaks and declaration of global pandemic, several vaccines across various platforms have been rapidly developed, trialled and licensed for use (Table 1.1). Whilst a number of these were developed using well-established vaccine technologies, some of the great success stories of the pandemic have been born in the newer technologies, mRNA and viral vectors, which resulted in an unprecedented acceleration of vaccine development timelines.

Table 1.1: List of COVID-19 vaccines which have been validated for use by WHO, or Emergency Use Listing (EUL) status, as of January 2022 (WHO, 2022).

Vaccine	Type	Manufacturer	EUL Approval Date
BNT162b2/Comirnaty	mRNA	Pfizer/BioNTech	31 December 2020
ChAdOx1-S/COVISHIELD	Viral Vector	Oxford/AstraZeneca	16 February 2021
Ad26.COV 2.S	Viral Vector	Janssen/Johnson & Johnson	12 March 2021
mRNA-1273/SpikeVax	mRNA	Moderna	30 April 2021
BBIBP-CorV	Inactivated Virus	Sinopharm	7 May 2021
CoronaVac	Inactivated Virus	Sinovac	1 June 2021
BBV152 COVAXIN	Inactivated Virus	Bharat Biotech	3 November 2021
Covovax/NVX-CoV2373	Protein Subunit	Novavax	17 December 2021
Nuvaxovid/NVX-CoV2373	Protein Subunit	Novavax	20 December 2021

Part of the success of these technologies can be attributed to the current available speed and cost of DNA synthesis and sequencing which have improved exponentially since their introduction. Additionally, the purification and synthetic encapsulation of mRNA-based vaccines into lipid nanoparticles (LNPs) for delivery as therapeutics is relatively simple and easy to scale-up. However, the long-term efficacy of these synthetic platforms remains to be seen in terms of longevity in the immune protection provided

and any unforeseen side effects. For these reasons, more traditional biologically-derived vaccine platforms have also been used to develop COVID-19 vaccines, though due to time required for these platforms we are only now beginning to see the outcomes to compare them as they progress to the end of clinical trialling and receive licensing.

The rise and divergence of multiple variants of the virus added another challenge to tackling the spread of COVID-19. Most of the vaccines originally developed for the virus target the spike protein or its components from sequences published in early 2020 which results in an antibody response specific against those parts of the initial virus strain that began to spread. However, by the end of 2020 approximately 5,000 mutations to the S protein had been identified and reported across new strains of the virus, and noted variants of concern Alpha (B.1.1.7), Beta (B.1.351), Gamma (P.1), Delta (B.1.617.2) and Omicron (B.1.1.529) have arisen with additional mutations compared to the original virus sequence with each divergence. Mutations leading to the Delta variant resulted in increased infection rates due to increased efficiency in transmission, while Omicron has been shown to evade the immune system and as of January 2023 was known to contain 32 mutations in the spike protein compared to the original Wuhan sequence (Mahboob *et al.*, 2023). With each new variant and mutation to the spike protein, it becomes a less recognisable structure to the antibodies raised against the original strain and reduces the power of the vaccines protection. This sequence of events means it is likely new vaccines will need to be continuously designed and trialled to combat the virus as it evolves within populations still experiencing high infection rates.

1.3 Exosomes as Antigen-Display Vehicles

The following section is adapted from a review paper published during my PhD which explores the potential of using exosomes as a potential vaccine platform (Dyball and Smales, 2022).

1.3.1 Exosome Composition and Biogenesis

Many of the newest vaccine platforms rely on products with vesicle-based elements for delivery or structural purposes. Extracellular vesicles (EVs) are naturally occurring vesicles in mammalian species which are released from all cell types and can be divided into three major categories with varied sizes and functions: apoptotic bodies, microvesicles and exosomes. Apoptotic bodies are between 100 – 5000 nm in diameter and are released by cells which are undergoing apoptosis, whilst microvesicles are 100 – 1000 nm in diameter and are formed and released via exocytosis of the plasma membrane (Hessvik and Llorente, 2018). Exosomes are the smallest of the three commonly recognised subcategories of EVs, measuring between 50 – 150 nm in diameter, however there has recently been reports of a smaller type of EVs referred to as ‘exomeres’ (Zhang and Lyden, 2019; Zhang *et al.*, 2018) which are <50 nm in diameter, but are not yet recognised as a subcategory of EV nor are they well characterised.

Exosomes were first described in the literature as ‘plasma dust’ in 1967 (Wolf, 1967) and eventually observed as entities released via endocytic pathways under investigation in rat (Harding, Heuser and Stahl, 1983) and sheep (Pan and Johnstone, 1983) reticulocytes in 1983. In time, the vesicles were termed ‘exosomes’ by Rose Johnstone who became a pioneer in the field, though they initially remained largely overlooked or disregarded as impactful tools until recent years. It is now recognised that these vesicles play a large part in cell-cell communication and that their properties and functions make them ideal candidates for use as biomarker and drug-delivery vehicles as well as potential viral and cancer vaccines. The natural roles of these vesicles are extensive and present themselves throughout many key systemic functions including: angiogenesis, apoptosis,

antigen presentation, inflammation, receptor-mediated endocytosis, cell proliferation and differentiation, and cell-signalling (Gurunathan *et al.*, 2019).

Exosomes are composed of a single lipid bilayer capable of encapsulating proteins, lipids and nucleic acid molecules, often those associated with the cell-type origin of the exosome. Although origin cell-type heavily influences molecular composition and cargo of exosomes, they do have several protein markers which have been determined to be unique to exosome populations regardless of origin, including; tetraspanins (CD81, CD63, CD9); flotillin; cytosolic heat shock proteins (HSP70 & HSP90); Rab proteins (Rab5 & Rab7); annexins; TSG101 and major histocompatibility complexes (MHCs) (Jeppesen *et al.*, 2019; Kalluri and LeBleu, 2020; Kowal *et al.*, 2016; Mashouri *et al.*, 2019; Pegtel and Gould, 2019; van Niel, D'Angelo and Raposo, 2018). These marker proteins are often associated with mechanisms involved in generic exosome formation and release. There are a number of databases, ExoCarta (www.exocarta.org) (Mathivanan and Simpson, 2009), Vesiclepedia (www.microvesicles.org/) (Kalra *et al.*, 2012) and Exosome-RNA (<https://exosome-rna.com>) (Kim *et al.*, 2015) which catalogue marker proteins of exosome populations and subpopulations from various cell-type origins.

Exosome release from cells occurs when multivesicular bodies (MVBs), which gather intraluminal vesicles (ILVs) formed via endosomal budding, fuse with the plasma membrane and introduce these ILVs to the extracellular space, after which they become known as exosomes (Dreyer and Baur, 2016) (Fig 1.5). The formation of ILVs, destined to later be released as exosomes, can occur through multiple pathways: the ESCRT pathway; the ceramide pathway or the syndecan-syntenin-ALIX pathway.

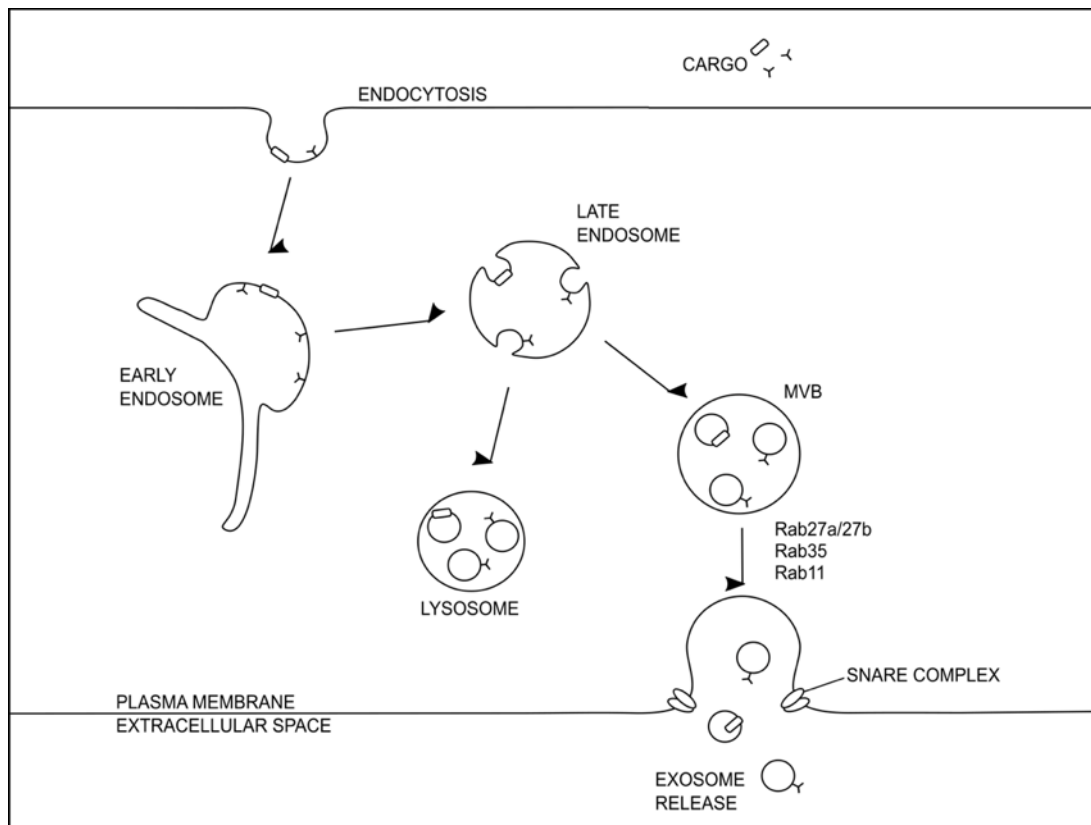


Figure 1.5: Schematic depicting exosome formation and release from cells. Cargo taken in by endocytosis is sorted at early endosomes which is then packaged into either lysosomes for degradation, or multivesicular bodies (MVB) containing intraluminal vesicles (ILV) formed by budding of late endosomal membranes. ILVs are then released as exosomes into the extracellular space when MVBs fuse with the plasma membrane. (Dyball and Smales 2022)

1.3.1.1 The ESCRT Pathway

The ESCRT-dependant formation of exosomes is executed first using the endosomal sorting complexes for transport (ESCRT) machinery, assembled from four protein complexes (ESCRT-0, -I, -II and -III), which facilitate inward budding of endosomal membranes. In late endosomes, ESCRT-0 clusters ubiquitylated cargoes after which ESCRT-I and -II enable membrane budding at the site of clustered ubiquitylated cargoes followed by ESCRT-III initiating membrane scission to complete the process and form ILV-containing MVBs (Hurley and Hanson, 2010) (Fig 1.6). This vesicle formation falls into a pathway which can then traffic the original ubiquitylated cargo either to lysosomes for degradation or to the plasma membrane for release to extracellular space as exosomes. In the case of exosomal release, MVB trafficking to the plasma membrane is achieved via microtubules by Rab GTPases, after which SNARE (soluble N-

ethylmaleimide-sensitive fusion attachment protein receptor) complexes mediate the fusion of MVBs with the plasma membrane (Mathieu *et al.*, 2019) (Fig 1.5).

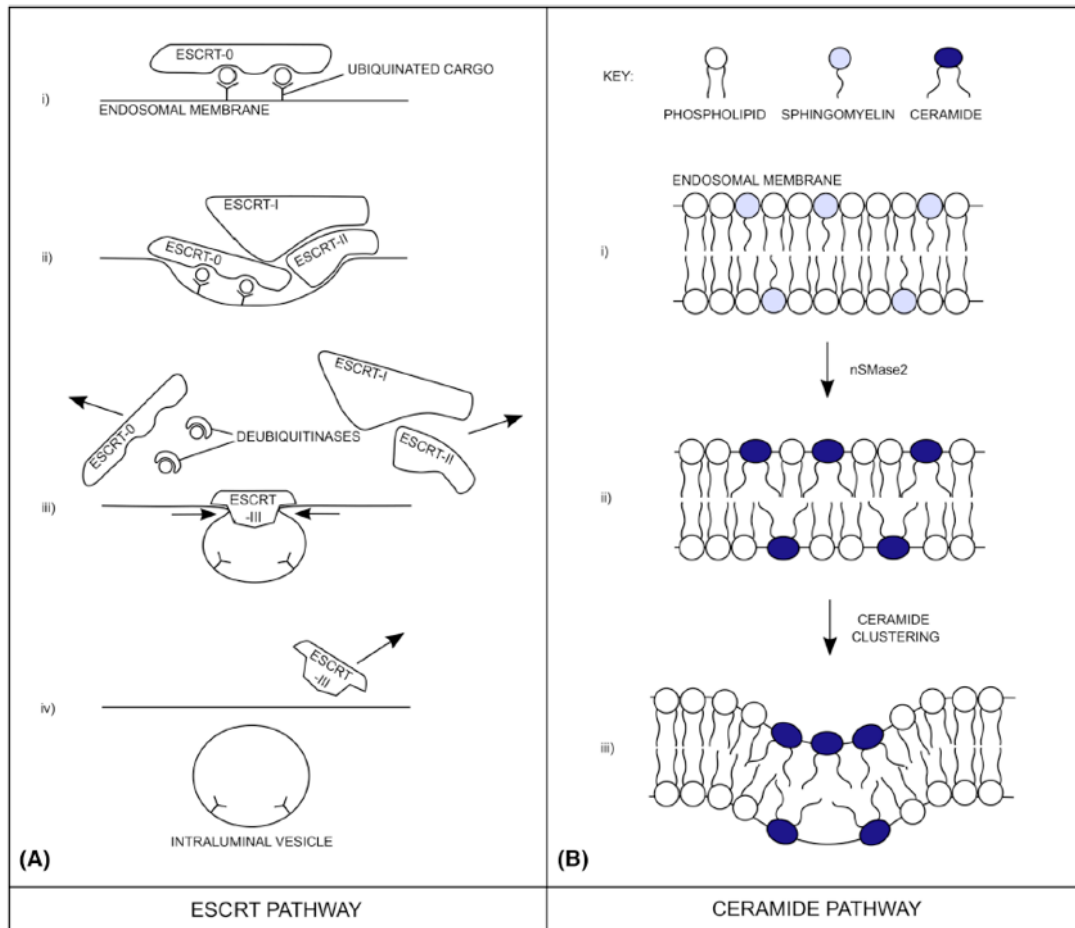


Figure 1.6: Vesicle formation via the ESCRT Pathway in which ubiquitinated proteins at the endosomal membrane are recognized by ESCRT-0 (i), which then binds with ESCRT-I and -II to begin invagination of the endosomal membrane (ii). This process results in the budding of the endosomal membrane, encapsulating the ubiquitinated cargo which is then deubiquitinated (iii), and the vesicle is formed when the membrane opening of the developing bud is fused by ESCRT-III (iv). (B) Endosomal membrane budding for vesicle formation via the Ceramide Pathway in which conversion of sphingomyelin (i) to ceramide within the membrane by nSMase2 (ii) results in clustering of ceramide to create the curvature of the membrane (iii) due to its more branched, unsaturated fatty acid tail structures. (Dyball and Smales 2022)

1.3.1.2 The Ceramide Pathway

Formation of MVBs is also possible independently of ESCRT machinery, through the curvature of membranes via a lipid modifying enzyme, nSMase2 (a type II sphingomyelinase), which converts sphingomyelin to ceramide (Trajkovic *et al.*, 2008). The resulting clustered ceramides produced in sphingolipid-rich membrane lipid

microdomains generates 'lipid rafts' which trigger invagination and budding of the membranes to form vesicles (Skryabin *et al.*, 2020) (Fig 1.6).

1.3.1.3 The Syndecan-Syntenin-ALIX Pathway

Another pathway by which MVB formation can occur is via the adaptation of endosomal membrane for ESCRT budding machinery via tripartite syndecan-syntenin-ALIX complexes (Baietti *et al.*, 2012; Fares, Kashyap and Zimmermann, 2017). Transmembrane syndecans, a major group of cell surface heparan sulphate proteoglycans (HSPGs) prominent in cell surface signalling, bind molecules via their heparan sulphate (HS) chains (Park, 2018) leading to syndecan clustering and the formation of assemblies that can recruit syntenin-1 and ALIX for membrane budding (Roucourt *et al.*, 2015). Syntenin-1, a cytosolic factor, contains two PDZ domains which facilitate the recruitment of syntenin to membranes due to their high affinity for syndecans, whilst the N-terminal interacts with ALIX, or PDCD6IP, completing the complex and creating a site for interaction for ESCRT protein TSG101 and CHMP4 via the three LYPX(n)L motifs present on ALIX (Baietti *et al.*, 2012).

The tetraspanin CD63 is also capable of binding with the PDZ domains of syntenin and is often found to co-accumulate with syntenin and ALIX in exosomes grouped as CD63⁺ subpopulations, which seem to bypass lysozyme degradation (Baietti *et al.*, 2012). CD63, along with other tetraspanins (CD9 and CD81), are commonly included in proteomic profiles of exosome biomarkers and can be found in tetraspanin-enriched microdomains which have been speculated to operate as 'specialised cargo platforms' which could direct components to exosomes (Perez-Hernandez *et al.*, 2013).

1.3.2 Exosomes: Cellular Messengers and Mediators

1.3.2.1 The Role of Exosomes in Immunity

Exosomes can be thought of as ‘messengers’ in cell-cell communication, they are known to carry cargo between cells and are capable of triggering direct immune responses via antigen presentation to immune cells (Agarwal *et al.*, 2014; Wolfers *et al.*, 2001; They, Ostrowski and Segura, 2009; Shenoda and Ajit, 2016; Wang *et al.*, 2018; Montecalvo *et al.*, 2008) or delivering nucleic acid molecules, including DNA (Takahashi *et al.*, 2017), mRNA (Valadi *et al.*, 2007), microRNAs (Valadi *et al.*, 2007; Fernandez-Messina *et al.*, 2020; Montecalvo *et al.*, 2012; Pegtel *et al.*, 2010; Santos *et al.*, 2018; Zheng, Zhou and Wang, 2020) and long non-coding RNAs (Conigliaro *et al.*, 2015; Kang *et al.*, 2018), via the internalisation of exosomes by endocytosis into recipient cells. Harvested, naturally-occurring exosomes and engineered exosomes have been investigated for delivery of specific microRNAs (Li *et al.*, 2018; Shimbo *et al.*, 2014), siRNAs (Lasser, 2015; Seyfizadeh *et al.*, 2019) and antigens (Bliss *et al.*, 2020; Anticoli *et al.*, 2018; Ferrantelli *et al.*, 2018; Kuate *et al.*, 2007) to specific targets in attempts to harness this natural ‘shuttling’ ability, with work also ongoing for their potential use as drug delivery nanoshuttles (Hong *et al.*, 2018).

During infection, these capabilities allow exosomes to take on roles as mediators and messengers for the immune system by carrying pathogen-associated molecular patterns (PAMPs), unprocessed antigens and even displaying antigens on the exosomal membrane via MHCs when released from infected cells (Shenoda and Ajit, 2016; Chaput and They, 2011; Rodrigues *et al.*, 2018). Other cells are able to receive these immunogenic exosomes via cell adhesion at the cell surface through specific receptors, or by internalisation into recipient cell endocytic compartments (Chaput and They, 2011).

Exosomes released from infected cells bearing PAMPs are able to be recognised by toll-like receptors (TLRs) and thus can trigger innate immune responses when circulated, increasing the likeliness of immune detection of a pathogen. Simultaneously, infected cells can also release exosomes carrying antigens which are able to induce CD4⁺ and

CD8⁺ T cell responses via both direct or cross-presentation. Direct exosome-mediated antigen presentation sees the exosomes present an antigen MHC-peptide complex to specific T cells, whilst in cross-presentation exosomes transfer an antigen to antigen presenting cells (APCs) which, in turn, process and load the antigen onto their own MHCs

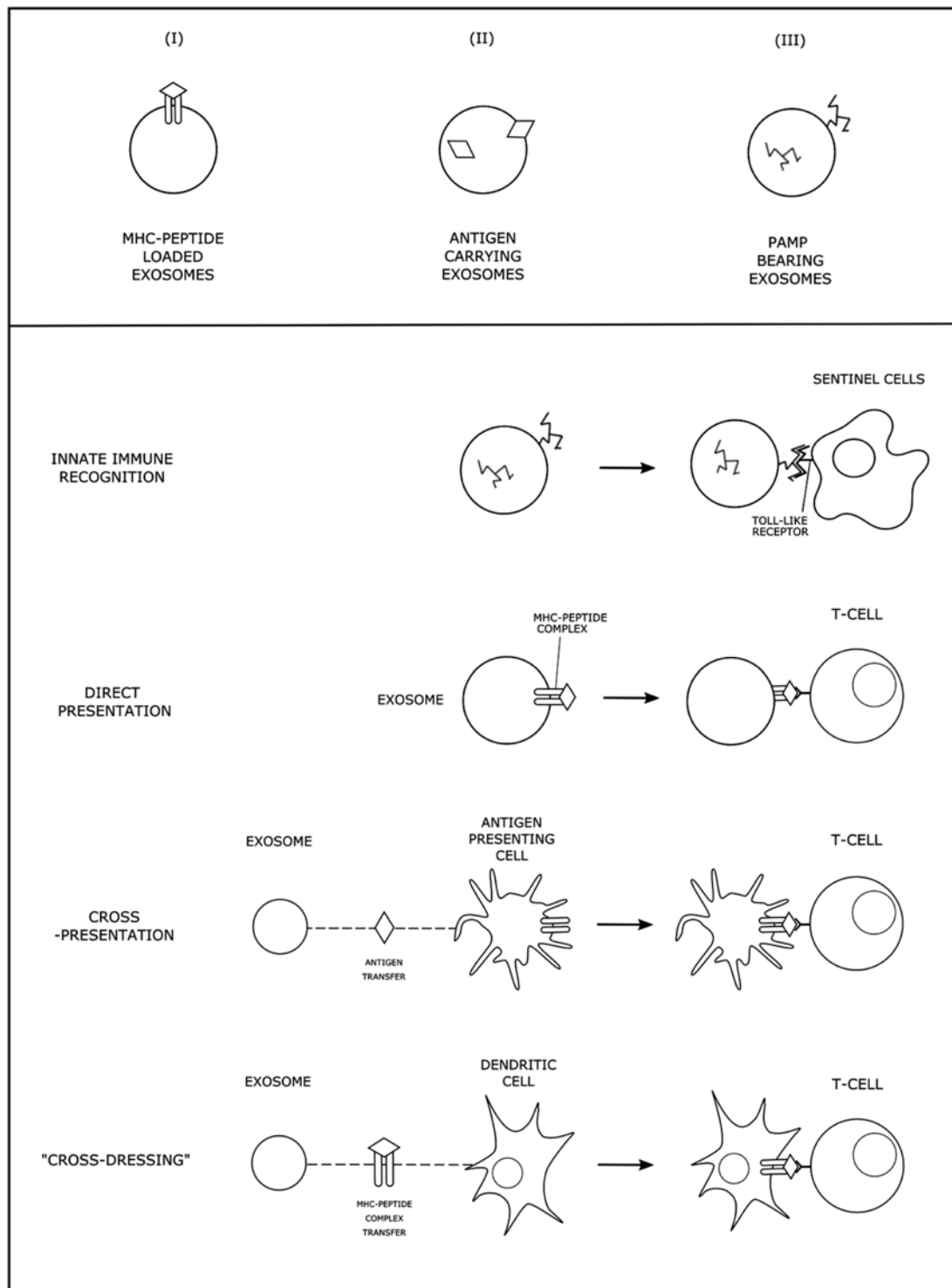


Figure 1.7: Variations on the types of exosome-cargo loading (I-III) and their possible presentation strategies to the respective immune cells, dependent on cargo type, to illicit immune responses. (Dyball and Smales, 2022)

for display (Shenoda and Ajit, 2016) (Fig 1.7). Another indirect method of exosome-mediated antigen presentation is known as 'cross-dressing', in which exosomes released from infected cells transfer antigenic MHC-peptide complexes specifically onto dendritic cells which then present the complex to T cells (Greening *et al.*, 2015a) (Fig 1.7). Exosomes derived from DCs, known as 'Dexosomes' (Dex), exploit this method of presentation by transferring antigenic MHC-peptides complexes onto naïve DCs in order to promote immune responses and have been trialled as an immunotherapy to treat cancers (Escudier *et al.*, 2005; Morse *et al.*, 2005; Zitvogel *et al.*, 1998).

1.3.2.2 Patient-Derived Exosomes as Inoculants

In addition to immunotherapy for cancer, exosomes have also sparked interest as a novel vaccine platform with studies carried out to explore the possibility of using exosomes harvested from the sera of infected patients as inoculants against viral (Anticoli *et al.*, 2018; Kuate *et al.*, 2007; Montaner-Tarbes *et al.*, 2016; Admyre *et al.*, 2006; Walker, Maier and Pober, 2009; Wang *et al.*, 2019; Di Bonito *et al.*, 2017), bacterial (Cheng and Schorey, 2013; Giri and Schorey, 2008) and parasitic (Li *et al.*, 2018) pathogens. The serum-derived exosomes in these studies were found to be capable of generating T cell responses in naïve hosts and the results were promising for the concept of developing an exosome-based vaccine platform which could confer immunity that is safer than traditional vaccine platforms but without the need for adjuvants or boosters that are routine in second generation vaccines.

However, these naturally produced exosomes would likely be unable to immunise against infections caused by enveloped viruses. Part of the replicative method for enveloped viral pathogens is to hijack host cell machinery, including pathways utilised in exosome biogenesis, in order to package and release new viral particles (Gould, Booth and Hildreth, 2003; Nguyen *et al.*, 2003). This hijacking of the exosome biogenesis pathways results in the production and release of exosomes that contain both PAMPs and host factors, allowing for immune evasion while simultaneously providing pathogen docking receptors and increasing infectivity (Rodrigues *et al.*, 2018). Consequently, the use of serum-derived exosomes may be unfavourable for enveloped viral infections or

any pathogen with similar complexities, instead genetically engineered exosomes with specific antigen display designs could be the best choice for an exosome-based vaccine strategy. Genetically engineered exosome cell lines would also be favourable in terms of manufacturing and regulation as they would allow more stable and controlled populations, with no pathogenic origins, to be produced for licensing and use in human vaccines.

1.3.2.3 Engineered Exosomes Expressed via Cell Culture and Isolation

Methods for engineering exosomes for carrying specific proteins have been investigated via expression, in controlled cell lines, of genetic constructs designed to influence the biogenesis and release of exosomes which can then be harvested for analysis. There are several strategies for exosome targeting constructs; an early strategy involved the exploitation of the C1C2 domain of lactadherin which mediates binding to lipid surfaces and exosomal-associated lactadherin secretion (Delcayre *et al.*, 2005). The replacement of the EGF-like domain of lactadherin with proteins of interest, tumour-associated antigens (TAA) CEA and HER2, resulted in the production of exosomes displaying these TAAs which were shown to improve antigen-specific immune responses and enhance anti-tumour therapeutic responses in mouse models (Delcayre *et al.*, 2005).

Another strategy investigated involved the re-appropriation of enveloped virus proteins involved in hijacking exosome biogenesis pathways for host-cell mediated viral replication, in order to create a type of exosome-targeted signal sequence. One such effort used a HIV protein, Nef, which when fused with an antigen of interest was then incorporated into exosomes in cells expressing the Nef^{mut} gene (Lattanzi and Federico, 2012). The Nef^{mut}-exosomes were compared to lentiviral Nef^{mut} VLPs carrying the same antigens and found to be capable of very similar levels of cross-presentation to immune cells (Lattanzi and Federico, 2012). Enveloped viral protein fusions as exosome-targeting signal sequences have also been tested by replacing transmembrane and cytosolic domains of the vesicular stomatitis virus (VSV) G protein, with the spike (S) protein of severe acute respiratory syndrome-associated coronavirus (SARS-CoV) (Kuate *et al.*, 2007) after SARS outbreaks in the early 2000's. However, despite the successful

generation of SARS-S⁺ exosome populations, murine models were found to only produce neutralising antibody titres exceeding those in convalescent sera of SARS patients when boosted with an adenoviral SARS-S viral vector vaccine (Kuate *et al.*, 2007), though this could be due to the tumour challenge-style testing model used to avoid direct work with the near-deadly virus.

Use of genetic material that has even partial origins in pathogenic organisms or therapies designed for use in humans is still undesirable, though the results do support the premise of exosome-based products for raising immunity to specific infectious agents. For this reason, a strategy that employs the natural cell machinery for targeting of proteins of interest into exosomes would be much more favourable. The ubiquitination of cargos for vesicle trafficking and lysosomal degradation pathways which link closely to exosome biogenesis pathways (Cheng and Schorey, 2016) is one such approach (Fig 1.8) that has been investigated for targeting proteins of interest for display on exosomes (Cheng and Schorey, 2013; Cheng and Schorey, 2016).

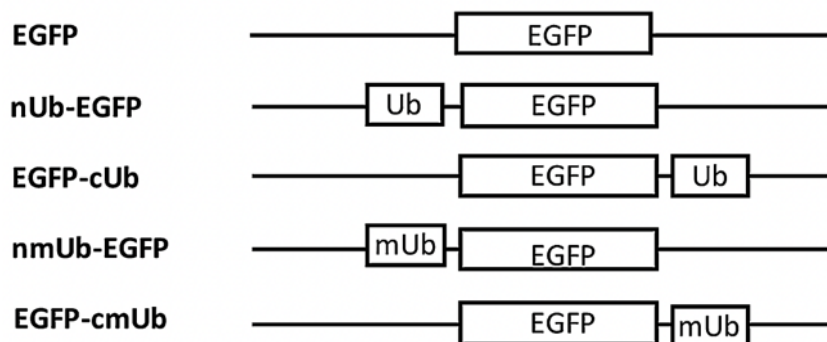


Figure 1.8: Ubiquitin-tagging gene constructs employed using eGFP as a fluorescent reporter to test if fusion with ubiquitin (Ub) /modified ubiquitin(mUb) results in trafficking to exosomes in HEK293 cells. (Cheng and Schorey 2016)

The expression of genetic fusions of ubiquitin with various proteins of interest (eGFP; HER2; *M. tuberculosis* antigens Ag85B and ESAT6) in human embryonic kidney 293 (HEK293) cell lines has shown to successfully result in the generation of exosomes containing the respective proteins of interest from each fusion (Cheng and Schorey, 2013). Furthermore, the Ag85B-ESAT6⁺ exosome populations were found to have a 10-

fold increase in Ag85B-ESAT6 concentrations compared to controls and their use in mouse models produced a direct correlation with the number of Ag85B- and ESAT6-specific INF- γ -secreting T lymphocytes observed (Cheng and Schorey, 2013).

Another strategy for directing proteins of interest into exosomes for surface display utilises tetraspanins, transmembrane proteins which are present on exosomal membranes and offer an anchor point for both internal and/or external display when fused with proteins of interest at the internal and/or external transmembrane loop domains (Stickney *et al.*, 2016) (Fig 1.9). This approach has shown some preliminary success with trimeric fusion proteins of CD9, CD63 and CD81 using fluorescent reporter genes GFP and RFP to demonstrate the potential for a simple exosome surface display technology. However, this approach has not been further explored to test the size limitations or efficacy using antigens for presentation to immune cells (Stickney *et al.*, 2016).

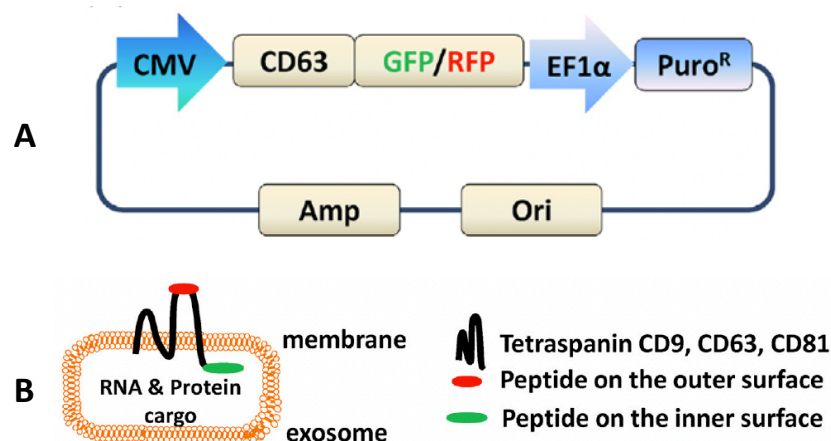


Figure 1.34: (A) The mammalian expression vector used to express CD63-GFP fusion proteins and its configuration within the plasmid. (B) Schematic of engineered exosomes for surface display of proteins of interest via fusion with tetraspanin proteins. Proteins can be fused at the extracellular transmembrane loop domain for external display (red oval, RFP), while those at the C-terminus are found on the inner surface (green oval, GFP). (Stickney, Losacco *et al.* 2016).

1.4 Exploring mAb Production and Development to Improve the Diversity and Availability of mAb Biotherapeutics

1.4.1 The Current Global Market

Whilst advancement of vaccine design and manufacturing allows for an improved proactive approach in tackling global health challenges, the same advancement in therapeutics such as biologics is also vital to allow reactive approaches to these challenges in cases where vaccines are unavailable, or to complement these. Biologics, drugs produced, synthesised or extracted from a biological source, currently financially dominate a huge portion of global pharmaceuticals; in 2018 the therapeutic monoclonal antibody market was valued at approximately \$115.2 billion USD globally and projected to reach \$300 billion USD by 2025 (Lu *et al.*, 2020).

1.4.2 Antibody Discovery and Hybridoma Technology

Novel antibody discovery has traditionally been achieved through hybridoma technology (Köhler and Milstein, 1975) in which antibody-producing B cells, which are usually short-lived, are fused with an immortalised myeloma cell line to produce hybridoma cells capable of continuous antibody production. In a natural infection, B cells of different lineages create pools of antibodies which bind to different epitopes of an antigen and are known as polyclonal antibodies. However, hybridoma technology allows for a cell line derived from a single B cell and therefore the production of monoclonal antibodies with a uniform specificity (Parray *et al.*, 2020). To initially trigger the expression of antibodies specific to antigens of interest, antigens are injected into mice of which the B cells are then collected, or alternatively B cells of those who have been immunised, infected or suffering from cancer are collected. These cells and the resulting antibody pools are then assessed to select high producers for immortalisation to start a monoclonal lineage for monoclonal antibody (mAb) production. Due to these mAbs originating in a non-human model, they have a higher immunogenicity when applied as therapeutics in humans. However, several methods exist for producing

humanized mAbs including CDR grafting (Jones *et al.*, 1986), phage display (Smith, 1985) and production of humanized mAbs in transgenic mice (Lonberg *et al.*, 1994).

1.4.3 Antibody Structure and Immunology

The five different classes of antibodies, or immunoglobulins are IgA, IgD, IgE, IgG and IgM, designated as such to correspond with their respective α -, δ -, ϵ -, γ - and μ -type heavy chains. Each of these classes have varied functions, structures and abundances and of them IgG is both the most abundant in the both the body and the biologics market. IgG's are composed of two identical heavy chains and two identical light chains which are bound together in a Y-shaped formation or some variation of this formation for each subclass (IgG1, IgG2, IgG3 and IgG4) which all utilize varied numbers of disulphide bonds to bind the chains together as well as a hinge. The light chains, which can be λ - or κ -type, together with the top half of the heavy chains form the antigen-

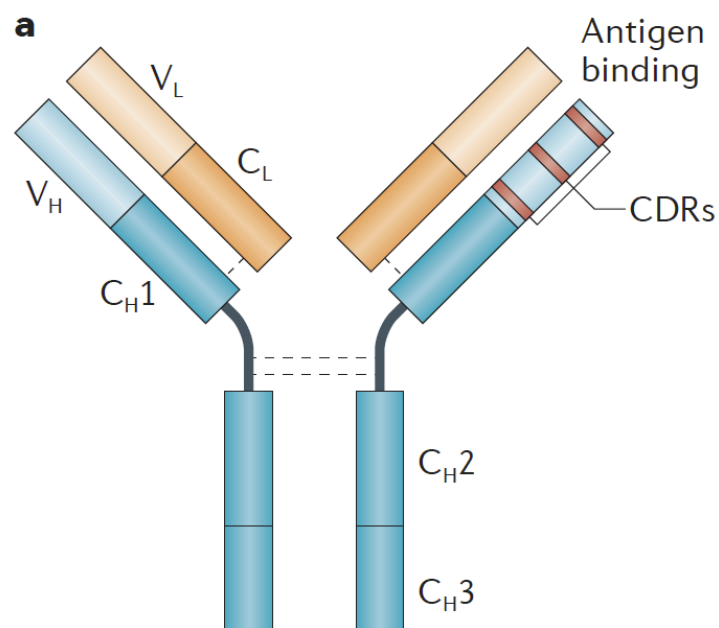


Figure 1.10: Schematic of the IgG antibody structure. Complementarity-determining regions (CDRs) are located in the variable heavy (V_H) and variable light (V_L) chains on each arm of the structure, together with the constant heavy chain-1 (C_H1) region they are referred to as a Fab (fragment antibody binding) region. The lower domains of the heavy chains, C_H2 and C_H3, form the Fc (fragment crystallizable) region (Lerner 2016).

binding (Fab) region which allows the molecules to bind to specific target antigens. The lower half of the heavy chains, located below the hinge region, forms the crystallizable

fragment (Fc) region which interacts with effector molecule receptors (Fig 1.10) (Lerner, 2016).

The N-terminal regions of both the heavy and light chains form a variable region, which includes a combination of framework regions (FR1, FR2, FR3 and FR4) interspaced with hypervariable complementary determining regions (CDR1, CDR2 and CDR3) capable of providing an immensely diverse library of sequences across these molecules. This ability to create vastly diverse populations of antibodies in response to infection allows the body to mount a defence against almost any foreign bodies encountered in an infection.

1.4.4 CHO Cells as a Platform for Optimised Monoclonal Antibody Production

Chinese hamster ovary (CHO) cells are the preferred system for the production of monoclonal antibodies due to their ability to convey post-translational modifications, folding and cleavage to produce biologics with low immunogenicity and high biological activity (Zhang *et al.*, 2022). They are also able to be cultured in suspension, serum-free, and combined with modern downstream technologies to allow for substantial scale-up and commercialised manufacture of biologics with titres of up to 10 g/L reported (Marichal-Gallardo and Alvarez, 2012). However, the investment required for such large-scale manufacturing puts a high cost on mAb therapies; exploration into enhanced, novel and cost-effective strategies for the engineering of CHO cell lines and the mAbs they produce is paramount for the field of bioprocessing. Elucidation of enhanced mAb production can be approached with several different or often combined strategies, including: expression vector engineering; host cell line engineering; antibody gene sequence optimization; and advanced bioprocessing techniques for high throughput screening (Zhang *et al.*, 2022; Priola *et al.*, 2016).

1.4.4.1 Vector Engineering Strategies

To deliver the sequences of biotherapeutics for expression in a cell, they are usually encoded and delivered by plasmids, or vectors. Vectors are generally comprised of

multiple sequences, in addition to the desired expression sequences, which play a role in either controlling expression of the recombinant protein(s), as selection markers, or in the replication of the vector itself. These can include gene promoters and terminators, signal peptides, metabolic or antibiotic selection markers, ribosomal binding sites, polyadenylation sites and an origin of replication.

Signal peptides (SPs) are short peptides present at the N-terminus of secretory proteins, capable of directing the protein to the ER and the secretory pathway (Owji *et al.*, 2018). Multiple studies have shown that using specific SPs for mAb expression results in better yields (You *et al.*, 2018; Peng *et al.*, 2016; Nagano and Masuda, 2014; Attallah *et al.*, 2017; Ramezani *et al.*, 2017; Gibson *et al.*, 2017; Haryadi *et al.*, 2015; Kober, Zehe and Bode, 2013) but natural antibody producing cells contain varied repertoires of SPs (Ling *et al.*, 2020). Studies examining optimisation of mAb production with different SPs have shown that each light- and heavy-chain of each mAb may require optimised SPs for obtaining the highest yields (Haryadi *et al.*, 2015; Kober, Zehe and Bode, 2013). The use of specific light- and heavy chain-specific SP sequences in CHO mAb-expression systems have been successfully employed to increase yields of 5 best-selling biosimilars (Haryadi *et al.*, 2015). Furthermore, tailoring different SPs to the chains of each biosimilars in this study showed that expression is variable depending on the SPs used and reinforces the evidence and need for SP optimisation for antibodies independently.

Further approaches for improving vector design for mAb production include codon-optimisation of the open reading frame sequences and inclusion of untranslated regions (UTRs) which have been shown to increase mAb yields in a CHO-based expression system by a further 50% in addition to improved signal peptides (You *et al.*, 2018). Vector design approaches can also include exploring different selection systems. Typically, in CHO cell expression systems for biotherapeutic production selection is mediated through metabolic control such as glutamine synthetase (GS) or dihydrofolate reductase (DHFR) selection markers. However, it has been shown that other selection systems can work in CHO cell lines such as pyroline-5-carboxylase synthetase (P5CS) for selection using proline-containing media as well as in conjunction with the classic GS selection for production of mAbs (Budge *et al.*, 2021).

Control of the HC:LC expression ratio is another consideration critical for mAbs expression and quality that can be controlled through expression vector design. Co-transfection of two vectors each containing HC or LC in different amounts during transfection can allow for controlled ratios in transient expression experiments (Zhang *et al.*, 2022). However, transfection of a single vector expressing both HC and LC controlled with different promoters and polyadenylation sites can give better control in stable transfections and triscistronic expression vectors designed to contain either internal ribosomal entry site (IRES) or furin-2A peptides to connect the LC, HC and selection genes are able to control HC:LC expression ratios with reduced transcription interference that can occur in single expression vectors for HC and LC (Zhang *et al.*, 2022). This control is desirable as excess light chain expression relative to heavy chain is favoured for both the expression and quality of antibodies (Ho *et al.*, 2013).

Expression of antibody chain sequences in CHO cell systems is routinely driven by strong viral promoters, such as cytomegalovirus (CMV) or simian virus 40 (SV40). However, these can be susceptible to epigenetic silencing and lack of regulatory control that has led to development of endogenous, inducible and synthetic promoters for regulated expression of recombinant proteins in CHO cells (Romanova and Noll, 2018). Endogenous promoters can better respond to the cellular state when used for gene expression, achieving lower cellular stress and greater stability in comparison to uncontrolled constitutive viral promoters (Nguyen *et al.*, 2019). Several cold-inducible promoter sequences have been identified allowing enhanced promoter activity after a temperature shift (Nguyen *et al.*, 2020) and provide another option for driving gene expression with a lower impact on cellular stress. Alternatively, synthetic promoters offer an approach for fine tuning expression of multi-gene vectors towards desired stoichiometries, though transcriptional activity using such promoters can deviate from the predicted outcomes (Patel *et al.*, 2021).

1.4.4.2 Cell Line Engineering Strategies

Genetic manipulation of the cells themselves provides another approach for improving recombinant protein titre. Due to the role that lipid metabolism plays in cellular processes which control the biosynthesis of recombinant proteins, lipid metabolism modifying (LMM) genes are a strong candidate for cell engineering to enhance the output of protein biosynthesis machinery. Overexpression of sterol regulatory element binding factor 1 (SREBF1), a global transcriptional activator of lipid biosynthesis genes, and stearoyl CoA desaturase (SCD1), in CHO cells expressing model secretory biotherapeutics has been shown to increase yields 1.5 – 9-fold (Budge *et al.*, 2020).

Another approach to CHO cell line engineering for enhanced expression of biotherapeutics utilise elements known to regulate secretion in antibody-producing plasma cells which have naturally evolved to have a high secretion capacity. One of the regulators identified, transcription factor BLIMP1/prdm1, was overexpressed in CHO cell lines resulting in an increase in recombinant IgG titres greater than 2-fold and cell-specific productivity greater than 3-fold. This was attributed to an increased endoplasmic reticulum size leading to enhanced protein synthesis and secretion capacity of the engineered CHO cell line (Torres and Dickson, 2021). Another group successfully overexpressed oncogenic PTEN (phosphatase and tensin homologue) C124S or G129E mutants, associated with cell growth, apoptosis and proliferation, in CHO cells that resulted in an increase in cell growth, culture viability and antibody titre in both transient and stable IgG-expressing CHO lines (Zhou *et al.*, 2021).

Conversely, inhibition via CRISPR-Cas9 gene editing of another gene involved in cell growth, CYLD lysine 63 deubiquitinase, in stable IgG-expressing CHO cells resulted in a 50% increase in antibody titre (Lu *et al.*, 2018). Whilst CRISPR-Cas9 mediated knockout of miR-744, a non-coding microRNA highlighted in high throughput miRNA screening as another influencer of cell proliferation and apoptosis, also resulted in a significant increase in antibody titres compared to controls (Raab *et al.*, 2019). These very different approaches, which each contribute to enhancement of antibody production, highlight the complexity of the landscape for cell line engineering which remains to be fully explored with the constantly improving genomic, transcriptomic and metabolic data for CHO cell lines.

1.4.4.3 Antibody Gene Sequence Optimization

Engineering of antibody sequences to create biotherapeutics that are easier to express in CHO cells or with reduced aggregation is a further strategy taken to enhance yields. Such developments have been made in the past to engineer humanised antibodies, and continue for individual antibodies to try and ensure these are ‘expressable’ whilst maintaining the specificity and activity of the individual antibody. This is undertaken alongside process development, new host cell identification and engineering of the host and/or expression system which are more universal approaches to enhancing recombinant protein expression. Thus, it is possible to examine antibody sequence and structure and undertake changes to particular regions which make a particular antibody difficult to express. This can be achieved using *in silico* screening to identify aggregation prone regions (APRs), which can contribute to the thermodynamic stability of an antibody, and designing variants which have sequence alteration to mitigate the effects and yield an increase in expression titres (van der Kant *et al.*, 2017). The combination of this approach with additional *in silico* techniques to identify potential post-translational modification (PTM) motifs that can be eliminated without impact to binding affinity or efficacy has also been shown to generate mAbs with reduced aggregation, increased stability and improved yields (Chae *et al.*, 2021). Additionally, alteration of the APRs as well as fine-tuning the electrostatically charged surface patches in the variable regions has been reported to reduce the viscosity of mAbs at high concentrations which can impede their development as a subcutaneously delivered therapeutic (Nichols *et al.*, 2015).

Protein engineering for improved expression and secretion is not restricted to mAbs either. For example, a computational analysis of two secreted proteins, TIMP-2 and TIMP-3, which share close sequence similarity but had very different expression levels in CHO cells allowed for the identification of regions which were responsible for the low expression of TIMP-3 compared to TIMP-2. Creation of a chimeric sequence, in which the identified problematic region of TIMP-3 was replaced with the corresponding sequence in TIMP-2, resulted in significant enhanced secretion of the chimera in a fully

glycosylated form compare to controls (Hussain *et al.*, 2018). The successful swapping or manipulation of sequences in antibody proteins could also provide solutions to high-value antibodies which suffer similar secretory bottlenecks.

1.4.4.4 Advanced Bioprocessing Techniques

In order to screen, select and scale-up high-titre antibody-producing cell lines of interest, high throughput methods are often employed to maximise process development at a lower cost. Initially clones can be produced and screened through limiting dilution methods and antibiotic or metabolic selection, but automation can increase throughput, through using approaches such as fluorescence activated cell sorting (FACS) and automated clone selection devices (e.g. ClonePix® (Molecular Devices)) for clone screening, or automated and miniaturized bioreactor systems (e.g. Ambr®15 (Sartorius Stedim)) for media and process optimisation (Priola *et al.*, 2016). Using combinations of these technologies and automation can shorten mammalian cell line development timelines from approximately 9 months down to several weeks/months with a decreased need for resources and labour (Tejwani *et al.*, 2021).

Of particular note, in the high throughput technologies for developing process optimisation and accurate scale-up predictions are Sartorius Stedim's ambr®15 and ambr®250 systems. The ambr®15 systems are capable of running up to 48 parallel culture vessels each with varied control of process parameters, including temperature/pH shifts and media/supplement optimisation in batch or fed-batch mode, and is well suited for complex design of experiment (DoE) approaches with high reproducibility (Wohlenberg *et al.*, 2022; Velugula-Yellela *et al.*, 2018). One caveat of this system is bioreactor volume, with a working volume of 10-15 mL the ambr®15 allows for process optimization with less resource input however minimal sampling and harvest volumes can be limiting for full analysis or purification. By using the ambr®250 systems this can be overcome as this instrument offers a larger maximum volume of 250 mL with much more flexibility in sampling and harvest volumes amenable to complete analyses. They are available in a modular or high throughput (include automated liquid handling robotic arm) format and can run 24 independently controlled vessels in

parallel. These systems can be used to provide reliable estimates of process performance and product quality up to the pilot scale (Manahan *et al.*, 2019).

1.4.4.5 Biosimilars

As the patents for biologics expire, this opens opportunities for the development of biosimilars and the potential for cheaper biotherapeutics. These products are very similar in design (they must have the same amino acid sequence but ‘similar’ other critical quality attributes such as glycosylation), production and administration to off-patent biologics but are not patentable themselves leading to lower prices (Torres-Obreque *et al.*, 2021).

One such off-patent biologic which has been used to successfully generate and market cheaper biosimilars is Trastuzumab. This humanised IgG1 antibody was generated in a CHO cell line by Genentech and targets the human epidermal growth factor 2 (HER2) (Lao-Gonzalez *et al.*, 2021). It has since been made commercially available by Roche under the brand name Herceptin® for the treatment of HER2-positive cancers (Robertson, 1998) and went off-patent in Europe in 2014 and the US in 2019. By 2020, there were five trastuzumab biosimilars approved by the EMA and FDA: Herzuma® (Mundipharma), Kanjinti® (Amgen), Ogivri® (Mylan), Ontruzant® (MSD) and Trazimera® (Pfizer), although they not all currently on the market in some countries with regulatory approval. The German market is one of those with all five commercially available and it has been predicted that the country’s potential annual savings would be in the range of €95.9 – €120.5 million if the Roche Herceptin® was replaced by the cheapest biosimilar (Trazimera® (Pfizer)), which undercuts the original drug price by 10.8% (Hübel, Kron and Lux, 2020). Survival analysis of a long-term study comparing Herzuma® (Mundipharma) treatment against Herceptin® (Roche) in patients with HER2-positive metastatic breast cancer found that there were no notable differences in final overall survival between the biosimilar and the original drug (Rugo *et al.*, 2021). These incredibly positive outcomes coupled with the potential reduction in costs for immunotherapies provides an excellent opportunity in manufacturing to invest in biosimilar developments prior to

biologic patent end dates so that economies can benefit from lower healthcare costs as soon as possible.

The success of biosimilars such as those designed to replace Trastuzumab have shown the importance of identifying biologics suitable for biosimilar development, which are scheduled to become off-patent in the near future. Strong candidates for this area of work include checkpoint inhibitors which have become major players in immunotherapy for the treatment of cancers. These antibody therapies target immune checkpoints such as cytotoxic T-lymphocyte-associated protein 4 (CTLA-4) and programmed death-1 (PD-1) and elicit anti-tumour responses to combat cancers (Franzin *et al.*, 2020). One of these antibodies is Nivolumab (Opdivo®), an IgG4 which binds to PD-1 receptors and has been shown to be an effective treatment in multiple advanced cancers which have evaded initial cancer treatments or unable to be surgically resected (Rajan *et al.*, 2016). It was first licensed for use by the FDA in 2014 and the EMA in 2015 for treatment of melanoma but has since been trialled and approved for uses in other cancers and in combination with other therapies. The patent for this biologic is due to expire in 2026 (EU)/2027 (USA) (Busse and Lüftner, 2019) and has strong potential for a successful translation into a biosimilar for a cheaper approach to the treatment of multiple cancers.

1.5 Concluding Remarks

Recent successes in the development of vaccine technologies have been underpinned by a lipid nanoparticle delivery system which can be described as synthetic analogues of extracellular vesicles such as exosomes. The potential strategies for the generation of recombinant exosomes and their reported involvement in immunity highlighted in this chapter, warrant the investigation and development of an exosome-based vaccine platform as a novel approach to vaccination. Furthermore, the emergence of a novel coronavirus, SARS-CoV-2, has resulted in an unprecedented global impact to public health and highlighted that vaccine development to tackle a pathogen with continuous mutations and immune evasion requires the investigation of novel and adaptive vaccine strategies. This chapter highlights the robust and well-established Chinese hamster ovary (CHO) cell expression platform, capable of withstanding engineering for the

manipulation of secretory pathways vital to exosome biogenesis, and a well-reported record for expression of multiple blockbuster biologics.

Concurrently, another global threat to public health, Dengue Fever, in the face of poor responses to vaccine technology compels the exploration of alternative strategies to tackle disease burden. Due to prevalence in countries with less developed medical therapies and complex biological interactions with vaccines, described in this chapter, optimisation of a newly discovered monoclonal antibody for enhanced yield using off-patent sequences from successful antibody products, in well-established expression systems such as CHO, could allow for a low-cost therapeutic strategy to combat disease where vaccines have failed.

1.6 Aims of This Study

The aims of the work described in this thesis were;

1. To develop and test a vector-based 'plug & play' fusion protein strategy using fluorescent reporter proteins for the generation of recombinant exosomes from CHO cell cultures, as a proof of concept as a potential novel vaccine platform.
2. To assess the proof of concept developed under aim 1, using antigenic targets identified against SARS-CoV-2, for its robustness for insertion of pathogen sequences of varying size and complexity in the ability to successfully produce recombinant SARS-CoV-2 antigen-bearing exosomes.
3. To optimise sequences of a newly identified anti-dengue antibody to produce a monoclonal lineage with improved expression in CHO cell cultures and identify production bottlenecks responsible in limiting its expression from CHO cells.

Chapter 2: Materials & Methods

All reagents used in this thesis were analytical grade or higher unless otherwise stated and sourced from standard suppliers such as Sigma Aldrich, Fisher Scientific, Promega or Thermo Fisher.

2.1 Bacterial Cell Culture Techniques

Escherichia coli (strain DH5 α) was used throughout this project as a vehicle for amplification of plasmid constructs for transfection into mammalian cells.

2.1.1 Liquid Media Culture

Luria-Bertani (LB) broth (per litre: 10 g Tryptone, 5 g Yeast Extract, 10 g NaCl) was used in liquid culture of *E. coli*, which were incubated overnight at 37°C and shaken at 200 rpm in volumes of 3 mL for subsequent mini-preps or 250 mL for subsequent maxi-preps.

2.1.2 Solid Media Culture

Luria-Bertani (LB) agar (per litre: 10 g Tryptone, 5 g Yeast Extract, 10 g NaCl, 15 g Nutrient Agar No. 2) was used to culture *E. coli* in petri dishes. Plates were inverted after inoculation and left in a static incubator at 37°C overnight.

2.1.3 Antibiotic Selection

Antibiotic (100 mg/mL Ampicillin, or 50 mg/mL Kanamycin) matching the selection gene of the plasmid being cultivated, was diluted into media at a ratio of 1:1000.

2.1.3 Competent Cells

E. coli (DH5 α) cells were made chemically competent using CaCl₂. Overnight cultures (3 mL) were used to inoculate 2 flasks of 50 mL Super Optimal Broth (per litre: 20 g Tryptone, 5 g Yeast Extract, 0.5 g NaCl, 10 mL 0.25 M KCl, 5 mL 2 M MgCl₂) which was then grown to an OD_{600nm} of 0.4 - 0.6. Cultures were then centrifuged at 3500 rpm for 15 minutes at 4°C, after which pellets were resuspended in 10 mL of ice-cold, filter-sterilised 100 mM CaCl₂ each and incubated on ice for 30 minutes. CaCl₂-cell suspensions

were centrifuged for 3500 rpm for 15 minutes at 4°C and the resulting cell pellets resuspended in 2 mL of ice-cold, filter-sterilised 100 mM CaCl₂ each, pooled and mixed with 1 mL sterile 80% glycerol. This preparation of CaCl₂ competent cells were then dispensed as 50 µl cryovial aliquots, flash-frozen on dry ice and stored at -80°C.

2.1.4 Transformations

Transformation of CaCl₂ competent *E. coli* (DH5α) cells with plasmid DNA or DNA ligation mixtures were carried out using a heat shock protocol. Competent cell cryovial aliquots (50 µl) were thawed on ice, mixed with 1 µl (≥10 ng) plasmid DNA or 5 µl DNA ligation mixture, and incubated on ice for 30 minutes. A heat shock step of 42°C for exactly 90 seconds was then applied, followed by immediate return to ice for 2 minutes and then addition of 450 µl LB broth before 1 hour incubation at 37 °C, shaking at 200 rpm. 100 µl of the culture was then plated onto LB agar and incubated at 37°C overnight.

2.1.5 Glycerol Stocks

Glycerol stocks were made of each culture containing completed and sequenced plasmids by mixing 500 µl of liquid culture grown overnight, with 500 µl sterile 50% glycerol in cryovials followed by immediate flash-freeze with dry ice and stored at -80°C.

2.2 Molecular Cloning Techniques

2.2.1 RNA Extraction

Cell pellets were taken from CHO-S cell cultures by centrifuging 2x10⁶ viable cells at 1000 rpm for 5 minutes, after which time the supernatant was discarded. RNA was then extracted using the QIAGEN RNeasy® Mini Kit following the protocol provided by the manufacturer. Extracted RNA concentrations were determined using a nanodrop instrument and stored at -80°C.

2.2.2 cDNA Synthesis (Reverse Transcription)

RNA extracts (4 µg) and 4 µl Promega™ Oligo (dT) 15 primer were topped up to a final total volume of 15 µl with RNase-free water and incubated at 70°C for 5 minutes, then transferred to ice for 2 minutes. Whilst on ice, 10 µl Promega™ M-MLV buffer (5X), 2.6

μl 10 mM dNTPs, 1.4 μl Promega™ RNaseIn ribonuclease inhibitor, 2 μl Promega™ M-MLV Reverse Transcriptase was added and topped up to a total final volume of 50 μl with nuclease-free water. This was then further incubated at 42°C for 1 hour, the resulting cDNA concentration was measured using a nanodrop instrument and stored at -80°C.

2.2.3 Phusion™ PCR

Polymerase chain reactions were carried out for DNA amplifications from cDNA, plasmid DNA and DNA string fragments in 100 μl reactions, containing 1 μl Phusion™ High-Fidelity DNA Polymerase (Thermo Scientific™), 20 μl High-Fidelity Buffer (5X), 4 μl Forward Primer (10 pmol), 4 μl Reverse Primer (10 pmol), 2 μl dNTPs (10 μM), 67 μl Nuclease-free water and 2 μl template DNA (100 ng/μl cDNA or 10 ng/ μl plasmid DNA and string fragments). These reactions were carried out in a thermocycler following the manufacturer’s recommended thermocycler program for Phusion™ High-Fidelity DNA Polymerase, shown below (Table 2.1), and reaction-specific custom-made primers (Table 2.2).

Table 2.2: Thermocycler program used for Phusion™ PCR reactions.

Cycle Step	Temperature	Time	Number of Cycles
Initial Denaturation	98°C	30 seconds	1
Denaturation	98 °C	10 seconds	35
Annealing	*T _m - 2°C	30 seconds	
Extensions	72°C	30 seconds/kbp	
Final Extension	72°C	7 minutes	1
Hold	4°C	-	-

*T_m = Primer melting temperature (°C).

2.2.3.1 PCR Primers

PCR primers used throughout the work described in this thesis are described in Table 2.2 below.

Table 2.3: List of custom primers used to amplify gene sequences via PCR, including the restriction enzyme site encoded and melting temperature (T_m) of each oligo.

Oligo Name	Sequence	Target Gene	Restriction Enzyme	T_m (°C)
PolyUbi_F	TATAAGCTTATGCAAATCTTCGTGAAGAC	Polyubiquitin	HindIII	61
PolyUbi_R	ATAGGATCCTTAATAGCCACCCCT	Polyubiquitin	BamHI	61
Ubi_NS_R	ATAGGATCCGCCACCCCTG	Ubiquitin	BamHI	61
eGFP_F	TATGGATCCATGGTGAGCAAGG	eGFP	BamHI	60.3
eGFP_R	ATACTCGAGTACTTGTACAGCTCG	eGFP	XhoI	61.3
GFP_NS_F	TATAAGCTTATGGTGAGCAAGGGC	eGFP	HindIII	61
GFP_NS_R	ATAGGATCCTTACTTGTACAGCTCG	eGFP	BamHI	61.3
Ubi_F	TATGGATCCATGCAAATCTTCGTGAA	Ubiquitin	BamHI	60.1
Ubi_R	ATACTCGAGTAGCCACCCCT	Ubiquitin	XhoI	59.8
mCh_R_S	ATACTCGAGCTACTTGTACAGCTC	mCherry	XhoI	61
GFPmCh_R_NS	ATAGGATCCCTTGTACAGCTCGT	eGFP/mCherry	BamHI	60.6
CD81_F	TATGGATCCATGGGGGTGGAG	CD81	BamHI	61.8
CD81_R	ATACTCGAGTCAGTACACGGAGC	CD81	XhoI	62.4
CD63_F	TATGGATCCATGGCGGTGAAG	CD63	BamHI	62.1
CD63_R	ATACTCGAGCTACATTACTTCATAGCC	CD63	XhoI	61.9
TSG101_F	TATGGATCCATGGCGGTGTCTGA	TSG101	BamHI	62.4
TSG101_R	ATACTCGAGTCAGTAGAGGTCATAA	TSG101	XhoI	61.6
mCh_S_F	TATGGATCCATGGTGAGCAAGGGC	mCherry	BamHI	64.4
mCh_S_R	ATACTCGAGCTACTTGTACAGCTCGTC	mCherry	XhoI	65
PUGFP_NS_F	TATGCTAGCATGGTGAGCAAGG	eGFP/mCherry	NheI	60.3
PUGFP_NS_R	ATAAAGCTTCTTGTACAGCTCGTCC	eGFP/mCherry	HindIII	61.3
PUmCh_NS_F	TATAAGCTTATGGTGAGCAAGGGC	mCherry	HindIII	61
PUmCh_NS_R	ATAGGATCCCTTGTACAGCTCGT	mCherry	BamHI	60.6
CD81_NS_R	ATACTCGAGGTACACGGAGCTG	CD81	XhoI	62.1
CD63_NS_R	ATACTCGAGCATTACTTCATAGCCACTT	CD63	XhoI	62.2
TSG_NS_R	ATACTCGAGGTAGAGGTCATAAGAC	TSG101	XhoI	63.2
GFP_S_Xho_F	TATCTCGAGATGGTGAGCAAGGG	eGFP	XhoI	62.4
GFP_S_Apa_R	ATAGGGCCCTTACTTGTACAGCTC	eGFP	ApaI	62.7
Den54_allLC_F	TATGGTACCGCCACCATGG	Den54	KpnI	58.8
Den54_allHC_F	TATGGCGCCGCCACCATG	Den54	KasI	60.5
Den54_OrigLC_R	ATACTTAAGTTAGCAAGAGTAGGAC	Den54	AflIII	58.1
Den54_newLC_R	ATACTTAAGTCAGCACTCGCC	Den54	AflIII	57.9

Den54_IgG1HC_R	ATAACTAGTTCACCTTGCCAGGGG	Den54	SpeI	60.6
Den54_IgG4HC_R	ATAACTAGTTCACCTTGCCCAGGG	Den54	SpeI	60.6
NewTsg101_S_R	ATACTCGAGTCACCTTTGCATAAGTGC	Tsg101	XhoI	61.9
NewTsg101_NS_R	ATACTCGAGCTTTTGCATAAGTGCC	Tsg101	XhoI	61.3
midmCh_Hind_F	TATAAGCTTATGGTGAGCAAGGGCG	mCherry	HindIII	63
midmCh_Kpn_R	ATAGGTACCCTACTTGTACAGCTCG	mCherry	KpnI	63
UBI_SPIKE_NS_F	TATGGATCCATGGTGAATCTGACCAC	tFLS	BamHI	63.2
UBI_SPIKE_NS_R	ATAAAGCTTGTGATGATGGTGTGGTGG	tFLS	HindIII	63.7
UBI_SPIKE_S_F	TATGCTAGCATGGTGAATCTGACCAC	tFLS	NheI	63.2
UBI_SPIKE_S_R	ATACTCGAGTCAGTGATGATGGTGTGG TG	tFLS	XhoI	66.8
ExoSPIKE_NS_F	TATAAGCTTATGGTGAATCTGACCACCA G	tFLS	HindIII	63.9
ExoSPIKE_NS_R	ATAGGTACCGTGATGATGGTGTGGT	tFLS	KpnI	63.2
UBI_RBD_NS_F	TATGGATCCATGCCCAATATCACCAAC	RBD	BamHI	63.4
UBI_RBD_NS_R	ATAAAGCTTGTGGTGTGGTGTGGTGG T	RBD	HindIII	63.9
UBI_RBD_S_F	TATGCTAGCATGCCCAATATCACCAAC	RBD	NheI	63.4
UBI_RBD_S_R	ATACTCGAGTCAGTGGTGTGGTGTGGT	RBD	XhoI	63.2
ExoM_RBD_NS_F	TATAAGCTTATGCCCAATATCACCAACCT G	RBD	HindIII	64
ExoM_RBD_NS_R	ATAGGTACCGTGGTGTGGTGTGGTGTGGT	RBD	KpnI	63.2
UBI_NCAP_NS_F	TATGGATCCATGTCCGACAACGGC	Nucleocapsid	BamHI	64.4
UBI_NCAP_NS_R	ATAAAGCTTGTGGTGTGGTGTGGTGTGG T	Nucleocapsid	HindIII	63.9
UBI_NCAP_S_F	TATGCTAGCATGTCCGACAACGGC	Nucleocapsid	NheI	64.4
UBI_NCAP_S_R	ATACTCGAGTCAGTGGTGTGGTGTGGT	Nucleocapsid	XhoI	63.2
ExoM_NCAP_NS_F	TATAAGCTTATGTCCGACAACGGCCC	Nucleocapsid	HindIII	64.8
ExoM_NCAP_NS_R	ATAGGTACCGTGGTGTGGTGTGGTGTGGT	Nucleocapsid	KpnI	65
UBI_SUB1_NS_F	TATGGATCCATGGGCGTGCACTC	S1	BamHI	64.2
UBI_SUB1_NS_R	ATAAAGCTTGGAGCCAGGAGAGTTGG	S1	HindIII	64.8
UBI_SUB1_S_F	TATGCTAGCATGGGCGTGCACTC	S1	NheI	64.2
UBI_SUB1_S_R	ATACTCGAGTCAGGAGCCAGGAGA	S1	XhoI	64.4

ExoM_SUB1_NS_F	TATAAGCTTATGGGCGTGCACTCCGT	S1	HindIII	64.8
ExoM_SUB1_NS_R	ATAGGTACCGGAGCCAGGAGAGT	S1	KpnI	64.2
UBI_SUB2_NS_F	TATGGATCCATGGCCTCTTCTGTGG	S2	BamHI	64.6
UBI_SUB2_NS_R	ATAAAGCTTGTGATGATGGTGATGGTGG T	S2	HindIII	63.9
UBI_SUB2_S_F	TATGCTAGCATGGCCTCTTCTGTGG	S2	NheI	64.6
UBI_SUB2_S_R	ATACTCGAGTCAGTGATGATGGTGATG	S2	XhoI	63.4
ExoM_SUB2_NS_F	TATAAGCTTATGGCCTCTTCTGTGGC	S2	HindIII	63.2
ExoM_SUB2_NS_R	ATAGGTACCGTGATGATGGTGATGGT	S2	KpnI	63.2
FLS_F_PteI	TATGCGCGCATGGTGAATCTGACCA	tFLS	PteI	64.6
FLS&S2_R_Bsp119I	ATATTCGAAGTGATGATGGTGATGGTGG T	tFLS/S2	Bsp119I	63.9
S1_F_PteI	TATGCGCGCATGGGCGTGCA	S1	PteI	63.5
S1_R_Bsp119I	ATATTCGAAGGAGCCAGGAGAGTTG	S1	Bsp119I	63
S2_F_PteI	TATGCGCGCATGGCCTCTTCTGT	S2	PteI	64.2
GFP_BP_F	TATGCGCGCATGGTGAGCAAGG	GFP	PteI	64
RBD_BP_F	TATGCGCGCATGCCAATATCACCA	RBD	PteI	64.6
NC_BP_F	TATGCGCGCATGTCCGACAACG	Nucleocapsid	PteI	64
GFP_BP_R	ATATTCGAAGTGTACAGCTCGTCCATG	GFP	Bsp119I	63.7
RBD&NC_BP_R	ATATTCGAAGTGGTGATGGTGATGATGG T	RBD/Nucleocapsid	Bsp119I	63.9

2.2.4 Reverse-Transcription PCR

2.2.4.1 Plate Protocol

The QuantiNova™ SYBR Green RT-PCR Kit (Qiagen) was used alongside custom primers (Table 2.5) following the recommended manufacturer's protocol for 20 µl reaction mixes (Table 2.3) and cycling conditions (Table 2.4) in a Bio-Rad DNA Engine Peltier Thermocycler with a Bio-Rad Chromo5 real-time detection module. To analyse the results generated, ThermoFisher QuantStudio Design and Analysis Software was used for relative quantification of RNA transcripts, using the housekeeping gene GAPDH as a baseline normaliser.

Table 2.4: List of components and volumes for each RT-PCR reaction for use with the QuantiNova™ SYBR Green RT-PCR Kit (Qiagen).

Reaction Component	Volume per 20 µl Reaction
2X QuantiNova™ SYBR Green RT-PCR Master Mix	10
QuantiNova™ SYBR Green RT Mix	0.2
10X Forward Primer	1
10X Reverse Primer	1
Template RNA (25 ng/ul)	2
RNase-free H ₂ O	5.8

Table 2.5: Cycling Conditions for RT-PCR reactions using the QuantiNova™ SYBR Green RT-PCR Kit (Qiagen).

Cycle Step	Time	Temperature (°C)	Ramp Rate
RT step	10 min	50	Fast Mode
PCR initial heat activation	2 min	95	Fast Mode
<i>2-step cycling</i>			
Denaturation	5 seconds	95	Fast Mode
Combined annealing/extension	10 seconds	60	Fast Mode
Number of cycles	40		

2.2.4.2 mRNA Transcript Relative Fold Change Calculations

To calculate the fold change ($2^{-\Delta\Delta Ct}$) in mRNA transcripts, the average cycle threshold (Ct) values were determined for target genes and the GAPDH gene in both the naïve CHO-S cell line and the related stable-expressing pool using the ThermoFisher QuantStudio Design and Analysis Software. These values were then used in the following equations to determine the mRNA transcript fold change of each transgene relative to GAPDH:

$$\Delta Ct (CHO) = Av. Ct (target gene, CHO) - Av. Ct (target gene, CHO)$$

$$\Delta Ct (Pool) = Av. Ct (target gene, Pool) - Av. Ct (target gene, Pool)$$

$$\Delta\Delta Ct = \Delta Ct(Pool) - \Delta Ct(CHO)$$

$$Fold\ Change = 2^{-\Delta\Delta Ct}$$

2.2.4.3 RT-PCR Primer List

Primers used in the RT-PCR work described in this thesis are described in Table 2.5 below.

Table 2.6: List of custom primers used in RT-PCR reactions, including melting temperature (T_m) of each oligo.

Primer Target	Oligo Name	Sequence	T_m (°C)
Heavy Chain 1	aHC1_F	AAAGGCCTGGAATGGATGGG	60.03
Heavy Chain 2	bHC2_F	TGCAGTCTCAGGTTCACTG	59.97
Heavy Chain 4	aHC4_F	CAGAAGTTCCGGGGCAGATT	60.04
Heavy Chain 5	bHC5_F	ACTTGGCGGATTCTGTTTCGT	59.97
Heavy Chain 1	aHC1_R	CTCAGGCCGTTCACTCCAT	60.04
Heavy Chain 1, 2 and 5	bHC125_R	CCCATCCATTCCAGGCCTTT	60.03
Heavy Chain 4	aHC4_R	AGAGCAGCTGTAGACTCGGA	60.03
Light Chain 1, 2 and 5	aLC125_F	CCGGCGTGTCTCTAGATTC	59.97
Light Chain 4	aLC4_F	GCTGCTGTTGTGTTGTCTG	59.97
Light Chain 1, 2 and 5	aLC125_R	GGAAGAGATGGCGTAGGAGC	59.97
Light Chain 4	aLC4_R	GAAGTCCTCAGGTTCCAGGC	60.04
GAPDH	GAPDH_F	GCCAAGAGGGTCATCATCTC	59.3
GAPDH	GAPDH_R	CCTTCCACAATGCCAAAGTT	55.3

2.2.5 Colony PCR Screening

To screen colonies growing on plates post-transformation, PCR reactions were carried out directly on a range of colonies per plate using primers specific to the target gene insert, with positive screens resulting in correct band sizes upon analysis of the PCR reaction by agarose gel electrophoresis. Each colony was picked with a sterile tip and suspended into 5 μ l nuclease-free water. Before discard, each tip was streaked onto a grid-labelled, fresh agar plate which was incubated overnight at 37°C once all colonies were suspended and streaked. To each 5 μ l cell suspension, 15 μ l GoTaq™ PCR master mix (per reaction: 4 μ l 5X GoTaq™ Buffer, 1.6 μ l MgCl₂, 0.4 μ l 10 mM dNTPs, 0.8 μ l 10 pmol Forward Primer, 0.8 μ l 10 pmol Reverse Primer, 7.3 μ l Nuclease-Free Water and

0.1 µl GoTaq™ DNA Polymerase) was added and run with a specific thermocycler programme (Table 2.6).

Table 2.7: Thermocycler program for colony PCR reaction protocol.

Cycle Step	Temperature	Time	Number of Cycles
Initial Denaturation	94°C	5 minutes	1
Denaturation	94°C	30 seconds	30
Annealing	50°C	30 seconds	
Extensions	72°C	1 minute/kbp	
Final Extension	72°C	7 minutes	1
Hold	4°C	-	-

2.2.6 Agarose Gel Electrophoresis

Gel electrophoresis of DNA was carried out in 1 or 2% agarose gels containing 0.5 g or 1 g agarose, respectively, and 2.5 µl Ethidium Bromide per 50 mL 1X TAE Buffer (1:50 dilution 50X TAE – 242 g Tris-Base, 57.1 mL acetate, 100 mL 0.5 M sodium EDTA). Gels were run using 1X TAE running buffer at constant voltage (100 V) for 1 hour before imaging using a UV filter.

2.2.7 Gel and PCR DNA Clean-up

The membrane-based Promega™ Wizard® SV Gel and PCR Clean-Up System was used to extract DNA bands from agarose gels and purify PCR products from excess nucleotides and primers in the reaction mix following the manufacturer's instructions.

2.2.8 Restriction Enzyme DNA Digests

Restriction digests were performed in either 10 µl or 20 µl reactions for the purpose of screening or ligating, respectively, with FastDigest® restriction enzymes (Thermo Scientific™) (Table 2.7) and in 100 µl reactions with New England Biolabs® restriction enzymes (Table 2.8).

Table 2.8: *FastDigest™ Restriction Enzyme double digest reaction compositions, both incubated at 37 °C for 1 hour.*

Component	10 µl Reaction	20 µl Reaction
FastDigest™ Buffer (10X)	1 µl	2 µl
Enzyme I	0.25 µl	1.5 µl
Enzyme II	0.25 µl	1.5 µl
Nuclease-Free Water	7.5 µl	15 µl - DNA volume
DNA	1 µl	2 µg

Table 2.9: *NEB® Restriction Enzyme double digest reaction composition, incubated at 37 °C for 1 hour.*

Component	100 µl Reaction
CutSmart® Buffer (10X)	10 µl
Enzyme I	2 µl
Enzyme II	2 µl
Nuclease-Free Water	86 µl - DNA volume
DNA	2 µg

2.2.9 Ligation Reactions

After enzyme restriction digested DNA fragments and/or plasmids were purified from agarose gels and eluted into 20 µl nuclease-free water, they were ligated together using Promega™ T4 DNA Ligase in 10 µl reactions (1 µl T4 Ligase Buffer, 3 µl digested plasmid backbone DNA, 5 µl digested gene insert DNA, 1 µl T4 DNA Ligase) incubated at either 4°C overnight, or room temperature for 4 hours.

2.2.10 Plasmid DNA Purification

Plasmid DNA was extracted and purified from 3 mL or 250 mL *E. coli* cultures using QIAGEN Mini or Maxi Kits, respectively, following the manufacturer's instructions.

2.2.10 Plasmid DNA Sequencing

All genetic constructs created were sequenced using commercial Sanger Sequencing through a third party (GENEWIZ®) and samples were prepared in accordance with their submission guidelines.

2.3 Mammalian Cell Culture

2.3.1 Revival of Cell Lines from Cryopreservation

A cryovial containing 1 mL (1×10^7) of Gibco™ CHO-S cell-line was removed from cryopreservation and placed in a 37°C water bath until the moment of thaw, and then added to 29 mL Gibco™ CD CHO chemically defined media, supplemented with L-Glutamine (8 mM), in a sterile 125 mL Corning® Erlenmeyer shake flask. The flask was then exposed to 5% CO₂ gas for 10 seconds, sealed and then incubated at 37°C and shaken at 140 rpm. Cultures were then routinely passaged for a minimum of 3 passages before use.

2.3.2 Routine Cell Culture Passage

Cultures were routinely passaged twice a week with cell counts ($\times 10^6$ /mL) and culture viability (%) determined using a Beckman Coulter® Vi-CELL™ Analyzer. New cultures were seeded at a cell concentration of 0.2×10^6 viable cells/mL in 8 mM L-Glutamine Gibco™ CD CHO media and exposed to 5% CO₂ gas for 10 seconds, sealed and then incubated at 37°C and shaken at either 140 rpm in 125 mL Corning® non-vented flask cultures (20-30 mL max volume) or 220 rpm for 50 mL falcon tube cultures (10 mL max volume).

2.3.3 Cell Growth Curves

2.3.3.1 Batch Cultures

For each CHO-S cell line, a 30 mL culture was set up with an initial seeding density of 0.2×10^6 viable cells/mL and incubated at 37°C and shaken at 140 rpm in 125 mL Corning® non-vented flasks. For each day of the growth curve, a 500 µl sample was taken from each culture and run through the Beckman Coulter® Vi-CELL™ Analyzer diluted 1:2 with

Gibco™ CD-CHO media to record the cell concentration and culture viability. Each culture was then re-gassed with 5% CO₂ for 10 seconds and the cell concentration and culture viability were then recorded each day and plotted using Microsoft Excel to assess the growth phase and ‘health’ of each flask. Cultures were discontinued once culture viability reduced to <60%.

2.3.3.2 Fed-Batch Cultures

For each CHO-S cell line, a 30 mL culture was set up with an initial seeding density of 0.2 x10⁶ viable cells/mL and incubated at 37°C and shaken at 140 rpm in 125 mL Corning® non-vented flasks or 250 mL/500 mL flask. The cultures were supplemented with Gibco™ CHO CD EfficientFeed™ B media according to the feeding protocol 3 provided by the products supplementary information (Table 2.9). For each day of the growth curve, a 500 µl sample was taken from each culture and run through the Beckman Coulter® Vi-CELL™ Analyzer diluted 1:2 with Gibco™ CDCHO media to record the cell concentration and culture viability. Each culture was then re-gassed with 5% CO₂ gas for 10 seconds and the cell concentration and culture viability records were then plotted against culture time in days using Microsoft Excel to assess the growth phase and health of each flask. Cultures were discontinued once culture viability decreased below <60%.

Table 2.10: Feeding Schedules and Volumes (as percentages of total culture volume) for fed-batch style culture using Gibco™ CHO CD EfficientFeed™ B (as recommended by manufacturer).

Day	Feed Additions (% Culture)	
	Condition 3	Condition 10
0	15	-
1	-	-
2	-	-
3	10	10
4	-	-
5	-	-
6	10	10
7	-	-
8	-	-
9	10	10
10	-	-
11	-	-
12	-	10

2.3.3.3 Ambr® 250 Fed-batch culture

The ambr® 250 Modular system (Sartorius) was used to grow CHO cell cultures under fed-batch conditions (Condition 10, Table 2.9) with online monitoring and control loops to keep process parameters at pre-determined setpoints (Table 2.10).

Table 2.11: Process detailing the parameters and setpoints used for CHO-S cultures grown in the Sartorius ambr® 250 Modular system.

Parameter		Setpoint / Value
Cell Line		CHO-S (D1A-8 and D2B-1)
Media		Gibco™ CD CHO Medium
Initial Fill Volume (mL)		170
Post-Inoc Volume (mL)		180
Number of Vessels		2
Process Length (days)		14
Seeding Density (x10 ⁶ vc/mL)		0.2
Temperature (°C)		37
Stir Speed (RPM)		350
Dissolved Oxygen (%)		50
Antifoam		None
pH	Setpoint	7
	Deadband	0.05
	Acid Control	Sparged CO ₂
	Base Control	1 M NaCO ₃
Sampling	Scheduled	Daily (AM)
	Sampling Volume (mL)	2
	Purpose	Cell Counts & Western Blot Analysis
Fed Batch	Media	Gibco™ CHO CD Efficient Feed B
	Bolus Days	3, 6, 9 and 12
	Bolus (% BR Vol.)	10

Each reactor was initially filled with sterile Gibco™ CD CHO medium and left for a period of 4 hours to allow hydration of each bioreactor vessel's sensors and probes. After

hydration, temperature control was initiated and the system left until the setpoint (37°C) was achieved before switching on the remaining process parameters. Reactors were then each inoculated from 125 mL shake flask cultures to produce a final vessel volume of 180 mL with seeding density targets of 0.2×10^6 viable cells/mL. From this point on, the automated system controlled the process parameters and maintained setpoints through control loops (Table 2.10). Samples were taken every morning for the duration of the cultures, after which a programmed bolus feed of Gibco™ Efficient Feed™ B was delivered by the system on feed days.

2.3.4 Transient Transfections

2.3.4.1 Electroporation

Transient transfection by electroporation was carried out with 100 µl containing 20 µg of non-linearised plasmid DNA diluted in filtered TE buffer and 700 µl culture containing 1×10^7 viable cells at 300 V, 900 µF in 4 mm BioRad Electroporation cuvettes. Each cuvette was then washed immediately with warm media and then transferred to 125 mL Erlenmeyer shake flasks containing 18.5 mL warm media. The flasks were then incubated at 37°C with shaking at 140 rpm for 24, 48 or 72 hours before harvesting material.

2.3.5 Stable Cell Line Construction

2.3.5.1 Plasmid DNA Linearisation

Complete linearisation of plasmid DNA for stable transfection required that DNA was digested overnight at higher concentrations (to that performed in Table 2.9) and with only a single restriction enzyme. 50 µg of plasmid DNA per transfection was digested overnight with the appropriate NEB® restriction enzyme in 100 µl reactions (2.5 µl enzyme, 10 µl buffer, 50 µg DNA, topped up to 100 µl final volume with nuclease-free water). The digestion/linearisation of the DNA for each digest was confirmed by running the material on an agarose gel.

2.3.5.2 Transfection

Electroporation was carried out for stable transfections with 100 μ l containing 40 μ g of linearised plasmid DNA diluted in filtered TE buffer and 700 μ l culture containing 1×10^7 viable cells at 300 V, 900 μ F in 4 mm BioRad Electroporation cuvettes. Each cuvette was then refreshed immediately with warm media and then transferred to T75 flasks containing 18.5 mL warm media. The flasks were then incubated at 37°C in static incubators supplied with 5% CO₂ for 24 hours.

2.3.5.3 Addition of Selection Agent

24 hours after electroporation, flasks were supplemented with a further 5 mL of media containing a volume of selection agent that gave the appropriate final selection agent concentration. Flasks were then returned to static incubation at 37°C, 5% CO₂ for a further 6 days.

2.3.5.4 Passaging from Static to Suspension Conditions

Cell counts of the static cultures were performed every 7 days to track cell concentration and culture viability. Until culture viabilities reached >50-60%, cultures were refreshed with media by centrifuging at 1000 rpm for 5 mins and the resulting cell pellets being resuspended in 50 mL of fresh media containing appropriate concentrations of selection marker. The 50 mL was split in two and transferred to fresh T75 flasks for static incubation at 37°C, 5% CO₂. Once culture viabilities had reached >50-60%, splits were transferred to 125 mL Erlenmeyer shake flasks and incubated at 37°C, shaking at 140 rpm, and then routinely passaged afterwards.

2.3.6 Cryopreservation of Cell Lines

Stocks of cultures were cryopreserved in liquid nitrogen suspended in a freezing media composed of 92.5% standard media and 7.5% (v/v) DMSO. Volumes of culture containing 1×10^7 viable cells were centrifuged at 1000 rpm for 5 minutes, and the pellets resuspended in 1 mL of freezing media and dispensed into cryovials. The cryovials were then flash frozen on dry ice, then stored at -80°C overnight before transferring to liquid nitrogen storage.

2.3.7 Monoclonal Cell Line Lineage Development

2.3.7.1 Limiting Dilution Cloning

For each cell line, cell cultures were taken and diluted to a density of 1×10^4 cells/mL with the stock medium it was cultured in (Gibco™ CD CHO media + 8 mM L-Glutamine + 750 µg/mL Hygromycin B), of which 200 µL (approx. 2000 cells) was pipetted into a single well (A1) of a 96 well plate. This was then serially diluted 1:2 vertically down the entire column 1 using the same stock medium. This row of wells was then serially diluted 1:2 horizontally for every row from column 1 – 12, again using the same stock medium. Plates were made in triplicate for each cell line and placed in 37°C static incubators supplied with 5% CO₂. After 24 hours, the wells of each plate were examined under a light microscope and any wells containing 1-3 cells were highlighted.

After highlighted wells reached an appropriate confluency (~2 weeks later), these cultures were transferred to 24-well plates and incubated for a further week with the same media and incubation conditions. Dot blot screening was then used to determine which of the highlighted cultures would be taken forward for each cell line out of the clones that survived the transfer to 24-well plate format. Scale-up from this point included transfer from 24-well plates to T25 flasks under static conditions, then transfer to 50 mL spin tubes followed by 125 mL Erlenmeyer flasks under shaking conditions. Each stage of scale-up was informed by western blot analysis to determine the expression profiles of clones throughout the process.

2.3.8 Cell Culture Protein Analysis

2.3.8.1 Cell lysate preparation

Lysis buffer (100 mL containing 0.48 g HEPES, 0.58 g NaCl, 0.216 g β-glycerophosphate, 1 mL Triton-X) was prepared with 1 Roche cOmplete™ Mini EDTA-free Protease Inhibitor Cocktail tablet per 10 mL and chilled. Volumes of cultures containing 1×10^7 viable cells were centrifuged at 1000 rpm for 5 mins. Supernatants were collected and stored at -20°C. Pellets were resuspended with 900 µl lysis buffer containing protease inhibitor and chilled on ice for 15 minutes before storing at -20°C.

2.3.8.2 Bradford Assay Determination of Protein Concentration

Lysates were diluted (1:20) with Milli-Q water and applied to a 96-well plate in triplicate, along with a range of 8 protein standard concentration solutions (BSA 0 – 400 μg). 200 μl Bradford reagent was then added to each well and after 5 minutes, the plate absorbances were read at a wavelength of 595 nm. Protein mass (μg) of each sample was determined using the gradient and intercept of the calibration curve given by the protein standards, applied to the average absorbance of each triplicate.

2.3.8.3 Protein Sample Preparation

20 μg of total protein for each sample was mixed with either reducing (per 10 mL: 2.4 mL 1 M Tris-HCl pH 6.8, 4 mL glycerol, 0.8 g SDS, 1 mL β -mercaptoethanol, 4 mg bromophenol blue, 2.6 mL ddH₂O) or non-reducing (per 10 mL: 2.4 mL 1M Tris-HCl pH 6.8, 4 mL glycerol, 0.8 g SDS, 4 mg bromophenol blue, 3.6 mL ddH₂O) loading dye at a 1:3 ratio (dye: sample). Samples were then boiled at 98°C for 10 minutes and centrifuged at 13,000 xG for 15 seconds.

2.3.8.4 Exosome Sample Preparation

For reduced preparations of exosomes, recovered from cell culture, loading dye (per 10 mL: 2.4 mL 1 M Tris-HCl pH 6.8, 4 mL glycerol, 0.8 g SDS, 4 mg bromophenol blue, 3.6 mL ddH₂O) was mixed with 1 M DTT at a ratio of DTT 1:4 dye immediately prior to sample prep. This DTT-loading dye was then added to neat exosome sample at a ratio of dye 1:3 sample. Samples were then boiled at 98°C for 10 minutes and centrifuged at 13,000 xG for 15 seconds.

2.3.8.5 SDS-PAGE (Gel Electrophoresis)

Polyacrylamide gels were cast using 1 mm cassettes with a 5% polyacrylamide stacking gel layer and either an 8%, 10% or 12% polyacrylamide resolving gel layer (Table 2.11). Gels, once loaded with samples and a protein ladder (Fisher PageRuler™ Plus Protein Ladder) were run in electrophoresis tanks with 1X SDS running buffer (10X: 144.4 g glycine, 10 g SDS, 30 g Tris in 1 litre ddH₂O, pH 8.8) at 100 V for 30 minutes followed by 150 V for 90 minutes.

Table 2.12: Composition of the varying percentage of polyacrylamide gels used in SDS page. Each column represents volumes required to make 4 gels.

Components	Gel Layer Polyacrylamide Percentage			
	5% (Stacking)	8% (Resolving)	10% (Resolving)	12% (Resolving)
30% Polyacrylamide (37.5:1)	3.4 mL	8.53 mL	10.7 mL	12.8 mL
1M Tris Buffer (pH 6.8)	2.5 mL	0	0	0
1.5M Tris Buffer (pH 8.8)	0	8 mL	8 mL	6.3 mL
10% SDS	200 µl	320 µl	320 µl	320 µl
10% Ammonium Persulphate	200 µl	320 µl	320 µl	320 µl
TEMED	20 µl	32 µl	32 µl	32 µl
ddH ₂ O	13.6 mL	14.8 mL	12.7 mL	10.5 mL

2.4 Analysis & Purification Techniques

2.4.1 Western Blotting

2.4.1.1 Protein Transfer from Gel to Membrane

After gel electrophoresis, protein was transferred from the polyacrylamide gels to nitrocellulose membranes via a current of 0.75 mA for 1 hour at 4°C whilst submerged in 1X transfer buffer (20% methanol, 10% 10X buffer: 15 g tris, 72 g glycine, 10 g SDS per litre).

2.4.1.2 Membrane Immuno-Blotting

After protein transfer, nitrocellulose membranes (blots) were washed in 1X TBS-T (1% Tween-20, 10% 10X TBS pH 7.6: 24.2 g Tris, 80 g NaCl per litre) then blocked in 5% milk-TBS-T (w/v) at room temperature for 30 minutes. Blots were then transferred to primary antibody solutions appropriately diluted in 5% BSA-TBS-T (w/v) as appropriate (Table 2.12) and incubated at 4°C overnight on a shaking apparatus. After primary antibody incubation, blots received 5 x 5-minute washes with 1X TBS-T and were then incubated

with the corresponding secondary antibody (Table 2.12) (unless primary antibody was HRP-conjugated) diluted 1:1000 in 5% milk-TBS-T for 1 hour on shaking apparatus at room temperature. A final set of 5 x 5-minute washes were then carried out and 1 mL of ECL reagent was applied to blots for 5 minutes before developing the images.

2.4.1.3 Dot Blots

Sample loading onto nitrocellulose membrane was conducted by transferring 50 μ L of neat cell culture from 96-well plates into the 96-wells of a microfiltration blotting device (Bio-Rad Bio-Dot[®] apparatus) that had nitrocellulose membrane which had been submerged in 1X TBS buffer before placement in the device. Once samples were applied, the base connector was attached to a vacuum pump and the valve opened to produce suction on the membrane until all samples were drawn through the membrane into the base plate wells. The nitrocellulose membrane was then carefully removed from the apparatus and the standard western blot protocol (see section 2.4.1.2) was applied to complete the procedure.

2.4.1.4 List of Antibodies used in this Study

The antibodies used throughout the work described in this thesis are described in Table 2.12 below.

Table 2.13: List of primary and secondary antibodies (including product codes) and each of the corresponding recommended dilution factors and (when applicable) secondary antibody types for western blotting (WB) and Immunofluorescence (IF).

Antibody	Brand/ Product Code	Use/ Dilution Factor	Secondary Antibody Type
<i>Primary Antibodies</i>			
Anti-GFP	Research Monoclonal Antibody Service, (CRUK)	WB, 1:5000	Anti-mouse
Anti-mCherry	Abcam, ab167453	WB, 1:2000	Anti-rabbit
Anti-Heavy Chain (Fc)	Sigma, 29764	WB, 1:4000	Anti-rabbit
Anti-Light Chain (κ)	The Binding Site, AP015	WB, 1:10000	N/A*
Anti-Light Chain (λ)	The Binding Site, AP017	WB, 1:10000	N/A*
Anti- β -actin	Sigma, A5441	WB, 1:5000	Anti-mouse
Anti-Ubiquitin	Abcam, ab19247	WB, 1:1000	Anti-rabbit
Anti-CD63	Santa Cruz, sc-365604	WB, 1:1000	Anti-rabbit
Anti-CD81	Santa Cruz, sc-166029	WB, 1:1000	Anti-rabbit
Anti-CD9	Abcam, ab263019	WB: 1:1000	Anti-rabbit
Anti-HIS	Sigma, SAB1305538	WB, 1:1000	Anti-mouse
Anti-Heavy Chain	Abcam, ab200699	IF, 1:100	Anti-mouse
Anti-Light Chain (κ)	Origene, AP21453AF-N	IF, 1:100	Anti-goat
Anti-Light Chain (λ) FITC conjugate	Origene, AP3205FC-N	IF, 1:10	N/A*
Anti-Calnexin	Abcam, ab22595	IF, 1:100	
<i>Secondary Antibodies</i>			
Anti-mouse HRP conjugate	Sigma, A4416	WB, 1:1000	N/A*
Anti-rabbit HRP conjugate	Sigma, A6154	WB, 1:1000	N/A*
Anti-mouse FITC	Sigma, F0257	IF, 1:100	N/A*
Anti-rabbit FITC	Sigma, F9887	IF, 1:100	N/A*
Anti-mouse TRITC	Sigma, T5393	IF, 1:100	N/A*
Anti-rabbit TRITC	Sigma, T5268	IF, 1:100	N/A*
Anti-goat AlexaFluor647	Abcam, ab150131	IF, 1:200	N/A*
Anti-mouse AlexaFluor647	Abcam, ab150115	IF, 1:200	N/A*

* HRP-conjugated, no further antibody required.

2.4.2 Confocal Microscopy

Cell cultures were adhered and fixed to coverslips for visualisation of fluorescence of antibody-conjugated fluorescent tags via a Zeiss™ Confocal Microscopy and edited for comparison using Zen® Black Zeiss™ software.

2.4.2.1 Cell Culture & Adherence to Coverslips

Cells at a density of 2×10^5 cells/mL were grown on round 13 mm coverslips (coated with poly-L-lysine) in 24 well plates and incubated at 37°C for 1 hour to allow adherence to take place.

2.4.2.2 Cell Fixation: Methanol Protocol

After removal of the culture medium and a PBS wash, ice cold methanol was applied to each coverslip to fix and permeabilise the adhered cells, and then rinsed again with PBS.

2.4.2.3 Cell Fixation: Polyformaldehyde Protocol

After removal of the culture medium and a PBS wash, chilled 4% paraformaldehyde (PFA) was applied for 2 minutes. The PFA was then aspirated and a 0.1% Triton solution applied for 2 minutes. After aspiration of the Triton, two PBS washes were applied to remove any residual PFA or Triton solutions.

2.4.2.4 Antibody Conjugation

After fixation, 250 µL of blocking solution (3% w/v BSA in PBS) was applied to the coverslips and incubated at room temperature for 20 minutes. They were then incubated each with 25 µL of primary antibody (Table 2.12), overnight at 4°C. Using a washing solution of 0.1% Tween-PBS (v/v) the coverslips were then washed 4 times for 5 minutes each by transferring across wash solution droplets. They were then, in low light conditions, incubated with 25 µL of an appropriate secondary antibody dilution (Table 2.12), for 2 hours at room temperature. Continuing in low light conditions, the coverslips were then washed 4 more times with wash solution as before and 50 µL of DAPI stain (10 mg/mL) was applied before washing a further three times. Coverslips

were mounted onto microscope slides using ProLong™ Diamond Antifade Mountant ready for imaging via a confocal microscope.

2.4.3 Enzyme-Linked Immunosorbent Assay (ELISA)

2.4.3.1 Capture Antibody Plate Coating

96-well plates were pre-coated overnight at 4°C with 100 µL per well of coating buffer (0.8 g Na₂CO₃, 1.47 g NaHCO₃, per 500 mL H₂O, pH 7.0) containing 1.66 µL/mL of capture antibody, IgG F(ab)₂ (goat, anti-human).

2.4.3.2 Blocking

Plates were then washed twice with wash buffer (5.84 g NaCl, 1.15 g Na₂HPO₄, 0.29 g NaH₂PO₄·H₂O, 3.72 g EDTA, 200 µL Tween-20, 10 mL L-butanol, per 1 L H₂O, pH 7.2) and then incubated for 1 hour at room temperature with 200 µL per well of blocking solution (1.59 g Na₂CO₃, 2.93 g NaHCO₃, per 1 L H₂O) which for every 200 mL had 1 g casein dissolved in overnight.

2.4.3.3 Sample & Detection Antibody Application

Samples were diluted using sample buffer (12.1 g Tris (HCl), 5.84 g NaCl, 200 µL Tween-20, 1 litre H₂O, pH 7.0) and plated out as well standards (serially diluted known concentrations of IgG diluted into sample buffer) after two washes to remove the blocking solution. Samples and standards were incubated for 1 hour at room temperature, followed by two washes and then application of 100 µL per well of secondary antibody (anti-human kappa light chain (bound and free) HRP conjugate raised in goat), diluted in wash buffer (1:10,000), and incubated for a further 1 hour at room temperature.

2.4.3.4 Substrate Application and Absorbance Measurement

Plates were washed a final two times before applying 100 µL of TMB substrate solution (0.01 % (w/v) TMB in DMSO) to each well and allowed to develop for 15 minutes. The reaction was stopped using 50 µL 2.5 M H₂SO₄ per well and the absorbance measured at 450 nm wavelength.

2.5 Antibody Recovery & Purification

2.5.1 Fast Protein Liquid Chromatography

Purification of the anti-dengue antibodies was carried out via fast protein liquid chromatography (FPLC) using an ÄKTA™ pure system and attached Fraction Collector F9-C (GE Healthcare) connected to a 5 mL HiTrap Mab Select™ SuRe™ (Cytiva) column for protein A chromatography. For each run, 2 L of 'Buffer A' (100 mM Sodium Phosphate (68.4 mL 1 M monobasic NaH_2PO_4 , 31.6 mL 1 M dibasic Na_2HPO_4); 150 mM NaCl in ddH₂O, pH 7.2) and 1 L 'Buffer B' (100 mM Sodium Citrate in ddH₂O, pH 3.5) were prepared and 0.22 µm filtered for connection to the ÄKTA™ pure system.

The column was first equilibrated with 10 column volumes (CV) of Buffer A at a flow rate of 2.5 mL/min. Then the full volume of the sample was applied to the column and flow-through collected via the fraction collector. After sample application, a column wash was executed using 10 CV of Buffer A at a flow rate of 2.5 mL/min, with flow-through also collected. To elute captured antibody from the column, 10 CV of Buffer B at a flow rate of 2.5 mL/min was applied and the resulting elutions collected as 6x 8.5 mL fractions in 15 mL falcon tubes containing 900 µl neutralising buffer (1 M Tris-HCl, pH 9). The column was then washed with 5 CV of Buffer A at a flow rate of 2.5 mL/min and flow-through collected. The system was reset and the column re-equilibrated before running subsequent samples for purification.

2.5.2 Product Concentration and Buffer Exchange

To concentrate and buffer exchange the purified antibody elution fractions recovered from the FPLC, 50 KDa molecular weight cut-off (MWCO) spin filters were used. 1X PBS was first applied to the filter and centrifuged at 4,000 rpm for 5 minutes to wet the filter membrane. The initial PBS was then discarded from the collection tube and each elution fraction of purified antibody transferred into the spin filter. This was then centrifuged at 4,000 rpm for 5 minutes until the fractions reach approximately the 200 µL mark on the filter. The liquid from the collection tube was discarded and fresh PBS buffer added to the filter. This was then centrifuged again at 4,000 rpm for approximately 2 minutes, until the filter level reached between the 300 – 500 µL mark. The resulting volume still

retained in the filter section, containing antibody in PBS, was then transferred to a sterile tube for storage at -20°C.

2.5.3 Exosome-Specific Protocols

2.5.3.1 Exosome Recovery from Cell Cultures

For the recovery of exosomes from cell culture supernatant, the Invitrogen™ Total Exosome Isolation (from cell culture media) Kit was used following the recommended protocol provided by the manufacturers.

2.5.3.2 Dynamic Light Scattering Analysis

Dynamic Light Scattering (DLS) analysis of exosome samples was performed on a Litesizer 500 (Anton Paar) particle analyser using pre-set parameters for the detection of exosomes. Each exosome sample was diluted 1:20 into a clean cuvette with 0.22 µm filtered 1X PBS and gently mixed using a pipette tip before loading into the analyser. Each sample was analysed as a series of 10 measurements which were recorded and downloaded for further analysis using Microsoft Excel software.

Chapter 3: Exploring the *In Vitro* Loading of Proteins of Interest into Exosomes as a Novel Cell-Based Vaccine Platform in Chinese Hamster Ovary Cells

3.1 Introduction

The work described in this chapter set out to explore the generation of recombinant exosomes bearing proteins of interest from CHO cell cultures. In order to direct proteins into exosomes two targeting vector design strategies were investigated. The first was based around a ubiquitin tagging strategy previously demonstrated by Cheng *et al* (2015) in which ubiquitin fusion proteins were expressed in human embryonic kidney (HEK293) cells to generate exosomes carrying target ubiquitin-fusion proteins. The first section of this chapter details the generation of ubiquitin-fused fluorescent reporters eGFP and mCherry in pcDNA 3.1 hygromycin (+) vectors, their expression in CHO cells and the profiling of the resulting exosomes generated. Both fluorescent reporters were fused with either a C-terminal or N-terminal ubiquitin tag sequence which encodes a single unit of the ubiquitin molecule, or an N-terminal polyubiquitin tag sequence (Figure 3.).

The second targeting vector strategy was based around the exosome surface display technology described by Stickney *et al* (2016) which harnesses the known exosome marker protein tetraspanins CD9, CD63 and CD81, to create tri-fusion proteins. When these are expressed in HEK293 cells this reportedly leads to the generation of recombinant exosomes which are able to display fluorescent tags both internally and externally by fusing the sequences at the transmembrane domain loops of each tetraspanin. The second section of this chapter therefore details the creation of exosome markers fused with the fluorescent reporter eGFP in pcDNA 3.1 hygromycin (+) vectors, their expression in CHO cells and the profiling of the resulting exosomes generated. Initially, the exosome markers CD63, CD81 and Tsg101 were explored with either a C-terminally or N-terminally fused eGFP sequences to first test expression with

a single fluorescent reporter, but after poor expression of the Tsg101 fusions in transient cultures this was no longer considered as a strategy for targeting in order to focus on variations of tetraspanin-based targeting. These variations included both CD63 and CD81 with either an N-terminal eGFP fusion or a mid-gene eGFP fusion at the second external transmembrane loop domain (Figure 3.).

Each strategy was initially assessed by producing the appropriate vectors and then analysing protein expression and targeting to exosomes via transient transfection of the vectors. Western blotting was first used to assess if the fusion proteins were expressed by/in CHO cells at detectable levels. After this, stable cell line pools were created and exosomes harvested from these when cultured under batch conditions using the commercially available Total Exosome Isolation Kit™ (ThermoFisher). The exosome preparations were then profiled by a number of analytic approaches including western blotting, confocal microscopy and size distribution analysis via dynamic light scattering (DLS).

The intention of the work described in this chapter was to generate a proof-of-concept vector design that could be easily modified to express and target to exosomes other proteins of interest as a potential novel vaccine platform. Included in this overall aim was the analysis of the differences between exosomes produced by the targeting vectors within each strategy, as well as comparison between the two overall strategies, to identify the most effective vector composition for recombinant exosome production in an industrially relevant mammalian cell line.

3.2 Results

3.2.1 Generation of Ubiquitin-fusion vectors

To express each ubiquitin-target fusion protein the commercially available pcDNA 3.1 Hygromycin (Invitrogen) plasmid was used. The genes for the target ubiquitin-target fusions were inserted into the multiple cloning site where transcription is driven by an enhanced CMV promoter with a bGH polyA signal at the 3' end (Fig 3.1).

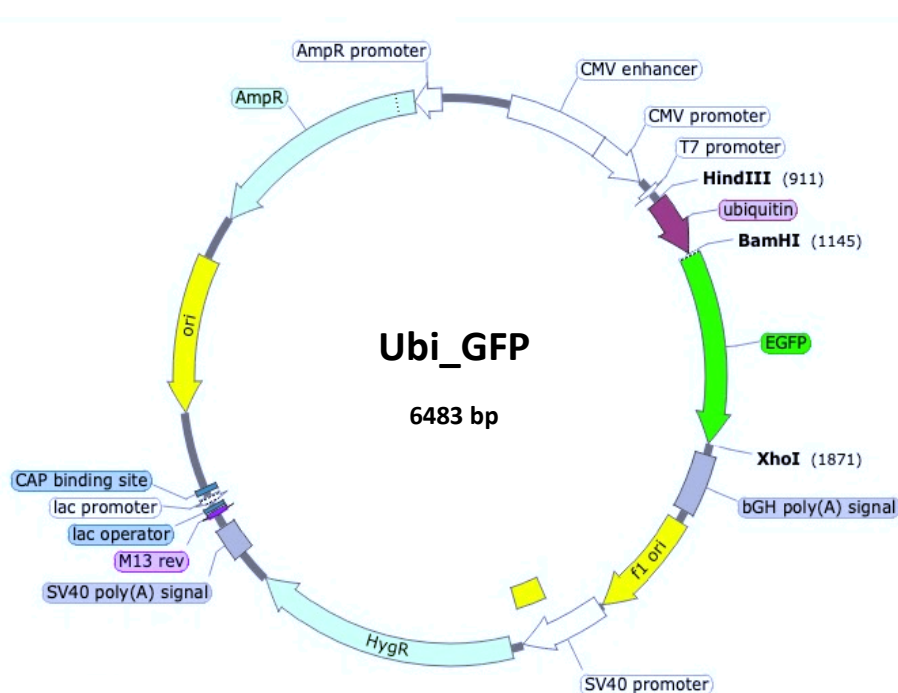


Figure 3.1: Vector map showing the 3.1 hygro plasmid backbone layout with the Ubi_GFP fusion protein gene sequence inserted at the multiple cloning site which is flanked by an enhanced CMV promoter and a bGH polyA terminator. The vector also includes ampicillin and hygromycin resistance genes for use in bacterial and mammalian systems respectively.

The CHO polyubiquitin (NCBI Ref: NM_001244381.1) sequence and a single ubiquitin unit sequence (taken from NCBI Ref: NW.003711167.1) were codon optimised for *Cricetulus griseus* (Chinese hamster) codons, synthesised as geneART strings (ThermoFisher) and subsequently cloned into the vector using traditional PCR restriction enzyme digest and ligation procedures as outlined in Chapter 2. The fluorescent reporters eGFP and mCherry were also inserted into the vectors on their own as controls in the orientations shown in Figure 3.2 via the same procedures, with stop codons removed between the fusion sequences to ensure translation into a single peptide.

CONTROL CONSTRUCTS



TARGETING CONSTRUCTS

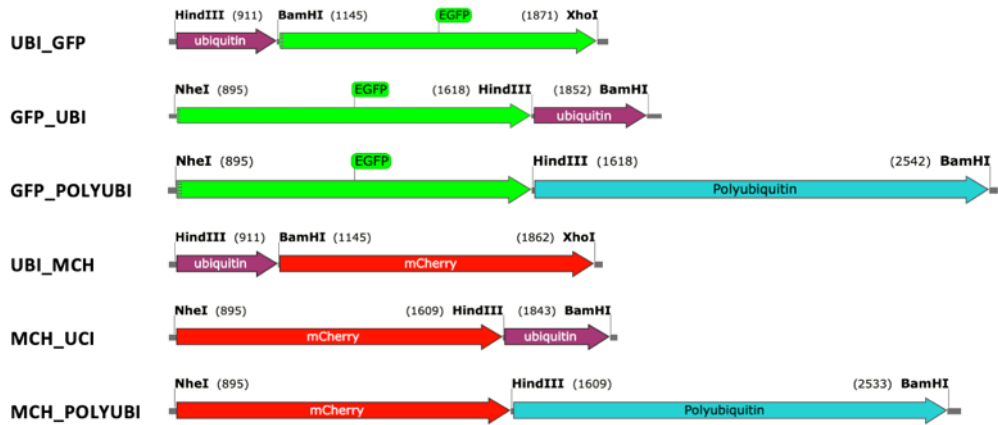


Figure 3.2: Schematic of the ubiquitin-based vector cassettes and respective control vector cassettes created and described throughout this chapter. Also shown are the restriction enzymes insertion sites used to clone sequences into the 3.1 hygro plasmid backbone. The annotated name used for each construct is shown on the left of each schematic.

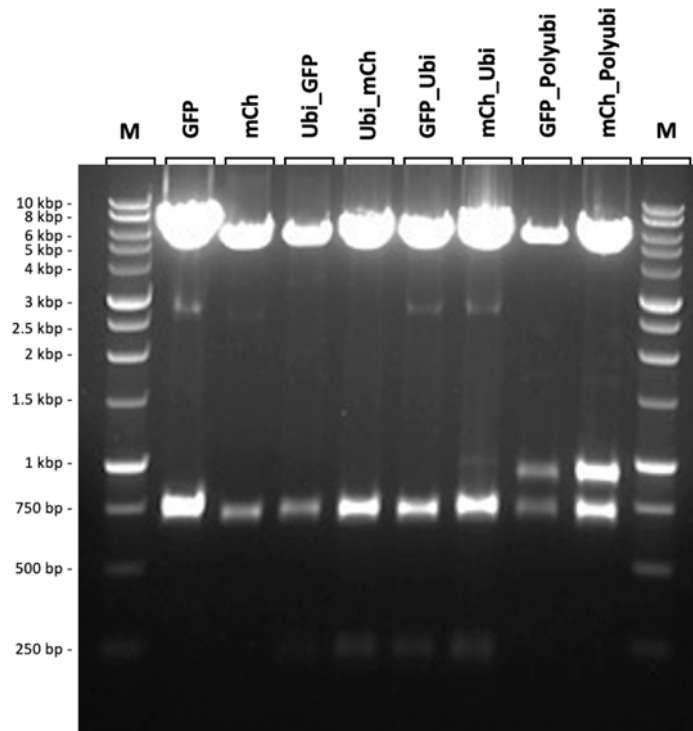


Figure 3.3: 1% Agarose DNA gel analysis of test restriction digests from finalised cloned ubiquitin vectors with 1 kbp DNA markers (M). Restriction enzymes for each lane: GFP (HindIII, BamHI); mCh (BamHI, XhoI); Ubi_GFP and Ubi_mCh (HindIII, BamHI, XhoI); GFP_Ubi, mCh_Ubi, GFP_Polyubi, mCh_Polyubi (NheI, HindIII, BamHI).

Each vector was then sequenced by Sanger sequencing to confirm the sequences contained no mutations or frame shifts and amplified for transfection in *E. coli* cultures, using maxi-prep kits (QIAGEN) to extract the plasmids. Each amplified vector was then re-screened via DNA digest to confirm the amplification process was successful (Figure 3.3) using enzymes which flank both ubiquitin and the reporter genes for each construct to release the target insert. The digests were run on 1% agarose gels and imaged under UV light to allow visualisation of the dropout band patterns with expected band sizes of 239 bp for ubiquitin, 711 bp for GFP and mCherry, and 918 bp for polyubiquitin (Figure 3). Once confirmed as authentic, the vectors were transiently transfected, via electroporation, into CHO-S cells for initial assessment to determine if each fusion protein was expressed correctly by the cells before moving onto stable cell line construction.

3.2.2 Expression Assessment of Ubiquitin-Fusion Vector Expression in CHO Cell Lines

3.2.2.1 Transient Expression

After transfection of 20 µg of non-linearised plasmid DNA for each vector into naïve CHO-S cells, cultures were incubated for 4 days before harvesting cell pellets to analyse protein expression via western blot. After pellet lysis and sample preparation with a non-reducing loading buffer, SDS-PAGE gels were blotted and antibody probed with anti-mCherry and anti-GFP with an anti-β-actin probe as a loading control (Figure 3.4). The mCherry signal was present in all lysates that had been transfected with a vector containing the mCherry sequence, including the mCherry-only positive control line, and appeared in multiple band sizes which were absent in the negative controls. mCherry-fusion lysate lanes showed bands at around 27 kDa (red arrow, Fig 3.4A), the expected size for mCherry alone, and a band of approximately 35 kDa – the expected size of a mCherry-ubiquitin fusion protein (blue arrows, Fig 3.4A).

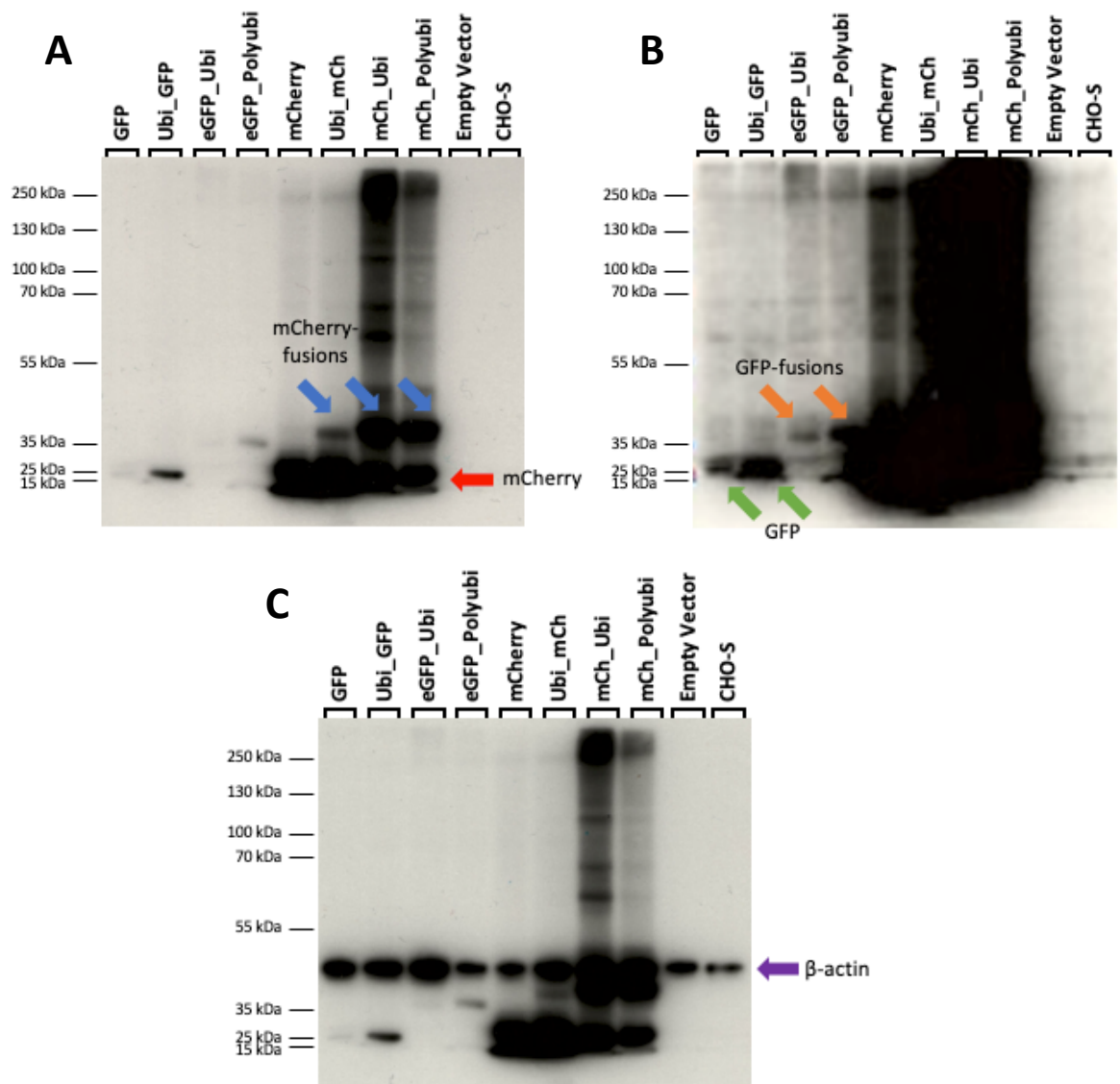


Figure 3.4: Western blotting of cell pellet lysates collected from transient transfection of CHO-S cells with ubiquitin-based fusion sequence containing vectors. (A) Anti-mCherry probe, 10 second exposure, red arrow shows mCherry size, blue arrows show mCherry-fusion bands. (B) Anti-GFP probe, 90 second exposure, green arrows show GFP sizes, orange bands show GFP fusion bands. (C) Anti- β -actin probe, 10 second exposure, purple arrow shows β -actin band sizes.

The GFP signal was also present in all lysates which had been transfected with a vector containing the GFP sequence, including the GFP-only positive control line, and absent in the negative controls (Figure 3.4). The GFP signal also showed two band sizes of around 27 kDa and 35 kDa which would correspond to GFP alone (green arrows, Fig 3.4B) or a GFP-ubiquitin fusion (orange arrows, Figure 3.4B), respectively. There were also bands at higher apparent molecular weights present on the blots in lanes for each of the

reporter gene-fusions, including the single-ubiquitin transfected lysates as well as the polyubiquitin transfected lysates (Figure 3.4). An anti- β -actin probe of the blot showed relatively even loading across all lanes (purple arrow, Figure 3.4C) and confirmed that the decreased signal seen with anti-GFP probing was not due to increased loading amounts. Residual banding patterns on the blot from the anti-mCherry (Fig 3.4A) and anti-GFP probes (Figure 3.4B) were also visible but were attributed to re-probing the same blot again without stripping the blot beforehand. Overall, expression was observed from ubiquitin-based vectors and the appropriate controls and therefore each vector was taken forward to create stable cell lines for analysis of any exosome populations produced.

3.2.2.2 Generation of CHO Cell Pools Stably Expressing Target Ubiquitin-Fusion Proteins for Exosome Delivery

3.2.2.2.1 Confocal Microscopy analysis of the stable CHO-S cell pools

For each ubiquitin-based vector, stable cell lines were constructed using linearised plasmid DNA of each ubiquitin-based vector as outlined in Chapter 2. After application of antibiotic (hygromycin B) selection and a recovery period in static incubation, samples were taken from each cell pool construction for confocal microscopy imaging to assess the fluorescence levels and determine if each construct transfection resulted in successful protein expression.

Multiple images (n=3) were taken under 63x magnification with oil immersion on a ZEISS confocal microscope for each stable cell pool with DAPI solution applied to slides during preparation as a nuclear stain. DAPI staining fluorescence was captured using the 405 nm laser (blue channel), along with images captured from either the 458 nm laser (green channel) or the 514 nm laser (red channel) to assess GFP or mCherry fluorescence, respectively, dependant on cell pool. Channel images were then merged using ZEISS ZEN software to create overlay images for comparison and assessment of fluorescence (Fig 3.5 & 3.6).

GFP and mCherry fluorescence was present in all GFP and mCherry stable cell pools, respectively, whilst there was no signal in the negative control (CHO-S host) as expected. Thus, the microscopy provided indicative evidence that all stable cell pool selections had successfully resulted in the isolation of cells where the plasmid DNA was integrated into the genome and thus the stable pools were able to express the target fluorescent reporter and reporter-fusion genes. The GFP-only positive control and the GFP_Ubi pool showed the strongest fluorescence overall for the GFP cell pools (Fig 3.5), whilst the mCherry pools all showed good expression in cells with mCherry expressed and some very strong fluorescence in cells of the mCh_Ubi pool (Fig 3.6).

With the confirmation of expression from these images, the stable cell pools were moved to shaking culture conditions and passaged until viabilities >90% were achieved when they were banked and used for exosome isolation and further analysis.

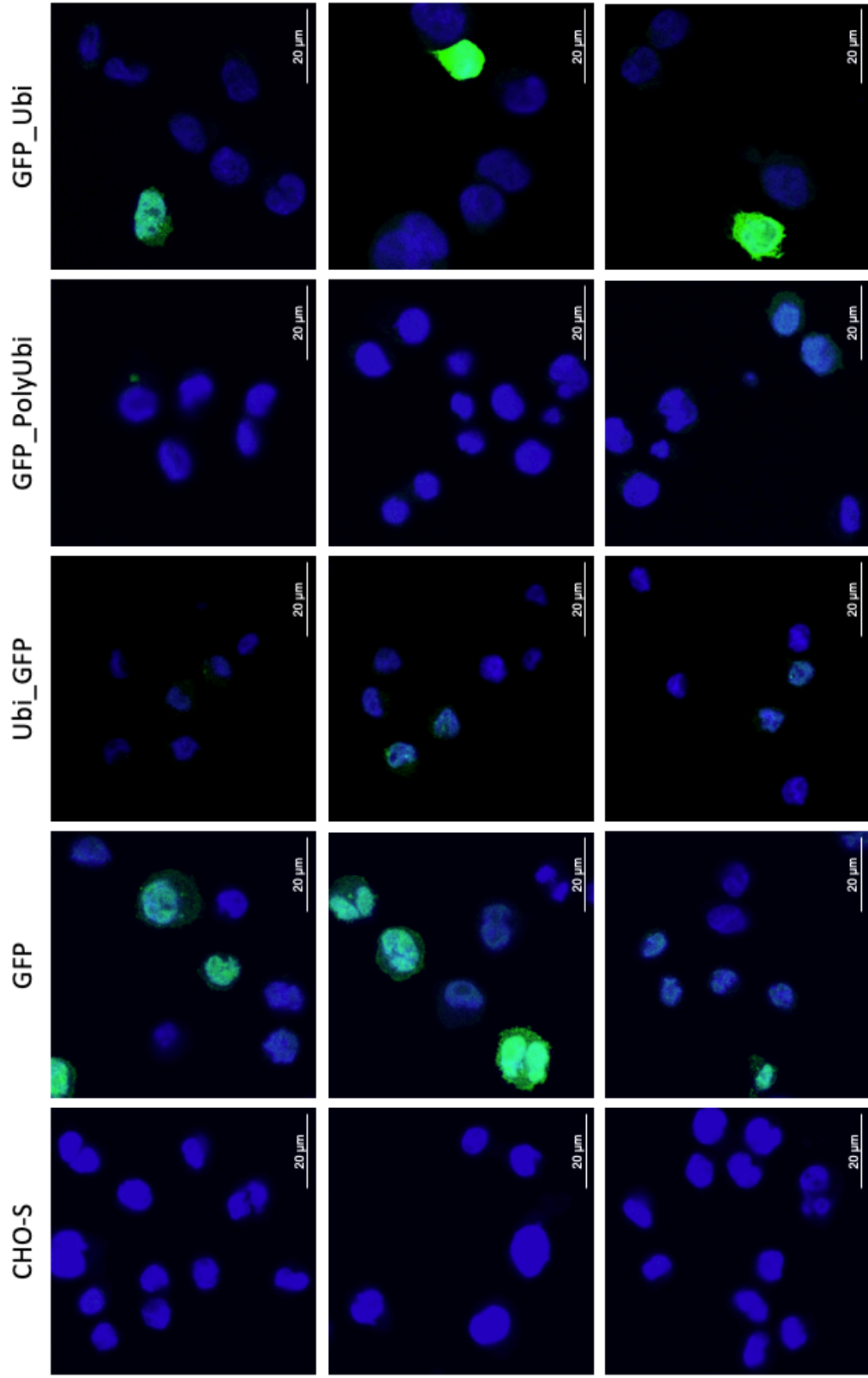


Figure 3.5: Merged channel ZEISS confocal microscopy images for each ubiquitin-based GFP stable cell line, alongside positive (GFP) and negative (CHO-S) control cell lines, in triplicate, showing the co-localisation of the nucleus (blue) and GFP (green) at 63x magnification plus oil immersion.

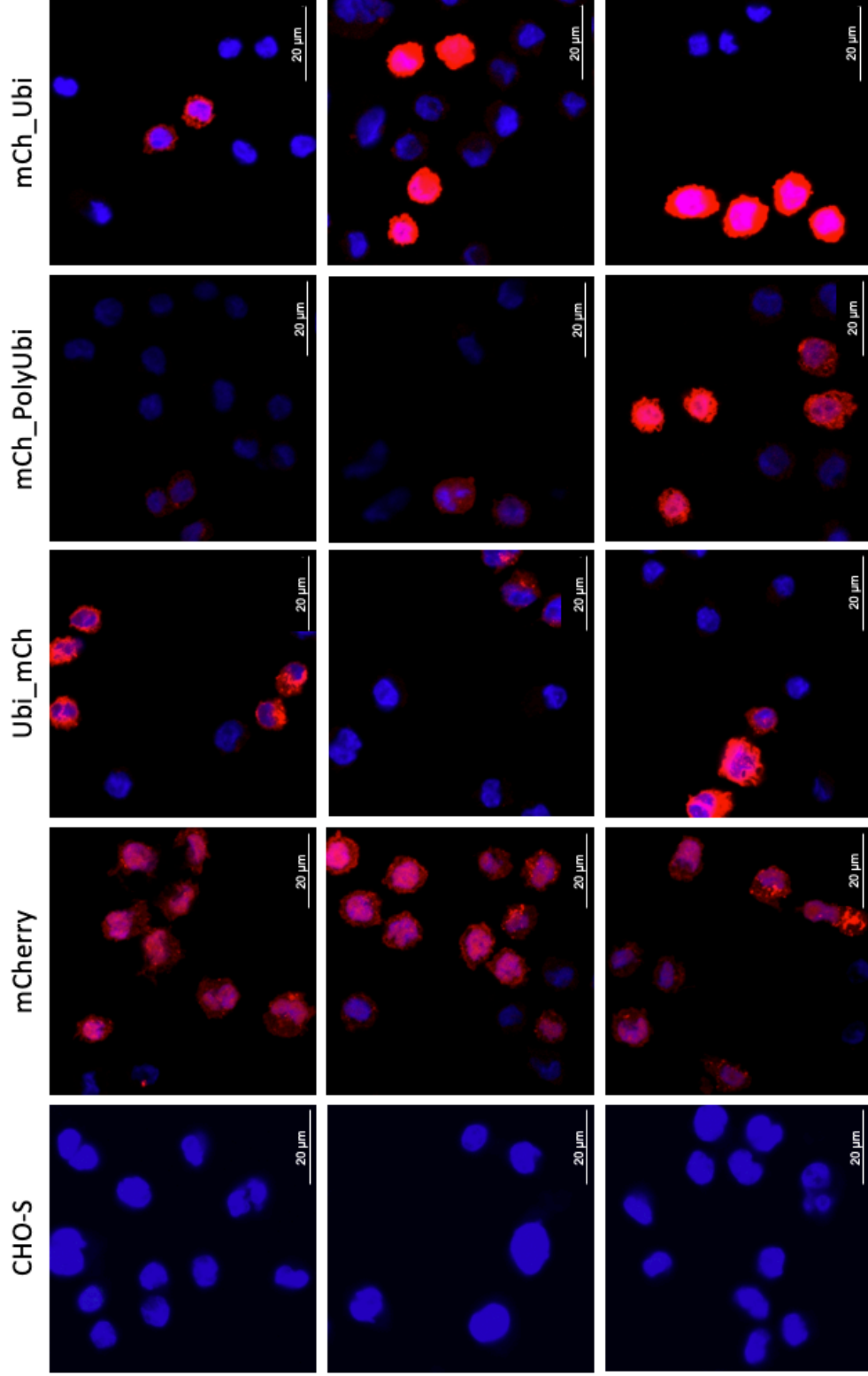


Figure 3.6: Merged channel ZEISS confocal microscopy images for each ubiquitin-based mCherry stable cell line, alongside positive (mCherry) and negative (CHO-S) control cell lines, in triplicate, showing the co-localisation of the nucleus (blue) and mCherry (red) at 63x magnification plus oil immersion.

3.2.2.2.2 Western Blot Analysis of Ubiquitin-Fusion Protein Expression in Stable Pools

Once stable pool cultures for all ubiquitin-fluorescent fusion targets were fully recovered and transferred to shake culture conditions, 10 mL of each cell line was grown for 4-days at 220 rpm, 37°C in 50 mL falcon tubes and cell pellets and supernatants were collected and exosome preps carried out on 5 mL of the supernatant to produce 250 µL exosome-PBS suspensions. In order to visualise banding on western blots for the exosome suspensions, a DTT-reducing buffer was added and the samples boiled to lyse the vesicles. This sample preparation was applied to all sample types from all cell lines and loaded onto SDS-PAGE gels followed by transfer to nitrocellulose for western blot analysis (Fig 3.7).

When probed with anti-GFP, the GFP cell pools all showed a similar banding pattern in the exosome suspension lanes with bands around 250 kDa present as well as smaller bands near to 130 kDa in size. There were also bands in the cell pellet lysate lanes of 25 kDa for the GFP-only control line and the Ubi_GFP cell line, and 35 kDa for GFP_polyubiquitin and GFP_ubiquitin cell lines (Fig 3.7). Though the bands present in the exosome suspensions were unexpectedly high, these were not present in the control samples and suggest successful translation and targeting of the target reporter gene into exosomes for each ubiquitin-fusion cell pool. However, the high molecular weight nature of the discrete bands observed could suggest multimerization of the target-fusion when in exosomes. Alternatively, they could be an artifact of intrinsic peroxidase activity due to lengthy exposure times used on these blots.

In the anti-mCherry probe, all mCherry cell pools showed a strong two-band pattern in the cell pellet lysate lanes, though these two bands were around 20 and 30 kDa for the mCherry-only control pool and the Ubi_mCh cell pool, with higher molecular weight bands of around 25 kDa and 35 kDa observed in the mCh_polyubiquitin and mCh_ubiquitin cell pool samples (Fig 3.7). This difference in observed band size between the differently orientated constructs mirrors that of the GFP cell pools but for mCherry was present as a two-band pattern. Unlike the GFP cell pools, the signal for mCherry was not present in all exosome suspension samples with bands of approximately 25 kDa in

the ubi_mCh and mCh_ubi cell pools but these were not observed elsewhere. Additionally, these bands in the ubi_mCh and mCh_ubi exosome cell pools were much closer to the predicted molecular weight expected for mCherry which suggests that these constructs successfully targeted the reporter into the exosomes produced by this

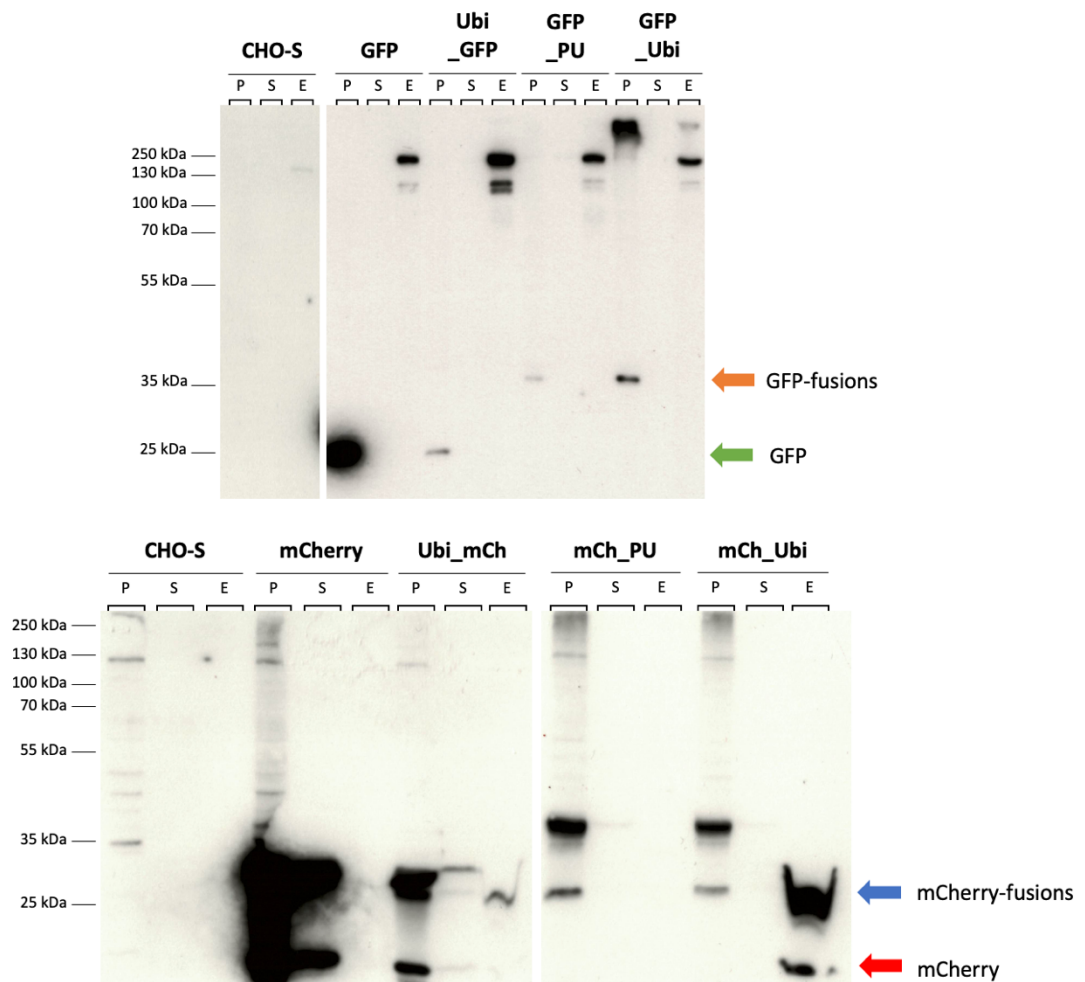


Figure 3.7: Western blots of cell pellet lysates (P), supernatants(S) and exosome suspensions (E) for each of the ubiquitin stable cell pools, each prepared with a DTT-reducing buffer and boiled prior to loading. (A) Anti-GFP probe, 10 minute exposure (B) Anti-mCherry probe, 1 minute exposure.

cell line.

3.2.2.2.3 DLS analysis of exosome preparations

Although the characterisation and definition of exosomes is far from exact, one of the major defining characteristics of exosomes agreed upon throughout the literature is that

of their size having to be between 50 – 150 nm in diameter. Therefore, the size of the vesicles isolated using the commercially available exosome isolation kit was assessed. To complete the assessment of the size distribution of exosomes isolated from the CHO-S host cell line and those from engineered pools designed for recombinant exosome production, the exosome-PBS suspensions isolated from cell culture supernatants were diluted with filtered PBS and examined via dynamic light scattering (DLS) on a Litesizer™ 500 (Anton Paar) instrument. In generating the size data, 10 measurement series were taken for each of the exosome suspensions, averaged, graphed and a log₁₀ transformation applied to produce a particle size distribution analysis for the exosome isolates from each cell line (CHO-S host) or stable cell pool.

The particle diameter size observed in the CHO-S host control exosome suspension showed a singular peak with a maximum around 261 nm, around the expected exosome size range (Fig 3.8A & Fig 3.9A). The presence of a singular peak in the host control provides evidence that the commercial kit exosome isolation method did not co-isolate any larger extracellular vesicles and any deviation was a result of differing exosome sizes. The GFP-only control (Fig 3.8B) showed a singular peak in the expected exosome size range but with a much wider distribution than the host control profile, suggesting the presence of larger particles. The mCherry-only control (Fig 3.9B) showed a much wider particle size distribution with no major defined peak in the exosome range. It should be noted that there were peaks <10 nm throughout the data that are likely to be dust or debris.

The size distribution from cell pools generated with GFP as a reporter all showed two main peaks, one large peak similar to that seen in the profile of CHO-S exosomes and another lower intensity peak at larger size confirming the presence of much larger particles with a diameter range between 1000-10,000 nm (Fig 3.8). The second peak at the larger particle size distribution had almost equal intensity in the Ubi_GFP exosome suspension with the first peak in exosome size range, but not in GFP_Ubi and

GFP_Polyubi suspensions where it was much reduced in size compared to the very predominant CHO-S exosome peak near 100-1000 nm.

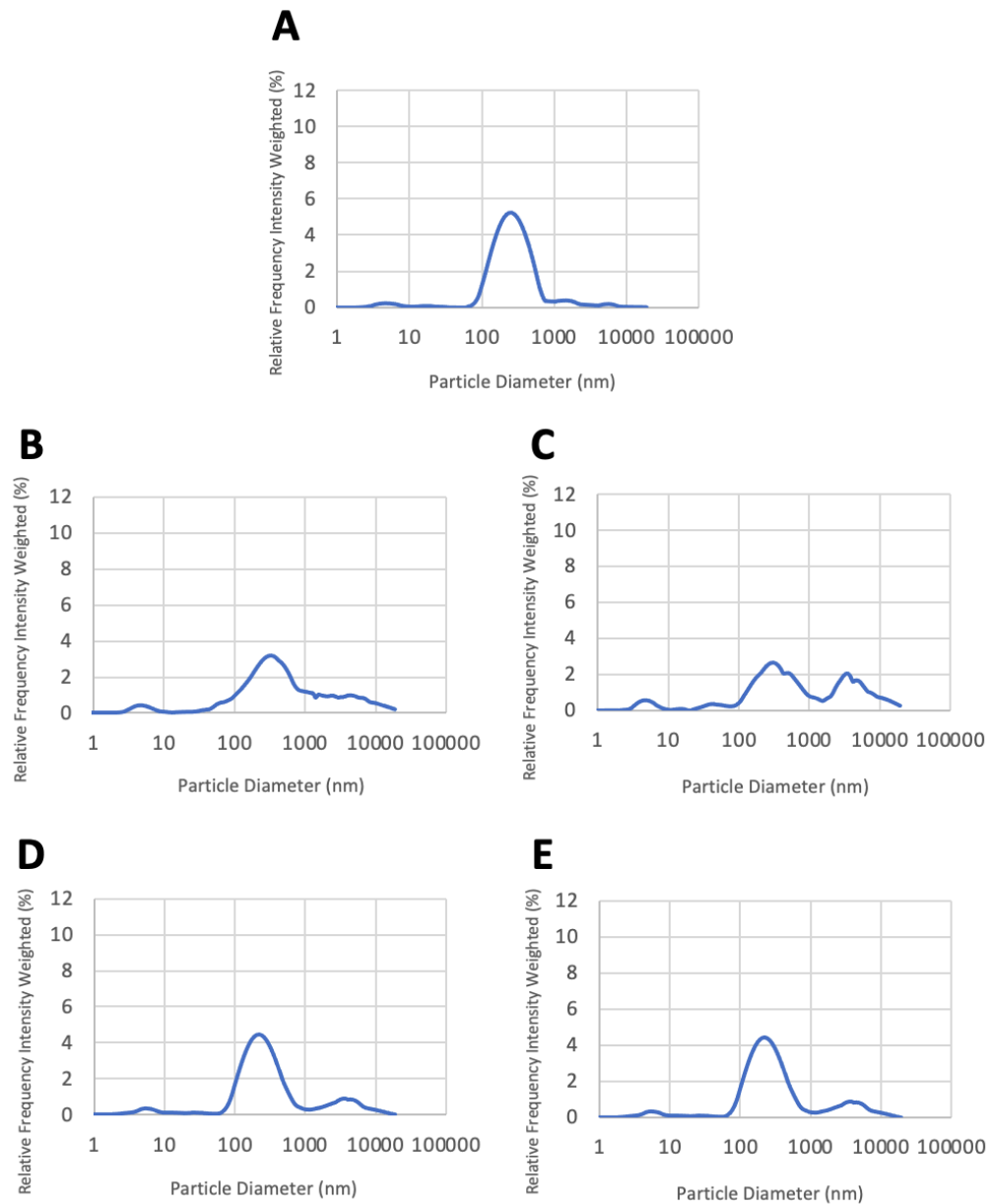


Figure 3.8: Particle size distribution of exosome preparations from for the ubiquitin-based GFP stable cell pool exosome suspensions, including (A) negative control (CHO-S), (B) positive control (GFP only), (C) Ubi_GFP, (D) GFP_Ubi, and (E) GFP_Polyubi exosome suspensions. Each graph shows the average DLS measurements (n=10) for relative intensity frequency weight (%) vs. particle diameter (nm) with a log10 scale applied.

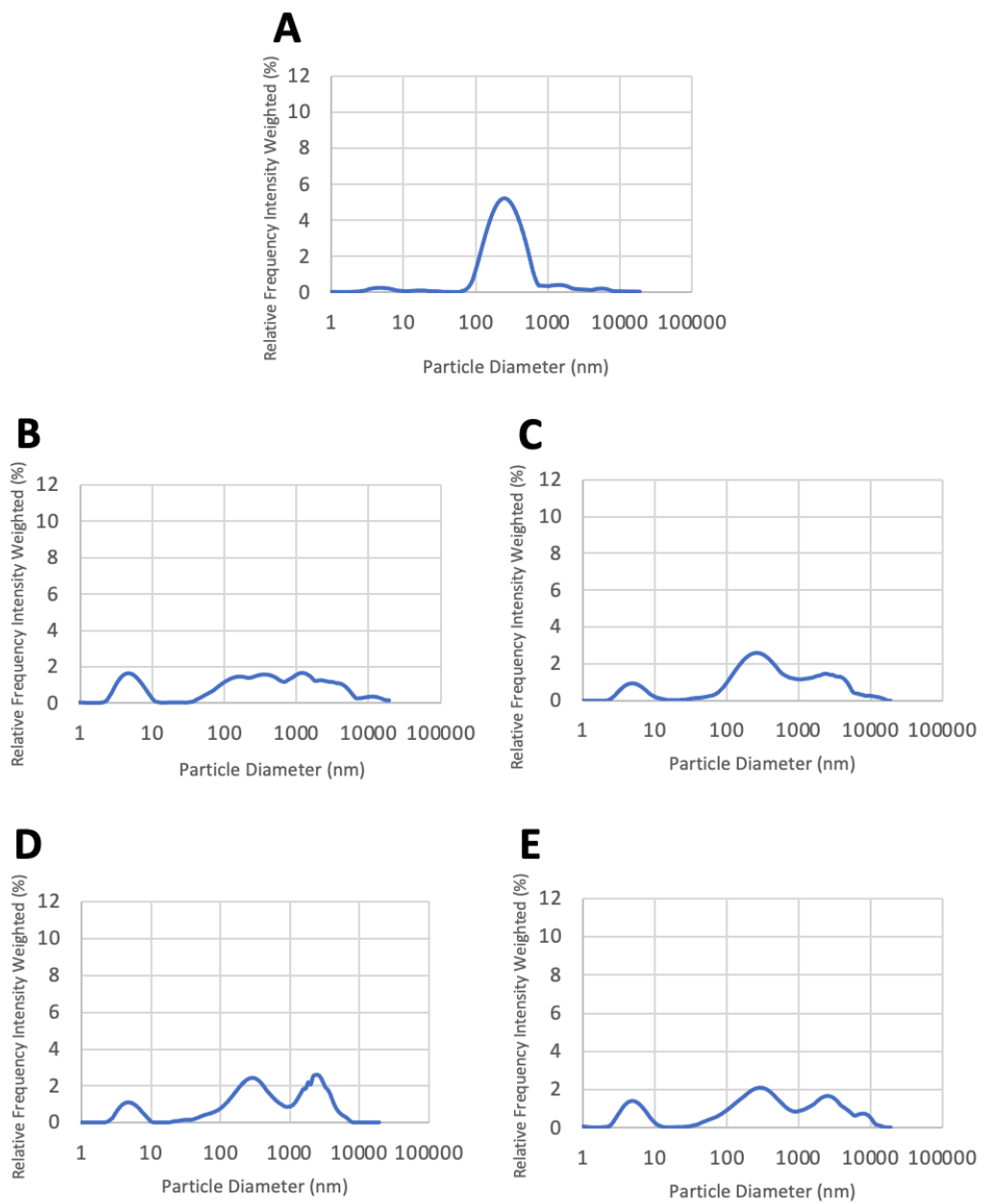


Figure 3.9: Particle size distribution of exosome preparations from for the ubiquitin-based mCherry stable cell pool exosome suspensions, including (A) negative control (CHO-S), (B) positive control (mCherry only), (C) Ubi_mCh, (D) mCh_Ubi, and (E) mCh_Polyubi exosome suspensions. Each graph shows the average DLS measurements ($n=10$) for relative intensity frequency weight (%) vs. particle diameter (nm) with a log₁₀ scale applied.

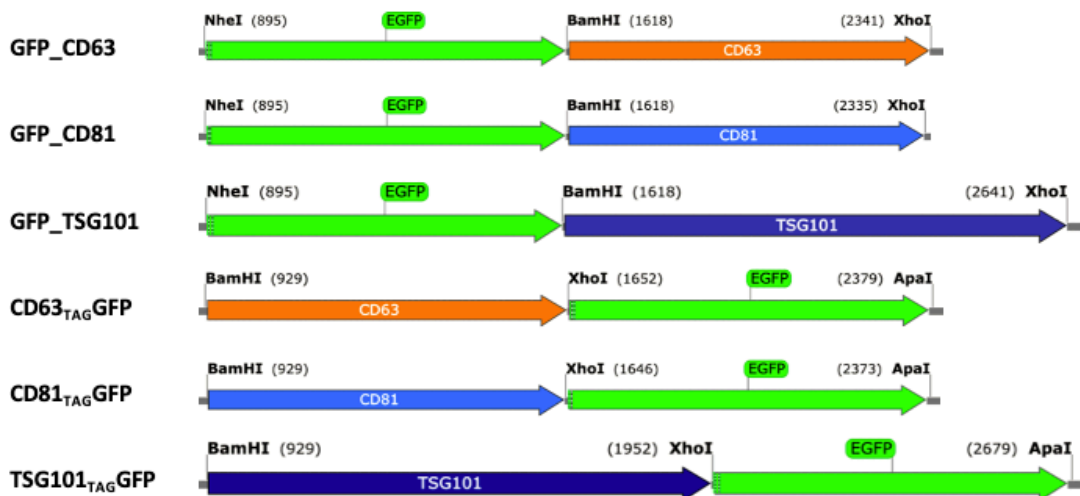
A similar second peak indicating the presence of larger particles was present in the analysis of exosome suspensions from the cell pools generated using mCherry as a reporter but these profiles lacked the distinct CHO-S exosome peak near 100-1000 nm which was instead part of a wider series of size distributions observed (Fig 3.9). These profiles were more similar to the particle size distributions observed in the Ubi_GFP exosome suspension (Fig 3.8C).

3.2.3 Generation of Exosome Marker-Fluorescent Report Fusion Based Vectors

CONTROL CONSTRUCT



TAGGED GENE FUSION CONSTRUCTS



MID-GENE FUSION CONSTRUCTS

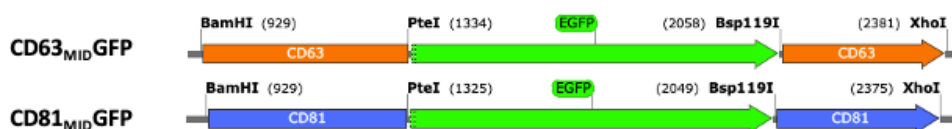


Figure 3.10: Schematic of the exosome marker-eGFP based vector cassettes and respective control vector cassette created and used throughout this chapter. Also shown are the restriction enzymes insertion sites used to clone sequences into the commercially available 3.1 hygromycin plasmid backbone.

In order to explore the exosome marker-based display strategy for expression of genes of interest on recombinant CHO-S exosomes, two sets of genetic constructs were designed. The first set included the C-terminal and N-terminal tagging of exosome markers CD63, CD81 and Tsg101 with fluorescent reporter GFP and removal of any stop codons between the two for translation as a single fusion peptide (Fig 3.10).

Due to the tetraspanins transmembrane nature and mid-gene extracellular loop domains, a second set of constructs encoding the CD63 and CD81 genes with a GFP sequence was created, intended for external display of the GFP from the exosome (Fig 3.10). To design these constructs, sequences for CD63 and CD81 were taken from NCBI Reference Sequence XM_003506207.5 and XM_027408862.2, respectively, then codon-optimised for *Cricetulus griseus* (CHO) codons and re-designed to include a mid-gene cloning site at the extracellular loop domains of each before being synthesised as DNA strings (Twist Biosciences). The mid-gene cloning site design included two restriction enzyme recognition sites, *PteI* and *Bsp119I* (ThermoFisher FastDigest), which flanked a filler sequence to allow dual enzyme binding at close proximity in double digests (Fig 3.11). The CHO Tsg101 sequence was identified as NCBI Ref: XM_027410472.1 from which primers were designed and successfully cloned out of synthesised cDNA from genomic DNA extracted from CHO-S cells.

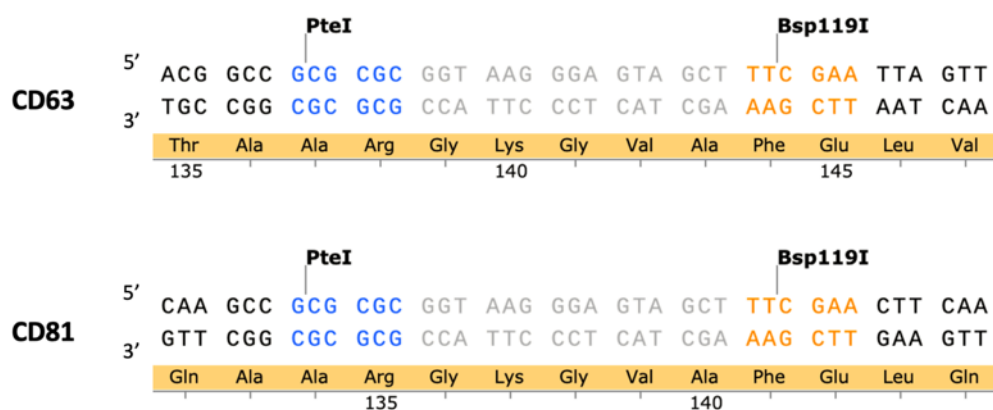


Figure 3.11: Double-stranded DNA and amino acid view of the restriction site sequence inserted into both CD63 and CD81 to create a mid-gene cloning site. The sequence is comprised of restriction sites *PteI* (blue) and *Bsp119I* (orange) flanking a filler sequence (Gly, Lys, Gly, Val, Ala) and is inserted after Ala-136 and Ala-133 for CD63 and CD81, respectively.

To express each of these fusions, and the GFP control, the pcDNA 3.1 Hygromycin (Invitrogen) plasmid was used and the sequences inserted into the multiple cloning site as described earlier in this chapter (Fig 3.1) for the ubiquitin-based vectors. For mid-gene fusion constructs, once the DNA string was inserted into the pcDNA 3.1 Hygromycin vector, the GFP gene sequence was inserted via digestion and ligation at the mid-gene restriction sites. Tagged fusion constructs were tagged with a GFP sequence by cloning in via the appropriate vector multiple cloning sites for each construct (Fig 3.10). Each vector was then sequenced by Sanger sequencing to confirm the sequences contained no mutations or frame shifts and amplified for transfection in *E. coli*. Each amplified vector was then re-screened via DNA digests to confirm the amplification process was successful (Fig 3.12). Due to each segment of the tetraspanin-based vectors having near-equal sequence length, whole gene fusion cassettes were digested out of the finalised vectors and compared with a control vector containing only the tetraspanin sequence from earlier in the cloning process (Fig 3.12A & Fig 3.12B), whilst the Tsg101 vectors were able to be fully digested to show both sequences (Fig 3.12C).

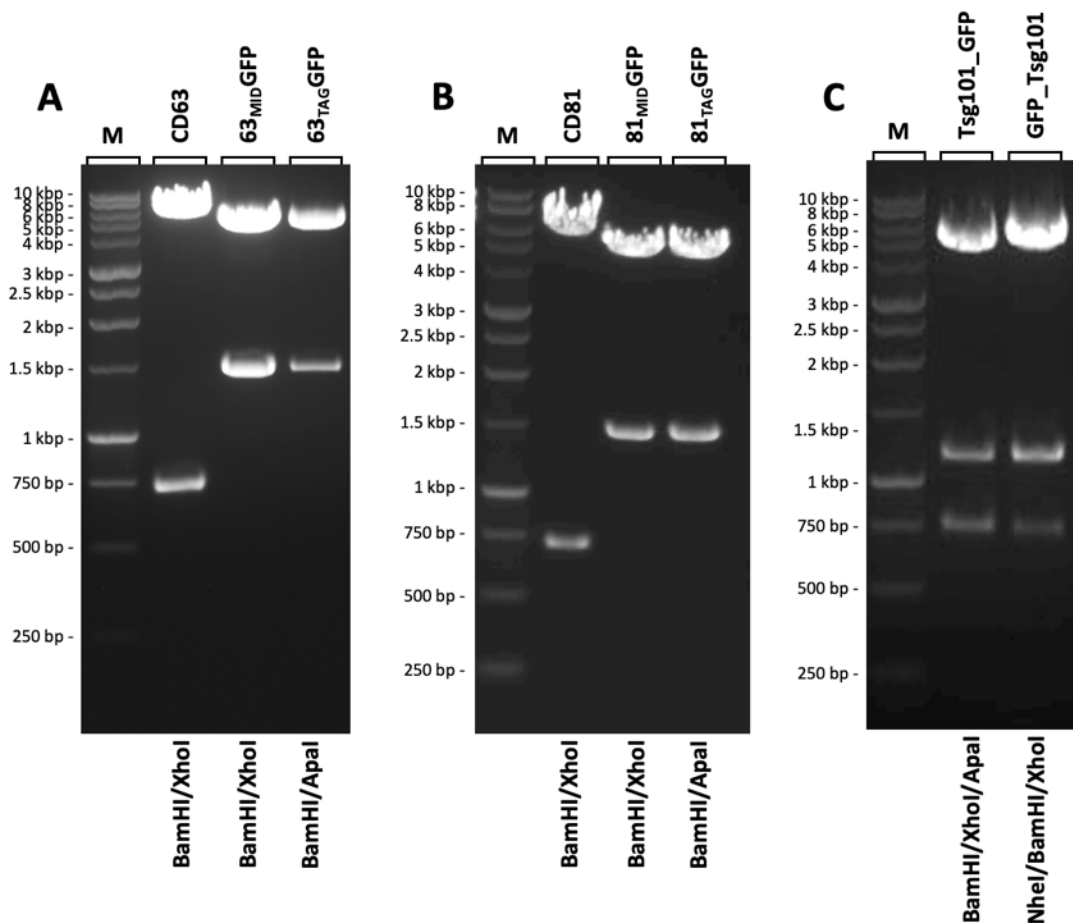


Figure 3.12: 1% Agarose DNA gel analysis with 10 μ L volumes of test restriction digests from finalised cloned exosome marker-based vectors with 1 kbp DNA markers (M). (A) CD63-only vector digest vs CD63-GFP fusion digests. (B) CD81-only vector digest vs CD81-GFP fusion digests. (C) Tsg101 full vector cassette digests.

All digests were run on 1% agarose gels via electrophoresis and imaged under UV light to produce dropout band patterns with band sizes of 717 bp for CD63, 711 bp for CD81, 1,175 bp for Tsg101 and 711 bp for GFP. Once confirmed, the vectors were each transiently transfected, via electroporation, into CHO-S cell cultures for initial screening to assess if each fusion protein was expressed correctly by the cells before moving onto stable cell line construction.

3.2.4 Expression Profiles of Exomarker-based Vector Cell Lines

3.2.4.1 Transient Expression of exosome marker-eGFP fusions in CHO cells

After transfection of 20 μ g of non-linearised plasmid DNA for each of the exosome marker tagged gene fusion vectors into naïve CHO-S cells, cultures were incubated for 4 days before harvesting cell pellets to analyse protein expression via western blot. After pellet lysis and sample preparation with a non-reducing loading buffer, 20 ng of each lysate was loaded into SDS-PAGE gels for electrophoresis and subsequent western blotting, probing with anti-GFP and an anti- β -actin probe as a loading control (Fig 3.13).

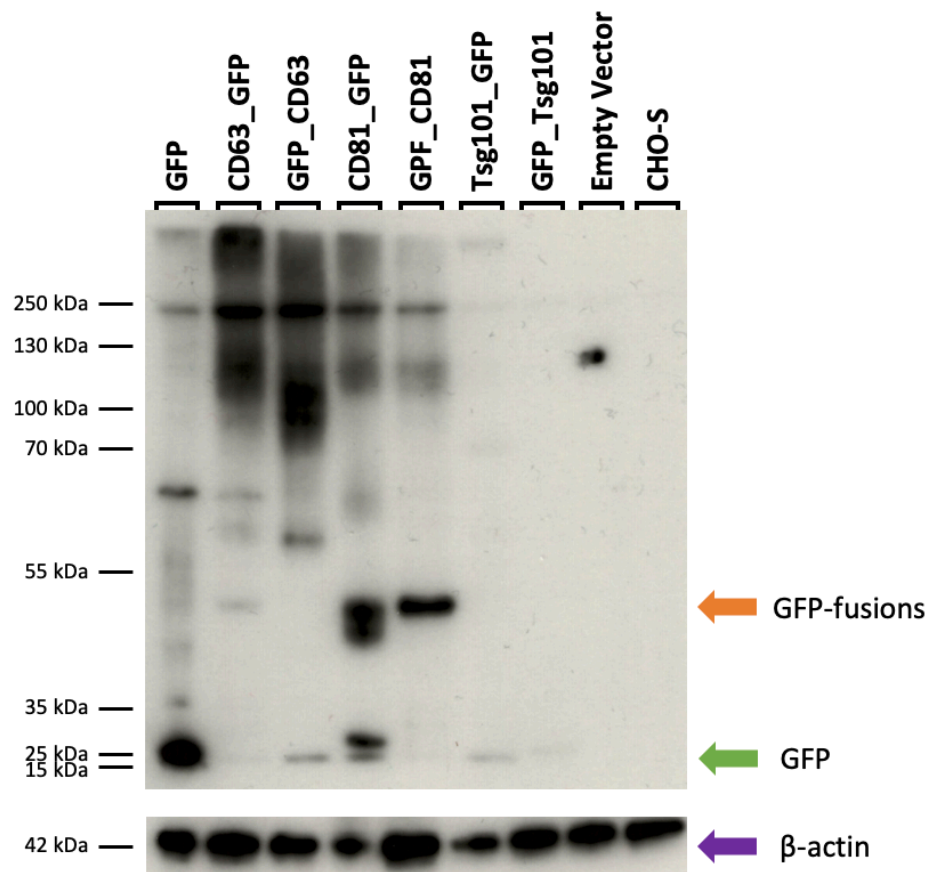


Figure 3.13: Western blot analysis of cell pellet lysates collected from transient transfection of CHO-S cells with exosome marker-based vectors. (Top) Anti-GFP probe, 3 minute exposure. (Bottom) Anti- β -actin probe, 10 second exposure.

The GFP signal was present in the lysate of cells transfected with the GFP-only vector and absent from both the empty vector-transfected and non-transfected CHO-S cell culture lysates as expected. From the exosome marker-based transfections, tetraspanin CD63 and CD81 transfections showed bands at various molecular weights but for Tsg101 transfections there was little to no signal with the anti-GFP antibody. Bands at expected

molecular weights for GFP (27 kDa), CD63 (26 kDa) and CD81 (26 kDa) were present in all tetraspanin transfection lysates as well as a higher band just below 55 kDa, the approximate size of the GFP-fusion products expected from these vectors. In addition to this, there was also a band observed in the GFP-only and tetraspanin transfection lysates at around 250 kDa (Fig 3.13). The loading control anti- β -actin probe for the blot showed relatively even loading for each lane. From this data, it was decided that the Tsg101 fusion vectors would not be taken forward in this work due to the extremely low, or lack of any apparent, expression. The other tetraspanin-based vectors showed strong expression and the vectors containing C-terminal GFP tags were taken forward to create stable cell lines alongside the mid-gene fusion tetraspanins. This was done to explore the efficiency of protein targeting into exosomes using transmembrane exosome markers with a reporter designed to display either internally or externally.

3.2.4.2 Generation and Characterisation of Stable CHO-S Cell Pools Expressing Tetraspanin Exosome Marker-eGFP Fusions

3.2.4.2.1 Confocal microscopy analysis of the stable CHO-S cell pools

For the C-terminal GFP-tetraspanin vectors and mid-gene fusion GFP tetraspanin vectors, stable cell pools were constructed using linearised plasmid DNA of each vector as outlined in Chapter 2. After application of antibiotic selection and a recovery period in static incubation, samples were taken from each cell pool for confocal microscopy imaging to assess the fluorescence levels and determine if each construct resulted in successful protein expression.

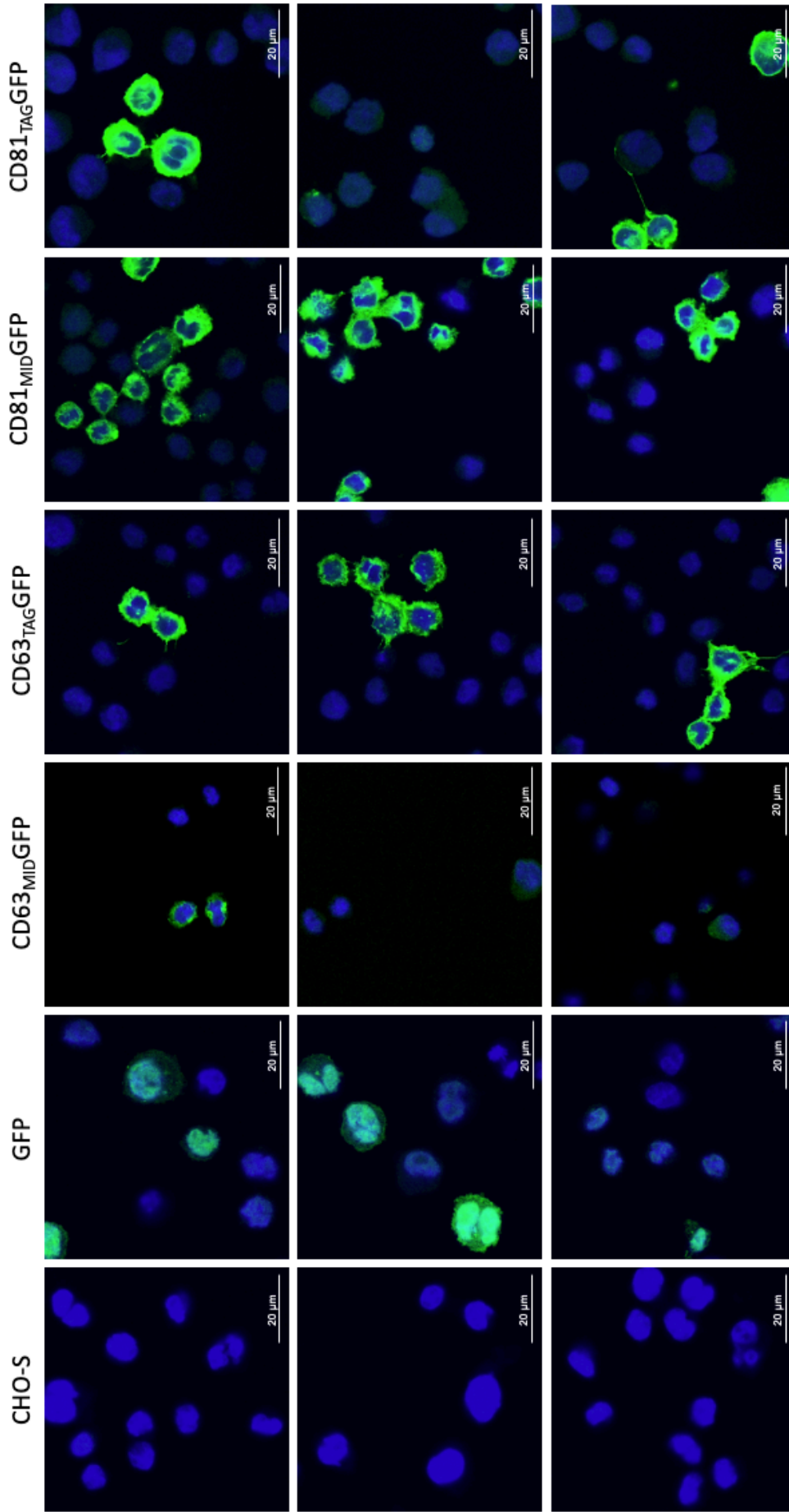


Figure 3.14: Merged channel ZEISS confocal microscopy images for each tetraspanin-based GFP stable cell line, alongside positive (GFP) and negative (CHO-S) control cell lines, in triplicate, showing the co-localisation of the nucleus (blue) and GFP (green) at 63x magnification plus oil immersion.

As previously described in this chapter (Section 3.2.2.2.1), confocal microscopy was carried out for each cell line on a ZEISS confocal microscope under 63x magnification with oil immersion with a DAPI nuclear stain applied to produce multiple images (n=3) per cell line. DAPI staining fluorescence was captured using the 405 nm laser (blue channel), along with images captured from the 458 nm laser (green channel) to assess GFP. Channel images were then merged using ZEISS ZEN software to create overlay images for comparison and assessment of fluorescence (Fig 3.14).

GFP fluorescence was present in all cell pools, except the negative control (CHO-S host) and was indicative that stable integration of the plasmid DNA had been successfully achieved and the antibiotic selection had isolated cell pools that expressed the fusion-fluorescent reporter genes (Fig 3.14). The GFP fluorescence signal was considered strong in all GFP cell pools except CD63_{MID}GFP which had GFP present but at a much lower intensity than in the other samples. The stable cell pools were then moved to shaking culture conditions and passaged until cultures were setup for exosome isolation and further analysis.

3.2.4.2.2 Western Blot Analysis of Tetraspanin-eGFP expression in the Stable CHO-S Pools

Batch cultures were harvested for the collection of cell pellets and supernatants for lysate and exosome preparation on day 4 of culture. The resulting cell pellet lysates, supernatant and exosome-PBS suspensions from each cell line were then reduced using a DTT-based loading buffer and boiled for 10 minutes before loading onto SDS gels for electrophoresis followed by western blotting (Fig 3.15). Using an anti-GFP probe, GFP signal was observed at the expected molecular weight (27 kDa) in the GFP-only positive control lysate and was found in the exosome suspensions of all of the tetraspanin-based cell pools, except the CD63_{TAG}GFP pool, as a distinct band at around 250 kDa in size (Fig 3.15). This band at approximately 250 kDa was also observed in the GFP only exosome preparation. A band was also observed just below 130 kDa in the GFP-only and CD81_{TAG}GFP line exosome suspensions and CD81_{MID}GFP line cell pellet lysate. The exosome suspension for the CD81_{TAG}GFP line also had the band seen in the transient

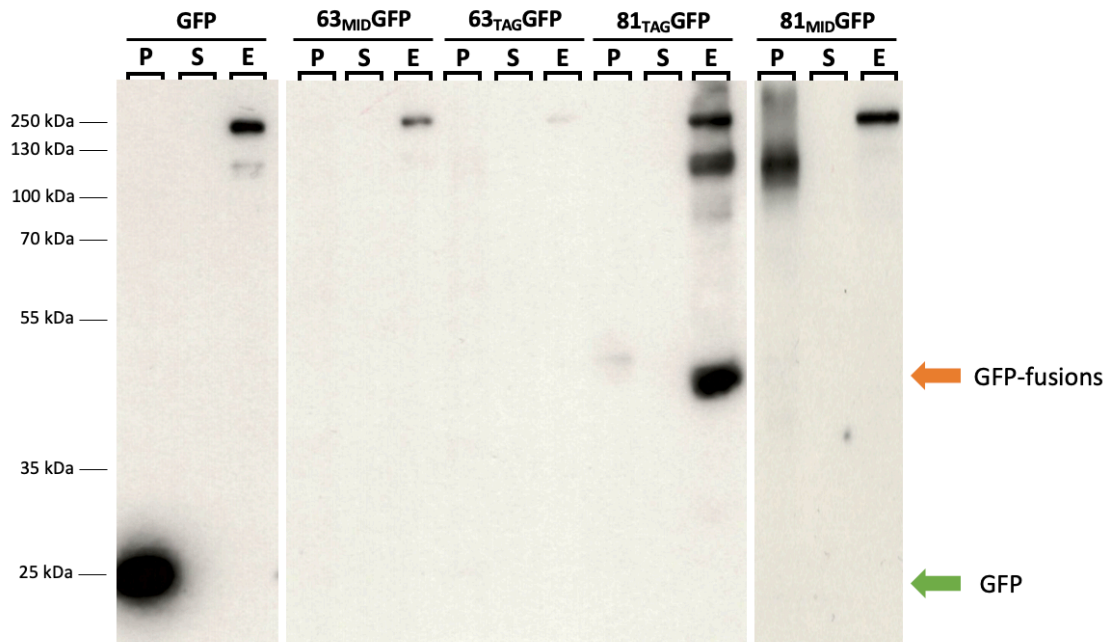


Figure 3.15: Western blots of cell pellet lysates (P), supernatants(S) and exosome suspensions (E) for each of the tetraspanin-based stable cell lines, each prepared with a DTT-reducing buffer and boiled prior to loading, blotted with an anti-GFP probe and exposed for 5 minutes.

data between 35 - 55 kDa consistent with that for the CD81-GFP fusion protein. Overall, the bands present in this data suggest that a distinct GFP multimer is being targeted into the exosomes of each cell pool, including the GFP-only positive control, in an unexpected observation. The nature or makeup of this high molecular weight band is unknown though as previously stated it may be the result of intrinsic peroxidase activity due to the length exposure time of the blot. However, the presence of a band in the CD81_{TAG}GFP line exosome suspension at the approximate expected molecular weight for a CD81-GFP fusion protein, suggests that this approach has successfully facilitated the introduction of the target fusion into the exosome population as the monomer CD81-GFP molecule.

3.2.4.2.3 DLS Analysis of Exosomes from the Different Stable Tetraspanin-eGFP Fusion Protein Cell Pools

Exosome suspensions prepared from each stable cell pool were diluted 1:20 with filtered PBS to a volume of 1 mL and analysed by DLS via a Litesizer™ 500 (Anton Paar) to determine the particle sizes present. The resulting measurements (n=10) of each suspension was averaged, graphed and a log₁₀ applied to produce the particle size

distribution analysis for each cell line exosome suspension (Fig 3.16). Each resulting data set was compared with those generated for the native CHO-S and GFP-only cell line exosome suspensions to assess if the targeting-eGFP fusion proteins affected the size distribution of the exosome populations produced. Each suspension showed a peak around but above 100 nm, the predicted exosome size range. This peak had a much lower intensity in the CD63_{MID}GFP derived samples where there was a very intense peak close to 1000 nm average particle diameter which was not observed in any of the other exosome suspensions (Fig 3.16C). The size distribution across the other tetraspanin-based cell pool exosome suspensions showed some similarity in profile with a peak between 1000 – 10000 nm, which was also previously observed in the exosome suspensions prepared from cell pools using a ubiquitin-based targeting vector system (Section 3.2.2.2.3).

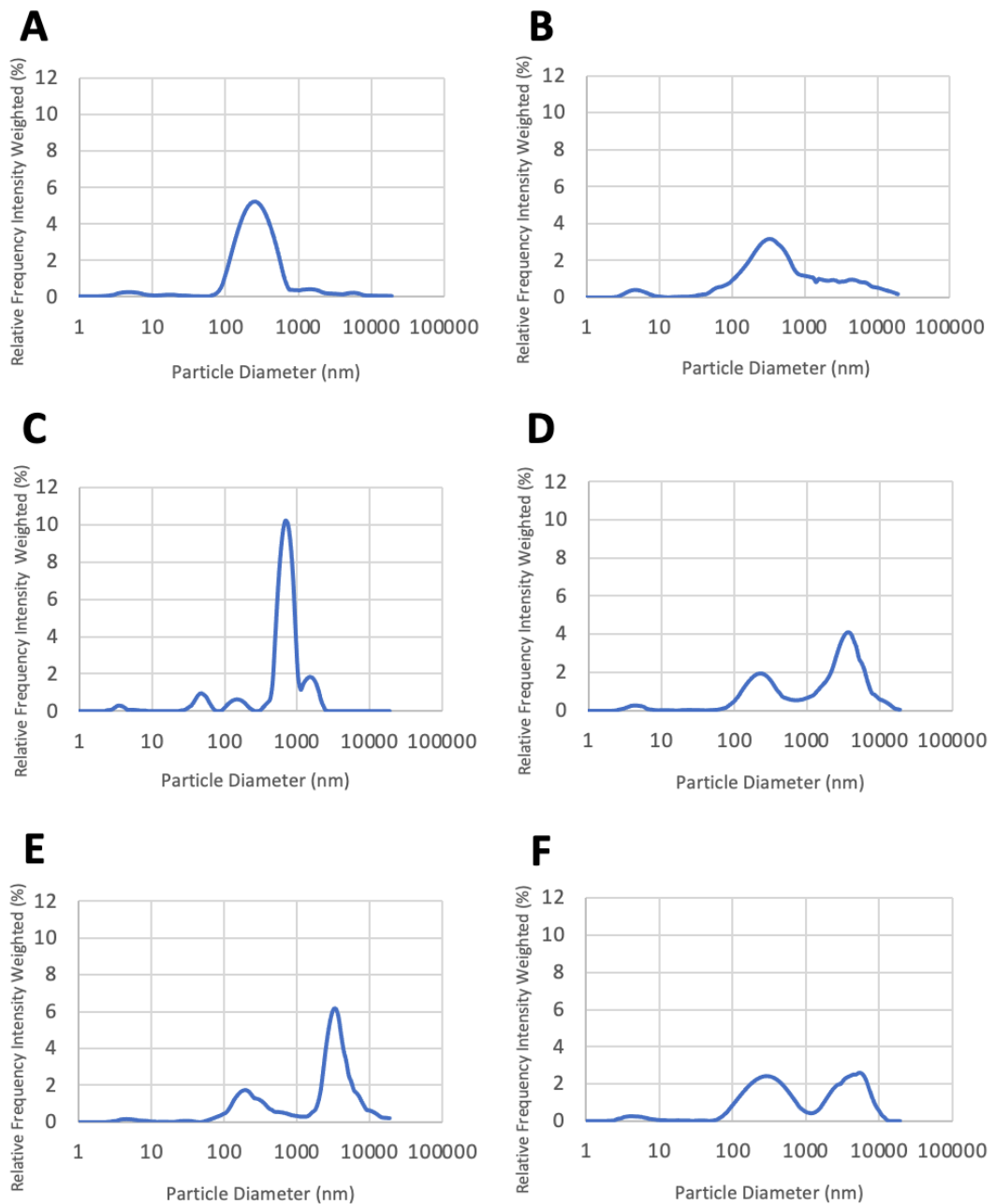


Figure 3.16: Particle size distribution for the tetraspanin-based GFP stable cell line exosome suspensions, including (A) negative control (CHO-S), (B) positive control (GFP only), (C) CD63_{MID}GFP, (D) CD81_{TAG}GFP, (E) CD81_{MID}GFP, and (F) CD81_{TAG}GFP exosome suspensions. Each figure shows the average DLS measurements ($n=10$) for relative intensity frequency weight (%) vs. particle diameter (nm) with a log₁₀ scale applied.

3.3 Discussion

3.3.1 Transient Data

3.3.1.1 Ubiquitin

After transient transfection of the generated ubiquitin fusion proteins described in this chapter into CHO-S cells, western blot analysis of ubiquitin-mCherry fusion proteins (Fig 3.4) confirmed the fusions Ubi_mCh and mCh_Ubi were present as full-length fusions as well as the unfused reporter mCherry. Presence of unattached mCherry is likely to be due to either degradation of some of the fusion protein between the ubiquitin and mCherry portion of the molecule or that only the mCherry portion of the transcript is translated. The mCh_Polyubi protein expression banding pattern in (Fig 3.4) also mirrors the pattern seen in the single-ubiquitin fusion proteins despite polyubiquitin's larger predicted molecular weight. This could be indicative that either the mCherry was the only sequence which was successfully translated in this protein, or that the polyubiquitin, which is made of several small units of ubiquitin which can be broken down (Ohtake *et al.*, 2018), after initial translation as an mCherry fusion underwent rapid degradation and was cleaved the fusion molecule within the cell. Ubiquitin itself is known to attach to proteins in order to facilitate their degradation (Ohtake *et al.*, 2018; Chen, Chen and Huang, 2019) and removal from the cell via vesicles and so it is possible that ubiquitin has promoted degradation of the ubiquitin fusion proteins. However, this would mean that the ubiquitin only portion of the molecule is degraded and the full mCherry left intact. More likely is that only the mCherry is produced (as described above) or the area linking between the mCherry and ubiquitin is susceptible to proteolysis and is thus cleaved. Fusion proteins are often reported to be susceptible to such proteolysis due to presence of cell-derived proteases (Chakrabarti *et al.*, 2016). Transient data analysis of the ubiquitin-GFP fusion proteins (Fig 3.4) showed a very similar pattern of expression between those proteins with the same ubiquitin-to-GFP orientation as seen in the ubiquitin-mCherry fusion proteins. Though overall signal produced by the anti-GFP antibody was weaker than that from the anti-mCherry, this is

likely due to antibody affinities and binding of the secondary rather than any difference in protein expression levels as the GFP and mCherry molecules are similar in size. The similarity between the two sets of ubiquitin-fusions is perhaps not surprising considering the nature of the two fluorescent proteins and similar conclusions with respect to presence of full-length fusion protein and GFP-only sized protein presences.

Both mCherry and eGFP-ubiquitin fusion expression profiles showed stronger full-length fusion proteins for those with an N-terminal reporter orientation with respect to the ubiquitin molecule. This could be indicative that this orientation yields the strongest structural composition for ubiquitin fusions that are the most stable and turned over more slowly than other orientations, or that the mRNA transcript is more stable and hence there is more transcript leading to higher expression or that the transcript is more efficiently translated in the orientation. Interestingly, results reported by Cheng & Schorey (2016) claimed that orientation had no effect on expression of a GFP-ubiquitin fusion proteins produced by transient transfection of HEK293 cells. However, they also observed, though not to a degree of statistical significance, that of the cells transfected with a GFP-ubiquitin fusion, those with C-terminal ubiquitin tagging had the highest transfection efficiency and produced the highest levels of fluorescence (Cheng and Schorey, 2016).

Additionally, in all the lysates of non-control transfected cells a band of varying strength throughout the lanes was present at around 250 kDa. It is possible that this may be due to aggregation or multimerization but the very distinct nature of the band observed is not consistent with general aggregates or multimer formation of a single band of an exact size. Another explanation could be that is the result of the reporter-fusions being incorporated into structures that could not be reduced. Nevertheless, the results from the transient data allowed for the confident assessment that each construct was able to be expressed by CHO-S cells and so could be used to generate stable cell pools for further investigation.

3.3.1.2 Tetraspanins

Transient transfection of CHO-S with tetraspanins-GFP fusions (Fig 3.4) generated in this chapter resulted in varied expression across the different tetraspanins examined. Both CD81-GFP fusions were present at a size which indicated the desired fusion protein product, whilst only the C-terminally fused GFP-CD63 yielded a full-length fusion protein which could indicate that CD81 is the most stable of these tetraspanins for expression as a fusion protein. Both the CD63 and CD81 constructs with a C-terminal GFP tag orientation did not result in proteins approximate to the size of GFP, indicating the intact fusions were the major species produced in this fusion orientation with minimal 'GFP only' from cleavage observed in the ubiquitin-fusion proteins. Based on the promising observations of their transient expression, these two C-terminally tagged tetraspanin constructs were taken forward to create stable cell pools for further investigation alongside another CD63 and CD81 with a mid-gene fusion of GFP configuration which were then generated for exploration of external exosome surface display due the insertion of GFP at an external transmembrane loop domain of each tetraspanin (Stickney *et al.*, 2016).

The other exosome marker-based constructs were designed with the exosome marker Tsg101 and upon blotting with anti-GFP showed little to no expression of any GFP or GFP fusions in the cell lysates. These two constructs were assessed as unsuitable for production of the desired fusion protein and were not taken any further forward.

3.3.2 Stable Fusion Protein Expression

3.3.2.1 Ubiquitin

Assessment of stable cell pools expressing each ubiquitin-fusion protein via confocal microscopy showed fluorescence in each pool and indicated that both the fluorescent reporter genes GFP and mCherry, regardless of orientation or length of their respective ubiquitin fusions, were able to be expressed. Although this data alone does not confirm the presence of the ubiquitin molecule on the fluorescent reporters in any of the cell pools. Patterns of expression conserved between the GFP and mCherry cell pools showed that the fusion orientations with the strongest fluorescence were those with a

N-terminal reporter and C-terminal single ubiquitin: GFP_Ubi and mCh_Ubi. This may be because that for this conformation of targeting vector, cells (1) express the fusion protein very well and are able to generate high concentrations due to an impact on the mRNA stability, translatability of the mRNA, or that the fusion protein is most stable in this conformation, (2) that the fusion protein is expressed well intracellularly but unable to be trafficked into exosomes efficiently resulting in high fluorescence in fixed and mounted cell images, or (3) the fusion protein is expressed intracellularly and builds up due to further packaging into vesicles through exosome biogenesis pathways before release from the cell. With regards to (3), unfortunately, confocal microscopy does not have sufficient resolution to visualise exosomes which are in the 50 – 150 nm range, and so this cannot be confirmed with these images. Nevertheless, the data confirmed that the ubiquitin-fusions were able to be stably expressed and showed the fluorescent reporter component of each of the fusion protein to be functional.

During further analysis to determine if full-length fusion proteins was expressed or any reporters were directed to their exosome populations it was discovered that simple non-reducing buffer and a boiling step for sample preparation in western blot analysis could not elucidate any detection of protein in exosome preparations. An investigation of different sample preparation methods revealed that breakdown of exosomes for protein analysis on western blots revealed that use of a strong reducing agent, DTT, to the sample buffer is necessary and perhaps shows the membraned vesicle nature of exosomes could mean they are difficult to breakdown for a full picture of protein content in this manner of interrogation.

Nevertheless, the more intensive sample preparation was able to produce antibody-mediated detection of proteins in the exosome preparations of these cell pools. Unsurprisingly, a similar pattern of expression to that seen in the transient data for the cell pellet lysates of the ubiquitin-fusion proteins. Additionally, exosomes from each ubiquitin-GFP fusion stable cell pool, including the GFP-only positive control, contained a protein species that was recognised by the anti-GFP antibody and thus each contained at least the GFP portion of the fusions. The banding pattern in each exosome lane showed a band of around 250 kDa and a weaker doublet band at approximately 130

kDa, in alignment with such bands observed in transient cell lysate data, the strongest of which for the Ubi_GFP exosomes.

One possible explanation for the high molecular weight exosome GFP bands is that GFP and GFP-fusions have been packaged into exosomes and that the proteins are either aggregated or bound to other exosome proteins. Another possibility is that the exosomes aggregate or are malformed due to interference of the biogenesis pathways from the GFP fusions and despite a strong reducing agent being present in the samples, higher than expected banding is observed. Interestingly, the positive control GFP-only cell line produced an exosome population positive for GFP upon blotting. In light of the very strong band seen in the cell pellet lysate, it could be hypothesised that GFP is packaged or encapsulated in the exosomes without a targeting fusion through sheer expression overload in the cell, as overexpression of proteins in CHO cells has been reported to potentially result in sequestration and loading onto exosomes (Steć *et al.*, 2023). These cells may have trafficked the GFP control protein to vesicles for export and/or degradation without specific exosome targeting fusions as observed in the case of exosomes shuttling cell-specific cargo in cell-cell communication (Kalluri, 2016).

For the mCherry-ubiquitin fusion cell pools the pattern of expression in cell pellet lysates also mirrored that of the transient data, however there were differences to those observed in the GFP lines. mCherry-ubiquitin pools showed presence of the reporter in the supernatant lanes for the mCherry-only positive control and Ubi_mCh, which was not observed in the GFP-ubiquitin fusion pools. However, signal in the cell pellet lysates for these pools was very strong and it is possible that the strength of expression from the mCherry and Ubi_mCh pools resulted in material in the supernatant due to the sheer volume of mCherry expressed by these cells.

Interestingly, despite this clearly strong expression in the mCherry-based pools, of the exosomes isolated only two of the exosome populations were found to have mCherry present, Ubi_mCh and mCh_Ubi, with a weak single band observed and a very strong double band, respectively. The presence of the smaller band in the mCh_Ubi exosome lane could be due to instability of mCherry fusions as proposed for the banding pattern

observed in the cell pellet lysates. This is also supported by the lack of mCherry in the positive control mCherry-only exosome population as the cells would likely not become 'overloaded' with the protein and begin exporting naturally via vesicles, as posited for the GFP control result, if the mCherry protein is present at lower levels at this time. Despite this, an overwhelmingly positive takeaway from the mCherry cell pool blots is that, unlike the GFP cell pools, band sizes in exosome lanes for mCherry pools appeared close to the predicted sizes of the reporter gene intended to be targeted into the exosomes and the data thus supports that this method of expressing ubiquitin-tag targeting vectors can target a protein of interest into exosomes produced by CHO-S cultures.

3.3.2.2 Tetraspanins

Confocal microscopy of the stable tetraspanin-fusion protein cell pools, revealed GFP fluorescence was also present in all of cell pools generated and suggests that these fusion proteins are also able to be expressed with a functional GFP component. However, the number of cells expressing the fluorescent protein varied from pool to pool suggesting expression of tetraspanin-GFP fusions with functional GFP is more varied with CD81_{MID}GFP showing the highest number of fluorescent cells and CD63_{MID}GFP the lowest. Unfortunately, due to the heterogeneous nature of cell pools, whether these observed differences are significant is not possible to determine from this data alone, though generally the CD81-fusions seem to show better GFP fluorescence than the CD63-fusions. One cell pool that did visibly lack fluorescence intensity on a cell-by-cell basis was the CD63_{MID}GFP fusion pool, an indication that the fusion protein produced within this pool is either difficult to express, or turned over more rapidly than other fusions, or exported from cells at a much faster rate than the other pools. Overall, each stable cell pool was observed to express some GFP and indicated that the cells could successfully express at least the GFP component of the tetraspanin fusions.

GFP presence in the exosome suspension of each tetraspanin-based cell pool except that of CD63_{TAG}GFP during western blot analysis (Fig 3.15), suggests that the tetraspanin-

based fusion proteins are also able to direct their reporter, GFP, into exosome populations. Although these results show that of the two tetraspanins fusions, CD81 yields better results. As observed in the transient cell lysates (Fig 3.13) and the western blot data for the ubiquitin-based cell pools (Fig 3.4 & Fig 3.7), GFP is also detected 250 and 130 kDa rather than the predicted weight for a GFP fusion or GFP alone. For the tetraspanin-based lines, the only pool which deviated from this observation with a band that corresponds to the predicted fusion protein molecular weight was CD81_{TAG}GFP, with a band present just below 55 kDa. As discussed previously, the high molecular weight bands present for GFP in exosome preps could be due to aggregation or malformation of exosomes produced by these cell pools, though the correct band size present in the CD81_{TAG}GFP exosome suspension suggests that this cell pool was able to produce intact fusion proteins which were trafficked into exosomes without degradation. The differing results between CD81_{TAG}GFP and CD81_{MID}GFP could be due to interference of CD81s natural incorporation into exosomes by the presence of a mid-gene GFP insertion preventing or interfering with trafficking more than a C-terminal GFP tag. This was not observed in the CD63 vectors though and may reflect the sensitivity of the different exosome tetraspanin proteins specifically when fused with GFP and the subsequent impact on trafficking into exosomes, as it has been previously reported that CD63-enriched exosomes excel over CD81-enriched exosomes in promoting GFP-loading of exosomes (Silva *et al.*, 2021).

3.3.3 DLS Data

Consistent profile differences between the DLS profiles of fusion protein exosome populations to that of the control cell exosomes suggest that the expression of the fusion proteins does indeed influence the size of a portion of exosomes produced from these cell pools. Combined with the detection of reporter proteins in exosome samples isolated from each cell culture during western blot analysis, it is likely this is due to some level of successful direction of the reporter target proteins. Production of exosomes from a single cell type can be often heterogeneous with multiple exosome sub-populations containing varied protein profiles is common when the proteomic composition is examined (Han *et al.*, 2022; Karimi *et al.*, 2022). In the case of the multiple peak DLS

profiles observed in this chapter, increased frequency intensity peaks would logically identify whether recombinant exosomes or natural exosomes are the dominant species produced for each cell pool. Furthermore, the very large molecular weights identified by antibody probe binding in western blot analyses would suggest the peaks identified at higher particle diameters in the DLS profiles correspond to recombinant exosome profiles. Though the vastly increased peak diameters in comparison to natural exosomes of these potential recombinant exosome species would suggest that there is a serious structural differences conferred by integration of the fusion proteins or reporter components, possibly due to aggregations or malformations.

Unfortunately, most published data on exosomes which have been engineered or protein cargo-loaded that report on size of the vesicles examined, describe diameter sizes between 40 – 300 nm (Lozano-Andrés *et al.*, 2019) (Meyer *et al.*, 2017) (Steć *et al.*, 2023) (Chandrasekera *et al.*, 2023) (Beit-Yannai, Tabak and Stamer, 2018; Osteikoetxea *et al.*, 2022; Silva *et al.*, 2021), which suggests the DLS data showing large-diameter exosome subpopulations are perhaps not the result of integration with fusion proteins, though size-based exosome isolation methods may create a selection bias in these outcomes. This is particularly highlighted by Meyer *et al* (2017) who also report on exosomes which were loaded with a CD63-GFP fusion and showed no evidence of the fusion proteins resulting in an increased diameter such as that seen in this chapter. Additionally, Silva *et al* (2021) describe the loading of GFP onto exosomes through overexpression of tetraspanins CD63 and CD81 with no large increases to exosome diameter.

However, there is one report that exosome preparations can cluster and/or aggregate before dilution in buffers (such as PBS) during analysis (Chandrasekera *et al.*, 2023) and so it is possible that the yield of exosomes obtained in this work impacted the clarity of the DLS data. In fact, initially the exosome preparations were analysed using DLS as undiluted samples with poor results and the 1:20 dilution with PBS was necessary (Fig 3.8, Fig 3.9 and Fig 3.16). Additionally, it has been posited that increased exosome concentrations can increase the possibility of exosome:exosome interactions, yielding exosome dimers as cells release exosomes to interact with incoming exosomes from

other cells as part of their cell-cell communication function (Beit-Yannai, Tabak and Stamer, 2018). Furthermore, a comparison of CHO-S cell-derived exosomes harvested at days 3 and 5 of culture (Skrika-Alexopoulos and Smales, 2023) has shown a slight shift in size of exosomes harvested on day 5. This could be due to increasing concentrations of exosomes as culture time goes on and could support the theory of exosome:exosome interactions, particularly in cases with a strong subpopulation triggered by overexpression engineered into the cells which may skew the size profiles further.

It should also be considered that in cell populations which have been transfected, to express non-native proteins or overexpress proteins, cells may be undergoing greater levels of stress than un-transfected native cells and therefore more prone to shedding particles which would lead to a skewing of DLS data from increased levels of non-exosome particles.

If indeed increased size distribution profiles are a result of exosome heterodimers or similar interactions, it should be noted this may have an effect on the potency of the recombinant exosomes as a potential vaccine platform due to the potential masking or exposure of the exosome surface display proteins this work aims to achieve.

3.3.3.1 Ubiquitin

If dual peak profiles observed in this dataset are indeed representative of two distinct populations; natural and recombinant exosomes, it is possible that the different relative frequency intensities between the different tagging orientations is indicative of their efficiency to target a protein of interest into exosomes. If recombinant exosomes are more prone to aggregation and result in a peak in the particle size distribution of exosome populations at larger diameters, DLS data analysis of the ubiquitin-GFP exosome populations suggests that the Ubi_GFP protein conformation is more efficiently able to direct the reporter GFP than the others examined here due to its higher relative frequency peak at the increased particle diameter.

Interestingly, the positive control mCherry-only exosome suspension yielded no discernible exosome particle-sized peaks during DLS profiling. This may be due to either (1) low exosome concentration for this cell pool, (2) poor formation of exosomes by this cell pool, (3) poor isolation of exosomes from culture media of this pool, or (4) degradation of the exosomes in suspension. However, dual-peak profiles generated by the ubiquitin-mCherry pools suggest the lack of exosome-associated peaks in the control mCherry profile were likely due to a lower yield of exosomes in this particular pool for reasons that cannot be identified by this dataset. Though it may explain why no mCherry was present in the mCherry positive control exosome samples examined in western blotting despite very high levels of mCherry in the cell lysate and supernatant and presence of GFP in the GFP controls which seems to show protein can be directed to exosomes in cases of over-expression.

A large particle diameter peak with the greatest relative frequency intensity was observed in the mCh_Ubi exosome suspension, counter to the configuration identified as most efficient at exosome targeting in the ubiquitin-GFP data. Analysis of DLS data combined with the western blot analysis, in which mCh_Ubi exosomes had the strongest mCherry band, indicates successful targeting of mCherry into the exosomes of cells expressing these constructs, particularly mCh_Ubi. This could mean that while generation of ubiquitin fusion proteins can be effective in targeting proteins into exosome populations, it may also be some-what dependent on the protein of interest, even between very similar protein targets. However, the overall two peak pattern observed in the ubiquitin-mCherry DLS profiles is very similar to that observed in the ubiquitin-GFP DLS data and suggests, following the assumptions for identification of recombinant exosome sub-populations using combined DLS and western blot analysis, expression of a protein of interest as a fusion with ubiquitin is a successful method for integration of a proteins of interest into exosomes.

3.3.3.2 Tetraspanins

Each of the profiles from the tetraspanin-GFP cell pools also showed two-peak profiles similar to the ubiquitin-based cell lines. As previously discussed, this two-peak profile

could be an indication that the fusions impact the exosome population, specifically the size of vesicles produced or their aggregation, and profiles with larger second peaks represent a greater impact of the fusion proteins on exosome sub-populations.

Interestingly, there was an apparent difference between the mid-gene GFP pools and the C/N-terminal tagged GFP pools between each of the CD63- and CD81-fusions, with mid-gene GFP fusions displaying a much sharper and distinct second peak. This is somewhat surprising considering the presence of protein at the expected molecular weight for CD81_{TAG}GFP exosomes. However, overall findings in the tetraspanin-fusion data and their similarity to the ubiquitin-based data is indicative of integration, in some form, of reporters into exosome populations.

3.4 Conclusions

This chapter explored two strategies for generating recombinant exosomes bearing proteins of interest via expression of proteins of interest (POI) fused with either ubiquitins or tetraspanins in CHO-S cells. Through western blotting and confocal of cell pools created for both strategies, the fluorescent reporter genes GFP and mCherry, regardless of orientation, length, or fusion protein, were able to be expressed and displayed functionality.

Of the ubiquitin-fusions, the noticeably stronger fluorescence was observed in those with a N-terminal reporter and C-terminal single ubiquitin: GFP_Ubi and mCh_Ubi. The presence of predicted band sizes during western blotting of exosome samples isolated from Ubi_mCh and mCh_Ubi suggests that the ubiquitin fusion strategy was successful in generating recombinant exosomes, particularly mCh_Ubi, which may provide the best orientation for this strategy: N-terminal POI and C-terminal single ubiquitin. Bands were also observed in the ubiquitin-GFP exosome sample during western blotting, the strongest of which was Ubi_GFP. However, these bands were present at a very high molecular weight and it's possible this is the result of either malformation or aggregation of exosomes from these cell pools. Interestingly, GFP was detected in the exosomes isolated from the GFP-only positive control cell pool alongside evidence of

strong intracellular expression and seems to support the loading of excess proteins into exosomes as a result of overexpression in CHO-S cells.

DLS profiling of the exosomes isolated from cell culture of each stable pool created in this chapter showed a trend divergence in the size distribution the exosomes into a two-peak profile compared with the single-peak profile of with those isolated from the naïve CHO-S host cell culture, suggesting that the expression of both ubiquitin- and tetraspanin-based fusion proteins has a strong impact on the exosome subpopulations of CHO-S cells. If the strength of the divergence in DLS profiles correlates to presence of recombinant exosomes and therefore the efficacy of the fusion proteins for exosome manipulation, it would seem the pools with the greatest second peak also match the microscopy and western blot analyses. The greatest relative frequency intensity for secondary peaks was observed in the mCh_Ubi and Ubi_GFP exosome isolates, meaning that while generation of ubiquitin fusion proteins can be effective in targeting proteins into exosome populations, it may also be some-what dependent on the protein of interest, even between very similar protein targets.

Concurrently, of the tetraspanin-fusions, CD81-fusions with GFP showed better fluorescence than the CD63-fusions during microscopy and produced greater signal in their exosome samples during western blotting, particularly CD81_{TAG}GFP which produced bands approximate to the predicted molecular weight of the fusion protein. These results suggest that CD81, particularly as an N-terminal fusion, is better suited for use in this strategy as it is able to direct POIs into exosome populations of CHO-S cells. Although, the correlation between these results and DLS is not observed in the tetraspanin-fusions, as the mid-gene GFP fusions of both CD63 and CD81 display a much sharper and distinct second peak despite the presence of the POI in exosomes of the CD81-fusions.

It is likely that the antibody-specific results of western blotting are most reliable in establishing the presence of the POIs in exosomes generated in each strategy, and as such the results for the mCh_Ubi cell pool have provided the most promising results

with bands of expected molecular weights without any aggregates and a strong fluorescence indicative that the POI retains its functionality.

Chapter 4: Investigating Exosome-Targeting Strategies for the Development of an Exosome-Based Vaccine Platform from CHO Cells using SARS-CoV-2 Display Antigens

4.1 Introduction

To further investigate the use of ubiquitin and tetraspanin fusion protein exosome-targeting strategies, the possibility of generating recombinant exosomes was explored, using SARS-CoV-2 antigen sequences as the proteins of interest. CHO cells were used as the production host to investigate the development of a novel exosome-based vaccine platform targeting COVID-19. The work built on the previous proof-of-concept work to design vectors which express exosome-targeting fusion proteins by replacing the fluorescent reporter sequences with SARS-CoV-2 antigen sequences to express ubiquitin-SARS-CoV-2 and tetraspanin-SARS-CoV-2 fusion proteins.

In order to achieve this, multiple antigen sequences were selected and designed to be cloned into both the ubiquitin and tetraspanin-based vectors to produce fusion proteins of each antigen. Due to the varying sizes and structural complexity of each antigen, this approach also allowed for the further examination of the effect of each exosome-targeting fusion proteins method on the ability of CHO cells to produce recombinant exosomes, previously not assessed in the proof-of-concept work. The SARS-CoV-2 antigen sequences used in this chapter were chosen from scientific literature and ongoing COVID-19 vaccine trials in which they have been highlighted as vaccine targeting candidates with excellent potential to produce a protective antibody response. The selected SARS-CoV-2 antigens included: a truncated full-length spike (tFLS) protein (lacking the transmembrane spanning domain of spike protein); spike protein subunits S1 and S2; the receptor binding-domain (RBD) of the spike protein; and the nucleocapsid (NC).

This chapter details the generation of the new SARS-CoV-2-fusion protein expressing vectors for stable transfection into CHO cells and the analysis of the subsequent exosome populations isolated from the resulting cultures. Isolation and analysis of exosomes throughout this section were performed using techniques identical to those described in the proof-of-concept work, with the exception of fluorescent microscopy which was not possible on the new non-fluorescing fusion proteins. Using the data collected from these analyses, the work assessed which SARS-CoV-2 antigen was most successfully directed into the exosome population of CHO cells. Comparisons between each exosome-targeting strategy using the SARS-CoV-2 antigens as proteins of interest were also carried out due to the varied size and complexity of each which could determine whether ubiquitin or tetraspanin-based exosome-based targeting provided a more robust method for the generation of recombinant exosomes as a potential novel vaccine platform.

4.2 Results

4.2.1 Generation of Ubiquitin-SARS-CoV-2 fusion sequences and constructs

To express each of the ubiquitin-SARS-CoV-2 fusion proteins the commercially available pcDNA 3.1 Hygromycin (Invitrogen) plasmid was used. The genes for the SARS-CoV-2 antigens of each fusion protein were inserted into the multiple cloning site in either a C-terminus (Fig 4.1) or N-terminus (Fig 4.2) orientation with respect to the inserted ubiquitin sequence, in the same manner as the ubiquitin-target fusion proteins previously described in Chapter 3. For each of the 10 ubiquitin-SARS-CoV-2 fusion protein-expressing vectors (Fig 4.3), the transcription of the ubiquitin-SARS-CoV-2 fusion protein coding sequences is driven by an enhanced CMV promoter with a bGH polyA signal at the 3' end.

The truncated full-length spike (tFLS) gene sequence was taken from sequences published by Wrapp *et al* (2020) detailing a cryoEM study of an engineered pre-fusion stable spike protein. The receptor-binding domain (RBD) and nucleocapsid (NC) genes

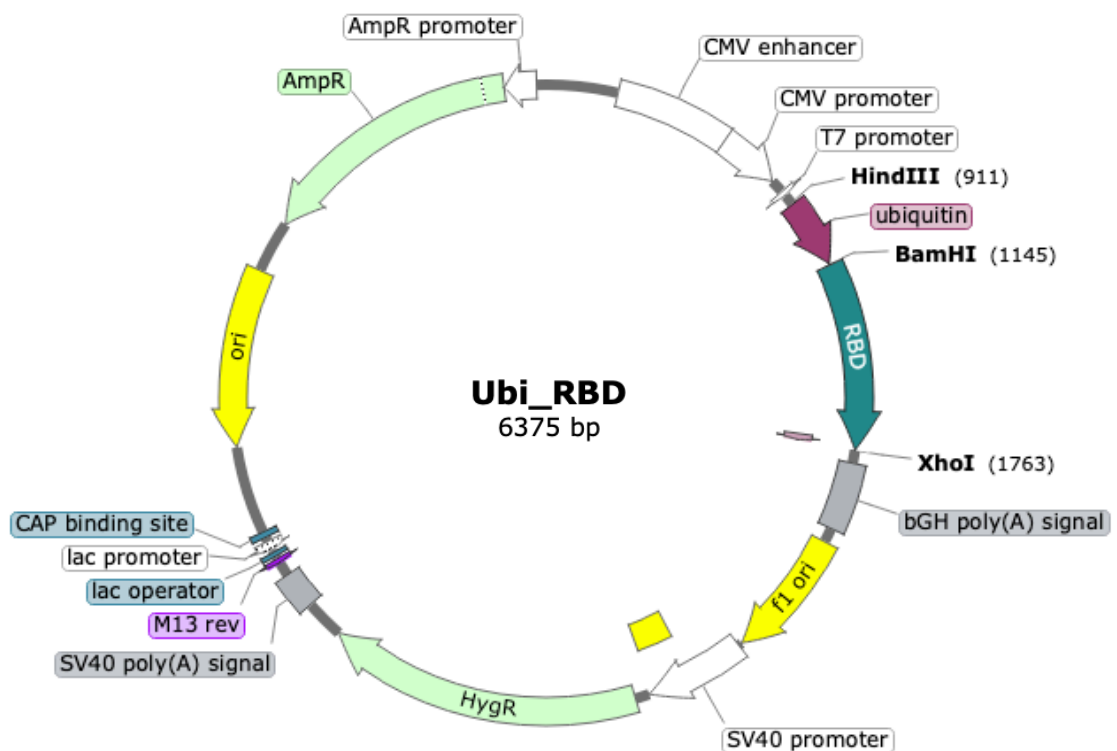


Figure 4.1: Vector map showing the 3.1 hygro plasmid backbone layout with the Ubi_RBD fusion protein gene sequence inserted at the multiple cloning site which is flanked by an enhanced CMV promoter and a bGH polyA terminator.

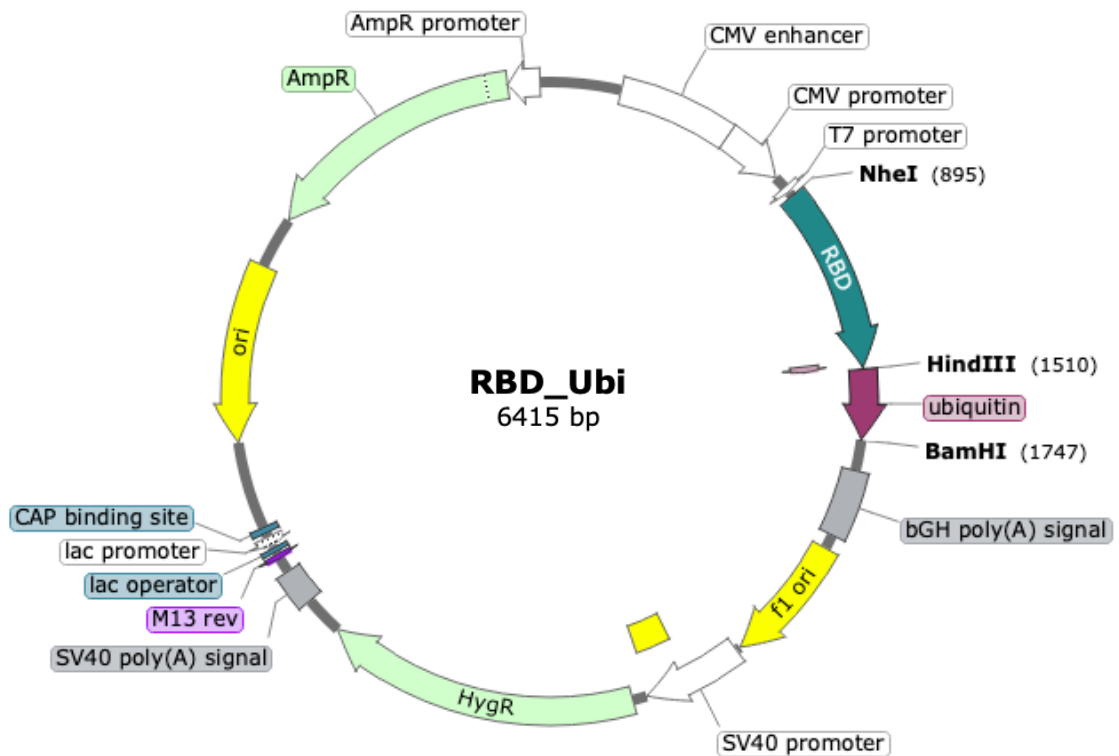
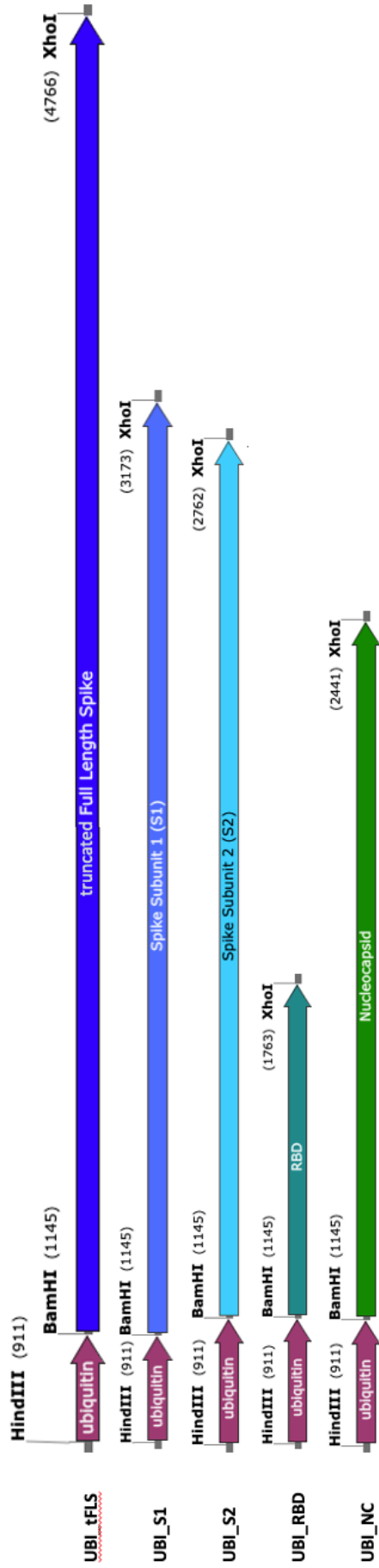


Figure 4.2: Vector map showing the 3.1 hygro plasmid backbone layout with the RBD_Ubi fusion protein gene sequence inserted at the multiple cloning site which is flanked by an enhanced CMV promoter and a bGH polyA terminator.

were amplified by PCR from available in-house geneART strings which contained the required gene sequences (GenBank ID: 7XRP_F and GenBank ID: YP_009724397.2, respectively) but that had been codon-optimised for expression in CHO cells. The spike protein subunits 1 and 2 (S1 and S2) were amplified from the tFLS gene as a template via PCR with primers designed to flank the regions of each subunit within the gene sequence at the mutated S1/S2 furin cleavage site within the spike protein. Furthermore, the tFLS, RBD and NC gene sequences were designed such that each included a His-tag at the C-terminus. It is noted however that as the S1 sequence was cloned out of the tFLS gene through PCR with a reverse primer which binds mid-gene, it is subsequently the only SARS-CoV-2 antigen sequence in this chapter which does not contain the His-tag. After amplification of each antigen gene selected as an exosome-display candidate, they were digested and ligated into vectors via traditional restriction enzyme cloning techniques (described in Chapter 2).

N-TERMINAL UBIQUITIN-COVID CONSTRUCTS



C-TERMINAL UBIQUITIN-COVID CONSTRUCTS

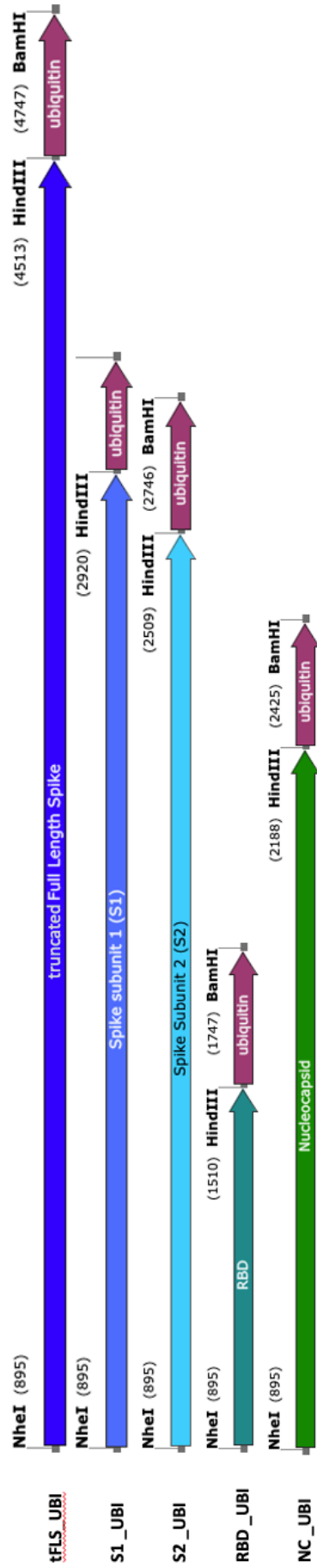


Figure 4.3: Schematic of the ubiquitin-SARS-CoV-2 vector cassettes and respective control vector cassettes created and described throughout this chapter. Also shown are the restriction enzymes insertion sites used to clone sequences into the 3.1 hygro plasmid backbone. The annotated name used for each construct is shown on the left of each schematic.

Once completed, the sequences of the ubiquitin-SARS-CoV-2 fusions in each vector were sequenced via Sanger sequencing to confirm the sequences had been successfully inserted with no mutations or frame shifts. They were then amplified for transfection in *E. coli* cultures using maxi-prep kits (QIAGEN) to extract the plasmid DNA and re-screened via DNA digest to confirm the successful amplification of each vector (Fig 4.4). The DNA digests were carried out using the restriction enzymes *HindIII*, *BamHI* and *XhoI* or *NheI*, *HindIII* and *BamHI* to release both inserted genes of either the N-terminus or C-terminus ubiquitin tagged sequences, respectively. The resulting digested DNA was analysed on 1% agarose gels to visualise the dropout bands under UV light. Each digest yielded a successful 239 bp dropout band for ubiquitin, and then successful dropout bands of 3612 bp for tFLS, 2019 bp for S1, 1608 bp for S2, 609 bp for RBD and 1287 bp for NC, each in the respective plasmids. After confirmation of a successful amplification of each plasmid, they were then taken forward for transfection into CHO-S cells.

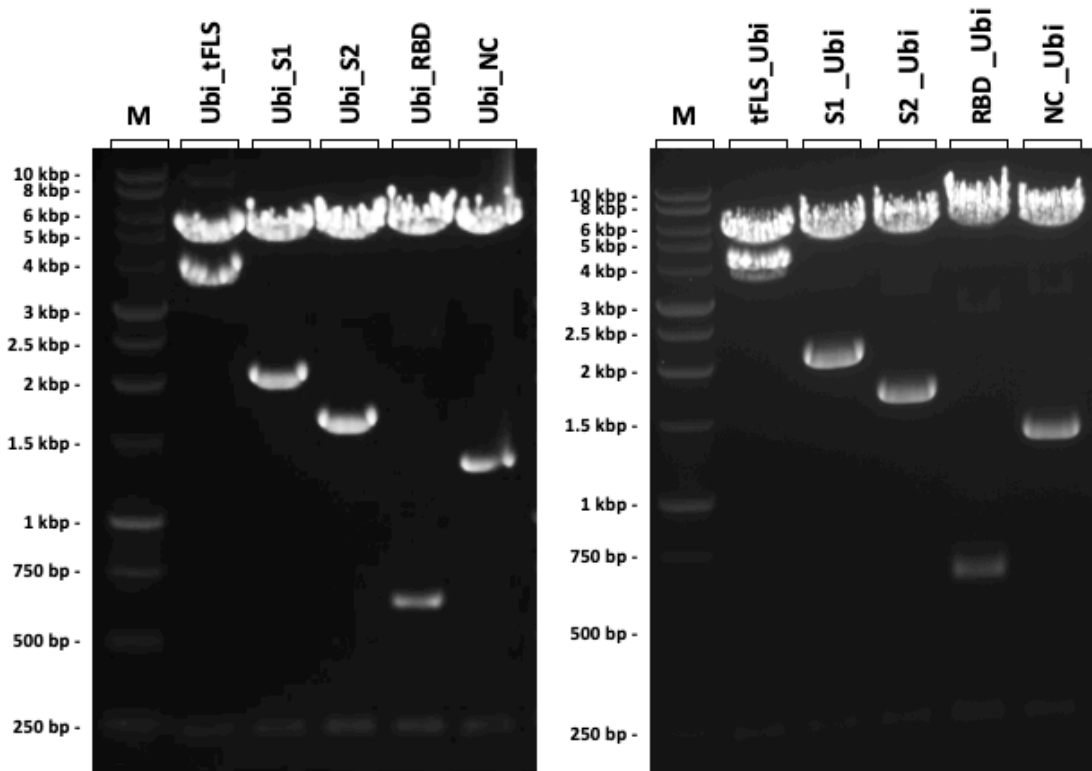


Figure 4.4: 1% Agarose DNA gel analysis of test restriction digests from finalised cloned ubiquitin-covid vectors with 1 kbp DNA markers (M). (Left) N-terminal ubiquitin-tagged sequences, digested with *HindIII*, *BamHI* and *XhoI*. (Right) C-terminal ubiquitin-tagged sequences, digested with *NheI*, *HindIII* and *BamHI*.

4.2.2 Western Blot Analysis of Ubiquitin-SARS-CoV-2 Fusion Protein Expression in Stable CHO-S Cell Pools

CHO-S cells were transfected with linearised plasmid DNA of each SARS-CoV-2-ubiquitin fusion protein expressing vector, and the resulting cells and supernatant were harvested from each cell pool after culture viability had recovered to >95% to analyse fusion protein expression. A cell pellet lysate and supernatant were collected from naïve host CHO-S cells and an exosome prep carried out on the supernatant for western blot analysis using antibody probes for exosome markers CD63, CD81 and CD9. Analysis using these markers (Fig 4.5) revealed the presence of a band for each in the exosome preps and provided evidence that the chosen method of exosome isolation from cell culture in this work was successful in isolating exosomes from CHO-S culture supernatants.

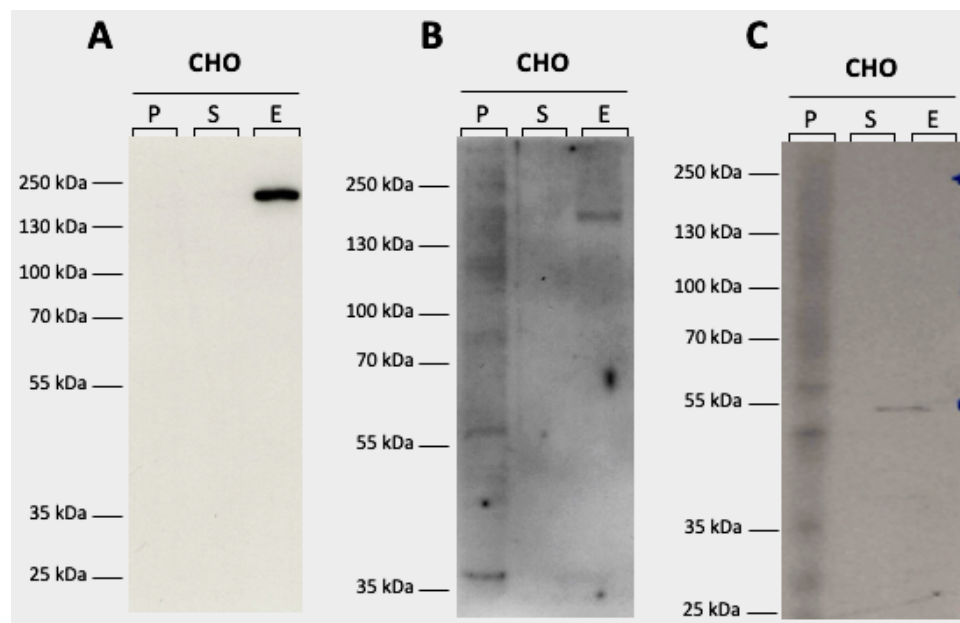


Figure 4.5: Western blot images of cell pellet lysates (P), supernatants (S) and exosome preps each taken from a CHO-S cell culture. (A) anti-CD63 probe (B) anti-CD81 probe and (C) anti-CD9 probe, 10 minute exposure.

To assess the expression of each ubiquitin-SARS-CoV-2 fusion protein, western blot analysis was conducted on the cell pellets, supernatants and exosome preps generated from each ubiquitin-SARS-CoV-2 fusion protein cell pool using anti-His (Fig 4.6) and anti-ubiquitin (Fig 4.7) antibody probes.

His-tag bands were present in all exosome prep lanes to varying degrees but all bands were the same size for each cell pool's exosome preps (Fig 4.6) regardless of the expected size of the fusion proteins (**Table 4.14**). His-tag bands were also present in all cell pellet lysates but at various sizes, including the CHO-S host cell pellet lysates. However, the CHO-S lysate only produced two strong bands at approximately 65 kDa and 50 kDa, whereas the SARS-CoV-2-ubiquitin cell pool lysates contained a third strong band at approximately 90 kDa. The only cell pool to produce a strong His-tag band in the supernatant was Ubi_NC, whilst there was some present in other cell pools (S2_Ubi, Ubi_S2, Ubi_RBD and Ubi_NC), the band was faint in comparison.

Table 4.14: A list of the approximate molecular weights for each of the ubiquitin-SARS-CoV-2 fusion protein components expressed in this section.

Protein Name	Abbreviation	Approximate Molecular Weight (kDa)
Truncated Full Length SARS-CoV-2 Spike Protein	tFLS	180-200
SARS-CoV-2 Spike Protein Subunit 1	S1	110
SARS-CoV-2 Spike Protein Subunit 2	S2	80
SARS-CoV-2 Receptor Bind Domain	RBD	21
SARS-CoV-2 Nucleocapsid	NC	45
Ubiquitin	Ubi	8

Overall, His-tag bands were present in the exosome preps of the cell pools expressing RBD and NC as ubiquitin fusion proteins regardless of ubiquitin tag orientation, whilst cell pools expressing a tFLS- or S2-fused protein yielded the strongest signal in the exosome preps. Interestingly, the reversal of the ubiquitin tag orientation in the tFLS and S2 fusion proteins produced opposite outcomes in the His-tag band intensity. The His-tag band in the exosome prep from Ubi_S2 was much stronger than that of S2_Ubi, whilst the band in the exosome prep from Ubi_tFLS was much weaker than that of tFLS_Ubi.

Western blotting of the ubiquitin-SARS-CoV-2 fusion protein expressing cell pools was also carried out using an anti-ubiquitin probe to further investigate expression of the fusion proteins (Fig 4.7). This was also necessary to examine the S1-fusion protein cell pools as the S1 sequence used to generate these pools did not contain a His-tag.

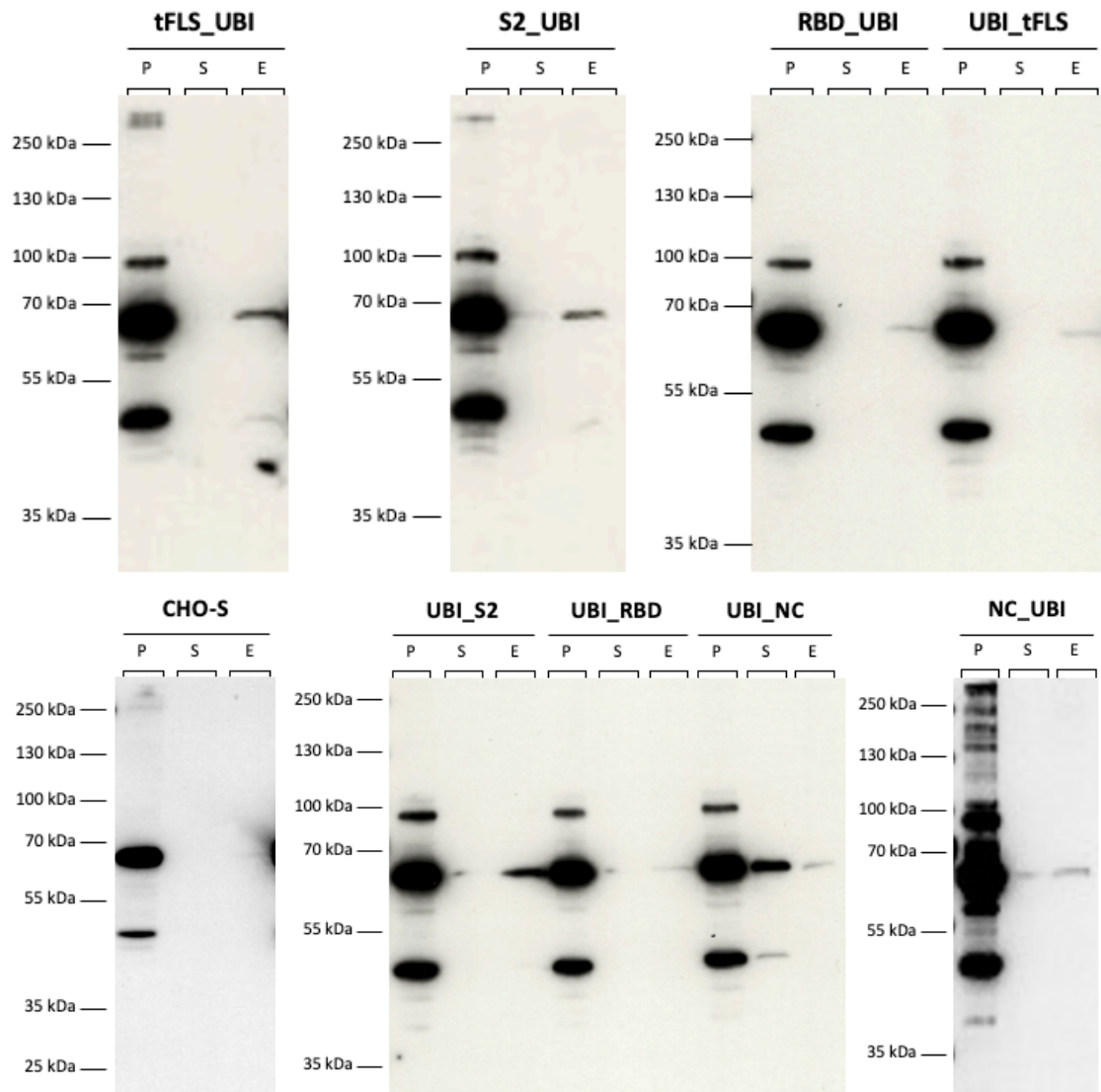


Figure 4.6: Western blot images of cell pellet lysates (P), supernatants (S) and exosome preps taken from each of the cell pools expressing SARS-CoV-2-ubiquitin fusion proteins containing a His-tag, using an anti-His antibody probe (exposure time 4 minutes).

Anti-ubiquitin probed blots of the cell pellet lysates, supernatants and exosome preps from ubiquitin-SARS-CoV-2 fusion protein cell pools confirmed the presence of ubiquitin across all the cell pellet lysates. However, there was also significant smearing across these lanes with no discernible banding in any of the lanes. Faint smearing was also present in all of the lanes containing exosome preps and overall, the anti-ubiquitin

probed blots did not show strong evidence of any bands which correspond to the predicted ubiquitin-SARS-CoV-2 fusion protein sizes or any their components.

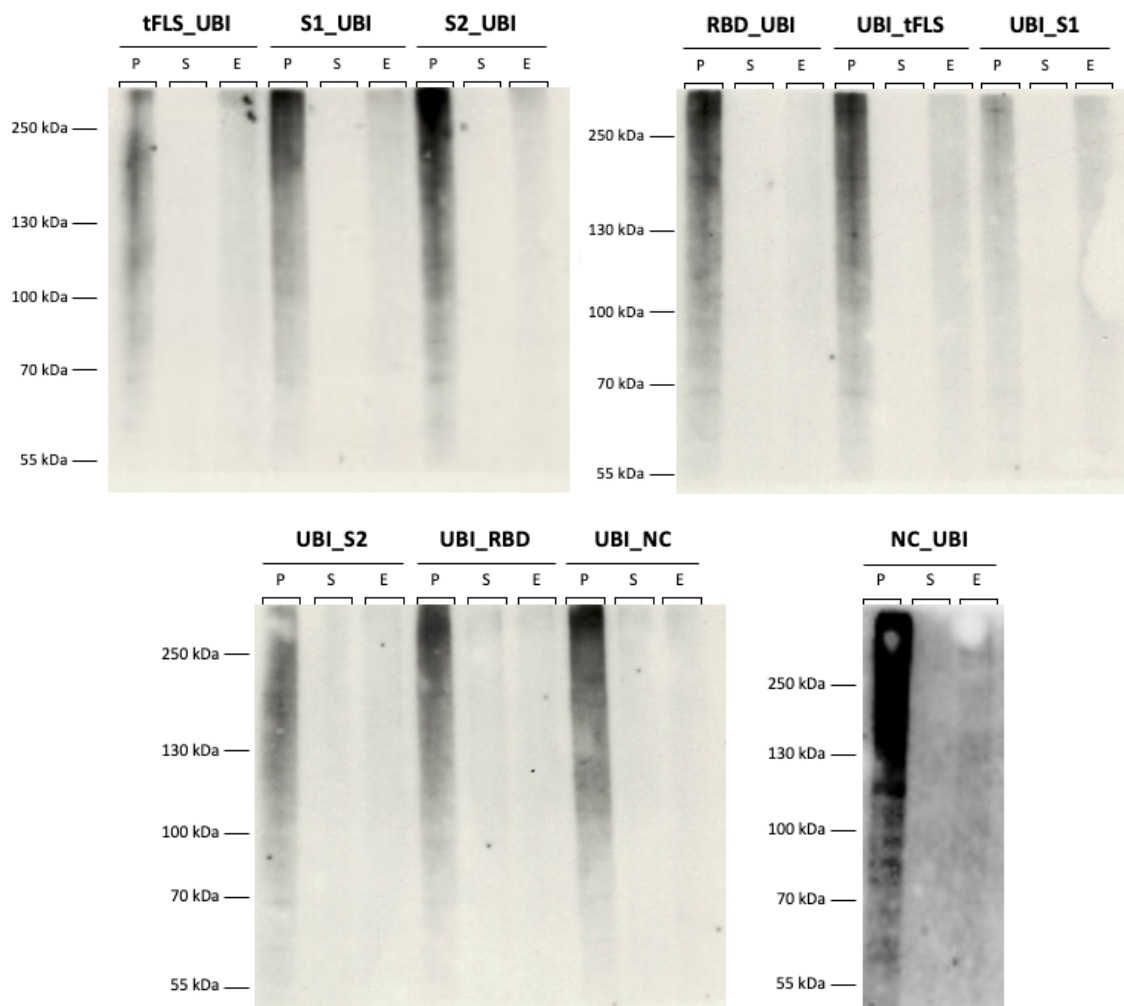


Figure 4.7: Western blot images of cell pellet lysates (P), supernatants (S) and exosome preps taken from each of the SARS-CoV-2-ubiquitin fusion protein expressing cell pools, using an anti-His antibody probe (exposure time 40 minutes).

4.2.3 DLS analysis of exosome preparations

The exosome prep suspensions isolated from cell culture supernatants for each cell pool were diluted with filtered PBS and examined by dynamic light scattering (DLS) and analysed and displayed on a logarithmic scale as previously described (section 3.2.2.2.3). The previously established control CHO-S exosome profile in Chapter 3 showed a singular peak close to the exosome diameter range generally accepted in the literature and was used as a baseline in these exosome particle size distribution analyses.

All of the particle size distribution profiles generated from the ubiquitin-SARS-CoV-2 fusion protein expressing cell pools showed a two-peak profile with the first peak matching the peak generated in the host CHO-S exosome profile (Fig 4.8 and Fig 4.9). Exosome profiles for all of the C-terminal (Fig 4.8) and N-terminal (Fig 4.9) ubiquitin-SARS-CoV-2 fusion protein expressing cell pools had a second peak with a higher relative frequency intensity in a particle diameter range between 1,000 – 10,000 nm, except for NC-Ubi which had two peaks of almost equal relative frequency intensity.

Comparison of the exosome profiles between the C-terminal and N-terminal ubiquitin-SARS-CoV-2 fusion protein expressing cell pools for each covid antigen showed an almost identical profile for those containing the tFLS, S1 and S2. The peaks in the exosome profile of Ubi_RBD and Ubi_NC (Fig 4.9) were much more distinct than RBD_Ubi and NC_Ubi (Fig 4.8), respectively, with narrower peaks and greater relative frequency intensities.

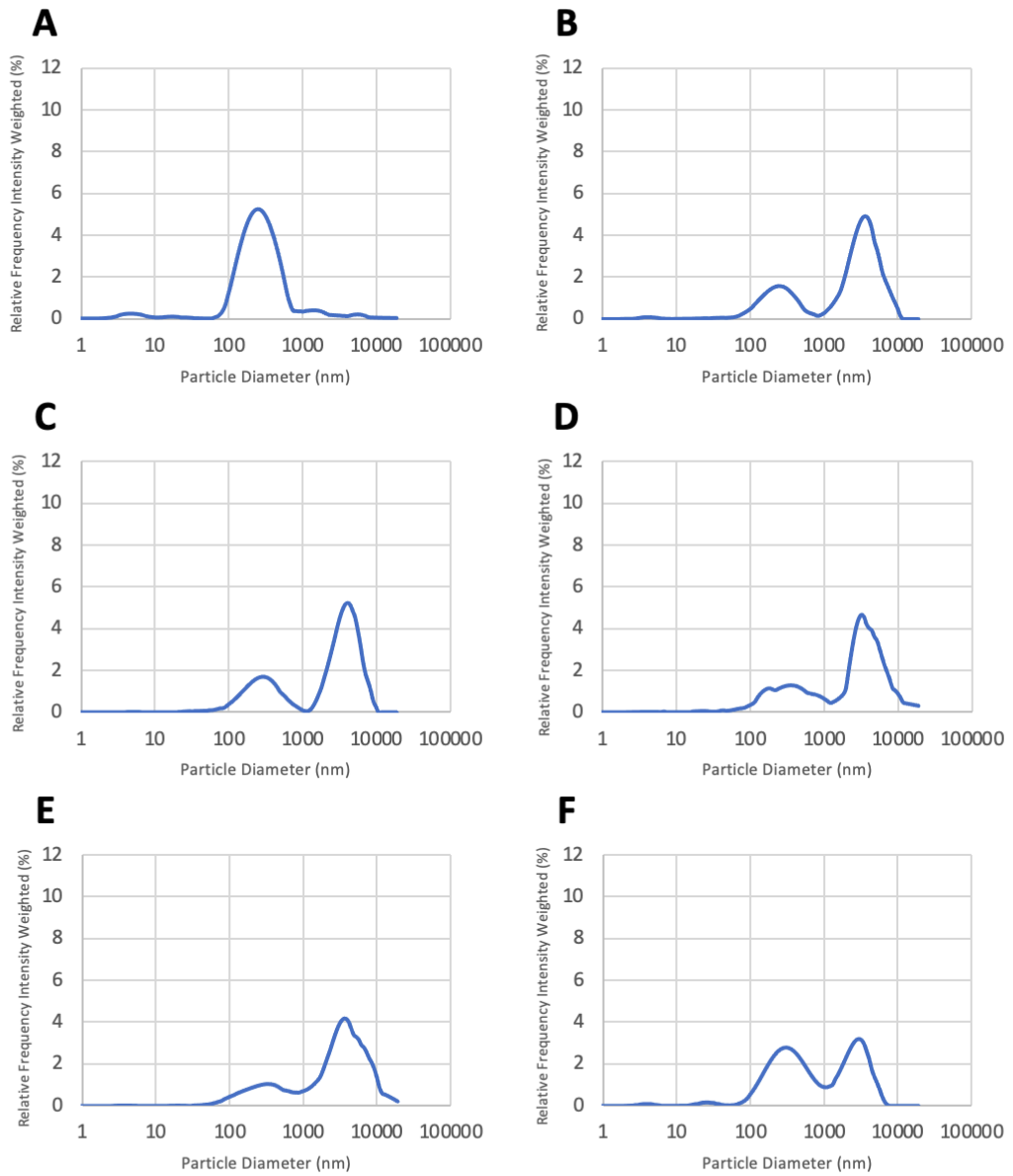


Figure 4.8: Particle size distributions of exosome preparations from the C-terminally tagged ubiquitin-SARS-CoV-2 fusion protein expressing stable cell pool exosome suspensions, alongside negative control (CHO-S) exosome suspensions. Each figure shows the average DLS measurement ($n=10$) for relative intensity frequency weight (%) vs. particle diameter (nm) with a log₁₀ scale applied.

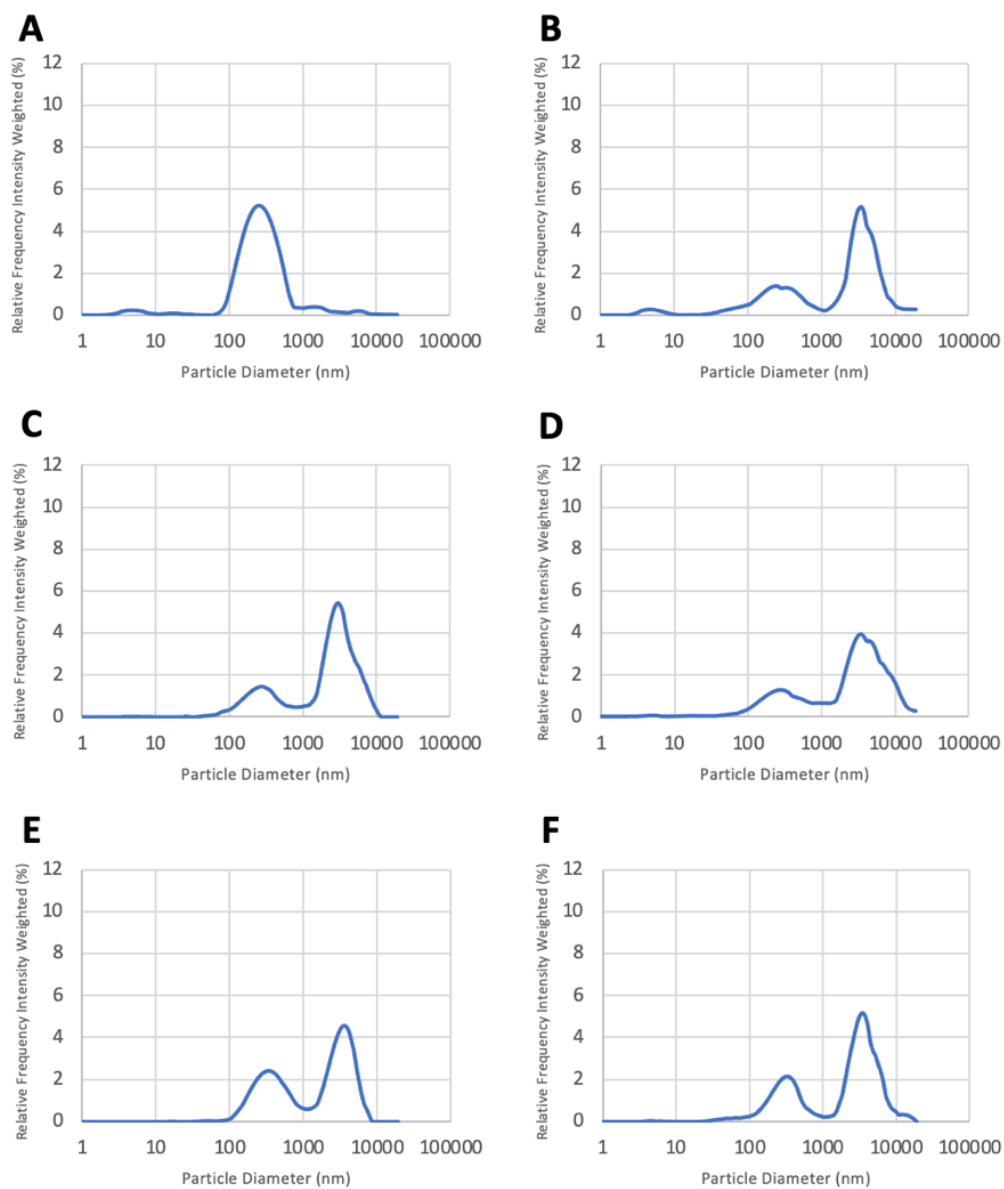


Figure 4.9: Particle size distributions of exosome preparations from the N-terminally tagged ubiquitin-SARS-CoV-2 fusion protein expressing stable cell pool exosome suspensions, alongside negative control (CHO-S) exosome suspensions. Each figure shows the average DLS measurement ($n=10$) for relative intensity frequency weight (%) vs. particle diameter (nm) with a log₁₀ scale applied.

4.2.4 Generation of Tetraspanin-fusion based vectors

Expression of the tetraspanin-SARS-CoV-2 fusion proteins was also achieved using the commercially available pcDNA 3.1 Hygromycin (Invitrogen) plasmid. Each tetraspanin, CD63 and CD81, were fused with each of the five selected SARS-CoV-2 antigens described in Section 4.2.1 for a total of 10 vectors. SARS-CoV-2 antigen sequences were inserted into the tetraspanin sequences using restriction enzyme insertion sites, as described in Chapter 3, after the tetraspanins had been cloned into the vector. Transcription of each tetraspanin-SARS-CoV-2 fusion protein coding sequences was driven by an enhanced CMV promoter with a bGH polyA signal at the 3' end (Fig 4.10 and Fig 4.11).

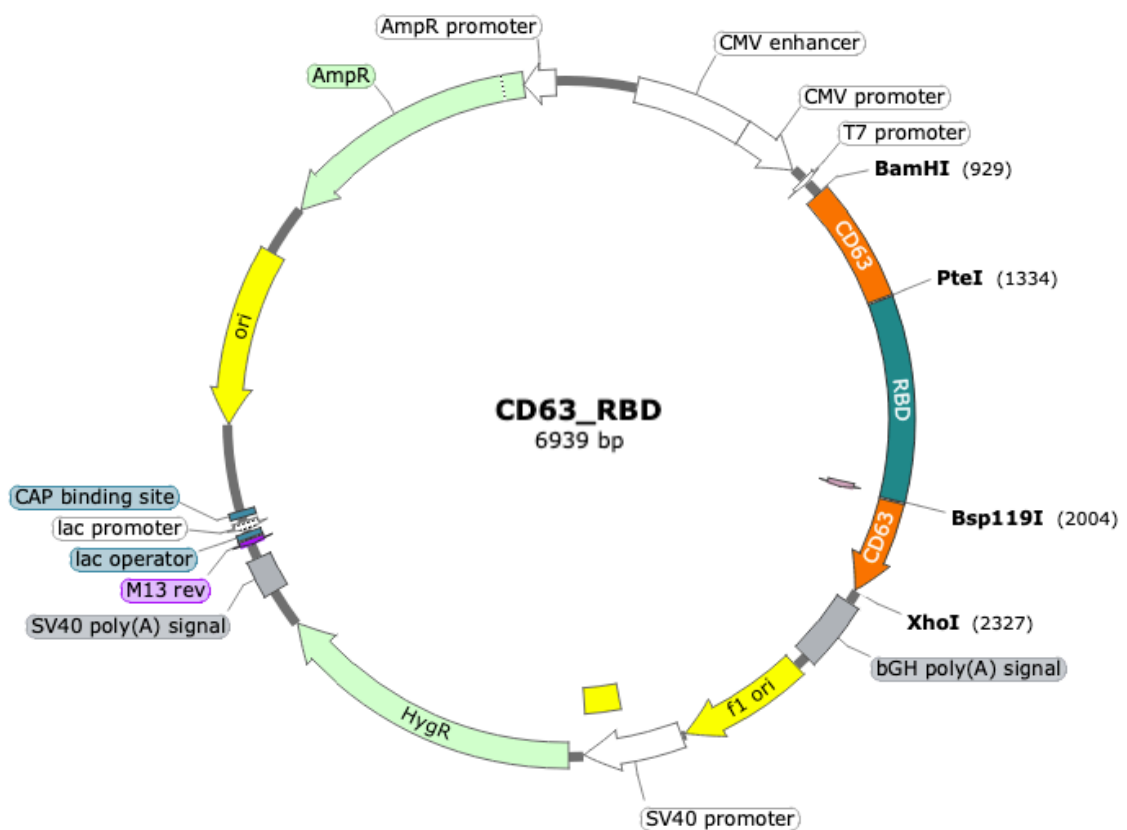


Figure 4.10: Vector map showing the 3.1 hygromycin plasmid backbone layout with the CD63_RBD fusion protein gene sequence inserted at the multiple cloning site which is flanked by an enhanced CMV promoter and a bGH polyA terminator.

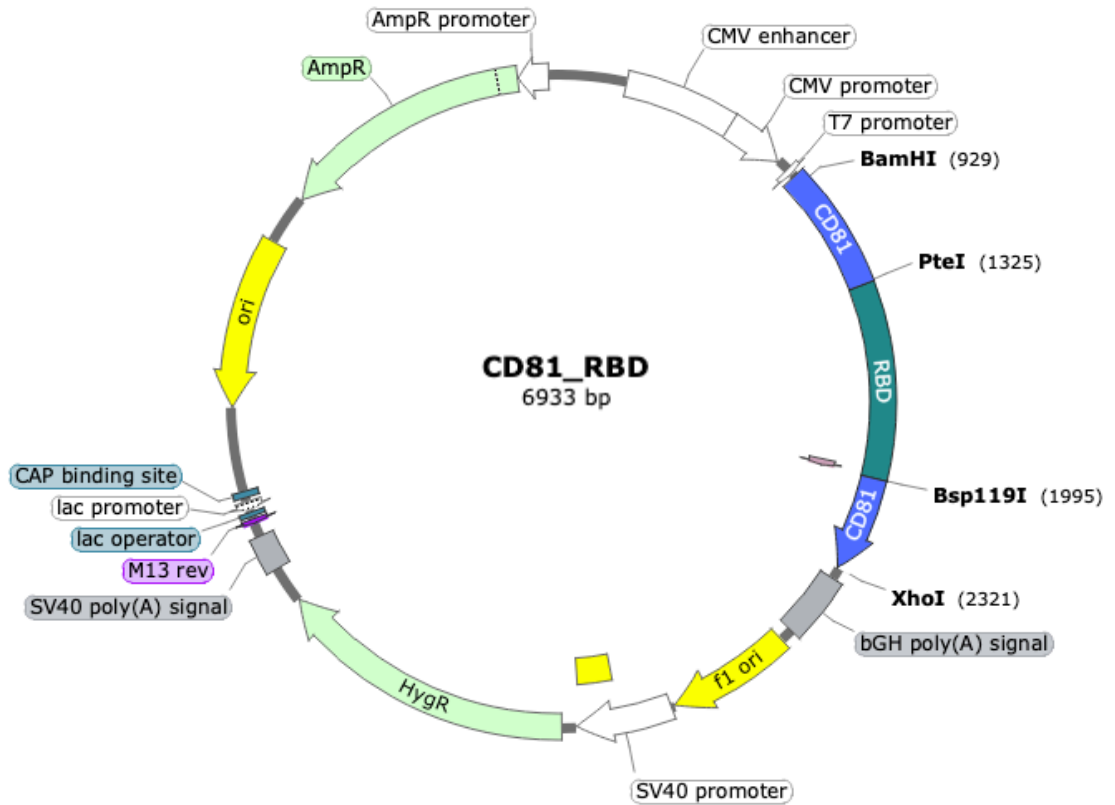


Figure 4.11: Vector map showing the 3.1 hygro plasmid backbone layout with the CD81_RBD fusion protein gene sequence inserted at the multiple cloning site which is flanked by an enhanced CMV promoter and a bGH polyA terminator.

After insertion of the tetraspanin-SARS-CoV-2 fusion protein sequences, each vector was sequenced via Sanger sequencing to confirm successful gene insertions into each plasmid with no mutations or frame shifts. They were then amplified for transfection in *E. coli* cultures using maxi-prep kits (QIAGEN) to extract the plasmid DNA and re-screened via DNA digest to confirm the successful amplification of each vector (Fig 4.12). The DNA restriction digests were carried out using the restriction enzymes *BamHI* and *XhoI* to release the full tetraspanin-SARS-CoV-2 fusion sequences and the resulting digested DNA analysed on 1% agarose gels to visualise the dropout bands under UV light.

The CD63-based plasmid digests yielded successful dropout bands of 4374 bp for tFLS, 2781 bp for S1, 2370 bp for S2, 1371 bp for RBD and 2049 bp for NC. The CD81-based plasmid digests yielded successful dropout bands of 4368 bp for tFLS, 2775 bp for S1, 2364 bp for S2, 1365 bp for RBD and 2043 bp for NC. Also shown in Fig 4.12, in the first lane of each gel, is the same restriction digest of each of the intermediate cloning

plasmids, 'CD63-only' and 'CD81-only', which show a dropout band of 762 bp and 756 bp, respectively. After confirmation of a successful amplification of each plasmid, they were then taken forward for transfection into CHO-S cells.

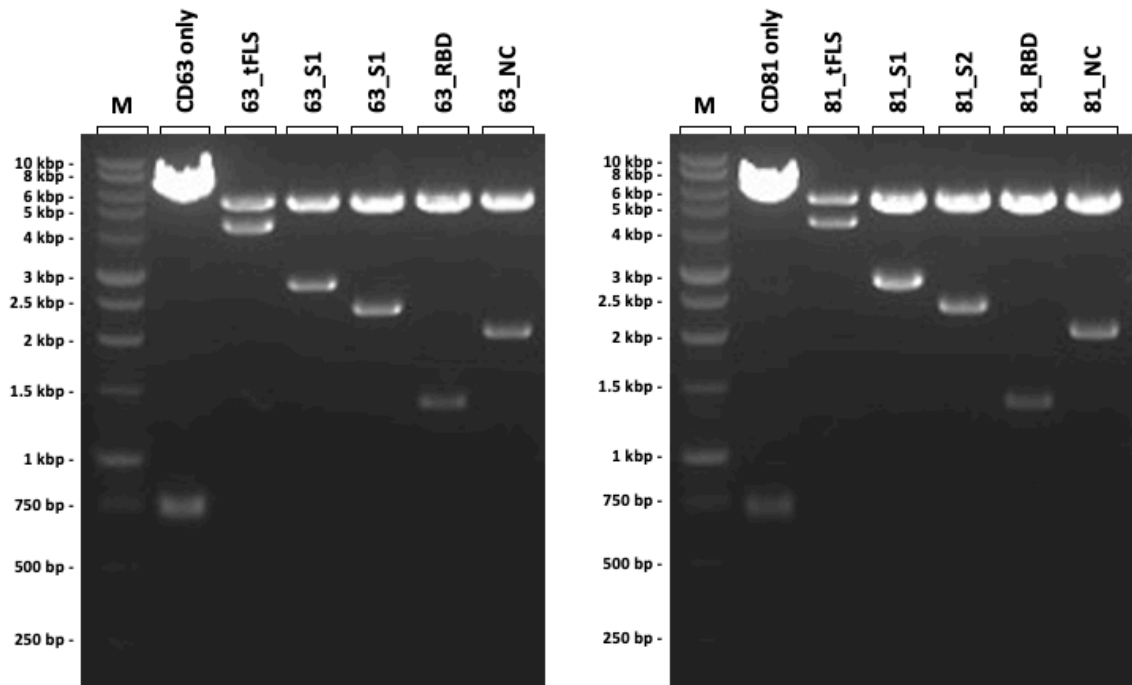


Figure 4.12: 1% Agarose DNA gel analysis of test restriction digests, using *Bam*HI and *Xho*I, on intermediate and finalised cloned tetraspanin-SARS-CoV-2 vectors with 1 kbp DNA markers (M). (Left) CD63-based sequences. (Right) CD81-based sequences.

4.2.5 Western Blot Analysis of Tetraspanin-SARS-CoV-2 Fusion Protein Expression in Stable CHO Cell Pools

CHO-S cells were transfected with linearised plasmid DNA from each tetraspanin-SARS-CoV-2 fusion protein expressing vector and maintained until a recovery of >95% culture viability had been achieved before analysis of each fusion protein expression. Cell pellet lysates and supernatants were harvested from each cell pool and exosomes prepared from the collected supernatants as described in Chapter 2. Western blot analysis using antibody probes for CD63 (Fig 4.13), CD81 (Fig 4.14) and His-tags (Fig 4.15) were carried out on the cell pellet lysates, supernatants and exosome preps for each cell pool generated to determine the presence of bands consistent with those expected for tetraspanin-SARS-CoV-2 fusion proteins (Table 4.15).

Table 4.15: A list of the approximate molecular weights for each of the tetraspanin-SARS-CoV-2 fusion protein components expressed in this section.

Protein Name	Abbreviation	Approximate Molecular Weight (kDa)
tFull Length SARS-CoV-2 Spike Protein	FLS	180-200
SARS-CoV-2 Spike Protein Subunit 1	S1	110
SARS-CoV-2 Spike Protein Subunit 2	S2	80
SARS-CoV-2 Receptor Bind Domain	RBD	21
SARS-CoV-2 Nucleocapsid	NC	45
Cell surface antigen CD63	CD63	25
Cell surface antigen CD81	CD81	25
Cell surface antigen CD9	CD9	25

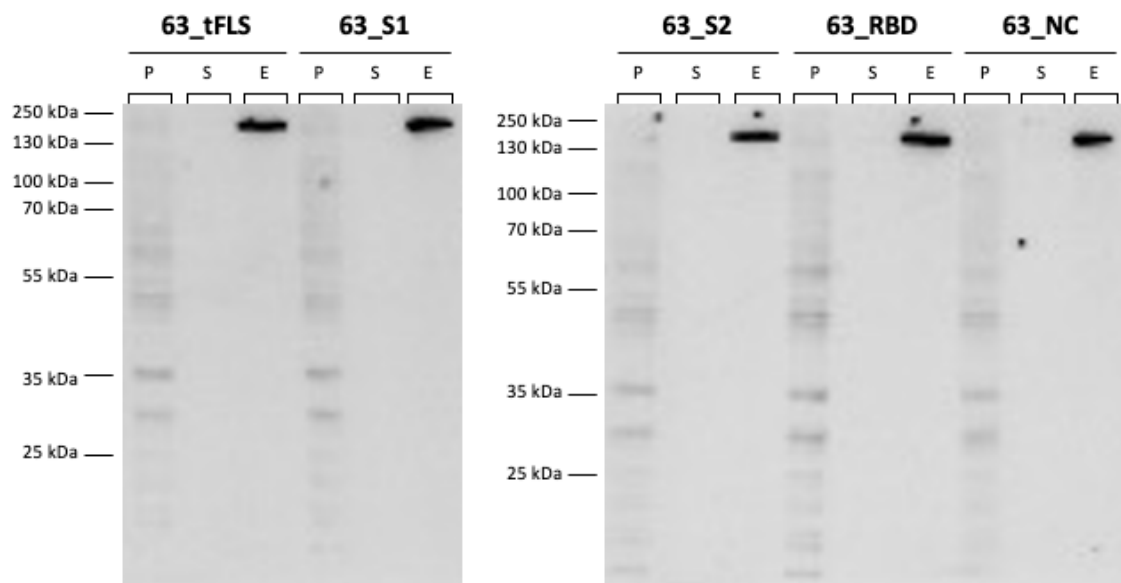


Figure 4.13: Western blot images of cell pellet lysates (P), supernatants (S) and exosome preps taken from each of the CD63-ubiquitin fusion protein expressing cell pools, using an anti-CD63 antibody probe (exposure time 30 minutes).

An anti-CD63 antibody probe of the cell pools transfected with CD63-SARS-CoV-2 fusion proteins showed extremely similar banding patterns in all of the cell pellet lysates examined, whilst the supernatant lanes from each pool showed none at all. Strong and distinctive bands were present in all of the exosome prep lanes for the CD63-SARS-CoV-

2 fusion protein cell pools at approximately 200 kDa, regardless of the varied molecular weights predicted for each fusion protein.

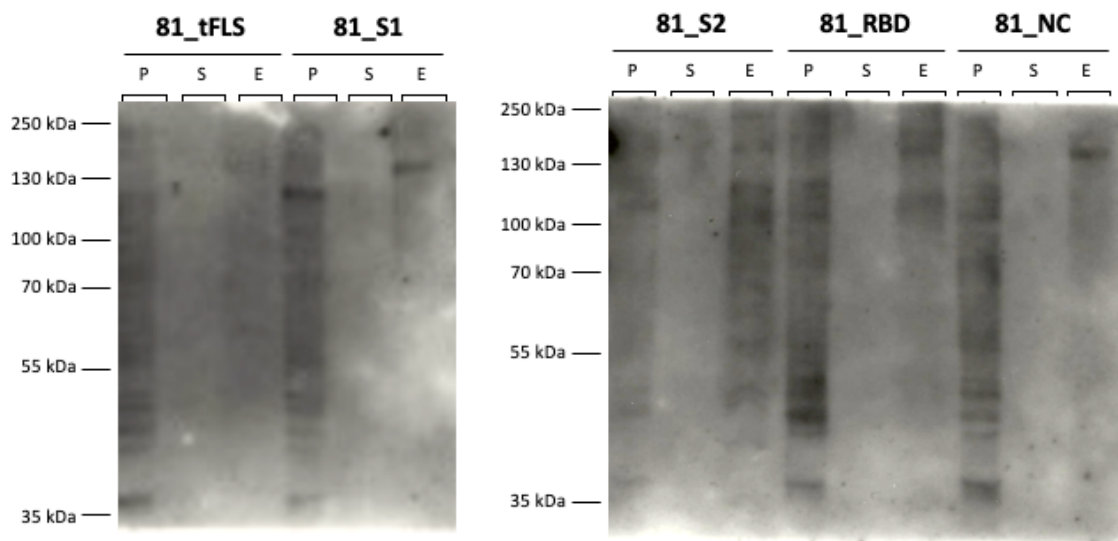


Figure 4.14: Western blot images of cell pellet lysates (P), supernatants (S) and exosome preps taken from each of the CD81-ubiquitin fusion protein expressing cell pools, using an anti-CD81 antibody probe (exposure time 40 minutes).

An anti-CD81 antibody probe of the cell pools transfected with CD81-SARS-CoV-2 fusion proteins also showed extremely similar banding patterns for each cell pellet lysate regardless of the various predicted fusion protein sizes, with no banding present in the supernatants from any cell pool. However, there was more variation in the banding present in the exosome prep lanes. Exosome prep lanes for the cell pools 81_S1, 81_RBD and 81_NC produced single bands approximately 150 kDa in size and there was also an extremely faint trace of a band of this size in the 81_tFLS exosome prep lane. This band size was also faintly present in the exosome prep lane of 81_S2, however there was also other faint bands of various sizes in this lane.

Anti-His antibody probing of all of the tetraspanin-covid fusion protein expressing cell pools (with the exception of 63_S1 and 81_S1) showed a similar banding pattern overall to that observed in the anti-His western blot analysis of the ubiquitin-SARS-CoV-2 fusion protein expressing cell pools in section 4.2.2 (Fig 4.6). His-tag bands were present in all exosome prep lanes to varying intensities but at an identical molecular weight of approximately 65 kDa, regardless of the expected size of the fusion protein for each

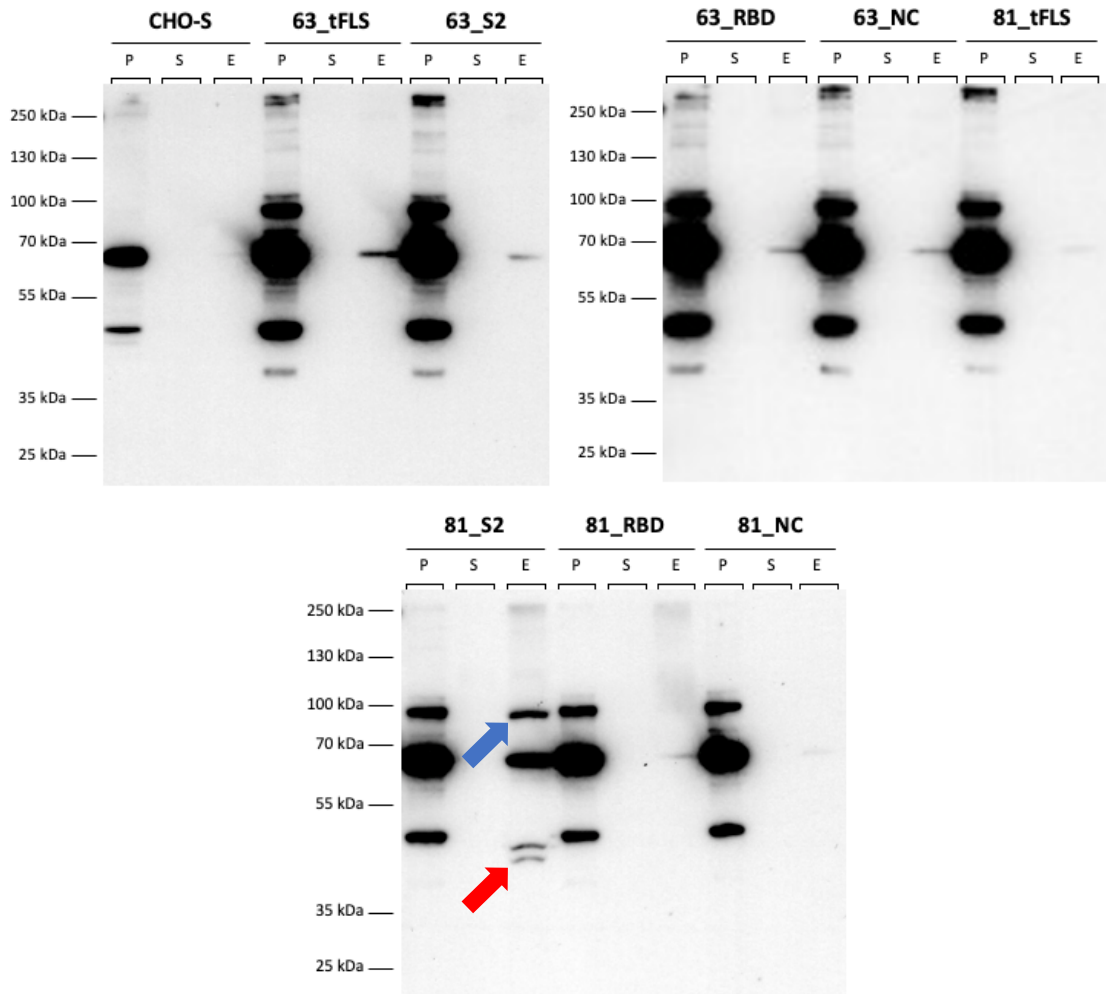


Figure 4.15: Western blot images of cell pellet lysates (P), supernatants (S) and exosome preps taken from each of the cell pools expressing tetraspanin-ubiquitin fusion proteins containing a His-tag, using an anti-His antibody probe (exposure time 4 minutes). Arrows highlight additional bands in the 81_S2 exosome suspension not present in the other pools or CHO-S control.

pool, with the exception of 81_S2 (Fig 4.15). The exosome prep lane for 81_S2 contained two distinct bands of approximately 65 and 90 kDa (marked by blue arrow, Figure 4.15) that mirror those present in the corresponding cell pellet lysate and a fainter doublet band just below the lysate's third 50 kDa band (marked by red arrow, Figure 4.15).

With the exception of 81_S2, the His-tag bands present in the CD63-SARS-CoV-2 fusion protein expressing cell pools appear stronger than those of the CD81-SARS-CoV-2 fusion protein expressing cell pools. Comparison of the band intensity between specific SARS-CoV-2 antigens fused with each tetraspanin showed no strong correlation that expression and direction into the exosome population of a cell is increased for any specific antigen regardless of tetraspanin fusion. However, the cell pools transfected

with RBD- and NC-fused proteins showed the weakest His-tag band strength in resulting exosome preps.

4.2.6 DLS analysis of exosome preparations

Particle size distribution profiles for the exosome suspensions isolated from each tetraspanin-SARS-CoV-2 cell pools were generated using DLS analysis and compared to the profile of CHO-S cell exosomes. Profiles generated from the CD63-SARS-CoV-2 cell pool exosomes all showed evidence of the CHO-S cell exosome peak to varying degrees, with the weakest evidence in the profiles of CD63_S1 and CD63_S2 (Fig 4.16). However, these two profiles also contained second peaks with a much higher relative intensity than any other peaks generated by the other CD63-SARS-CoV-2 cell pool exosomes. The CD63_tFLS and CD63_RBD exosomes also produced a two-peak profile though the particle diameter range for the former was much narrower than the latter, with the second peak of the CD63_tFLS profile presenting below 1000 nm in particle diameter. The profile from the CD63_NC exosomes showed similar but less distinct peaks of particle diameter to those from the CD63_RBD, which could be indicative of some degradation of the exosome sample used.

Analysis of the CD81-SARS-CoV-2 cell pool exosomes showed a two-peak profile in each, with the first peak matching the peak generated in the host CHO-S cell exosome profile (Fig 4.17). The second peak in all CD81-SARS-CoV-2 profiles was of higher relative frequency intensity between 1,000 – 10,000 nm in the particle diameter range, except CD81_tFLS which had two peaks of almost equal relative frequency intensity.

Comparison of the exosome profiles between the CD63- and CD81-SARS-CoV-2 cell pools exosome profiles for each SARS-CoV-2 antigen showed some similarity for those with the RBD present. However, none of the other antigens showed a common profile in both tetraspanin-fusion protein conformations.

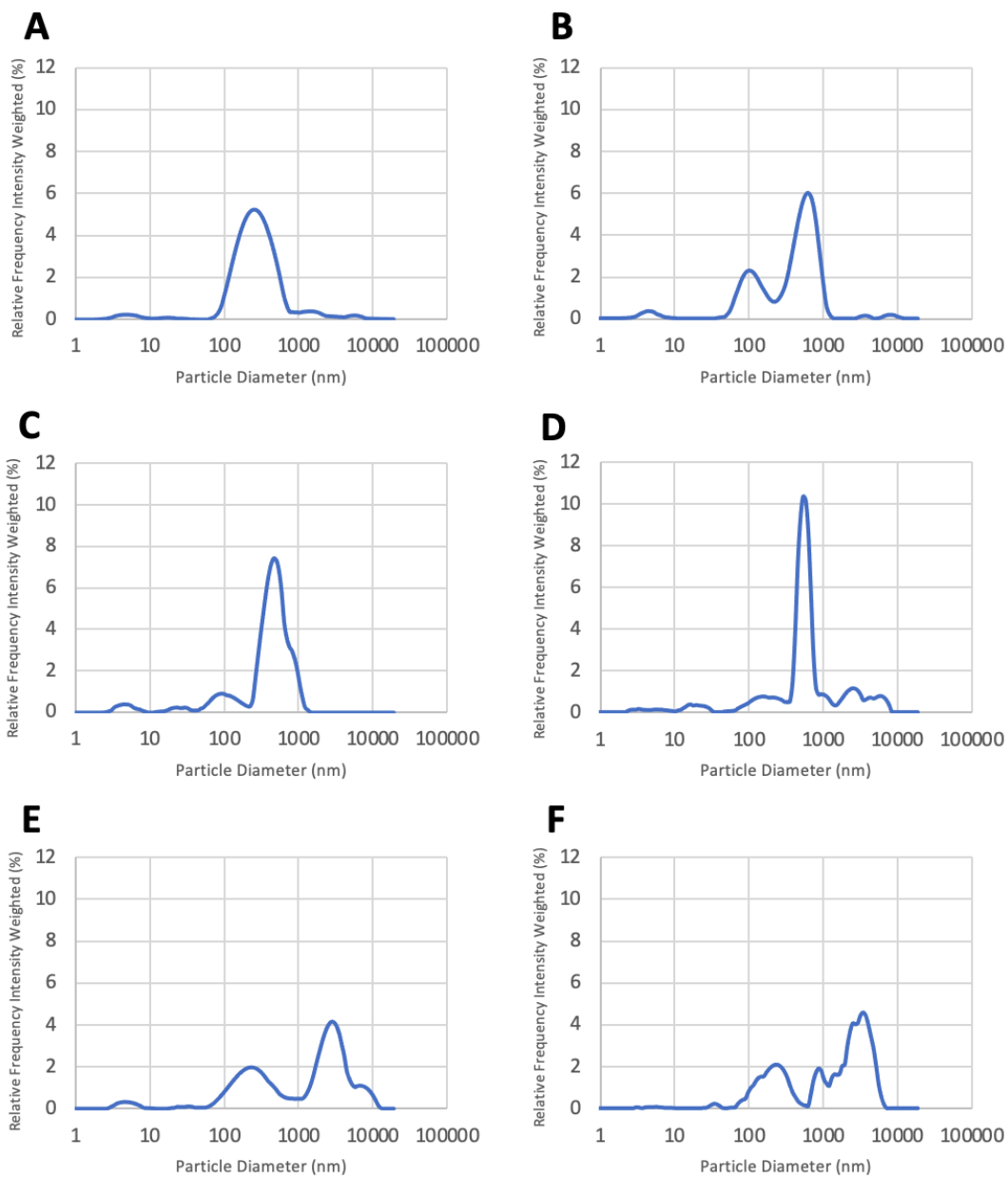


Figure 4.16: Particle size distributions of exosome preparations from the CD63-SARS-CoV-2 fusion protein expressing stable cell pool exosome suspensions, alongside negative control (CHO-S) exosome suspensions. Each figure shows the average DLS measurement ($n=10$) for relative intensity frequency weight (%) vs. particle diameter (nm) with a log₁₀ scale applied.

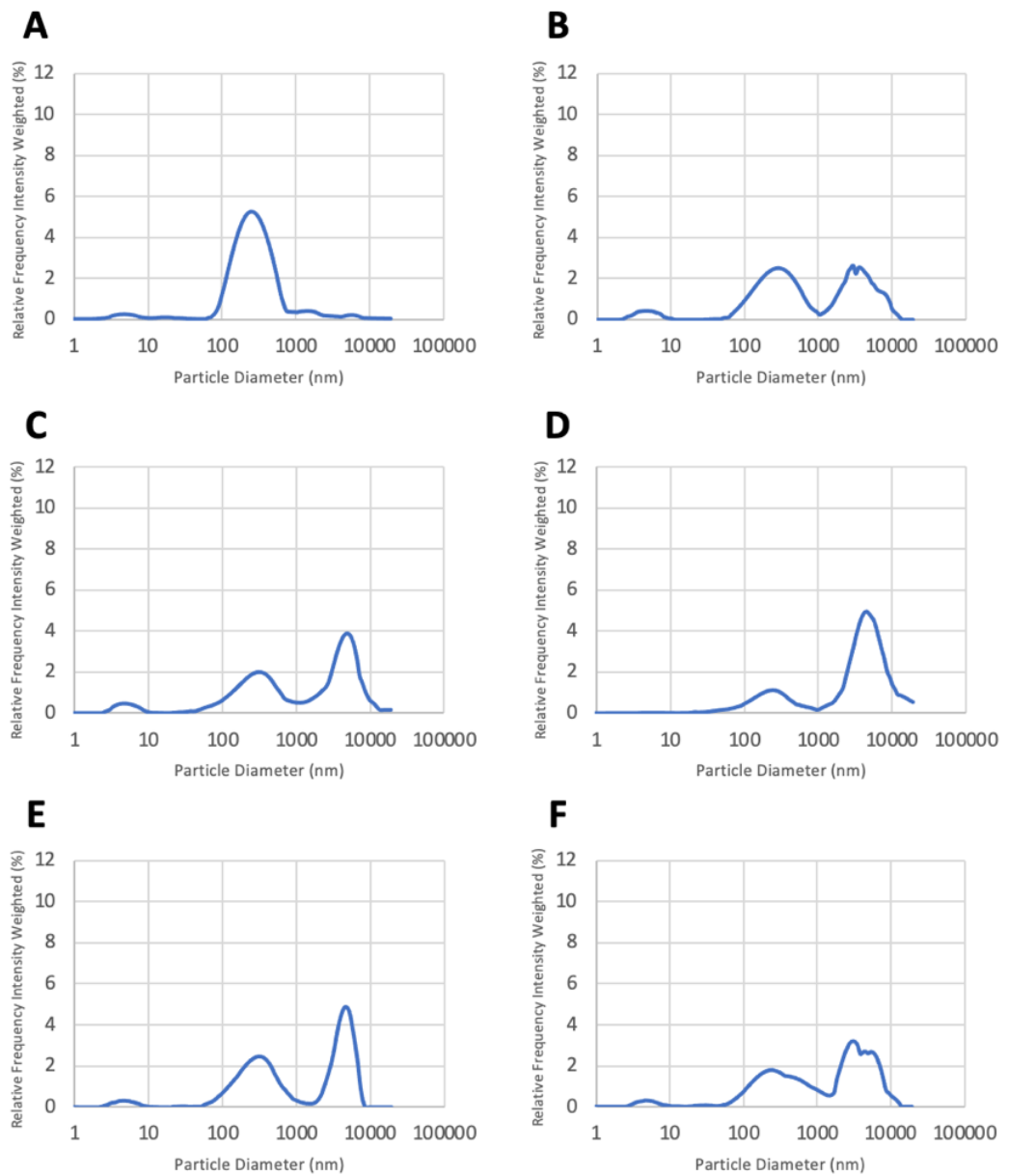


Figure 4.17: Particle size distributions of exosome preparations from the CD81-SARS-CoV-2 fusion protein expressing stable cell pool exosome suspensions, alongside negative control (CHO-S) exosome suspensions. Each figure shows the average DLS measurement (n=10) for relative intensity frequency weight (%) vs. particle diameter (nm) with a log10 scale applied.

4.3 Discussion

Following the transfection of CHO-S cells with vectors containing the ubiquitin-SARS-CoV-2 fusion proteins, western blot analysis with an anti-His probe revealed a consistent difference in the banding pattern between the non-transfected negative control and the transfected cultures (Fig 4.6). Bands present in the non-transfected CHO-S cell pellet lysate were unexpected but attributed to non-specific binding of this antibody to an endogenous CHO-S cell protein due to the repeated presence in negative controls. Additional banding present only in the transfected cultures strongly suggests that the transfected fusion proteins were expressed by the cells in some form, though the consistent sizing of the extra bands throughout the transfected cultures despite variable predicted sizes of each fusion protein is difficult to explain. It is possible that degradation occurs to each as a result of the ubiquitin tag to yield a common 'core' product.

Interestingly, this pattern was also observed in the western blot analysis of the cells transfected with tetraspanin-SARS-CoV-2 fusion proteins (Fig 4.15), despite the fusion of two targeting components both vastly different to ubiquitin. This would suggest that the differences observed in both sets of fusion protein transfections, compared to negative controls, is a result of a component present in the SARS-CoV-2 antigen sequences resulting in a common issue in fusion protein expression or folding.

Bands present in the exosome preps from the ubiquitin-SARS-CoV-2 (Fig 4.6) and tetraspanin-SARS-CoV-2 (Fig 4.15) transfected cells matching the 65 kDa sized band present in the corresponding cell pellet lysate of each culture may suggest successful targeting of proteins to exosomes. Due to the relatively even band intensity strength of anti-His throughout each of the cell pellet lysates in this analysis, the variation of band signal strength in the exosome prep lanes maybe representative of the targeting power of each ubiquitin-SARS-CoV-2 fusion protein. Under these two assumptions, it appears that the ubiquitin-SARS-CoV-2 fusion protein with the greatest targeting into exosomes is Ubi_S2, though the very faint banding in exosome preps of other fusion proteins with the N-terminal ubiquitin tag suggests this is not due to the orientation of the ubiquitin tag. In fact, the fusion proteins with the closest band intensity strength to Ubi_S2 were

tFLS_Ubi and S2_Ubi, which both contain the S2 sequence and could suggest this sequence is able to be incorporated into CHO-S cell exosomes more than the other SARS-CoV-2 antigens investigated here. When applying the same two assumptions to the tetraspanin- SARS-CoV-2 transfected cells, this increased incorporation of the S2 protein was also obvious in the CD81_S2 transfection of CHO-S cells which had the strongest banding intensity of any of the exosome preps generated. Furthermore, it appears that orientation of the ubiquitin tag in the case of the selected SARS-CoV-2 antigens used here had no significant impact on the expression of the fusion or targeting of antigens into exosomes. However, in the case of the tetraspanin- SARS-CoV-2 fusions, fusions with CD81 appeared to result in stronger exosome targeting than CD63.

The size of the band present in the blotted exosome preps at 65 kDa matches a band seen in the cell pellet lysate of the negative control (non-transfected CHO-S cells) rather than any of the extra bands seen in the transfected cell pellet lysates. This could mean that either (1) the additional 100 kDa protein product whose expression is triggered by transfection of ubiquitin- SARS-CoV-2 fusions is being degraded during its packaging into exosomes, or (2) transfection of ubiquitin-SARS-CoV-2 fusions triggers a mechanism in the cells which leads to **increased production** of exosomes, resulting in higher concentrations of general intracellular proteins on the exosome preps. However, this cannot be true for the CD81_S2 fusion which generated not only the strongest exosome prep bands but also bands not present in the non-transfected control (Fig 4.15). Western blot analysis of the exosome prep of CD81-S2 cells also gave the strongest evidence, of any of the antigens or targeting fusion strategies produced in this work, of successful direction of a protein into the exosome population of CHO-S cells.

Comparisons between the DLS data generated and western blot analysis of the ubiquitin-SARS-CoV-2 exosome preps, did not reveal any obvious relationship between the two data sets. As previously stated, western blot band intensity in the exosome preps may be indicative of the targeting power of each fusion protein with Ubi_S2, tFLS_Ubi and S2_Ubi (Fig 4.1) standing out as fusion proteins with the strongest exosome band intensity. However, there was not an increased relative intensity of any peaks present, or a shift in particle diameter ranges, for peaks in the DLS data for these

exosome preps (Fig 4.8 and Fig 4.9), when compared to the rest of the preps isolated from the ubiquitin-SARS-CoV-2 fusion protein-transfected cultures. The lack of difference in the DLS data between those highlighted in the western blot analysis and the rest of the cultures could mean that the presence of engineered exosomes evidenced from the western blot data were not at high enough amounts to be detected by the DLS-based particle size analysis. Alternatively, it could be an indication that the differences in exosome protein band intensities in blots are not representative of fusion protein exosome-targeting power.

In order to determine the actual composition of the exosomes isolated in this chapter; they would ideally be examined by mass spectrometry to confirm the protein components/constituents of each exosome population. This was attempted with the exosomes prepared in this chapter but unsuccessful due to the presence of polyethylene glycol (PEG) in the commercial kit used to isolate the vesicles from cell culture supernatants. Further work to achieve this might involve developing a method of exosome isolation which can separate out exosomes from supernatants in a high enough concentration for analysis without the need for PEG. Additionally, electron microscope imaging using immunogold staining to capture images of the exosomes at high resolution may be useful for determining if a specific protein has been successfully incorporated into exosomes.

Once a successful composition analysis has been completed then the next steps in developing this platform would be to test the potency of exosomes produced with these fusion protein expression strategies. Initially this could include an ELISA designed to detect the presence of the SARS-CoV-2 antigens incorporated into the exosomes which would give an indication of the ability of the engineered vesicles to be recognised specifically by the displayed antigens. If successful, this could be followed up with GFP-macrophage take-up assays and eventually clinical studies in mouse models for a better understanding of how the exosomes perform in a more complex environment.

Chapter 5: Optimisation, Expression and Profiling of Novel Monoclonal Antibodies for the Treatment of Dengue Fever

5.1 Introduction

This chapter describes the work carried out to optimise the expression of a difficult-to-express (DTE) novel anti-dengue antibody developed by collaborators in Mahidol University, Bangkok. The research group had previously created hybridomas using peripheral mononuclear blood cells (PBMCs) isolated from patients with secondary dengue infections resulting in the development of several human monoclonal antibodies (HumAbs) with promising cross-neutralising activity against the four DENV serotypes (Setthapramote *et al.*, 2012). Some of the HumAb clones were then further engineered for isotype switching to IgG-2 or IgG-4 and a mutation (N297Q) in the Fc region to reduce the affinity for Fc γ receptors and *in vitro* antibody dependent enhancement (ADE) (Ramadhany *et al.*, 2015; Injampa *et al.*, 2017). This chapter shows work to optimise one of the clones they developed and engineered at Mahidol University, clone 54 (Den54), which was not able to be expressed in the CHO-K1 cell lines they created.

Initial transfection of the original sequences into CHO-S cells confirmed the poor expression profiles of this molecule and the sequences were then further engineered to try improve secretion of the DTE Den54 antibody. To identify which region or domain(s) of the antibody structure were preventing successful secretion, four new molecule designs (D1 – D4) were created using the sequences from well-characterised antibodies, Trastuzumab and Nivolumab, to replace either the constant regions or both constant and framework regions of the antibody (Fig 5.4). In addition to this, each molecule was given new signal peptide sequences and codon-optimised for expression in a CHO host. A fifth molecule design (D5) was also created which retained the full original coding sequence of Den54 but with the new signal peptides and codon-optimisation for expression in CHO (Fig 5.4) as a control to determine if poor expression had been the result of poor translation or translocation prior to the secretory pathway.

The expression of each of these five designs was then examined through the creation of transient and stable-expressing cell lines as well as various stages of scale-up for the stable pools. Monoclonal cell lineages were developed from the pools and scaled up from single cell static culture conditions through to shake flask cultures and eventually a fed-batch ambr[®]250 process to examine the expression profiles throughout the process in an attempt to isolate a clone from each which could produce high titres of its respective antibody. This work also included an investigation of the effects of a temperature shifts and fed-batch conditions in order to boost antibody titres of a clone.

Finally, this chapter details an experimental investigation to identify the location of a production bottleneck for the non-hybridised D5 molecule were carried out. This investigation is formed of qRT-PCR data which examines the relative mRNA transcript levels of the heavy and light chain antibody sequences expressed to rule out any issues with translation of the sequences. Western blot analysis and an immunofluorescence study are then combined to highlight the localisation of a secretion bottleneck and identify the potential reasons for this molecule's poor secretion in CHO-S cells.

5.2 Results

5.2.1 Generation of Den54-native vectors

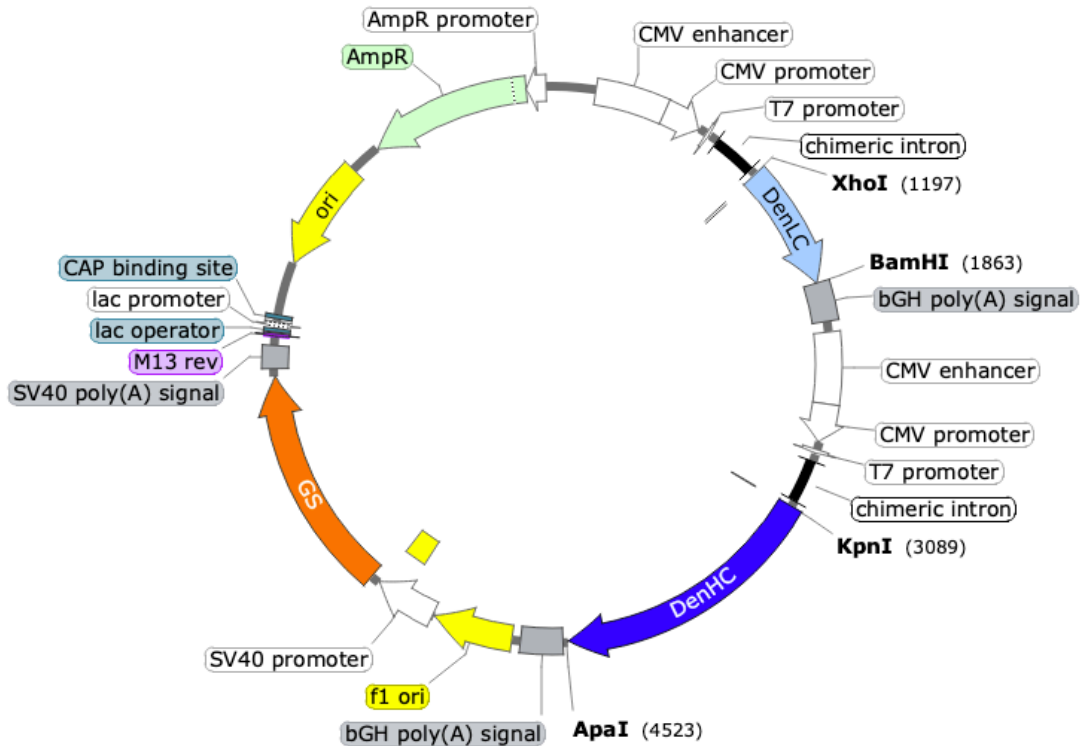


Figure 5.1: Vector map for pcDNA 3.1 GS which has the Den54 light and heavy chain sequences cloned into the restriction sites XhoI/BamHI and KpnI/ApaI, respectively, flanked by T7 promoters and bGH polyA signals. This vector also contains the metabolic selection marker glutamine synthase (GS) gene and antibiotic selection marker ampicillin resistance (AmpR) gene for mammalian and bacterial use, respectively.

To produce the DTE anti-dengue antibody, Den54, developed by our Thai collaborators, the original Den54 heavy chain (HC) and light chain (LC) sequences were acquired and submitted for commercial gene synthesis by GeneART (ThermoFisher) with the addition of universal primer binding sites for cloning. Once synthesised, the sequences were inserted into the pcDNA 3.1 GS plasmid (Fig 5.1) using traditional restriction enzyme cloning one sequence at a time (Fig 5.2A & B) with each replacing the corresponding heavy chain and light chain sequence for trastuzumab, an antibody known to be well expressed in this vector.

Once the Den54 sequences were correctly inserted and confirmed by Sanger sequencing, the vector was amplified, alongside the original trastuzumab vector and a vector with empty expression cassettes, using *E. coli* DH5 α cultures and purified via QIAGEN DNA Maxi-prep kits as described in Chapter 2 (section 2.2.10). The resulting vectors were used to transiently transfect CHO-S cell cultures and then the cell culture supernatant was harvested 72 hours post-transfection. Supernatants from each culture were analysed by SDS-PAGE followed by western blotting using an anti-heavy chain antibody probe specific to the Fc region (Fig 5.2C). Blotting showed that whilst the original trastuzumab control vector produced a banding pattern indicative of fully- and partially-formed antibody molecules, transfection of CHO-S cells with the anti-dengue antibody heavy and light chain containing vector showed no evidence of expression in supernatant samples at all.

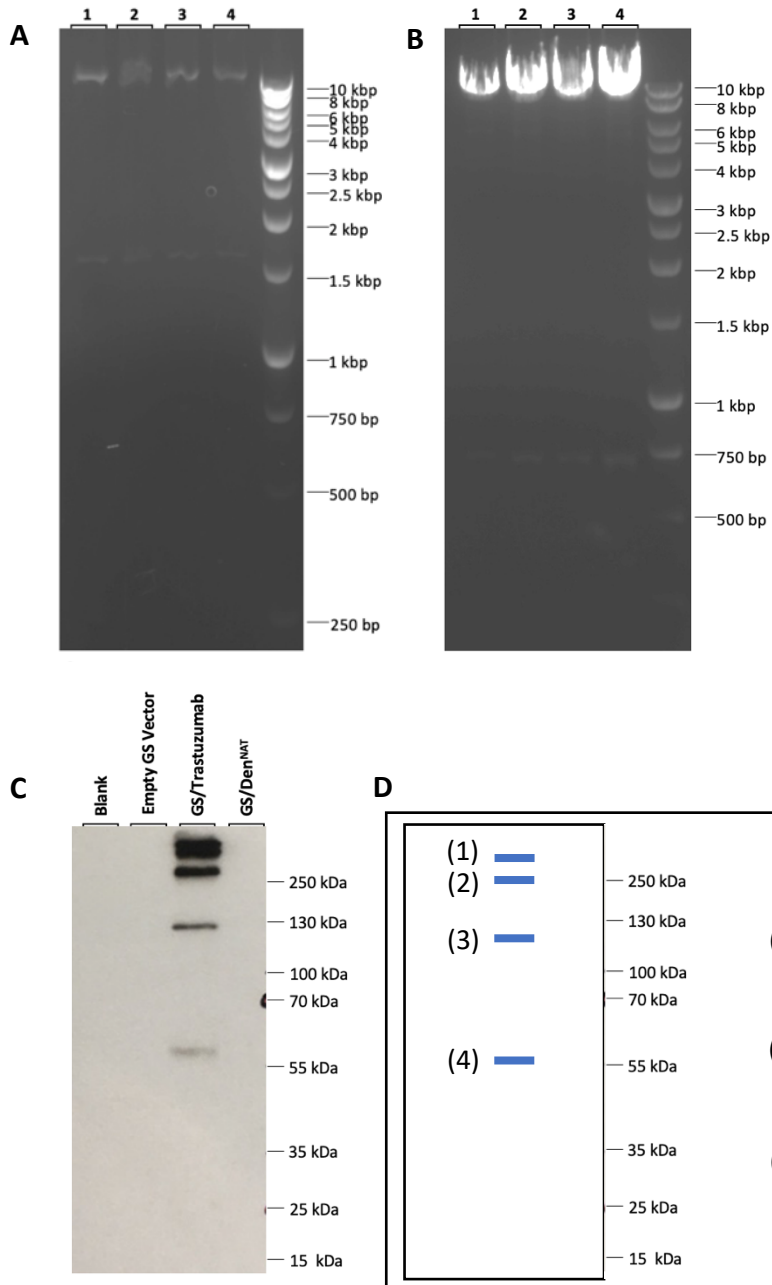


Figure 5.2: (A) 1% agarose gel loaded with test digests (*KpnI/ApaI*) for GS-Trast + DenHC ligation. (B) 1% agarose gel loaded with test digests (*KpnI/ApaI* for (A) + DenLC ligation. (C) Supernatant samples from a transient expression for 72 h of the Trast and Dengue antibody constructs analysed by western blot after running samples on a 12% SDS gel prepared with non-reducing buffers boiled. Probed for Heavy Chain (Fc) region (Sigma) with 30 second exposure. Negative controls: Blank (TE buffer only) and an Empty GS vector. Positive Control: Trastuzumab vector (GS backbone). (D) A schematic of the breakdown of expected antibody components from incomplete folding/expression which can bind to the anti-heavy chain probe: (1) fully-assembled antibody molecule; (2) two heavy chains bound with no light chain; (3) bound single heavy and light chain and (4) free heavy chains.

5.2.2 Redesign and engineering of anti-dengue antibody, Den54, amino acid sequences to improve secretory expression

To try and achieve a higher anti-dengue IgG4 Den54 antibody production and overcome possible protein synthesis difficulties, the Den54 LC and HC sequences were re-engineered into five new designs (Fig 5.4) to (i) maximise potential output and (ii) try to identify any problematic sequence components that underpinned the lack of observed expression. The designs included two variations of the hybridisation of the variable Den54 sequences with each of the two constant or framework sequences of the commercial antibody sequences of trastuzumab (IgG1, Drug Bank Accession Number DB00072) and nivolumab (IgG4, Drug Bank Accession Number DB09035) which are known to produce well in CHO cell lines.

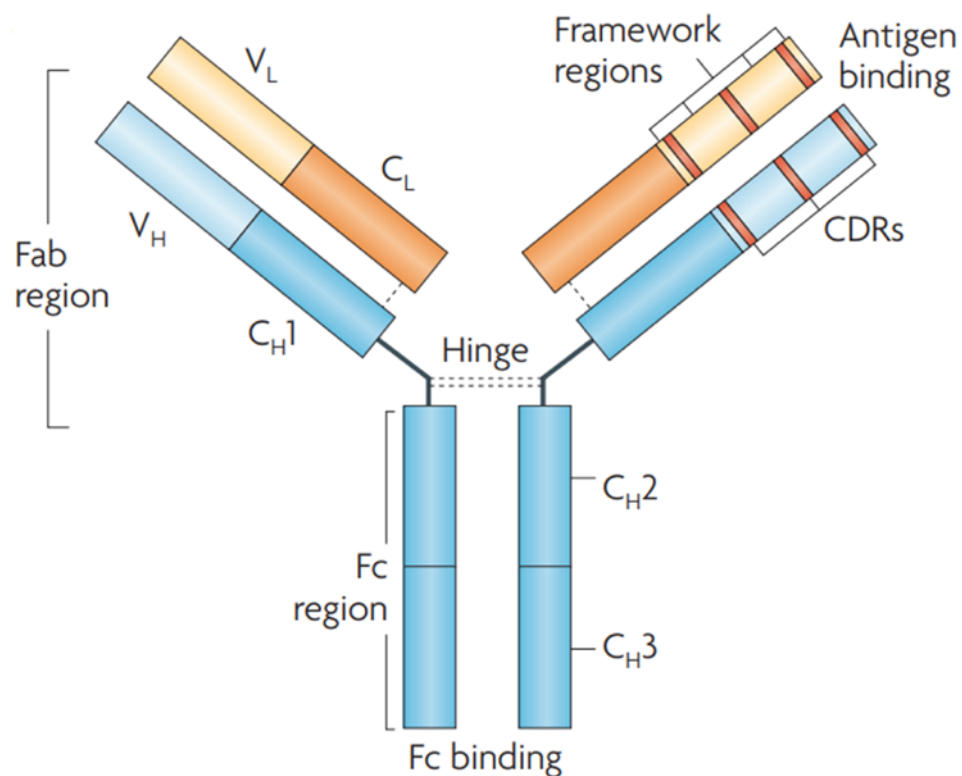


Figure 5.3: Annotated schematic of an IgG antibody molecule, including the variable heavy (V_L), variable light (V_H) and constant heavy domains (C_H1, C_H2 and C_H3). Complementarity-determining regions (CDRs) and framework regions are found in the antigen binding site in the Fab region. Constant heavy domains 2 and 3 form the crystallised fragment (Fc) region. (Hansel et al, 2010)

IgGs are composed of a light chain (LC) made of a constant (C_L) and variable (V_L) domain and a HC consisting of three constant heavy domains (C_{H1} , C_{H2} and C_{H3}) and a variable domain (V_H) (Fig 5.3, (Hansel *et al.*, 2010)). The V_L is further composed of framework regions and the complementary determining regions (CDRs) that bind to and recognise the antigen epitope. The first hybridisation set, D1 and D2 (Fig 5.4, molecules 1 and 2), were designed so that each was composed of the LC and HC constant region amino acid sequences (C_L and C_{H1} , C_{H2} and C_{H3}) of either the trastuzumab or nivolumab constant regions, respectively, and the variable regions (V_L and V_H) of Den54. This included the framework regions and complementary determining regions (CDRs) of the Den54 variable regions.

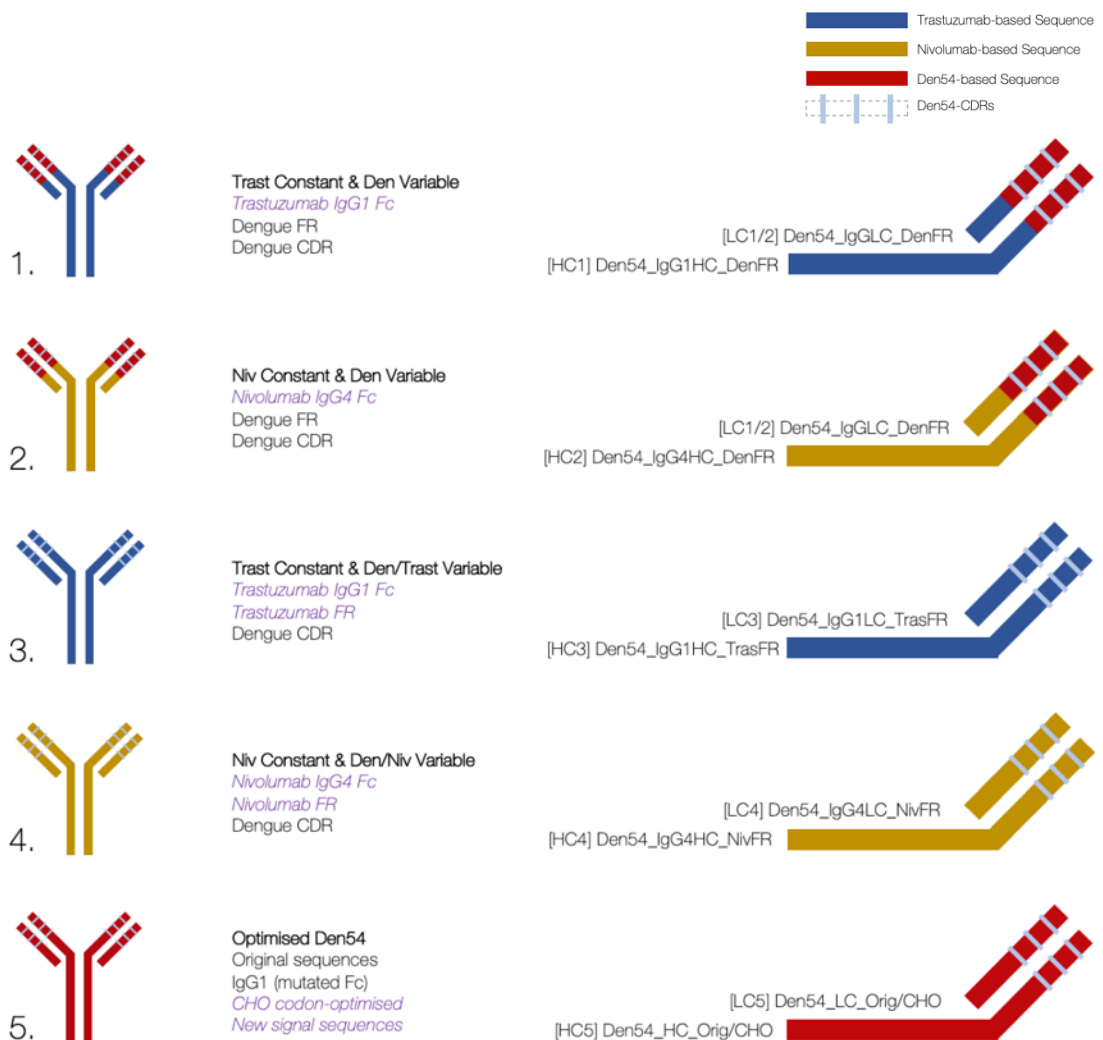


Figure 5.4: Schematic diagram showing the re-engineered of the anti-dengue Den54 amino acid sequence designs (molecules D1 – D5), with colour coding to represent sequence origins of each antibody region. Blue: trastuzumab sequence; Gold: nivolumab sequence; Red: Den54 sequence; and Light Blue bars: Den54 CDRs. (Left) Icons representing fully assembled antibody. (Right) Individual light and heavy chain sequences for expression vectors.

The second hybridisation set, D3 and D4 (Fig 5.4, molecules 3 and 4), were designed so that each was composed of the constant LC and HC sequences (V_L and C_{H1} , C_{H2} and C_{H3}) for the trastuzumab and nivolumab constant regions as in D1 and D2, but additionally also contained the variable framework regions from either trastuzumab or nivolumab with only the complementary determining regions (CDRs) matching the original Den54 sequences. The last redesigned molecule that was prepared of the original anti-dengue Den54 antibody (Fig 5.4, molecule D5) was composed of the original Den54 amino acid LC and HC sequences ($LC5$ and $HC5$) but where the transcript (mRNA) had been codon-optimised for Chinese hamster and there was a different ER signal sequence on the LC and HC (Haryadi *et al.*, 2015) known to express well in CHO cells.

5.2.3 Generation of Den54(1-5) vectors

Each of the re-engineered LC and HC sequences that make up the 5 new molecule designs (D1-D5) were commercially synthesised by GeneART (ThermoFisher). Upon arrival each of the LC and HC genes were cloned into the pcDNA 3.1 Hygromycin-Trastuzumab plasmid, after removing the Trastuzumab LC and HC genes, using traditional restriction enzyme cloning. Each of the new vectors therefore contained the LC and HC gene corresponding to the designs shown schematically in Figure 5.4. Due to the similarity in size of the inserted sequences to the original antibody chain sequences in the Trastuzumab plasmid used, screening for successful ligations entailed a double DNA restriction enzyme digest where at least one of the enzyme digestion sites was unique to the dengue sequence inserted and hence the resulting banding pattern, and hence confirmation of the required insert being present, could be assessed on an agarose gel by the number and size of bands observed (Fig 5.5).

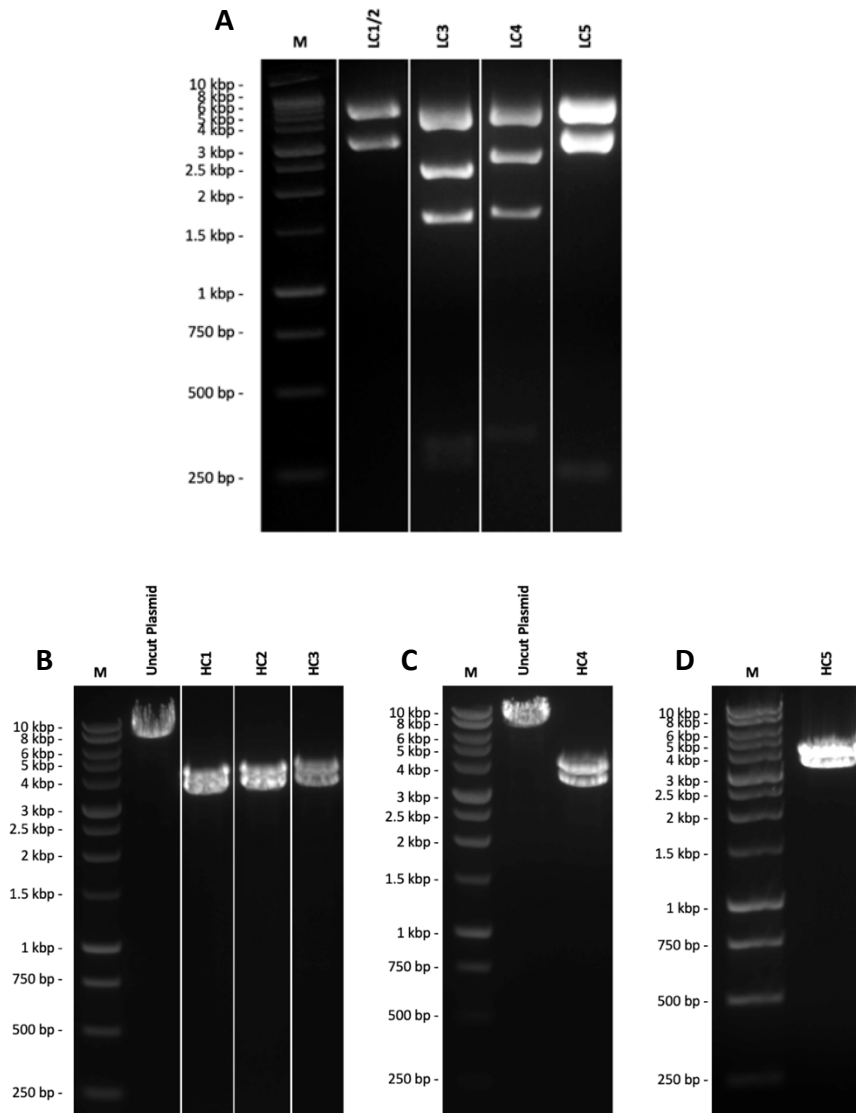


Figure 5.5: Restriction enzyme digest analysis of dengue plasmids D1 – D5 (Figure 5.3) on 1% agarose gels with a 1 kb DNA ladder marker. (A) LC1/2 and LC5 double-digested with *XhoI* and *ApaI*, LC3 and LC4 digested with *PstI*. (B - D) All plasmids digested with *BamHI*.

The light chains LC1/2 and LC5 were screened with FastDigest (ThermoFisher) restriction enzymes *XbaI* and *ApaI* which yielded two bands for a successful ligation; light chains LC3 and LC4 were screened using FastDigest (ThermoFisher) *PstI* which yielded three bands in a successfully ligated vector (Fig 5.5A). The heavy chains were all screened using FastDigest (ThermoFisher) *BamHI* for which successfully ligated vectors produced two bands (Fig 5.5B-D). After initial confirmation of the required inserts, each vector was sequenced using Sanger sequencing to confirm each gene had been inserted correctly with no mutations or frameshifts. Subsequently the plasmids were amplified in *E. coli* DH5 α and purified using commercially available QIAGEN DNA Maxi-prep kits, as detailed in Section 2.2.10 and then stored until required for transfection into CHO-S cells.

5.2.4 Expression Profiles of newly designed Den54 sequences: D1 – D5

5.2.4.1 Transient expression of different anti-dengue antibody designs

To initially determine that the newly designed anti-dengue antibody sequences were expressed at the protein level and could be detected in the supernatant after transient expression, each vector was transiently transfected into CHO-S cultures via electroporation. The resulting cultures were grown for 72 hours before harvesting the cell culture supernatant to be assessed for the presence of antibody by western blotting using an anti-HC (Fc specific) antibody probe (Fig 5.6). Blotting of the culture supernatants with the anti-HC antibody revealed that expression was observed for all of the antibody designed with a characteristic antibody banding pattern between 150 and 250 kDa, an indication that the protein observed was fully assembled (2 x LC and 2 x HC) antibody molecule. Vectors D1 – D4 all showed similar expression, whilst the D5 vector containing the optimised Den54 sequences and no hybridisation with other antibody sequences gave only a very faint band in comparison, suggesting that this was expressed at much lower amounts than the other 4 hybrid antibody designs.

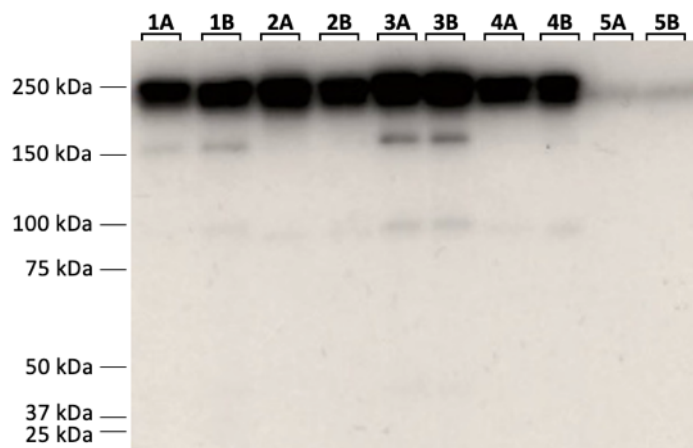


Figure 5.6: Western blot of CHO-S cell culture supernatants collected from transient transfections of the D1 – D5 vectors in biological duplicate 72 h post-transfection. A 10% SDS-PAGE analysis was undertaken with an anti-HC (Fc) primary antibody probe and 10 second exposure.

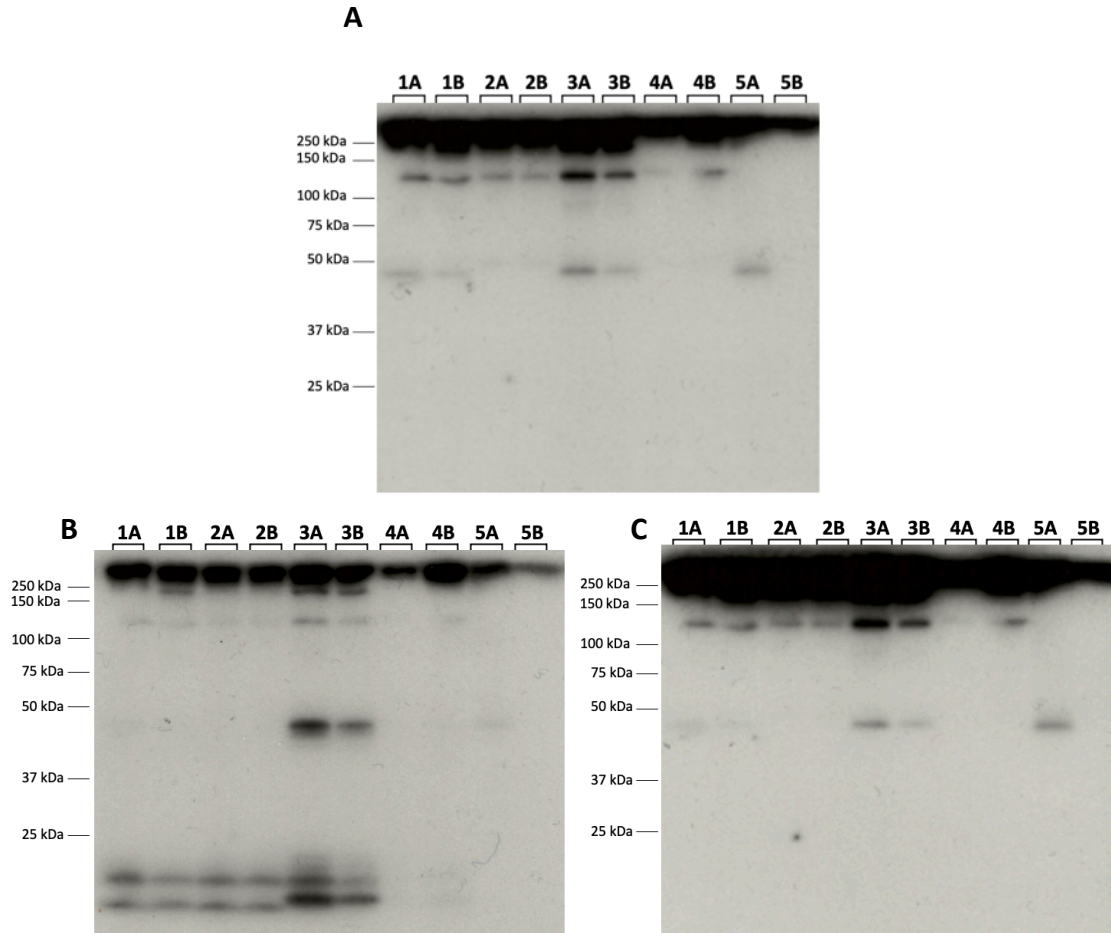


Figure 5.7: Western blots of culture supernatants collected from stable cell line pools, created with the D1 – D5 vectors. Prepared using a 12% SDS gel for electrophoresis. (A) Anti-HC (Fc) primary antibody, 5-second exposure; (B) Anti-LC (λ), 30-second exposure; (C) Anti-LC (κ), 10-second exposure.

5.2.4.2 Generation and characterisation of CHO-S stable anti-dengue antibody expressing cell pools

After confirming that the different anti-dengue antibody designs could be at least transiently expressed in CHO-S cells, to the next step was to generate recombinant CHO-S stable cell pools for each. To do this, CHO-S host cells were transfected by electroporation with linearised DNA in biological duplicate and incubated in static flasks for recovery and selection as described in section 2.3.5. The resulting cells, once recovered and scaled up to 20 mL volumes in shaking conditions, were sampled to examine antibody expression levels of each cell pool.

Western blotting of the supernatants from each line revealed that the pattern of expression for D1 – D5 shown previously in transient expression studies was maintained in stable cell pools. Although still the lowest producer, D5 visually appeared to express more protein in stable pools relative to the other cell pools (Fig 5.7). To further explore protein production, each supernatant was also probed using anti-LC- λ (Fig 5.7B) and anti-LC- κ (Fig 5.7C) antibodies to determine if any free light chain or light chain dimers were secreted by cells stably expressing the hybrid vectors (D1 -D4) and the optimised Den54 vector (D5), respectively. The blots showed the presence of light chains in D1 – D3 cell culture supernatants, but much less was apparent in D4 and D5 cell pool supernatants.

5.2.4.3 Fed-batch 100 mL production run of D1 – D5 stable cell pools

5.2.4.3.1 Western blot analysis of cell culture supernatant and cell lysates

To investigate the impact of scale-up and feeding on overall antibody production across the cell pools, fed-batch production runs were carried out with starting volumes of 100 mL and harvested when culture viability dropped below 80%. Western blotting of the supernatants collected from each culture at harvest showed the same pattern observed in lower volume batch-cultures in that D1-D4 molecules were present in the supernatant whilst there was little D5 anti-dengue molecule produced (Fig 5.8). However, when the cell pellet lysates were investigated this identified that the D5 optimised antibody, specifically in cell line 5A, was expressing and assembling antibody which was present intracellularly but that the protein was clearly retained intracellularly and was unable to be secreted out of the cell and into the culture media (Fig 5.8).

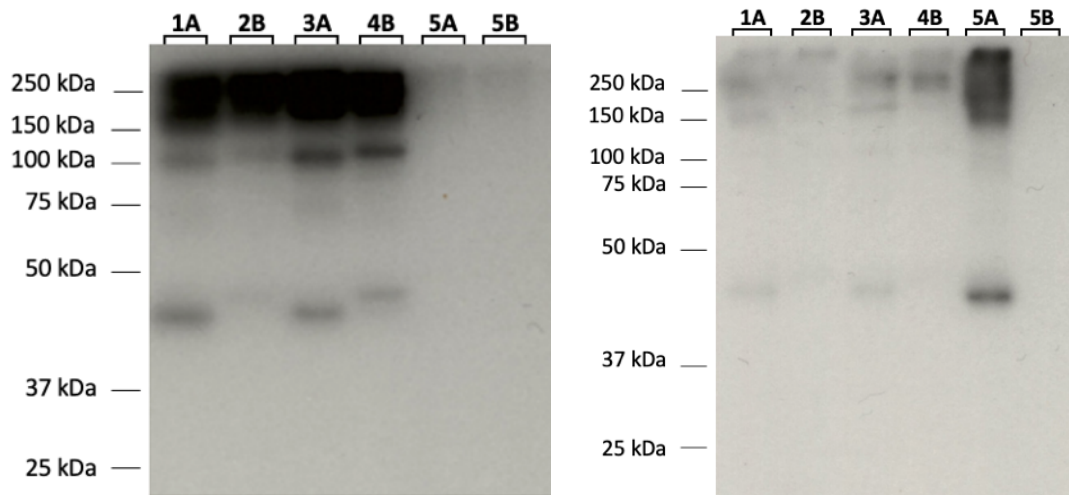


Figure 5.8: Western blot analysis of anti-dengue antibody present at harvest from the D1 – D5 stable cell pool 100 mL fed-batch production run. Samples were separated using a 10% SDS-PAGE and then probed with an anti-HC (Fc) primary antibody. (A) Cell culture supernatants, 1-second exposure; (B) Cell pellet lysates, 4-second exposure.

5.2.4.3.2 Protein-A affinity chromatography purification of secreted anti-dengue antibodies

Harvested fed-batch cultures were centrifuged to pellet the cells and cell debris and recover the supernatants, which were then filtered before application onto a Cytiva® mAb Select SuRe protein A column attached to a GE ÄKTA™ Pure fast-protein liquid chromatography (FPLC) system for purification. Purification and recovery of antibodies for the stable pools D5A and D5B were excluded from this process as the original western blot analysis of the harvest cell culture supernatant showed no or little presence of antibody (Fig 5.8A). The resulting elution fractions, flowthrough and washes were collected and again analysed by western blotting to determine the efficiency of the binding, washing and elution steps of the affinity chromatography process and track the presence or absence of antibody in each with an anti-heavy chain antibody (Fig 5.9).

Each of the recovered anti-dengue antibody products were present in the highest concentration (as determined visually from the western blot band intensity) within elution fractions 3-6 with a less intense signal in elution 2 (Fig 5.9). There was no, or very weak, signals for bands of the size expected for full-sized antibody products in the

flowthroughs or wash collections in each run, suggesting very little loss of antibody from poor binding (Fig 5.9).

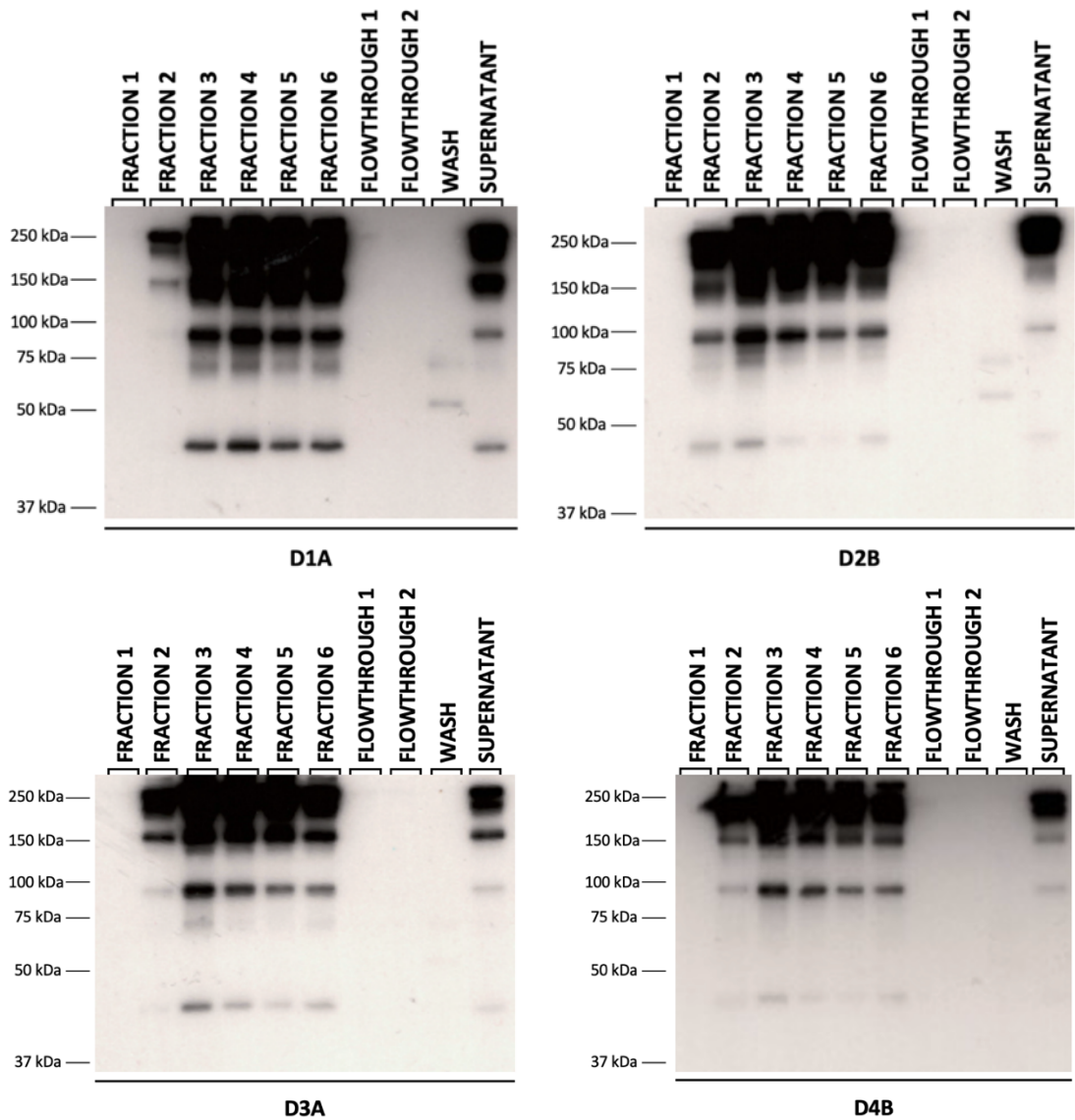


Figure 5.9: Western blot analysis of the harvested cell culture supernatants and the elutions, flowthroughs and washes collected during FPLC Protein A affinity chromatography purification of the secreted antibody from the supernatants harvested from 100 mL fed-batch productions runs of the D1- D4 stable cell pools. Prepared using a 10% SDS-PAGE gel for electrophoresis, probed with an anti-HC(Fc), 10-second exposure.

5.2.4.3.2 Assessment of concentration of purified antibodies using ELISA

Pooled elution fractions (3-6 from Figure 5.8) from each purification run were then passed through a 50,000 kDa molecular weight cut-off (MWCO) spin tube filter, buffer exchanged into PBS and collected as a concentrated antibody suspension of around 500 μL in volume. To determine the antibody concentration of each, an enzyme-linked immunosorbent assay was designed using an IgG F(ab)₂ capture antibody to pre-coat the plates (detailed in Section 2.4.3). Once the assay was optimised using a commercially-produced IgG, trastuzumab, each of the antibodies purified from stable cell pool fed-batch cultures were run in concentrations ranging from neat to 1:1000 diluted. However, the only concentration that produced a result were the neat samples and each were determined to have low concentrations of antibody (40-60 ng, Figure 5.10).

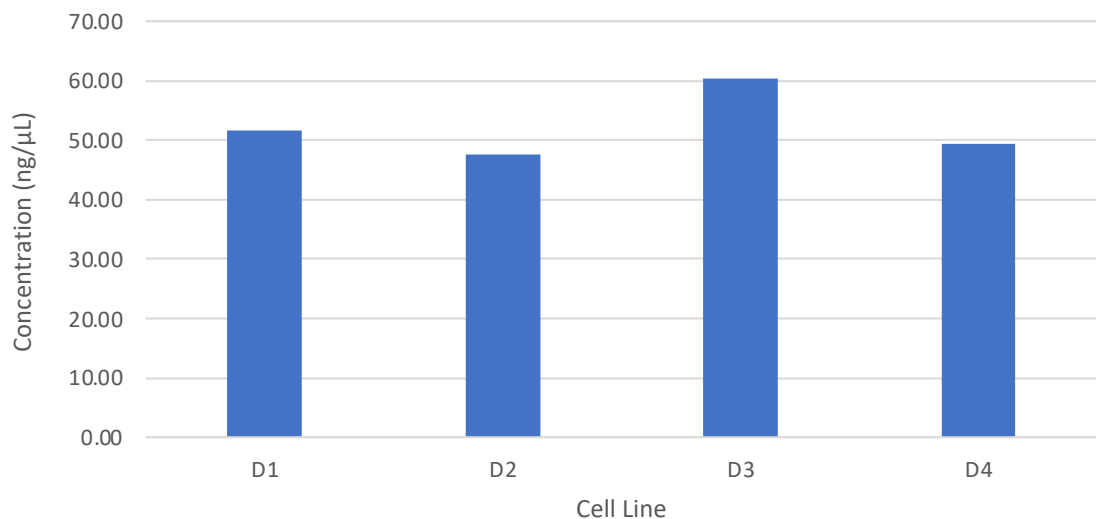


Figure 5.10: ELISA-determined concentration (ng/ μL) of each of the purified anti-dengue antibodies produced from the respective stable pool cell lines D1 – D4 (n=1)..

5.2.5 Initial Development of Monoclonal Stable Cell Lines Expressing Anti-Dengue Molecules D1 – D5

5.2.5.1 Limiting Dilution Cloning of Cell Pools

In an attempt to isolate higher expressing cells and ultimately boost the production of antibody, monoclonal cell line development was undertaken using three 96-well plates of limiting dilutions of each cell pool to separate out single cells from the pools as

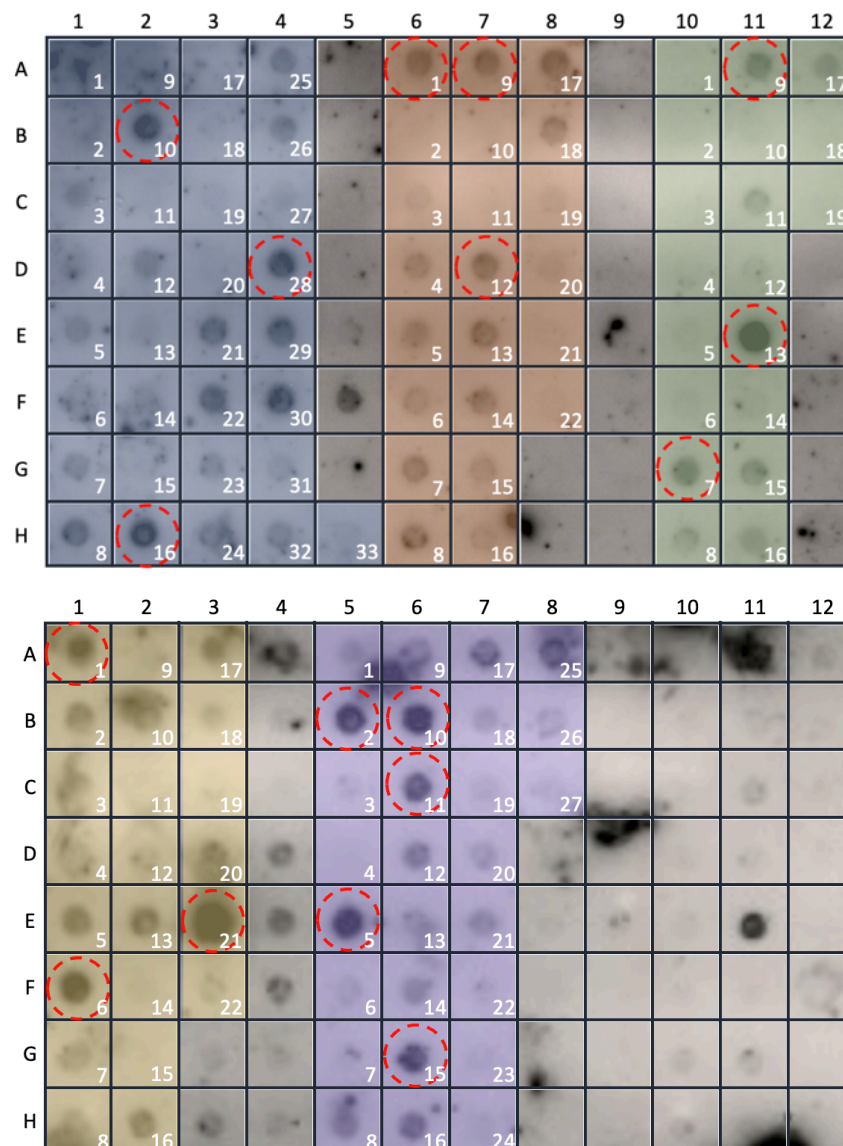


Figure 5.11: Western dot blot using 100 μ L of the cell culture supernatants of specific D1 - D5 clonal cell lines, grown in 96-well plates post-limiting dilution. Blots probed with an anti-HC (Fc) primary antibody and 20-minute exposure. Clones from each cell line are grouped and colour-highlighted: (Top) Blue = D1; Orange = D2; Green = D3; (Bottom) Yellow = D4 and Purple = D5. Clones selected for further scale-up are highlighted further with dashed red circles.

described in section 2.3.7.1. Once clones were isolated and cultivated, the supernatant

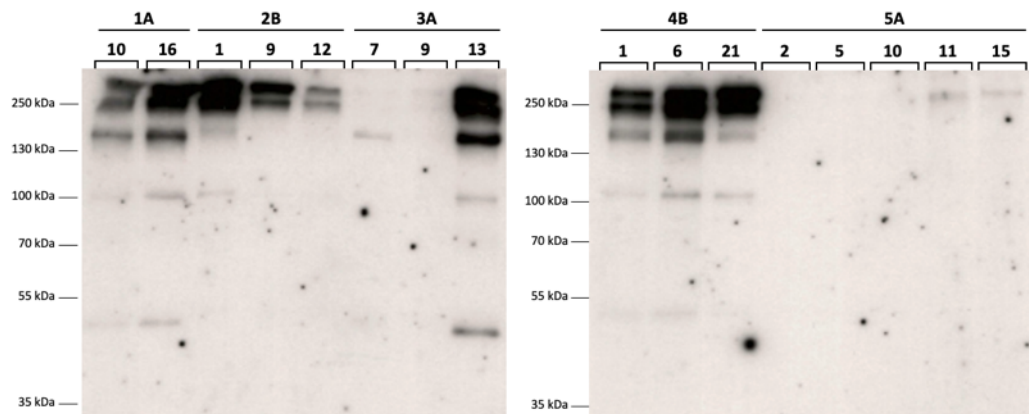


Figure 5.12: Western blot analysis of D1 – D5 expressing clones after scaling to static T25 flasks with 10 mL culture volumes. Analysis undertaken using a 10% SDS-PAGE gel for electrophoresis, probed with an anti-HC (Fc) primary antibody, 10-minute exposure.

from the wells the cells were cultured in were applied to a nitrocellulose membrane and blotted using an anti-HC(Fc) antibody probe to determine which clones gave the strongest signal and hence were likely to be considered higher antibody producers (Fig 5.11). The three clones for D1 – D4 and the five clones for D5, highlighted in Figure 5.11, were then taken forward for scale-up and further investigation.

5.2.5.2 Scale-up of monoclonal cell lines and determination of antibody expression profile: Growth in T25 static flask cultures

After cultivation in increasingly larger static well-style plates, the surviving clones were transferred into T25 static flasks in a total volume of 10 mL of culture medium and then the supernatant collected and re-assessed to investigate expression profiles. Western blotting of the collected supernatants showed that the clones selected for each cell line produced differing expression levels, as well as differences between each molecule (Fig 5.12). Once again, D1 – D4 cell lines had at least one with stronger expression of a fully assembled antibody product in the supernatant than other clones, whilst D5 clones showed minimal or no presence of product in every cell line. The two clones with highest expression for each cell line, as visually determined from the banding intensity, including cell lines for the D5 molecule, were selected and taken forward for further scale-up.

5.2.5.3 Scale-up of clones into spin tube shaking cultures and analysis of antibody expression by western blot

After T25 flasks, cells were adapted to suspension culture and cultured at the same volume but under shaking conditions of 220 rpm in 50 mL falcon tubes. After the culture viability of each line recovered to >90%, each culture was passaged at 0.2×10^6 viable cells/mL and grown for 72 hours before harvesting. The supernatants collected were then analysed by western blotting with an anti-HC(Fc) antibody probe and showed no major discrepancies between the banding patterns or expression levels observed in the previous T25 flask static cultures (Fig 5.13).

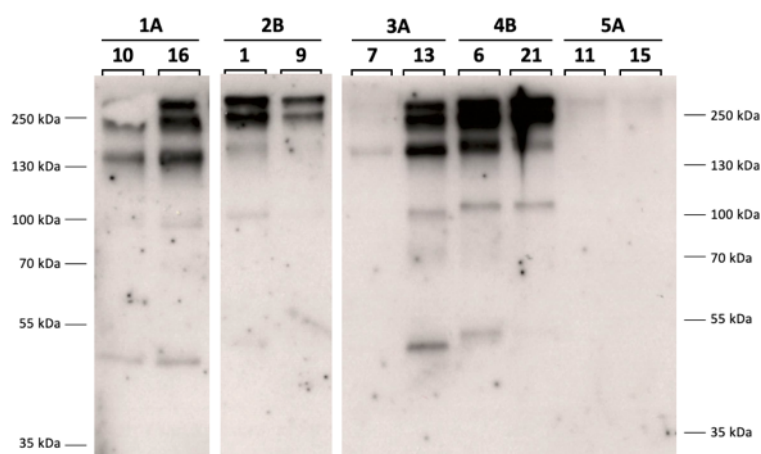


Figure 5.13: Western blot analysis of D1 – D5 clone cell culture supernatants after growing in suspension shaking incubation at 220 rpm in 50 mL falcon tubes in 10 mL culture volumes. Analysis undertaken using a 10% SDS-PAGE gel for electrophoresis, probed with an anti-HC (Fc) primary antibody, 30-second exposure.

5.2.5.4 Scale-up of clones to growth in E125 shake flasks and analysis of antibody production by western blot

The isolated clones were then transferred to suspension growth in 125 mL Erlenmeyer flasks in a total culture volume of 20 mL. Again, once culture viabilities recovered to >90%, cultures were passaged at 0.2×10^6 viable cells/mL and grown for 72 hours before harvesting. The western blotting of supernatants from the resulting cultures showed

more-or-less identical profiles for each cell line as seen at previous cell culture scales, with the exception of D3A-13 which appeared to have a different banding pattern with a stronger band around 250 kDa and weaker lower bands (Fig 5.14). Overall, throughout the scale-up process of the selected clones, there was no major changes in expression profile observed for any of the cell lines at each increasing level of cultivation.

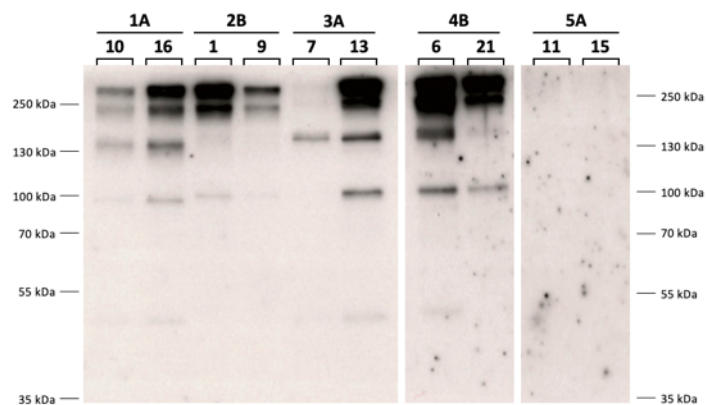


Figure 5.14: Western blot analysis of supernatant from D1 – D5 clones after growth at 140 rpm in 125 mL Erlenmeyer flasks in 20 mL culture volumes. Analysis undertaken using a 10% SDS-PAGE gel for electrophoresis, probed with an anti-HC (Fc) primary antibody, 30-second exposure.

5.2.6 Fed-batch production runs of D1 – D5 molecule expressing monoclonal cell lines

5.2.6.1 Culture growth and productivity profiles

Using the clones considered to have the best expression in E125 shake flasks, fed-batch production runs were set-up for each cell line in 500 mL vented shake flasks with a starting volume of 100 mL, seeded at 0.2×10^6 viable cells/mL. Each culture was incubated at 37°C, 5% CO₂ with shaking at 125 rpm for the duration of the run. The cultures were fed with Gibco™ Efficient Feed B using the feeding regimen described by the manufacturer. Sampling for cell counts (Fig 5.15B & C) and the assessment of protein expression via western blot (Fig 5.15A) were taken on feeding days 3, 6 and 9 as well as at final harvest.

With regards to both culture viability and longevity, D1A-16 and D5A-11 greatly surpassed the other three cell lines, whilst D4B-21 was the poorest performer overall

with an early decline in culture viability after peaking on day 6 at 12.07×10^6 viable cells/mL (Fig 5.15B). Interestingly, the closely matched growth profiles of D1A-16 and D5A-11 were not reflected at all at the antibody production level as assessed by western blot. The product analysis by western blot revealed a massive increase in protein expression between days 6 and 9 for the D1A-16 cell line but almost no expression throughout the entire run for the D5A-11 cell line (Fig 5.15A). The strongest signal present on the blots was that from the D2B-1 cell line at harvest on day 11, which also reached the highest viable cell concentration of 30.62×10^6 viable cells/mL on day 9 (Fig 5.15B).

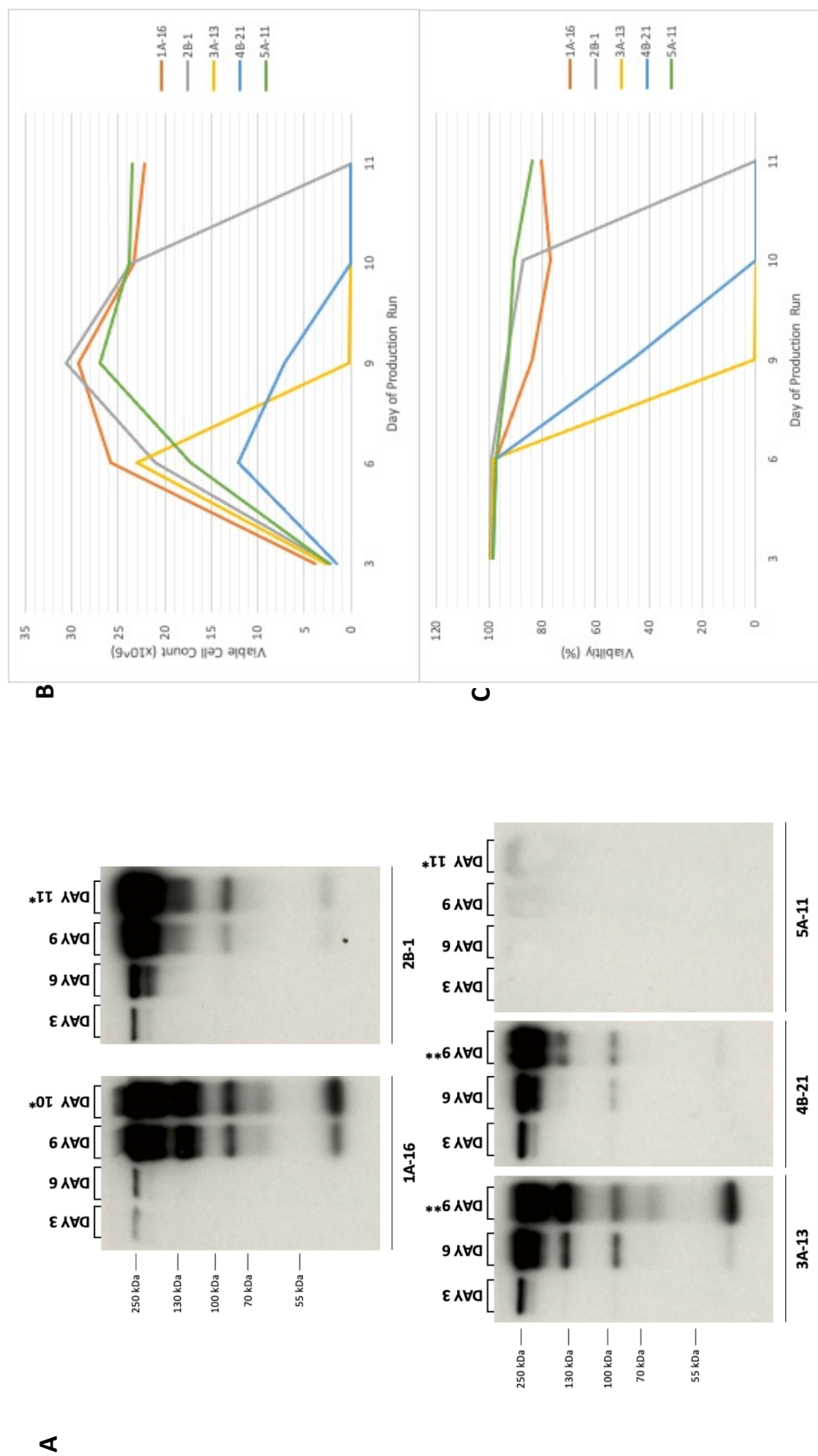


Figure 5.15: 100mL fed-batch production run sampling results from monoclonal lines D1A-16, D2B-1, D3A-13, D4B-21 and D5A-11. (A) Western blots of supernatants collected during culture sampling on feed and harvest days. Prepared using an 10% SDS gel for electrophoresis and probed with an anti-HC (Fc) primary antibody, 5-second exposure. (B) Viable cell counts of each culture over time (days) (n=1). (C) Viability percentages of each culture over time (days) (n=1).

5.2.6.2 Protein-A Affinity Chromatography Purification of Fed-Batch Monoclonal Cell Line Cultures

Harvested culture from the 500 mL flask fed-batch production runs was centrifuged at 4,000 x g and the resulting supernatant vacuum filtered using a 0.2 µm PES filter before purification on a mAb Select SuRe protein A column (Cytiva) via FPLC as described in section 2.5.1. Samples from the elution fractions and the collected flowthrough and wash were examined using western blot with the anti-HC(Fc) antibody probe to determine efficiency of column binding and elution (Fig 5.16). The blots showed strong bands around 250 kDa in elutions 2 – 6 of D1A-16, D2B-1 and D3A-13. D1A-16 and D3A-13 also showed minimal presence of antibody product in the flowthrough and wash collections, whilst D2B-1 showed weak evidence of bands in these lanes. D4B-21

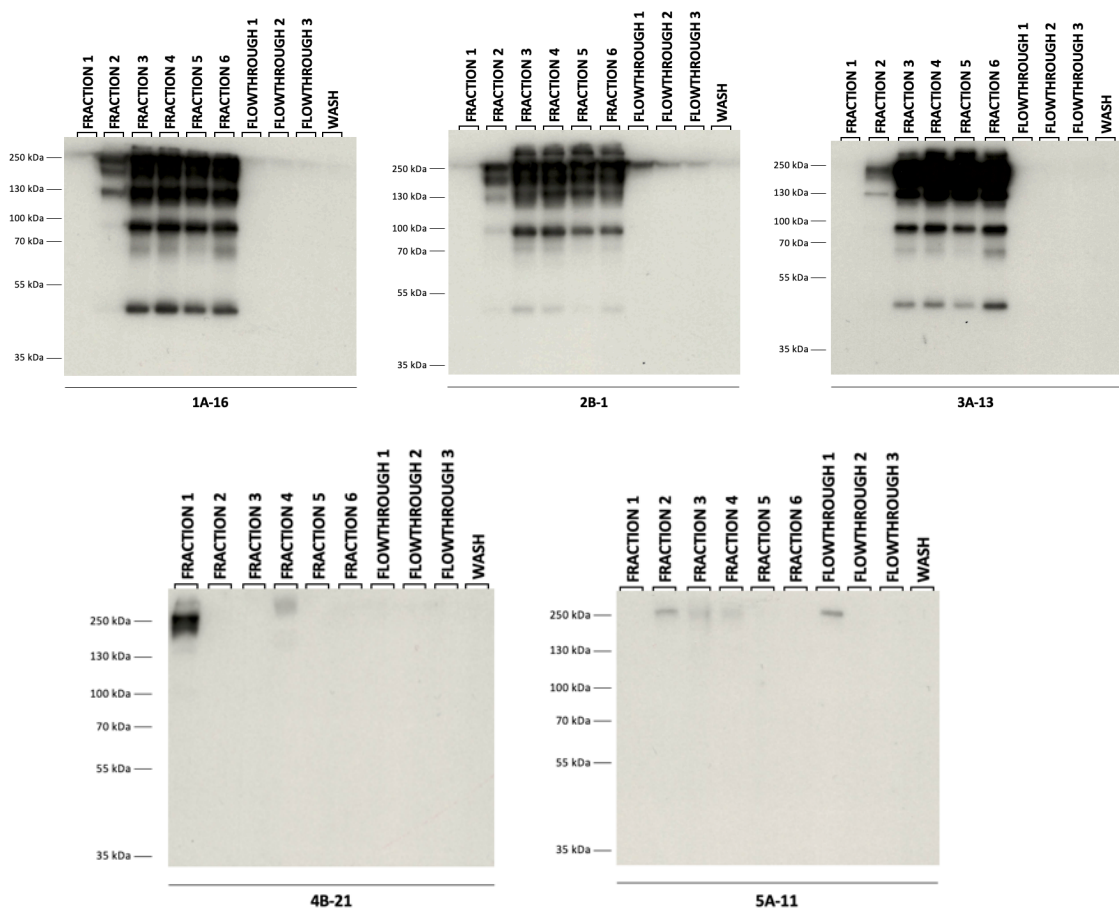


Figure 5.16: Western blot analysis of the elutions, flowthroughs and washes collected during FPLC Protein A affinity chromatography runs for the supernatants harvested from fed-batch production runs of D1A-16, D2B-1, D3A-13, D4B-21 and D5A-11. Analysis undertaken using a 10% SDS-PAGE gel for electrophoresis, probed with an anti-HC (Fc) primary antibody, 2-second exposure.

produced a single strong 250 kDa band in elution 1 with no bands in the flowthrough or wash collections either, whilst D5A-11 showed only a very faint 250 kDa band in elutions 2 – 4 and flowthrough 1.

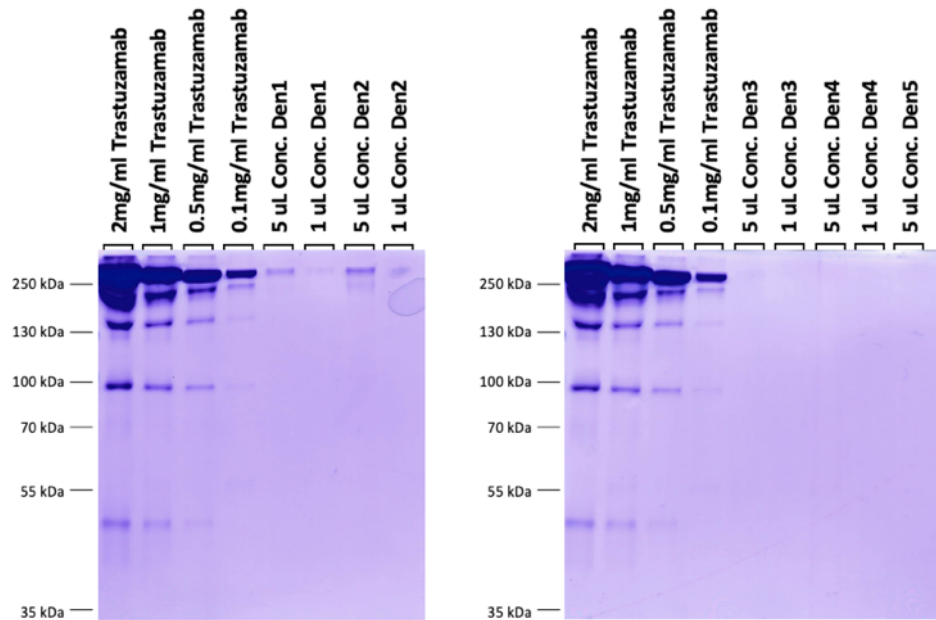


Figure 5.17: Coomassie blue-stained SDS-PAGE of the purified and concentrated monoclonal D1 – D5 antibody products in 1 uL and 5 uL volumes, alongside 5 uL volumes of commercially produced Trastuzumab in a standard concentration range.

After purification by Protein A chromatography, the elutions collected were pooled and applied to a 50,000 kDa molecular weight cut-off spin tube filter and buffer exchanged into 1X sterile PBS to a final volume of <1 mL, according to the manufacturer’s instructions. For visual assessment of concentration, each concentrated mAb was analysed on an SDS-PAGE alongside 5 uL of Trastuzumab standards ranging from 0.1 - 2 mg/mL, and bands visualised using coomassie blue stain (Fig 5.17). Of the concentrated purified mAb, cell cultures expressing molecules D1A-16 and D2B-1 yielded the strongest band at around 0.1 mg/mL compared to the trastuzumab control. Due to very faint banding in the coomassie gel comparison (Fig 5.17), a western blot was undertaken (Fig 5.18). While the heavy chain signal for the D1_8 and D3_11 molecules were still faint, blotting confirmed that D2_1 not only yielded the strongest titre from this run with approximately 0.5 – 1 mg/mL (using trastuzumab as a reference), but that the work to develop this cell line from a stable pool had resulted in an increase in expression.

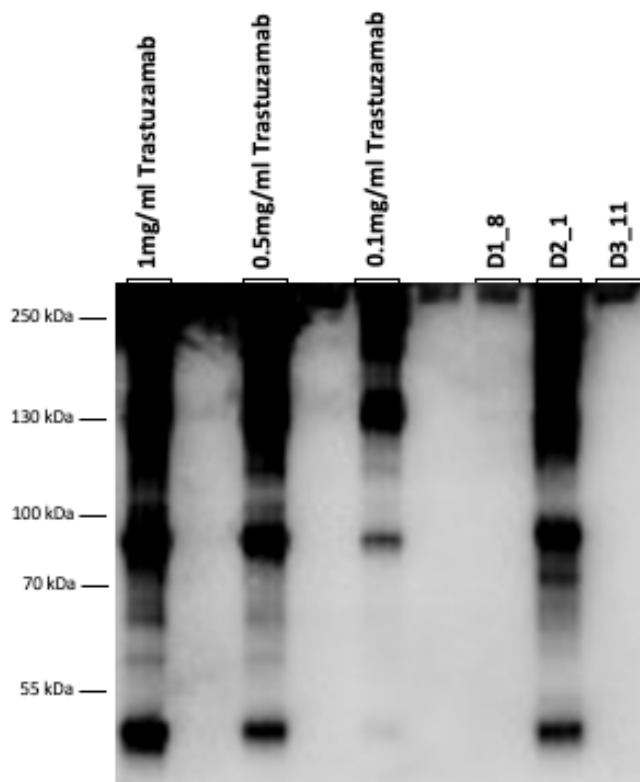


Figure 5.18: Western blot (anti-HC probe, 2-second exposure) comparison of purified antibody material from monoclonals D1_8, D2_1 and D3_11 with standard concentration range of commercially produced trastuzumab.

In order to further boost concentrations, a second round of limiting dilution cloning was undertaken to try and further isolate the highest producing clones from the cell lines generated in this section, which may not have been completely monoclonal due to the nature of limiting dilution cloning.

5.2.7 Second Round of Limiting Dilution Cloning for Generation of Monoclonal Stable Cell Lines Expressing Anti-Dengue Antibody Molecules D1 – D4

In order to try and further isolate high-producing clones, a second round of limiting dilution cloning of cell lines D1A-16, D2B-1, D3A-13, D4B-21 was undertaken. Isolated clones were then once again grown in progressively larger cultures and examined via western blot to identify those with the highest expression of the respective anti-dengue mAb for each cell line.

5.2.7.1 Scale-up Expression Profile: Spin Tube Shaking Cultures of Clones

Clones were scaled from the limiting dilution volumes up to 10 mL culture volumes and then moved to shaking culture conditions in 50 mL spin tubes grown with shaking at 220 rpm. The resulting cultures were sampled after 4 days of growth and western blots carried out to compare mAb expression levels (Fig 5.19). Expression from the new clones, derived from the D2B-1, D3A-13 and D4-21 cell lines, was fairly consistent with only minor differences in banding intensity between them. However, the clones isolated from cell line D1A-16 showed a larger discrepancy in band intensity between the three cell lines investigated with clone 8 being the standout with the highest antibody expression from those isolated from that line. Two new clones from each line deemed to have the highest expression from the western blot analysis were selected and taken forward for further scale-up and investigation.

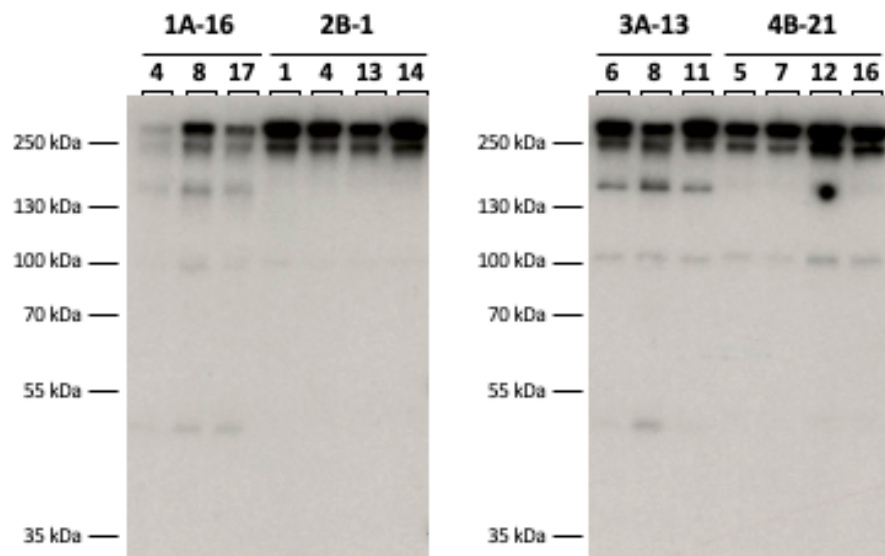


Figure 5.19: Western blot analysis of anti-dengue mAb from the clones produced from lines D1A-16, D2B-1, D3A-13 and D4B-21 after scaling to shaking incubation at 220 rpm in 50 mL falcon tubes with 10 mL culture volumes. Analysis undertaken on a 10% SDS-PAGE gel for electrophoresis, probed with an anti-HC (Fc) primary antibody, 2-minute exposure.

5.2.7.2 mAb expression profile of cell lines in E125 flask shaking cultures

Each of the new clones selected for high expression were transferred to 125 mL Erlenmeyer shake flasks and incubated with a shaking speed of 140 rpm in 20 mL volumes. After 4 days of growth, each culture was sampled and western blot analysis carried out to assess any changes in expression profiles before advancing to further scale-up (Fig 5.20). Despite previously showing expression, neither of the clones derived from D1A-16 showed any detectable antibody under larger shake flask culture conditions and there was a noticeably reduced antibody signal for the D3A-13 clones (Fig 5.20). However, the expression profiles of mAb from clones isolated from D2B-1 and D4B-21 mirrored the previous expression profile of these at lower volumes with the exception of the D2B-1 clone 14. In light of these results, the strongest expressors for each cell line were selected for a production run as well as both the weakly-expressing clones derived from D1A-16 to assess whether this was an aberrant result or that modified culture conditions could reproduce the previously observed expression levels.

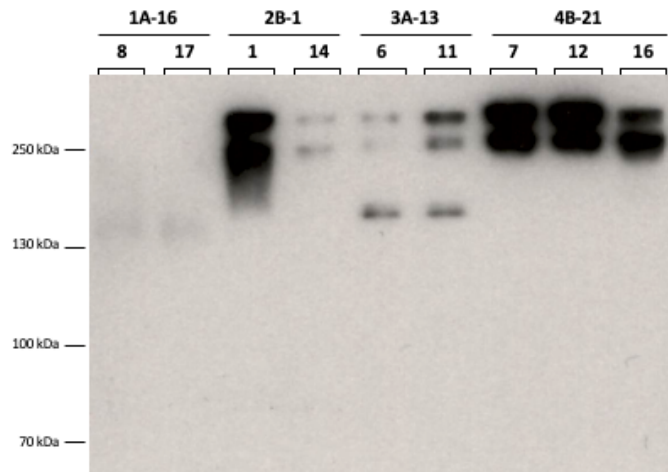


Figure 5.20: Western blots of the clones produced from lines D1A-16, D2B-1, D3A-13 and D4B-21 after scaling to shaking incubation at 140 RPM in 125 mL Erlenmeyer flasks with 20 mL volumes. Prepared using an 10% SDS gel for electrophoresis, probed with an anti-HC (Fc) primary antibody, 10-minute exposure.

5.2.7.3 Fed-batch Production Runs of D1 – D4 2nd Generation Monoclonals

5.2.7.3.1 Routine sampling to assess growth and productivity throughout culture

Each of the selected clones from the second round of limiting dilution cloning were grown for seeding a production run which followed the same conditions and feeding as described in section 5.2.6.1. Both the lowest and highest producers were grown in duplicate, to be pooled post-production run for purification in order to boost any production in the lower-producing lines and maximise the amount of mAb from the

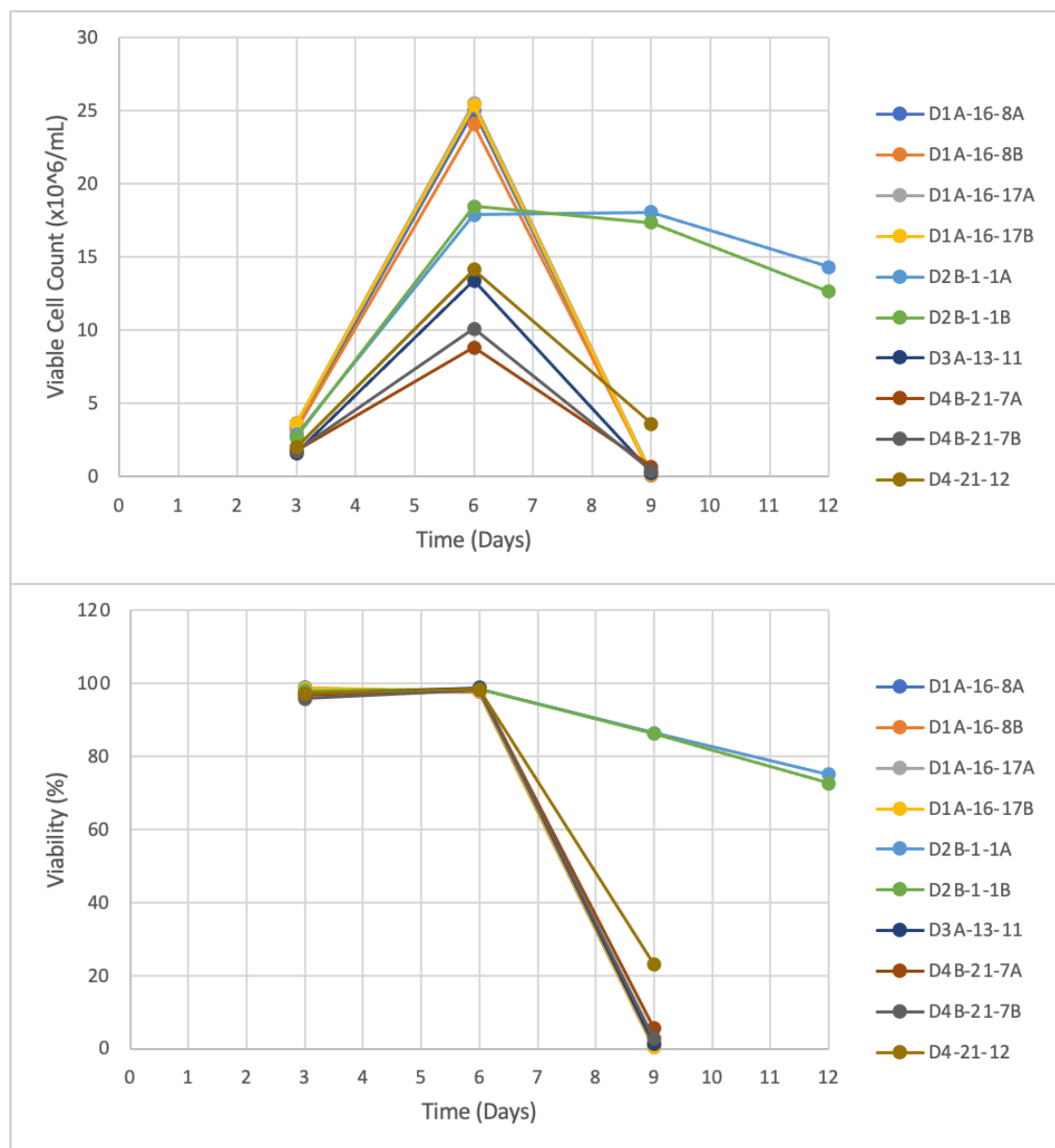


Figure 5.21: 100 mL fed-batch production growth characteristics from clones derived from cell lines D1A-16, D2-1, D3A-13 and D4B-21 (n=1). (Top) Viable cell concentrations of each culture over time (days). (Bottom) Culture viability of each culture over time (days) (n=1).

high-producers. The cultures were sampled on feeding days prior to feed addition to monitor their growth (Fig 5.21) and protein expression (Fig 5.22) profiles throughout the run.

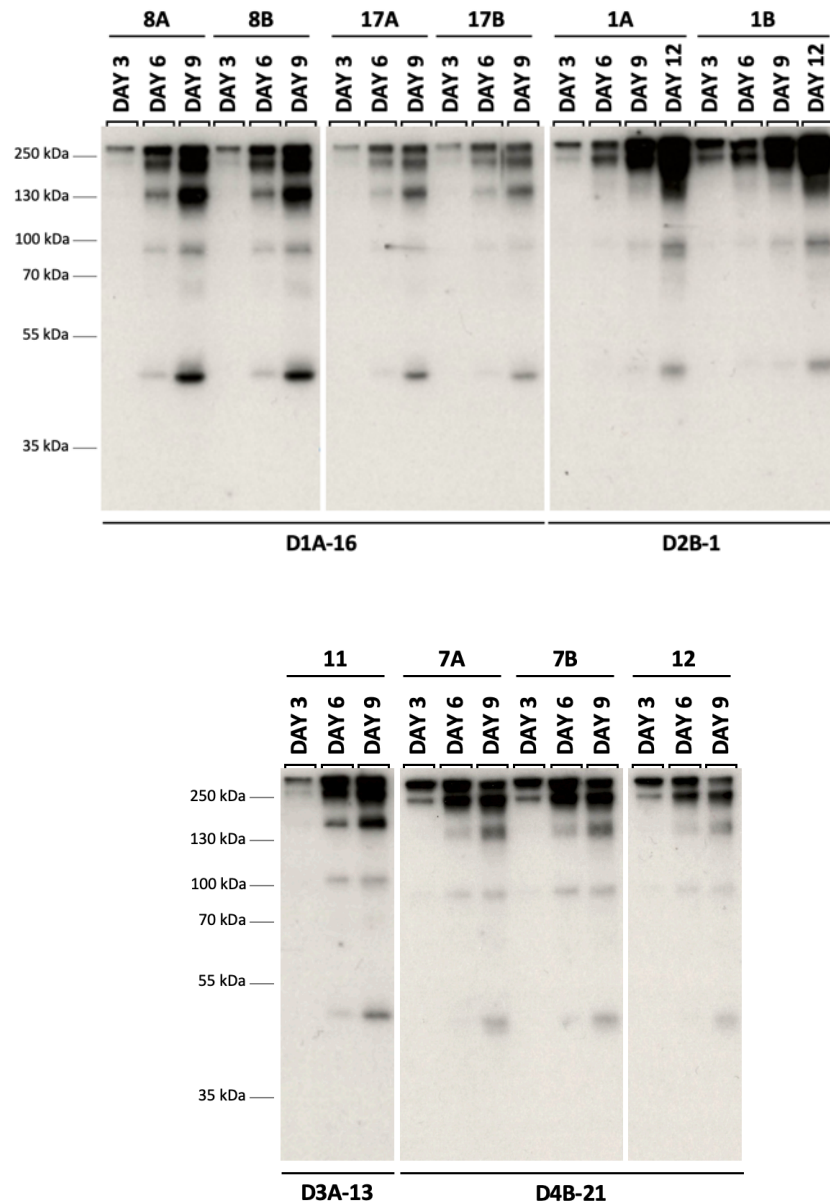


Figure 5.22: Western blot analysis of supernatants collected during culture on feed and harvest days for the clones derived from cell lines D1A-16, D2-1, D3A-13 and D4B-21. Analysed on a 10% SDS-PAGE gel for electrophoresis and probed with an anti-HC (Fc) primary antibody, 1-second exposure.

All of the cultures reached their peak viable cell concentration on day 6, with the highest concentrations observed in the D1A-16-derived clonal lines (Fig 5.21). However, all of the cultures dropped sharply in viability (%) by day 9 and were harvested at that time

point, except the D2B-1-derived clone cultures which maintained viability for longer and only dropped to below 80% culture viability on day 12 (Fig 5.21) at which point they were harvested.

Western blot analysis of the supernatants taken during culture showed increasing amounts of mAb in the supernatant with the highest concentrations being present on harvest days for all cultures (Fig 5.22). The D1A-16-17 clone cultures produced the weakest signal for each of the time points in contrast with the D1A-16-8 cultures, despite reaching almost identical viable cell concentrations. Overall, the strongest heavy chain signal of all the cultures was present in the day 12 samples of the D2B-1-1 cultures, though interestingly the banding pattern also shows that there was a greater ratio of full-sized antibody molecules to lower, fragmented antibody molecules in the D2B-1-1 cultures at harvest compared to those in D1A-16-8 and D3A-13-11 cultures (Fig 5.22).

5.2.7.3.2 Protein-A affinity chromatography purification of mAb from cell culture harvest supernatants

As described previously, filtered supernatants were prepared from each culture and loaded onto a protein A column to purify the anti-dengue mAbs. The resulting elution fractions, flowthroughs and washes were collected and analysed for western blotting (Fig 5.23). The western blot heavy chain signal was present in elution fractions 1 – 3 of D1A-16-8, D3A-13-11 and D4B-21-7 and elution fractions 1-4 of D2B-1-1 with very little leakage into flowthrough or washes for all four runs. This indicated that although elution of the mAb was not extensive, it was due to low concentration rather than poor binding. The elution fractions were pooled for each run, buffer exchanged into PBS and concentrated to a final volume of approximately 500 μ L. These concentrated mAbs were compared with standard concentrations of Trastuzumab on an SDS-PAGE as before (Fig 5.24) and showed that the only run to produce a clear band upon staining was D2B-1-1, though it looked to be weaker than the 0.1 mg/mL trastuzumab standard.

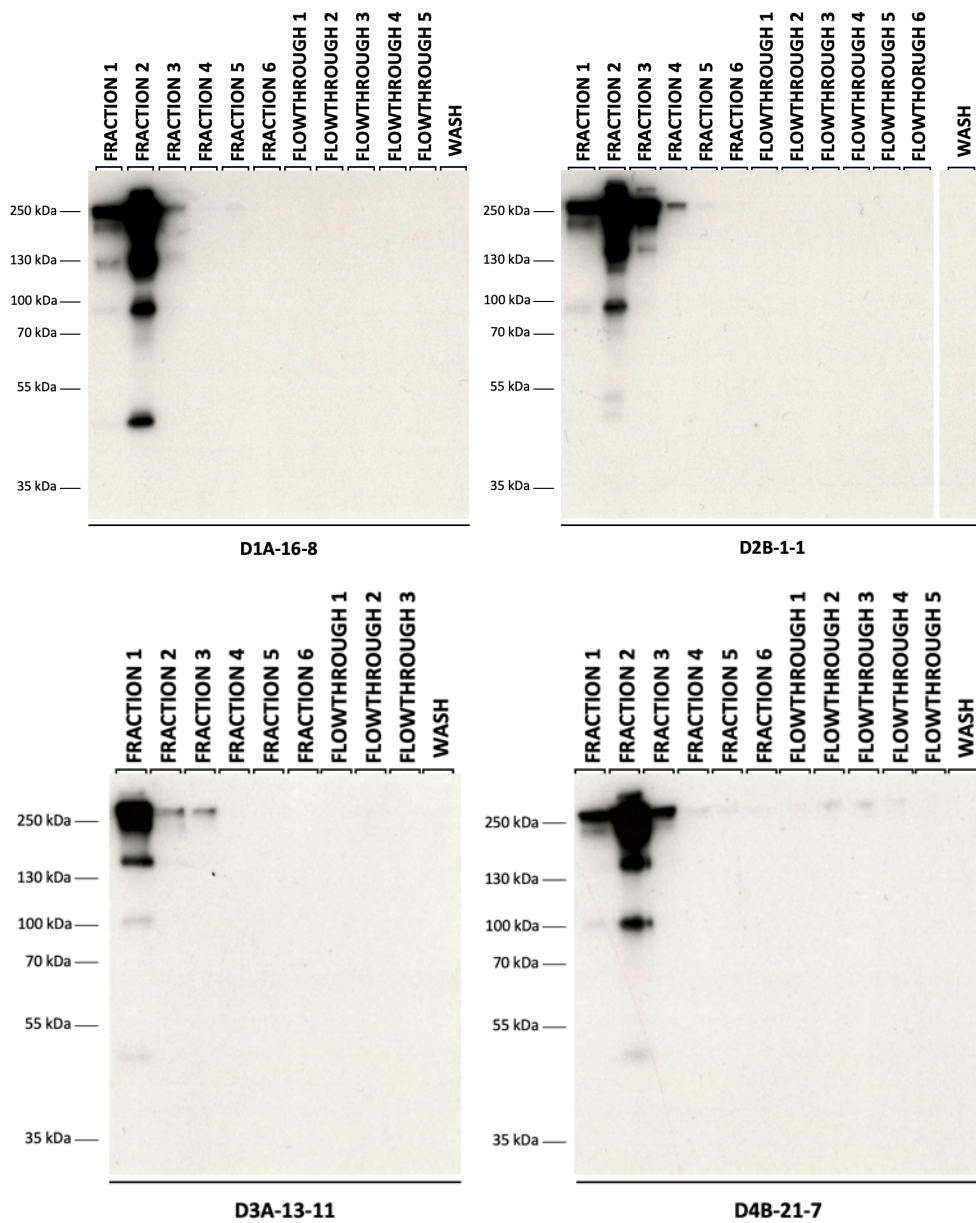


Figure 5.23: Western blot analysis of the elutions, flowthroughs and washes collected during FPLC Protein A affinity chromatography purification of mAbs from the supernatants of cell culture harvest from clones derived from D1A-16, D2B-1, D3A-13 and D4B-21. Analysed using a 10% SDS-PAGE gel for electrophoresis, probed with an anti-HC(Fc), 1-second exposure.

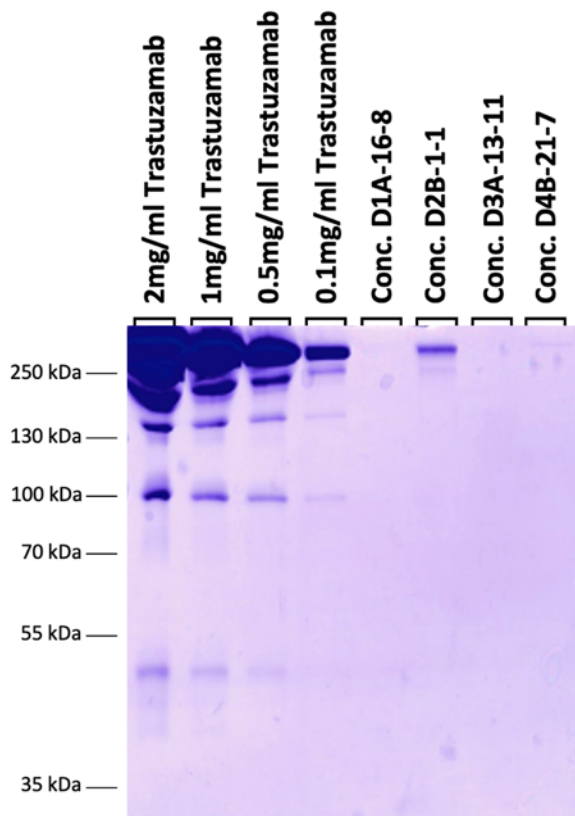


Figure 5.24: Coomassie Blue-stained SDS-PAGE analysis of the purified and concentrated antibody products from further monoclonal development of the cell lines D1A-16, D2B-1, D3A-13, and D4B-21. Lanes are loaded with equal volumes (5 μ L) alongside commercially produced Trastuzumab in a standard concentration range.

5.2.8 Optimisation of culture conditions to improve anti-dengue mAb product yields

5.2.8.1 Small-scale temperature shift experiments

In an attempt to try and increase antibody product titres further, a small-scale shake flask experiment was undertaken to explore the effect of varying temperature conditions on expression levels using the cell line with the highest titres so far, D2-1. Three flasks with a starting volume of 30 mL were prepared for a fed-batch run with three temperature conditions: (A) 32°C throughout; (B) 37°C until peak viable cell concentration was reached, then dropping the temperature to 32°C; and (C) 37°C throughout. Each culture was sampled daily for cell concentration and culture viability determination and to retain a small volume for western blot analysis of expression throughout the run.

5.2.8.1.1 Culture growth profiles and mAb productivity throughout culture

Using daily cell concentration data (Fig 5.25), the cells grown in condition B and C were estimated to be nearing peak viable cell concentration on day 5 and the flask for condition B was moved to the lower temperature of 32°C at this timepoint. After day 7, there was a divergence between conditions B and C in viable cell concentrations ($\times 10^6$ viable cells/mL) as expected, with condition C flask showing a decline in overall culture viability from this point forward whilst the condition B flask overall viability was maintained from this point forward. Although the condition A flask had the highest culture viability (%) of the three at the end of the run, the viable cell concentration never exceeded 3×10^6 viable cells/mL which was achieved in the other flasks after day 3. These differences were mirrored in the daily average cell diameters (μm) measured. Condition B and C flasks had very similar average cell diameter values until day 6, where upon the condition B flask cells were then increasingly larger with culture time. Meanwhile, the condition A flask cells showed a very different pattern of average cell diameter over time with a large increase on day 3 followed by a slow decline over time after this sharp peak.

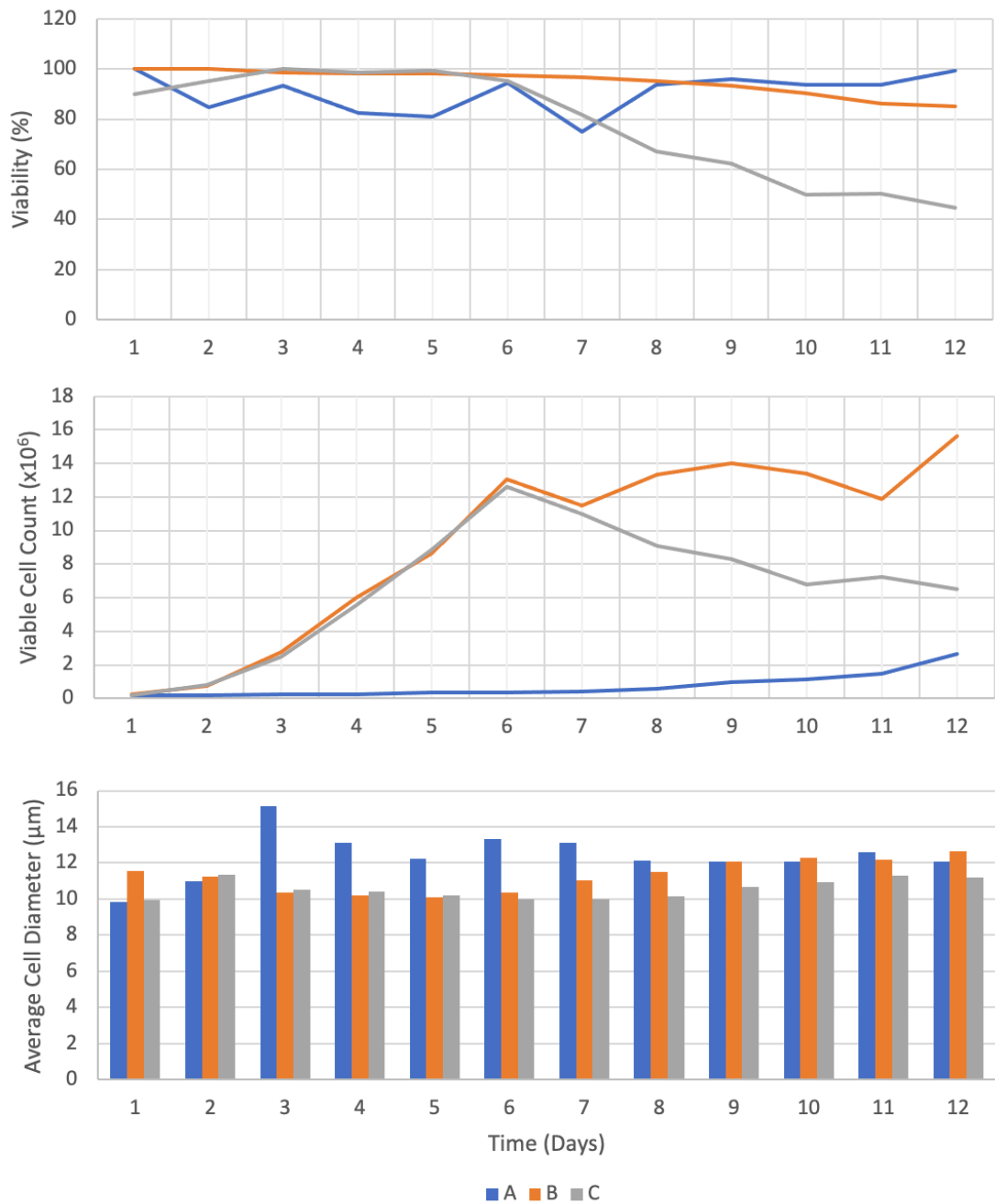


Figure 5.25: Daily cell growth, culture and size measurements (n=1) of the small-scale temperature optimization experiment showing: (Top) Daily culture viabilities (%); (Middle) Daily Viable Cell Concentrations (x10⁶); and (Bottom) Daily average cell diameters (μm).

5.2.8.1.1 Daily sampling to assess mAb productivity and yield with culture progression

Western blot analysis was undertaken to examine mAb product amounts in daily sampled supernatants (Fig 5.26) to investigate the effects of the various temperature conditions on secretory product yields. The blots showed the expected similar mAb levels for conditions B and C up until the temperature drop in culture B on day 6, as well as very low levels present in condition A, which mirrors the growth patterns of each. From day 6 to day 8, the culture grown under condition B outperformed that of condition C, whilst expression of mAb in culture condition A remained weak in comparison. With the exception of day 9, condition B resulted in the strongest mAb banding for all the remaining time points, with a clear difference in the antibody present

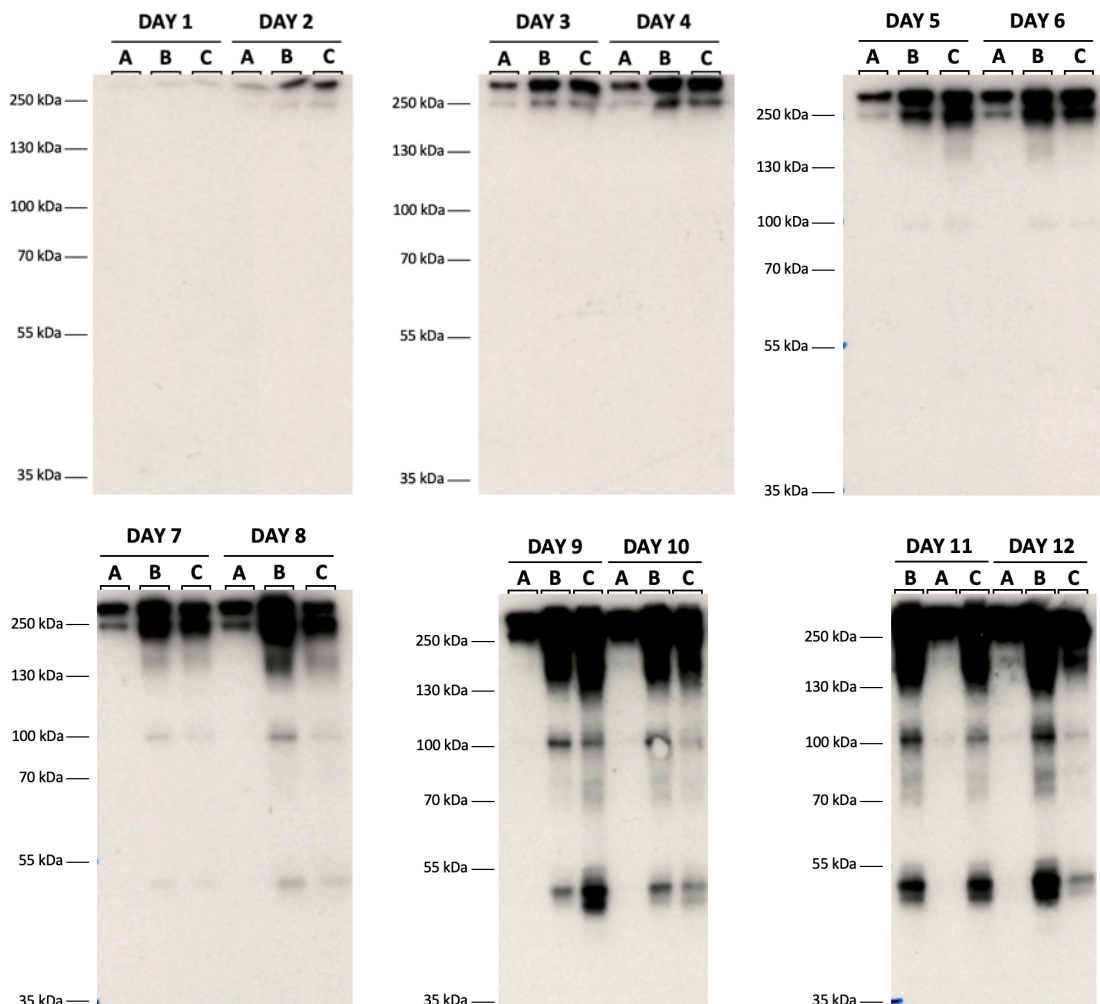


Figure 5.26: Western blot analysis of supernatants collected from daily sampling of the small-scale temperature shift experiment, analysed using a 10% SDS-PAGE gel for electrophoresis and probed with an anti-HC (Fc) primary antibody, 10-second exposure. Lanes: Condition A (32°C throughout); Condition B (37°C until day 6, then 32°C); and Condition C (37°C throughout).

at harvest on day 12. This small-scale data showed that expression of D2_1 was boosted when the culture incubation temperature was dropped from 37°C to 32°C when the peak viable cell concentration was reached (approximately day 6).

5.2.8.2 Larger-Scale Temperature Shift Production Run

The temperature shift condition was next taken forward and applied at a larger scale with a fed-batch production run of D2_1, carried out in equal volumes across four 1 L shake flasks with a total starting volume of 800 mL. The cultures were originally planned to receive Gibco™ Efficient Feed B at timepoints recommended by the manufacturer, as with previous runs, but daily viable cell concentration measurements initially showed a large drop in culture viability (Fig 5.27) and the feeding schedule was delayed until either the cells recovered or a new run could be started. As can be seen in Figure 5.27 the cultures did begin to recover on day 4 and a feeding schedule was re-incorporated into the run with feeds on days 7, 10, and 13. The cell cultures reached their peak viable cell concentrations on day 7, though the temperature was not dropped down to 32°C until day 8 as the expected peak concentrations were predicted to be higher from previous runs. Despite a stalled start, the drop in temperature allowed the cells to retain a >60% culture viability until day 17 when they were harvested. Average cell diameter (um) was also measured daily and showed a slow increase from around 10 µm to >12 µm by the end of culture (Fig 5.27).

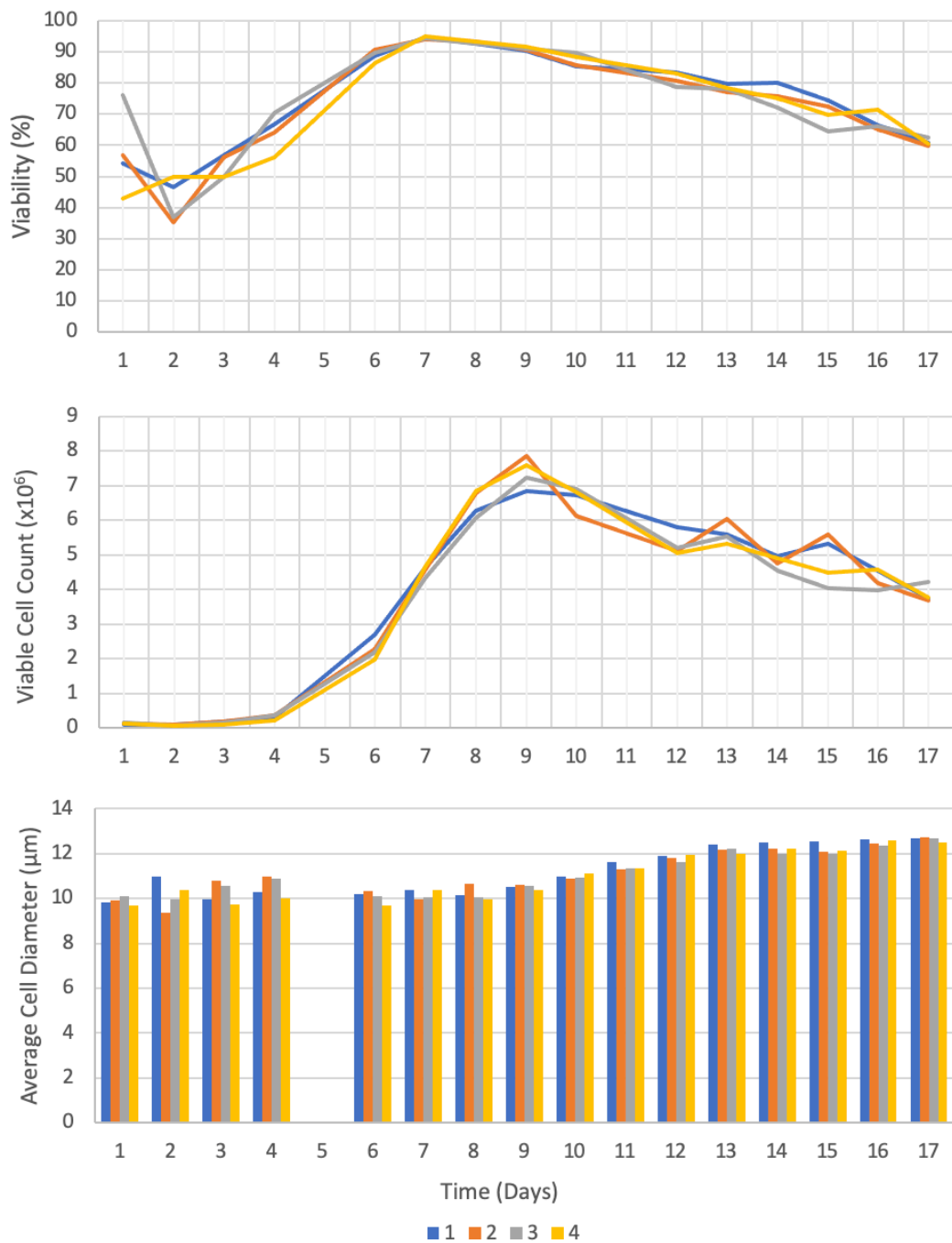


Figure 5.27: Daily viable cell concentrations, culture viabilities and cell size data for the larger-scale temperature optimized production run with four biological replicate flasks of one clone (D2_1), compared and monitored over 17 days: (Top) Daily culture viabilities (%); (Middle) Daily Viable Cell Concentrations ($\times 10^6$); and (Bottom) Daily average cell diameters (μm).

Western blot analysis was then used to determine mAb expression levels in the supernatants of the daily samples and showed no outliers between the four replicates. However, the amounts of mAb observed in daily samples mirror the stunted growth at the beginning of the run with very weak bands in the first 8 days of culture (Fig 5.28).

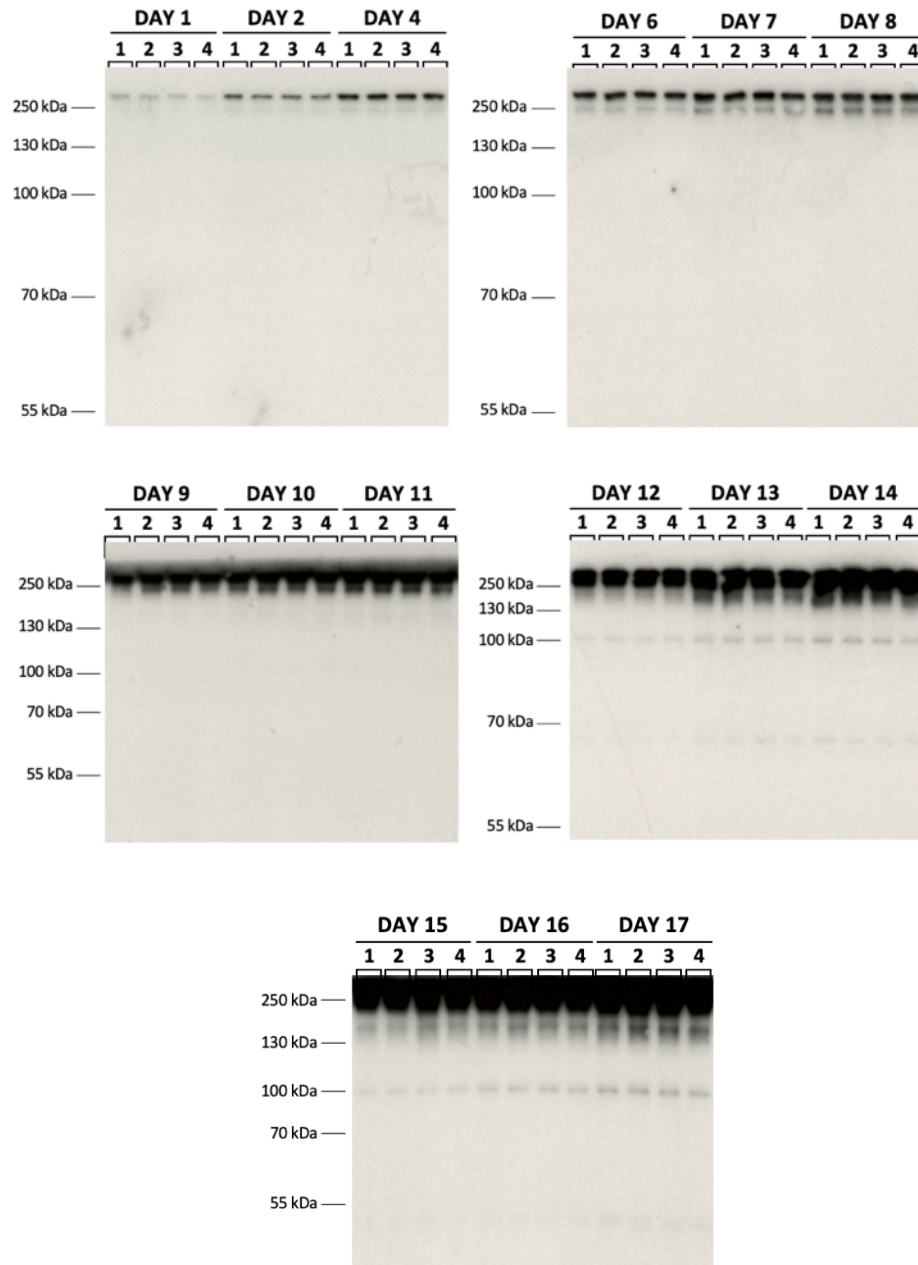


Figure 5.28: Western blot analysis of supernatants collected daily from the larger-scale temperature-optimized production run of clone D2_1, analysed on a 10% SDS-PAGE gel for electrophoresis and probed with an anti-HC (Fc) primary antibody, 10-second exposure. Lanes "1", "2", "3" and "4" each represent the corresponding replicate flask cultures.

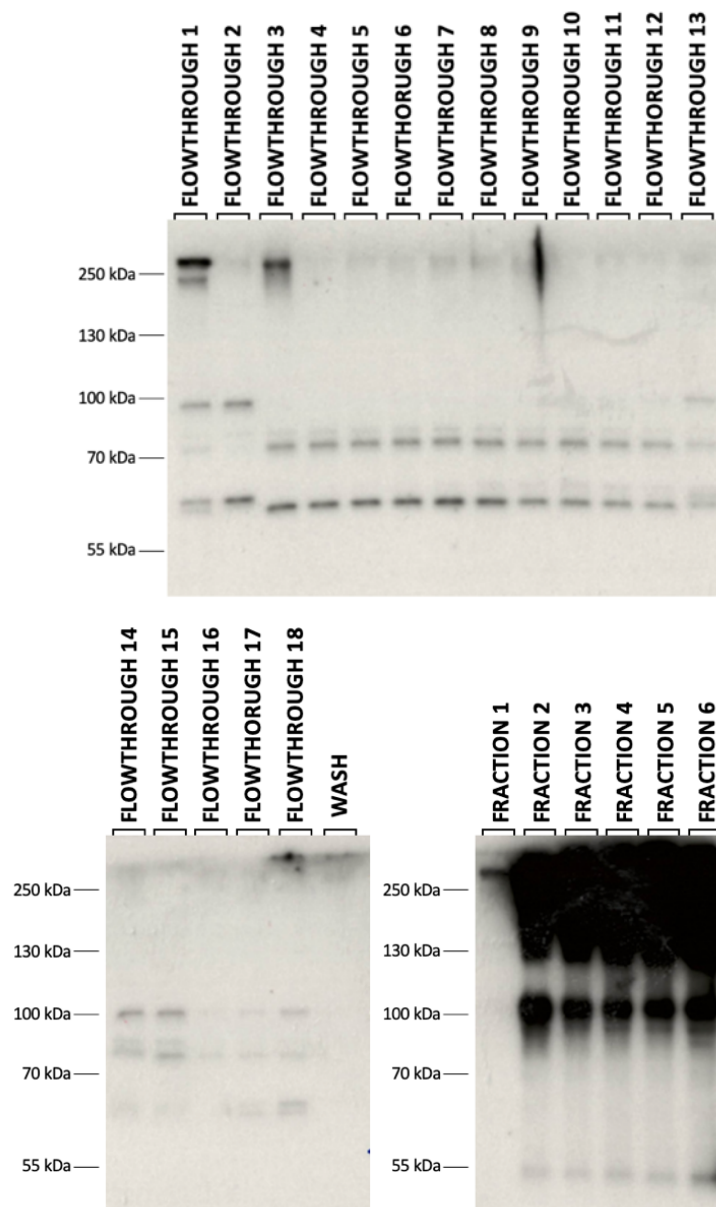


Figure 5.29: Western blot analysis of the flowthroughs, washes and elutions collected during FPLC Protein A affinity chromatography 1 Litre run of the supernatants harvested from the larger-scale temperature-optimized production run of clone D2_1. Analysed using a 10% SDS-PAGE gel for electrophoresis, probed with an anti-HC (Fc) primary antibody, 10-second exposure.

The final volume of the four cultures once pooled was just over 1.2 L and was centrifuged to separate the supernatant from cells and cell debris, which was then filtered and divided into two volumes of 1 L and 200 mL to run through a protein A column on an AKTA Pure FPLC system. The elution fractions, flowthroughs and washes were collected

for each run and western blotting carried out to assess the presence of the mAb throughout the purification process (Fig 5.29 and Fig 5.30). The analysis of the first run (1 L of supernatant applied to the column) showed that a very large portion of the full-sized antibody product was recovered with strong heavy chain signal present in the elution fractions 2-6 with a small band present in elution fraction 1 (Fig 5.29). However, there was a full length mAb heavy chain signal present in the first and third flowthrough collections indicating some full-sized antibody product did not bind to the column.

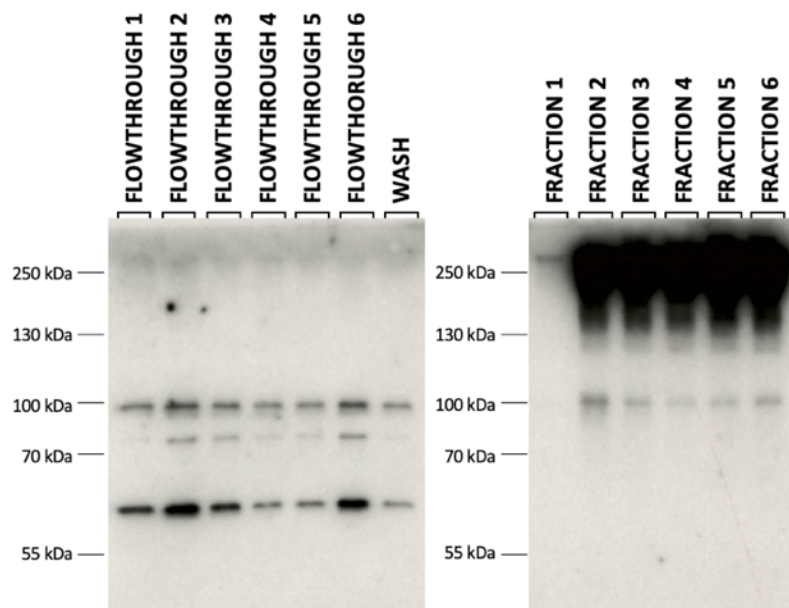


Figure 5.30: Western blot analysis of the flowthroughs, washes and elutions collected during FPLC Protein A affinity chromatography 200 mL run of the supernatant harvested from the larger-scale temperature-optimized production run. Analysed using a 10% SDS-PAGE gel for electrophoresis, probed with an anti-HC (Fc) primary antibody, 10-second exposure.

Analysis of the elutions, flowthroughs and wash that were collected in the second FPLC run (remaining 200 mL of supernatant) subjected to western blotting showed a strong mAb heavy chain signal again present in elutions 2 – 6 with a small amount in elution 1 (Fig 5.30). However, the flowthroughs and the wash for this smaller run showed no evidence of the presence of mAb heavy chain signal that would have indicated full-sized antibody product had failed to bind to the column.

The elutions from both runs were then pooled and passed through a 50,000 KDa molecular weight cut-off spin tube filter and buffer exchanged with PBS and

concentrated to a final volume of approximately 600 μ L. This concentrated final product was examined on a nanodrop spectrometer using an A_{280} measurement, which gave an approximate value of 0.62 mg/mL.

5.2.8.3 AMBR[®] 250 Fermenter Production Run of Two Anti-Dengue Producing Cell Lines

To try further boosting antibody product titres through increased culture longevity and control of pH and oxygen availability within the production runs, an automated bioreactor programme was designed to culture the two highest-producing cell lines produced in this chapter: D1A-16-8 and D2B-1. The programme design incorporated the optimised culture conditions developed in this chapter as well as the normal feeding strategy and base medium. Bioreactor stir-speeds, gas flows and dissolved oxygen setpoints were determined from literature citing CHO-S culture parameters in an ambr[®] 250 system (Synoground *et al.*, 2021; Hoshan *et al.*, 2019) and are detailed in Section 2.3.3.3. After a conditioning period overnight with media placed in the reactor and supplementary reservoirs filled accordingly, bioreactor 1 and 2 were seeded with D1A-16-8 and D2B-1, respectively, at 0.2×10^6 viable cells/mL (Day 0). Each bioreactor was sampled daily to monitor cell growth (Figure 5.31) and mAb expression levels (Figure 5.34), as well as real-time data collection from the ambr250 system for the entire run (Figure 5.32 and Figure 5.33). The automated real-time data included recording any deviations in temperature, pH, foaming and dissolved oxygen (DO(%)), with corrective measures automatically applied to minimise deviations outside of pre-set condition ranges. Both cultures grew well with similar viable cell concentrations observed until day 5, where the cell concentration and culture viability of D1A-16-8 suddenly declined and showed no signs of recovery by day 9 (Figure 5.31). In contrast, D2B-1 continued to grow and peaked at a cell concentration on day 6 of 20.67×10^6 viable cells/mL before entering a very gradual decline in culture viability which did not dip below 80% until day 13 (Figure 5.31). These peak cell concentrations were far in excess of those obtained in shake flask experiments previously reported in this chapter.

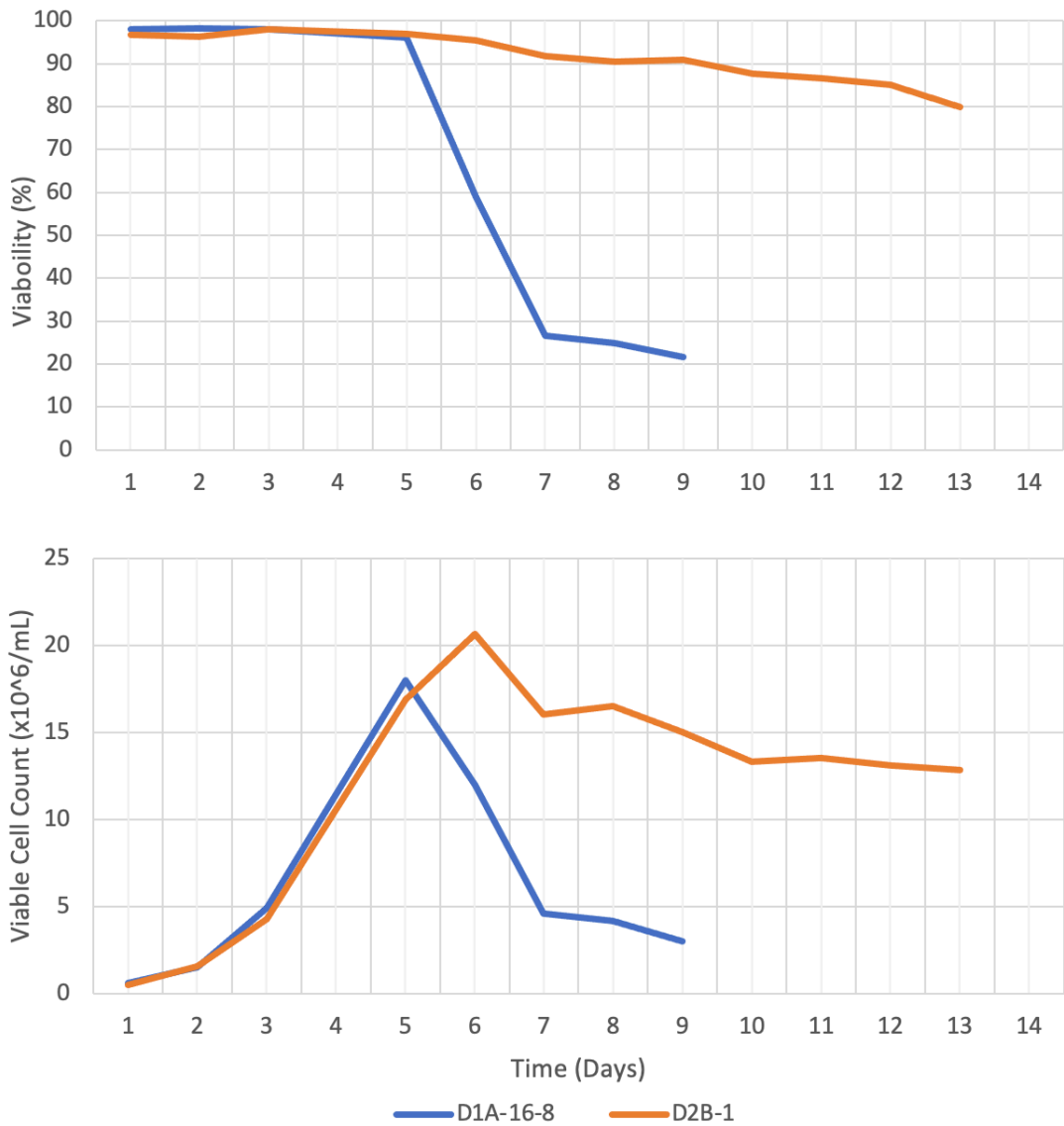


Figure 5.31: Growth measurements of cell lines grown under controlled ambr250 bioreactor conditions with reactor 1 and 2 growing cell lines D1A-16-8 and D2B-1, respectively (n=1). (Top) Culture viability (%) and (Bottom) Viable Cell Concentration (x10⁶ viable cells/mL) across culture on a daily basis.

The data plots generated from the real-time data collection of each bioreactor throughout the runs (Figure 5.32 and Figure 5.33) show a decline in dissolved oxygen over the first few days as culture cell concentration increased exponentially for both cultures. However, in bioreactor 1 over the course of day 3 base supplement (NaCO₃) was added to correct for the decrease in pH detected, with a total of 5 mL being added by day 4 (Figure 5.32). After a brief return to the pre-determined pH setpoint range for this run, a decline was detected again after day 6, for which more base was pumped into

the culture for a total of 5.8 mL added by day 9 at which point the cells did not recover and were harvested. In contrast, the same decline in pH was detected in bioreactor 2 but not until day 4 and the decrease more subtle, resulting in only 2.5 mL base volume addition which resulted in a steady return of the pH to setpoint range until the end of the run (Figure 5.33). However, by day 10 the foam sensor for bioreactor 2 showed a large increase which did not return to its baseline for the remainder of the run.

Despite the decline in the cell concentration and culture viability of D1A-16-8, western blotting of the daily samples for the presence of mAb showed a small increase in the heavy chain antibody signal with each day. The intensity of the band in the blots from the daily samples of D2B-1, however, was much stronger throughout except for the final day which was much weaker suddenly (Figure 5.34). The cultures were harvested from each bioreactor by centrifugation to separate cells and cell debris from the supernatant which was then filtered before purification via protein-A chromatography as previously described earlier.

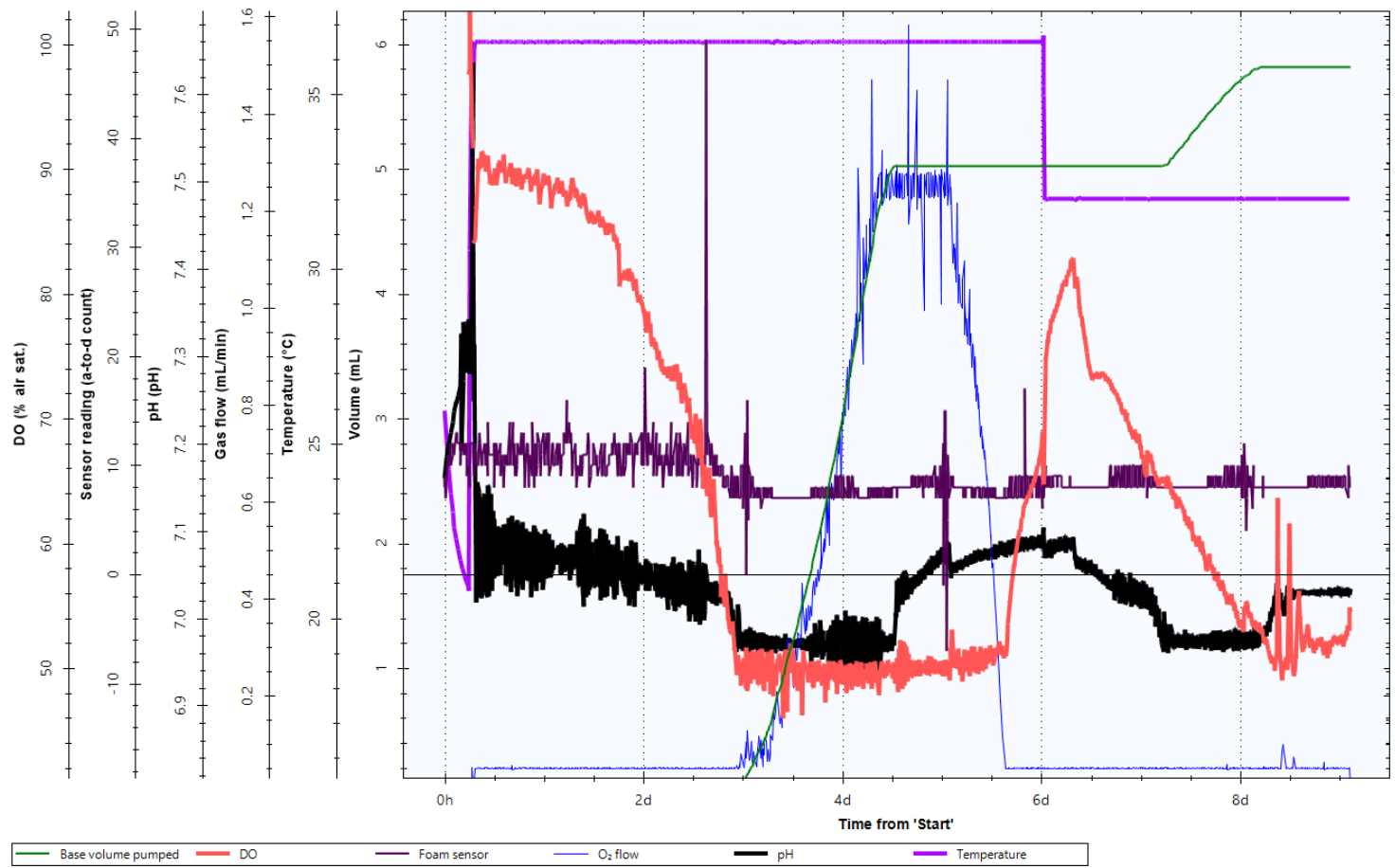


Figure 5.32: Combined trace graph produced in Sartorius' 'Results Viewer' software for bioreactor 1 (D1A-16-8 cells) which shows dissolved oxygen (DO%), foam sensor readings, pH, temperature (°C), volume of base added (mL) and gas flow (mL/min) of the bioreactor vessel over the 9 day process.

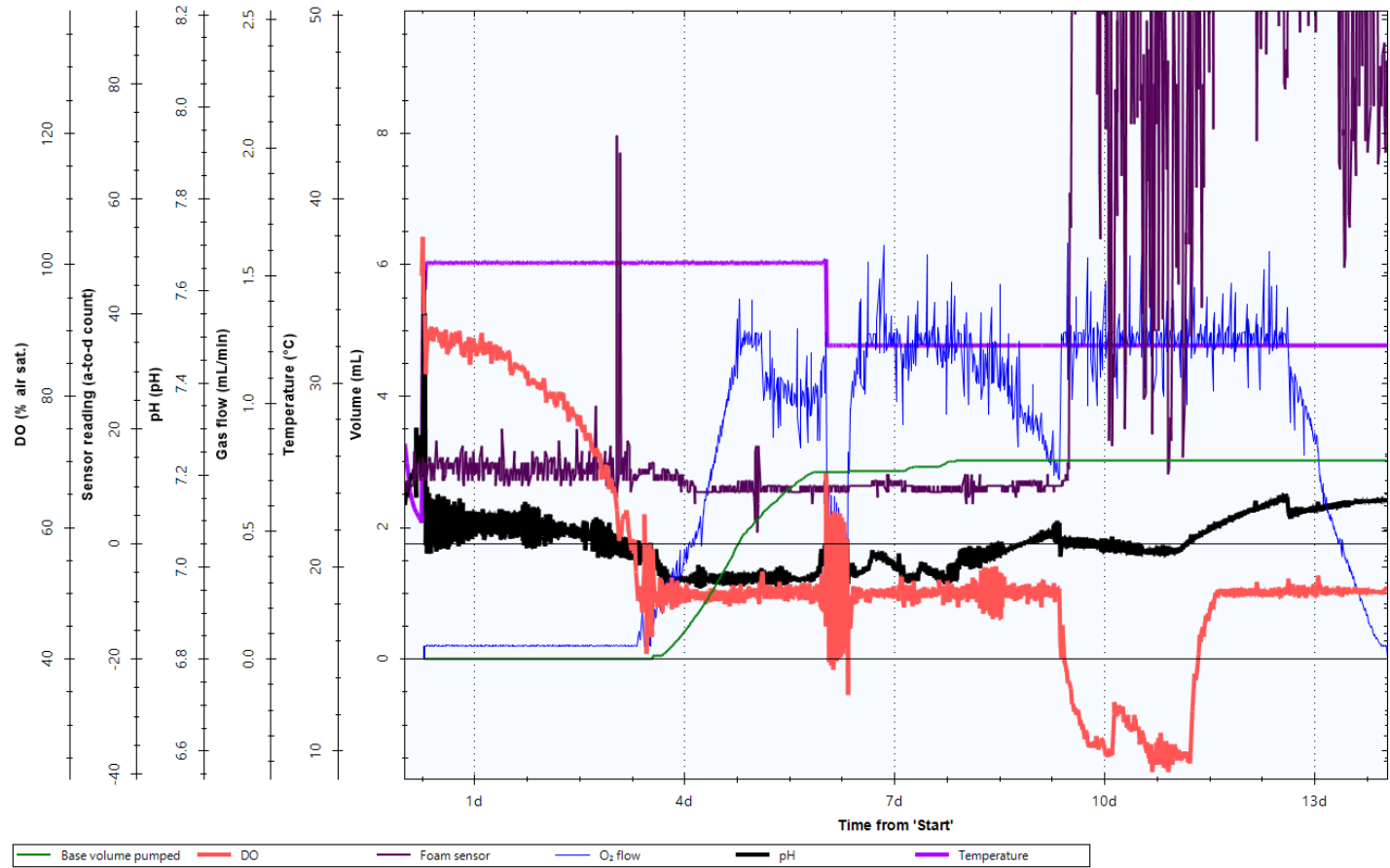


Figure 5.33: Combined trace graph produced in Sartorius' 'Results Viewer' software for bioreactor 2 (D2B-1 cells) which shows dissolved oxygen (DO%), foam sensor readings, pH, temperature (°C), volume of base added (mL) and gas flow (mL/min) of the bioreactor vessel over the 13 day process.

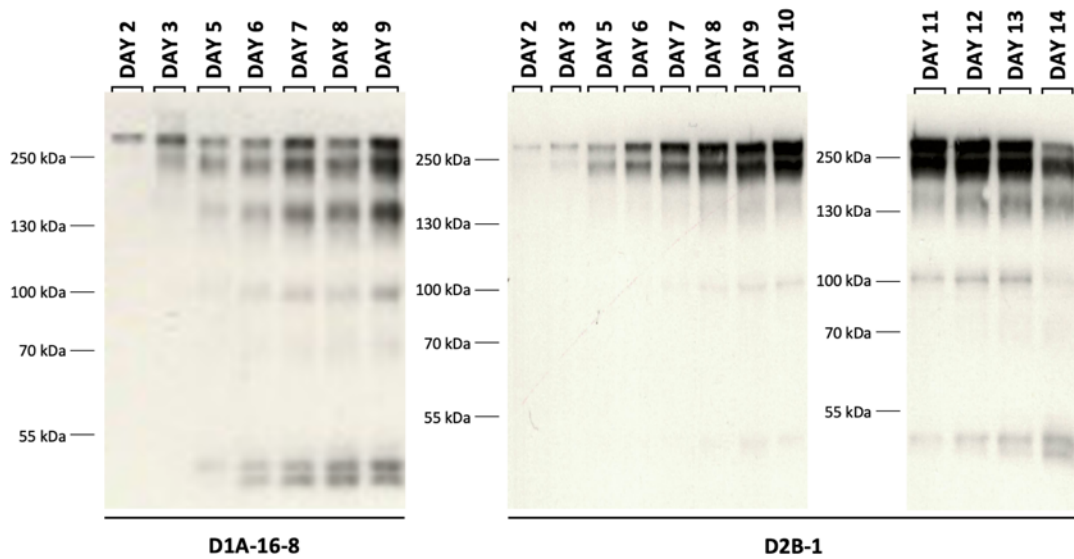


Figure 5.34: Western blot analysis of daily samples from the ambr250 bioreactors 1 and 2, growing cell lines D1A-16-8 and D2B-1 respectively. Analysis was undertaken on a 10% SDS-PAGE gel for electrophoresis, probed with an anti-HC (Fc) primary antibody, 30-second exposure.

After Protein-A purification, the elution fractions, alongside flowthroughs and washes, were analysed by western blot for the presence of mAb (Figure 5.35). The elution fractions 2-6 for both the D1A-16-8 and D2B-1 purifications showed the presence of mAb through the anti-heavy chain signal, with no signal present in either the flowthrough or washes. However, the signal strength in the elution fractions of these runs was moderate in comparison with banding intensity observed in previous

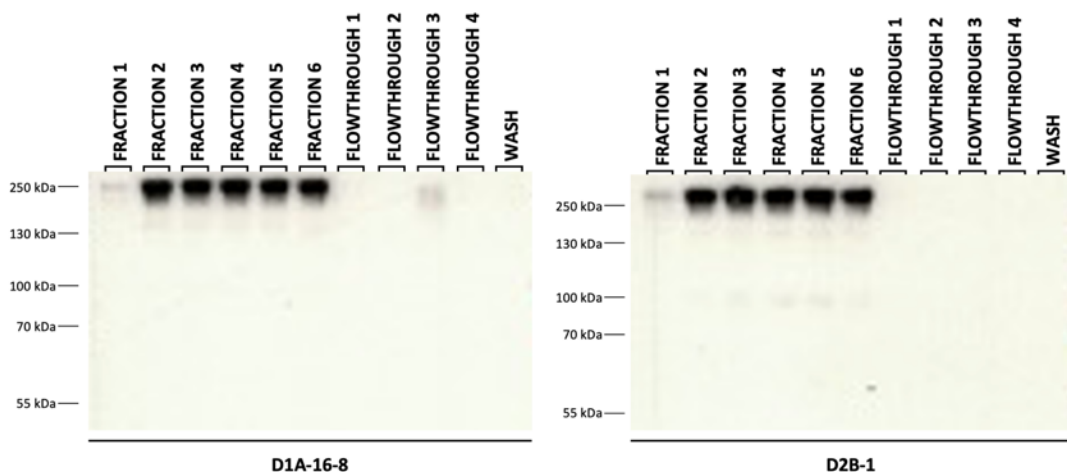


Figure 5.35: Western blot analysis of samples taken from the elution fractions, flowthroughs and washes produced during the purification of the the supernatants harvested from ambr250 bioreactors 1 and 2, growing cell lines D1A-16-8 and D2B-1 respectively. Analysed using a 10% SDS-PAGE gel for electrophoresis, probed with an anti-HC (Fc) primary antibody, 30-second exposure.

purification runs of similar or lower supernatant volumes (Figure 5.23 and Figure 5.30). Nanodrop $A_{280\text{nm}}$ measurements revealed a concentration of 0 and 0.02 mg/mL for the purified material from D1A-16-8 and D2B-1, respectively, and showed that in this instance culture using the ambr[®] 250 system had not led to an improvement in mAb titre.

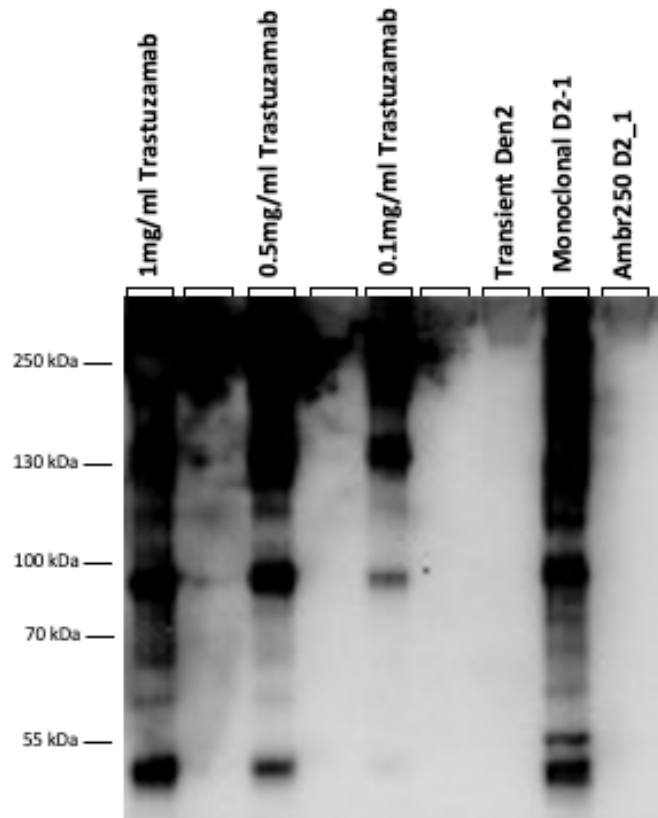


Figure 5.36: Western blot (anti-HC probe, 2-second exposure) comparison of purified antibody material from various D2-expressing cells grown with a temperature shift at peak cell concentration alongside a range of standard concentrations of commercially produced trastuzumab.

A direct comparison by western blot between all of the material purified from D2-expressing cell lines in which a temperature shift was applied showed that the monoclonal D2_1 cell line grown in shake flask conditions produced the highest final antibody titre (Figure 5.36). Visual comparison of the temperature shifted monoclonal D2_1 material with a trastuzumab standard concentration range in the western blot using an anti-heavy chain probe (Figure 5.36) suggested that the antibody concentration was in the range of 1 mg/mL, in the region of that suggested by nanodrop $A_{280\text{nm}}$ measurement which was 0.62 mg/mL.

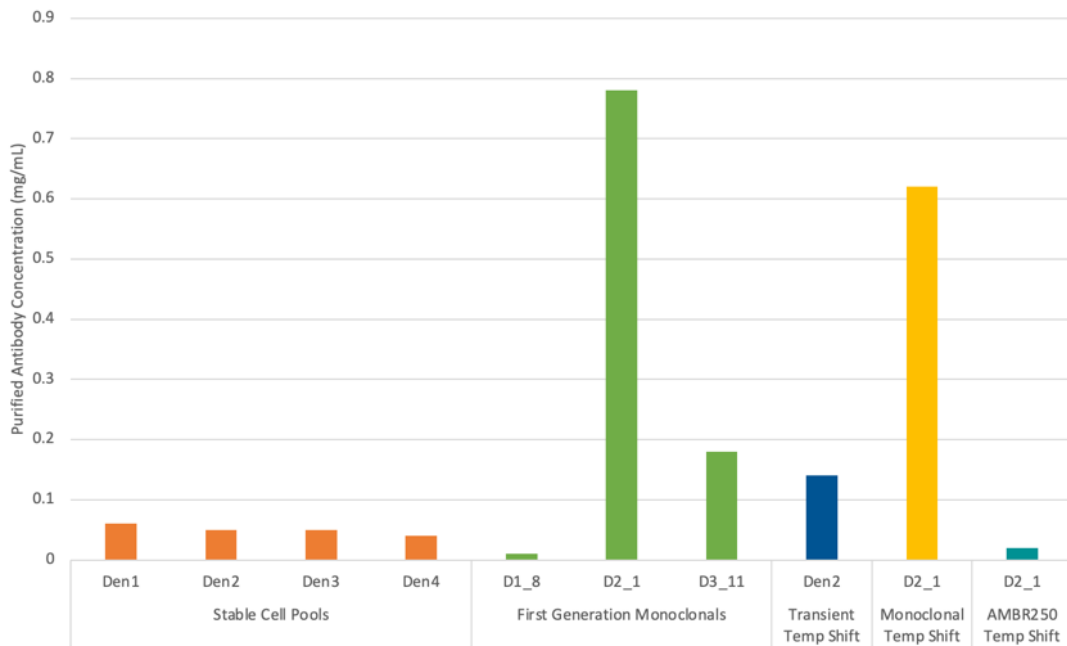


Figure 5.37: Comparison of A_{280nm} measurements of purified antibody material from cell pools and lines along the various stages of cell line and process development to improve titres. ($n=1$ for each mAb material which are pooled purified materials)

A final comparison of A_{280nm} measurements collected from purified antibody material produced from cell pools and lines showed the impact of cell line development and process optimisation investigations on titre for the anti-dengue cell lines created from re-engineered antibody sequences (Figure 5.37). Titre increase was generally seen after development of a monoclonal cell line from stable cell pools for D2- and D3-expressing cells, with D2_1 achieving the highest expression of any of the cell pools or clones developed throughout this work. Although initially shown at small-scale to improve expression, the implementation of a temperature shift did not improve the titres of the top-performing cell line, D2, when carried out with a transient pool, stable monoclonal and in an automated bioreactor vessel. However, it should be noted that the temperature shift run for the monoclonal D2_1 did suffer a drop in culture viability during the first few days of the process which may have affected the end titre.

5.2.8 Investigating Potential Bottleneck Points in Protein Production of Den54-Derived Antibodies

5.2.8.1 Western Blot Comparison of Den54-Derived Cell Pools and Lines Antibody Secretion

Expression of the original Den54 sequence using a pcDNA 3.1 GS plasmid transfected into CHO-S cells was not detectable in the supernatant when probed by western blot using an anti-HC (Fc) primary antibody (Figure 5.2). Re-engineering of the sequences to create trastuzumab or nivolumab hybrids and an optimised native sequence increased antibody production and resulted in the presence of a band for the intact IgG product on a western blot using the same anti-HC (Fc) primary antibody (Figure 5.38).

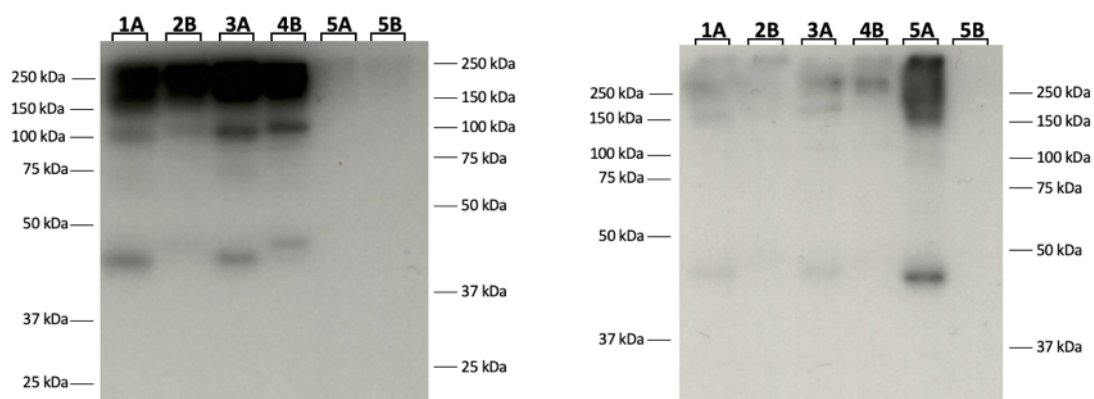


Figure 5.38: Western blots analysis comparing antibody intracellular or secretion levels from stable cell line pools D1A, D2B, D3A, D4B, D5A and D5B collected at harvest from the stable cell line 100 mL production run. Analysed on a 10% SDS-PAGE gel for electrophoresis and probed with an anti-HC (Fc) primary antibody. (A) Supernatants, 1-second exposure; (B) Cell pellet lysates, 4-second exposure.

However, there was a clear difference in the abundance of intact antibody product present in culture supernatant between the hybrid sequences and the optimised native sequence, with the latter producing very low levels in comparison with the former (Figure 5.38). To investigate the cause of this lower expression in the

optimised native sequence, immunofluorescence and mRNA analysis was undertaken to investigate the bottleneck in the secretory production of the protein.

5.2.8.2 Determining mRNA Transcript Levels of Heavy and Light Chains

Examination of mRNA levels in the stable cell line pools for D1 – D5 was carried out using qRT-PCR of RNA extracted from cell pellets of each cell line as outlined in Section 2.2.4. Primers were designed targeting the light and heavy chain of each cell line as well as two housekeeping genes, β -actin and glyceraldehyde-3-phosphate dehydrogenase (GAPDH), which were used as controls from which a fold-change in antibody chain transcription levels could be calculated (Table 2.5). To calculate fold change, first the difference in cycle threshold (Ct) was calculated between the test and housekeeping primer reactions of experimental samples (Δ CTE), and between the test and housekeeping primer reactions of a CHO-S control sample (Δ CTC). Fold changes were then expressed as $2^{-\Delta\Delta Ct}$, where $\Delta\Delta Ct$ is the difference between Δ CTE and Δ CTC. From these data the expression for each antibody chain was calculated (Figure 5.39).

The fold changes generated from this show that heavy chain and light chain mRNA levels for the optimised native sequence cell line pools, D5A and D5B, were among the most abundant and not limiting compared to other pools. Meanwhile, the stable cell line pools with the least abundant antibody heavy and light chain transcripts were D1A, closely followed by D2B. In addition to this, comparisons of the light and heavy chain mRNA expression levels of each cell pool show the smallest variation in the D5A and D5B, and the largest in D1A. The levels of HC and LC mRNA for each cell pool were not correlated with the amount of intact antibody secreted into the supernatants (Figure 5.38). Unfortunately, when reviving cryopreserved cell banks to generate qPCR data for mRNA expression data analysis, none of the banked stable cell pool vials for D3A survived the revival process and so this cell line was not able to be included in this analysis.

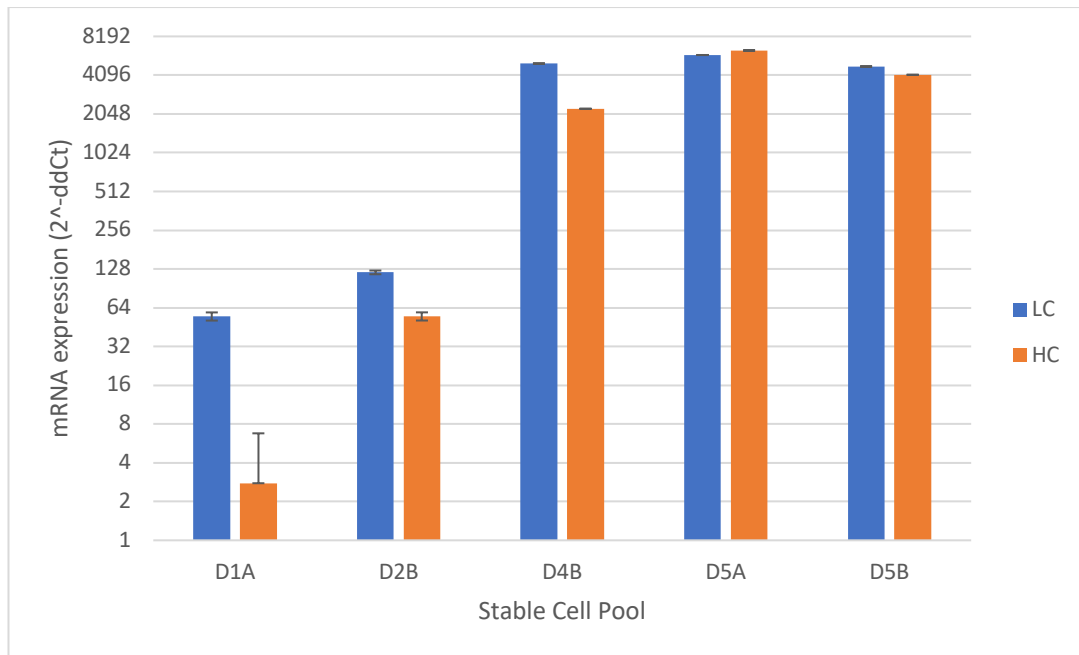


Figure 5.39: mRNA expression fold changes for the light (LC) and heavy (HC) chain of the different anti-dengue molecules determined from qPCR carried out on stable cell pools, using GAPDH as a housekeeping gene control. (n=3, error bars indicating variation between technical replicates for each qPCR reaction)

5.2.8.3 Immunofluorescence Imaging of Intracellular Heavy and Light Chains

To further investigate the production bottleneck of D5, immunofluorescent staining was carried out on D5 stable cell pool cultures which had been fixed to coverslips (described in Section 2.4.2) alongside trastuzumab-hybrid stable cell pool cultures, D1 and D3, and native CHO-S cells. The staining was performed with a DAPI nuclear stain and an anti-calnexin primary antibody bound to a TRITC-conjugated secondary antibody for visualisation of the endoplasmic reticulum (ER), alongside an anti-heavy chain primary antibody bound to a FITC-conjugated secondary antibody to show the presence of heavy chain molecules. Confocal microscopy was then used to take images, at 63x magnification with oil immersion, of the resulting fluorescence at individual wavelength channels from each cell pool type and then merged to highlight any co-localisation (Figure 5.40). DAPI and TRITC-conjugated anti-calnexin

each showed fluorescence throughout all the cell pools imaged as expected, highlighting the nuclei and ER, respectively (Figure 5.40). Imaging of the FITC-conjugated anti-heavy chain resulted in varying levels of fluorescence throughout the cell pool types, with low intensity in the D1 and D3 cells and a higher intensity in D5 (Figure 5.40).

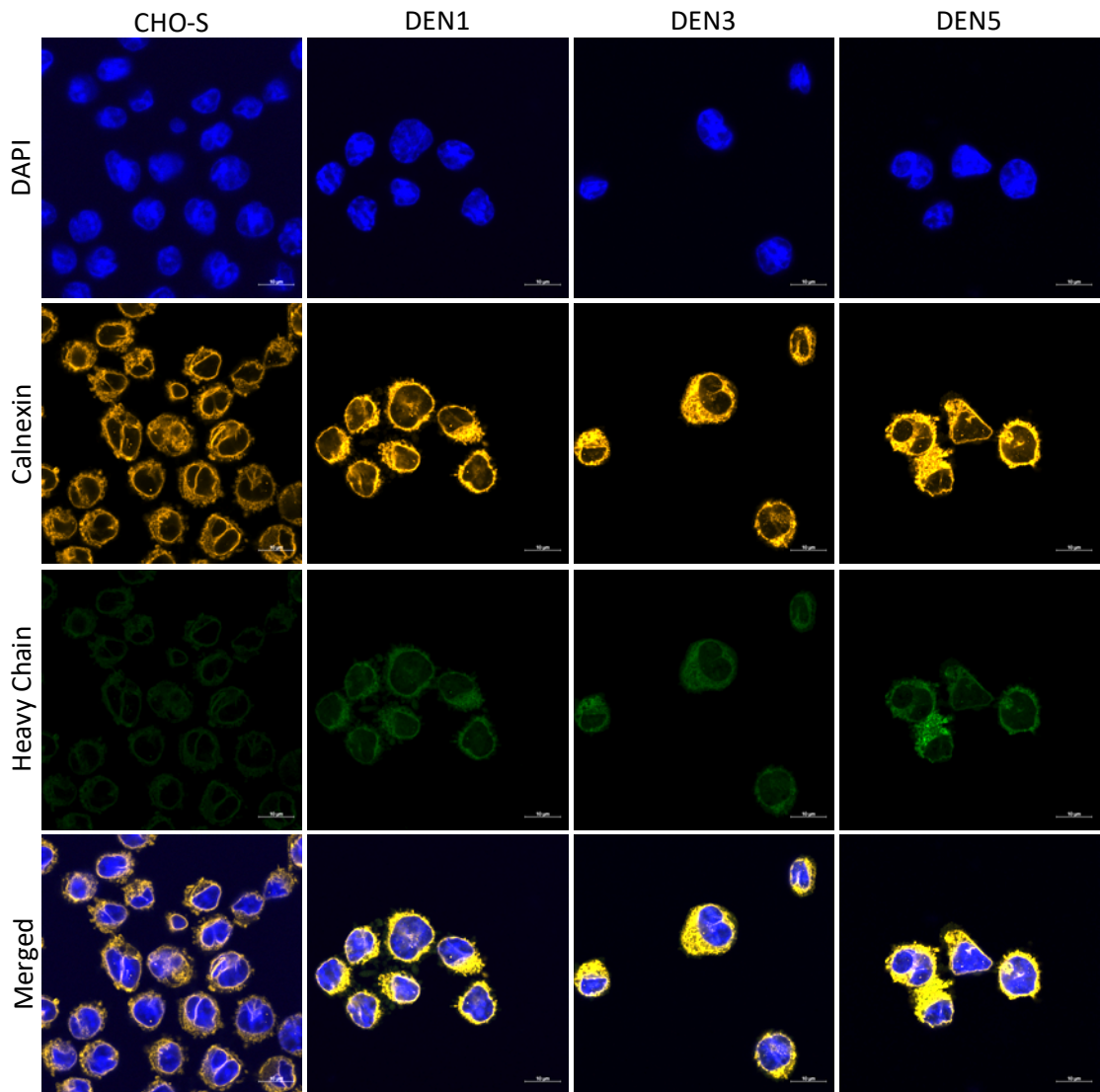


Figure 5.40: Images of the CHO-S native cell line and stable cell pools Den1, Den3 and Den5 after fixation and immunofluorescent staining collected by confocal microscopy at 63x magnification under oil immersion with a 10 um scale bar. Immunofluorescence stains include anti-calnexin (orange, ER marker) and anti-heavy chain (green), with a DAPI nuclear stain (blue) and are presented as viewed with individual channels and a merged view of all three.

Examination of the increased heavy chain fluorescence overlaid with calnexin fluorescence as a merged image in D5 cells shows that the increased presence of heavy chain appears to co-localize with the ER (highlighted by single arrows in Figure 5.41). The merged view of heavy chain and calnexin fluorescence for D1 however, shows faint heavy chain presence in the surrounding areas of calnexin staining which appears to be migrating away from the ER in small vesicle-like shapes (highlighted by double arrows in Figure 5.41).

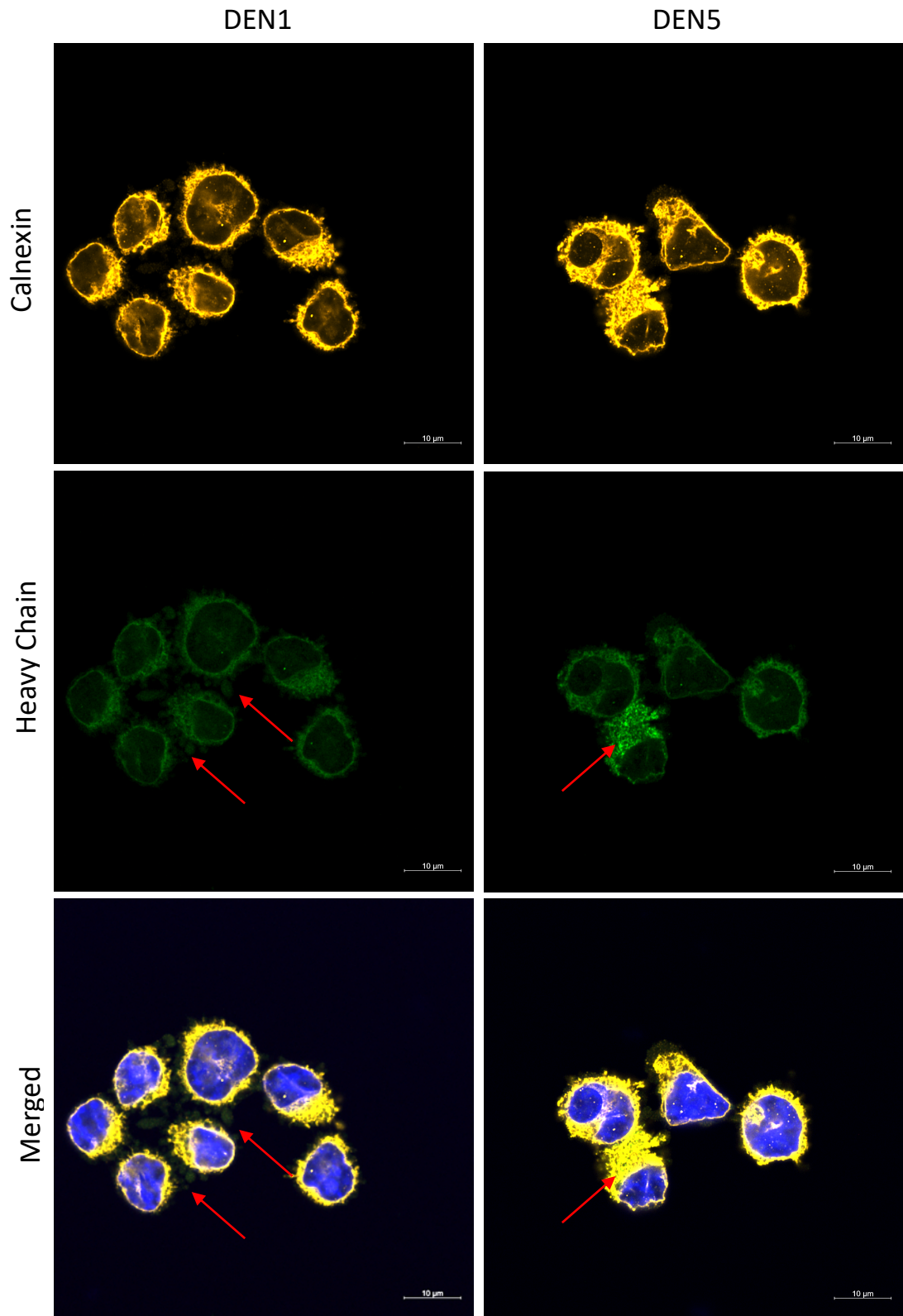


Figure 5.41: Enlarged confocal images of the immunofluorescent stained stable cell pools Den1 and Den5, comparing the anti-heavy chain localisation (top) with the merged view co-localisation of heavy chain, calnexin and DAPI (bottom) to show differences in heavy chain presence between the two cell pools.

Meanwhile, the images taken for D3 suggests a halfway point between the two, with no increased heavy chain apparent within the ER but also no heavy chain in the surrounding areas (Figure 5.40). Given that for the trastuzumab-hybrid lines, cells derived from the D1 pool were able to achieve the highest antibody expression, followed by those from the D3 pool and lastly the D5 pool which secreted little to no antibody, the immunofluorescent staining images and intracellular blots together suggest the D5 molecule is made in the cell but unable to be secreted and hence retained intracellularly.

5.3 Discussion

5.3.1 Re-design of Den54 sequences to incorporate elements of IgG molecules expressed well in CHO-S cultures to improve anti-dengue antibody production

Transfection of the original Den54 antibody sequences in a 3.1 GS plasmid into CHO-S cells resulted in no detectable expression of any antibody when the resultant supernatant was analysed by SDS-PAGE and western blotted with an anti-heavy chain probe. This was shown to be antibody sequence specific when compared with a positive control comprising an identical transfection with the same vector carrying Trastuzumab heavy and light chain sequences. To tackle the lack of expression of these sequences, they were re-designed into five alternative configurations (**Error! Reference source not found.**), D1-D5, which were all codon-optimised for expression in Chinese hamster and a new set of signal sequences grafted on, sourced from (Haryadi *et al.*, 2015), intended to make the molecule easier to express and hence obtain good yields of product.

The re-design of the sequences involved fusing regions of the Den54 heavy and light chains with those of antibodies which have been historically well-expressed and tolerated by CHO-S cells, trastuzumab and nivolumab, with the hypothesis that the new hybridized sequences would generate molecules more compatible for expression in CHO cells. D1 and D2 contained the most original anti-dengue antibody

sequences, with trastuzumab and nivolumab Fc regions, respectively, combined with the Den54 framework regions (FRs) and complementary determining regions (CDRs). The D3 and D4 molecules contained the least Den54 sequences and were identical to trastuzumab and nivolumab, respectively, except for the Den54 CDRs. The sequences for D5 were created through codon optimization of the original Den54 sequences, including a mutated Fc region, for expression in CHO cells and contained no trastuzumab or nivolumab hybridization.

With the high sequence similarity to trastuzumab and nivolumab, D1 and D2 were expected to express well as they only contained the small CDR sequences from the DTE Den54. However, FRs can give structural support to CDRs and a molecule with a mis-matched FR/CDR combination could also potentially have led to a less stable structure or one difficult to form. Additionally, this configuration would likely produce an antibody with very low binding efficiency in the presence of dengue fever antigens due to the lack of anti-dengue specific FRs which also support the CDRs in antigen binding (Gąciarz and Ruddock, 2017). Conversely, D3 and D4 which contain both the FRs and CDRs of the Den54 sequences could have greater difficulty in being expressed if these regions are responsible for Den54's DTE nature. However, the matching of Den54 FRs and CDRs could mean that D3 and D4 would have greater structural stability in the variable regions and were also likely to have better binding efficiency from the correct supporting FRs to the CDRs.

Of the five new configurations, D1-D4 were able to be expressed in CHO-S cultures following transient transfections and were present in culture supernatants as fully assembled (2 x HC and 2 x LC) molecules when examined via western blot. Thus, these data along suggest that elements of the constant regions of Den54 limited secretory productivity. The only configuration which did not express and secrete intense bands by western blot was antibody D5, the only set of sequences which had not been hybridised with the antibody sequences from Trastuzumab or Nivolumab and still retained the Den54 mutated Fc region. However, there was a very faint signal of mAb and heavy chain in the D5 supernatants of western blots which was not seen at all in the original Den54 supernatants. The data therefore shows that the

'optimisation' of Den54 to create the D5 sequences did result in a minor improvement of expression, but was outperformed by the other hybridized sequences.

To further investigate and potentially increase antibody production from these sequences, stable cell pools were created using the D1-D5 plasmids and then examined post-transfection at up to 100 mL volume fed-batch cultures to determine antibody titres and if there were differences between the sequence molecule variants. Post-transfection, the stable cell pools displayed almost identical expression profiles to those seen from the transient transfections, except for D5 which showed a very small increase in mAb expression as detected by heavy chain presence. However, in fed-batch suspension cultures at the 100 mL scale there was no increase in secretory D5 amounts. A direct comparison of the cell pellet lysates and supernatants taken from the fed-batch stable cell pools showed that intracellular mAb and heavy chain was present in one of the D5 pools suggesting the cells were able to express the molecule but there are limitations on its secretion from the cells. A similar observation has been reported with other antibodies when comparing the expression and secretion between 'standard' and DTE mAbs (Mathias *et al.*, 2020), where authors also explored the secretion and expression of each using immunofluorescent imaging, western blot analyses and RNA transcript analyses to determine the bottleneck in a DTE mAb. Interestingly, they also found that the DTE mAb sequences were indeed translated but unable to be secreted resulting in a build-up of the protein in the ER. However, further analysis found that the bottleneck was caused by improper folding due to poor disulphide bond formation in the light chains which was then triggering endoplasmic-reticulum-associated protein degradation (ERAD) pathways, resulting in abhorrent ER morphology which was not observed in the D5 cell pools during immunofluorescent microscopy. Though Mathias, Wippermann *et al.* 2020 shows some strong similarities and highlights a potential checklist of investigations for the poor secretion of D5, ultimately the differences in secretion between the D5 and D1-D4 antibodies seems to lie in the Fc region of the original Den54 sequences which were only present in D5.

For the cell pools that achieved higher secretory mAb concentrations, D1-D4 as shown by western blot, purification and concentration steps were undertaken on the fed-batch 100 mL culture supernatants and an ELISA performed to determine specific titres. The assays showed very low titres across each cell pool, with an average concentration of 50 ng/mL purified product, and there was also minimal difference between the cell pool titres suggesting that despite large differences in their sequence configurations, they all expressed similar amounts of product. The very low amounts of secretory D5 in contrast to D1-D4 therefore suggests that one severe DTE region of the Den54 sequence is located in the Fc region as the D5 molecule is the only molecule to retain this sequence region. Further, the intracellular data suggests the molecule can be assembled but is not secreted and thus the Fc region may have a structure non-compatible with secretory pathways or result in misfolding/aggregation and retention within the ER. However, this may not be the only characteristic of the sequences which hinders secretory expression as the stable cell pools for D1-D4, thought better than D5, also had low productivity compared to a standard trastuzumab molecule.

5.3.2 Development and Scale-Up of Monoclonal Lineages of each Redesigned Anti-Dengue Molecule

Cell pools by their very nature are heterogeneous and include several or numerous populations, each with varied levels of plasmid integration and sites after a transfection (i.e. different numbers of the genes may be integrated at different sites in the genome in different cells) (Kim *et al.*, 2011; Pilbrough, Munro and Gray, 2009). In order to isolate higher-producing cells and eliminate lower-producing cells to enhance the secretory titres achieved, limiting dilution cloning was performed to generate a monoclonal lineage from each cell pool. The clones from each pool which showed the highest antibody production by western analysis were gradually scaled up to 100 mL suspension cultures.

Initially dot blots were carried out on supernatants from the limiting dilution plates, revealing that there were large variations in expression of mAb from clones derived

from each cell pool and confirmed broad heterogeneity in each of the pools. This heterogeneity will likely contribute to reduced productivity over clonal cell lines. After the transfer of clones from 96-well plates to T25 flasks, western blot analysis revealed changes in expression profiles of several clones from those originally observed in the dot blot analysis. Such differences can be accounted for by a number of reasons including: stress from the transfer to larger surface volume areas; cultures established in the 96-well plates being polyclonal; silencing of gene expression over time (Patel *et al.*, 2018; Porter *et al.*, 2010; Veith *et al.*, 2016), or the presence of intracellular heavy chain from direct application of cells to the membrane in dot blotting masking lower secretory producing cell lines. The scale up of the surviving clones from T25 flasks onwards showed very little variation in their expression profiles suggesting that only the most resilient cells survived from this point on, though regrettably a direct comparison with the original pools was not included during the western blot screening for each scale-up stage. Consistently low expression from D5 clones compared to the others provides further evidence that cell presence in the dot blotting protocol had produced a false positive in the initial screening of D5 clones.

Once clones from each cell pool were established and successfully scaled up to 100 mL culture volumes, those with the strongest antibody production by western blot were run in a fed-batch production process. Clones D1A-16 and D2B-1 showed minimal expression on days 3 and 6 during exponential growth, then a sharp increase in expression after a plateau in cell growth on day 9. This showed a clear shift in cellular energy output from growth to productivity that has previously been described by others (Reinhart *et al.*, 2019) and suggests that these clones could produce higher mAb amounts from culture conditions which allow for a sustained stationary phase. Meanwhile, clones D3A-13 and D4B-21 showed a steady increase in both cell numbers and mAb titre throughout fed-batch culture. However, these cell lines did not survive as long as clones D1A-16 and D2B-1, which perhaps indicates that the antibodies produced strongly impact cell viability. Finally, D5A-11 showed a similar growth profile to D1A-16 and D2B-1 but virtually no secretory expression in supernatants.

Purification of the resulting production run supernatants by FPLC showed good binding and elution for D1A-16, D2B-1 and D3A-13 when samples from each step of the process were examined by western blot, but D4B-21 yielded very little antibody product after the purification process. This is likely due to an overall poor growth in comparison with the other cell lines during the production run, obtaining the lowest cell concentration and culture viability declined gradually before harvest compared to the other cell lines. After purification and concentration, a final coomassie-stained SDS-PAGE comparison revealed only D1A-16 and D2B-1 had a visible mAb protein band, of which D2B-1 was the strongest. When visually compared to the standard concentrations of trastuzumab the D2B-1 band concentration appeared to be just below 0.1 mg/mL with D1A-16 similar. Although this was still a low final yield, it was improved by a magnitude of order when compared with the initial yields from the D1 and D2 cell pool titres and suggests a successful selection of the higher-producing cells present in the original highly heterogenous cell pools.

Due to the initial variation in expression profiles during the early stages of scale up after the first round of limiting dilution cloning, a second round was performed in order to create cell lines which were statistically much more likely to be truly monoclonal and potentially give a further increase in antibody titres. The further limiting dilution cloning of the selected initial clones, followed by scale-up and blotting as carried out before, resulted in much less variation in expression profiles between the new clones for each cell line. This suggests that the initial clone selections were likely to be monoclonal in nature.

During the scale-up of the clonal lines from the second round of limiting dilution cloning, expression faltered at the E125 flask stage with western blotting revealing an absence of mAb as detected through an anti-heavy chain antibody in the supernatants of D1, D2, and D3-derived clones. Whilst this could have been due to stress from transfer to new culture conditions, the cells had previously been observed to have a strong tendency to prioritise growth before productivity. As samples for analysis were taken at the end of a single passage (72-96 hours), this may

explain the low mAb expression. For these reasons, surviving clones were taken forward into a fed-batch production run regardless of low expression at this point, unless a standout clone with good expression was available for a cell line. Antibody expression was subsequently apparent in the western blots of supernatant samples collected throughout the production runs of all selected cell line clones, even in those which had little expression at the E125 scale. It is noted that stability of secretory recombinant protein expression in CHO cells is a long-acknowledged issue (Marx *et al.*, 2022; Dorai *et al.*, 2012; Kim *et al.*, 2011; Barnes, Bentley and Dickson, 2003) that can result in the loss of expression from cell lines over time or very rapidly. Often this is attributed methylation and promoter silencing resulting in decreased transcription of the recombinant genes and epigenetic impacts although the mechanisms are likely to be diverse and are not fully elucidated.

The D2-derived clones consistently were better than the others in terms of both culture longevity and productivity. However, despite undertaking the additional round of limiting dilutions cloning this did not appear to result in the isolation of cell lines that were improved in terms of productivity over the initial clones. The only purified and concentrated mAb visible against a standard concentration range of trastuzumab on a coomassie-stained SDS-PAGE gel was D2B-1-1, which appeared to be less than the 0.1 mg/mL trastuzumab standard. The culture conditions were therefore investigated further as an alternative means to enhance anti-dengue mAb expression.

5.3.3 Manipulation of Culture Conditions to Improve Anti-Dengue mAb Yields of Each Engineered Molecule and Cell Line

A change in culture temperature has been widely reported to result in increased secretory yields of recombinant proteins from CHO cells (Xu *et al.*, 2019; McHugh *et al.*, 2020). Various mechanisms have been reported for this observation including increased recombinant transcript amounts, reduced cell death, improved folding fidelity and assembly, and a shift from the cell utilising resources to synthesis host cell proteins to recombinant protein (Donaldson, Dale and Rosser, 2021; Mason *et*

al., 2014; Fox *et al.*, 2004). From an initial small-scale temperature shift experiment, it was observed that cell concentration and culture viability could be sustained for much longer by shifting cells to a lower temperature of 32°C from 37°C once the culture had reached its peaked in cell concentration. Western blot analysis of supernatants harvested daily from different culture condition for mAb heavy chain presence showed that cultures that sustained cell concentration and culture viability, achieved by a temperature shift, exhibited increased secretory mAb amounts after the temperature shift. Lowering the temperature of the cultures as the cell population reached the stationary phase of growth results in increased culture time and as a result such cultures outperform cultures grown at 37°C throughout in terms of mAb product produced in line with other reported studies (Fox *et al.*, 2004; McHugh *et al.*, 2020; Torres *et al.*, 2021).

Due to the low antibody expression exhibited by the cell lines developed and described in this chapter, the temperature shift was scaled up to 4 x 200 mL fed-batch shake flask cultures ran in parallel to determine if the altered culturing process could produce higher levels of antibody than achieved in earlier large-scale production runs. Each scaled-up replicate culture displayed an almost identical growth pattern, however with peak cell concentrations between 6 – 8 x10⁶ viable cells/mL they did not reach the cell concentrations achieved in small-scale cultures which reached 12 – 13 x10⁶ viable cells/mL. The reduced peak cell concentrations could be attributed to the reduced culture viabilities after seeding the flasks, although the culture viability of all four cultures did begin to recover, alongside the cell concentrations, after day 4. The larger-scale cultures subjected to a temperature shift displayed a similar rate of decline in culture viability to the small-scale cultures, with cultures reaching approximately 80% viability at day 12. However, considering the delayed exponential and stationary phases of growth due to the reduced culture viability and growth at the beginning of the production run, the temperature shifted small-scale culture outperformed the large-scale cultures in maintaining a higher cell concentration and culture viability for longer.

Westerns blots of harvested supernatant samples from the temperature shifted large-scale cultures show little variation in mAb heavy chain levels between replicates, consistent with the growth data, however they were collectively lower than that seen in the first 8 days in the small-scale experiment carried out with the same cell line. This is possibly due to the lower cell concentration in the large-scale or due to the reduced culture viabilities at the beginning of the run, which also led to a delay in the temperature shift.

To explore if antibody titres could be improved using more controlled process parameters to increase culture longevity and cell 'health', the two highest producing cell lines developed were cultured in Sartorius® ambr250 sparged mammalian fermentation vessels with the integrated software controlling setpoints for each vessel. Process setpoints included pH, temperature, agitation, and dissolved oxygen (DO), with a temperature shift to 32°C programmed for day 6 and a feeding schedule programmed to replicate the timing and volumes of feeding schedules used in the small-scale temperature shift culture. By culturing the cell lines in a closed system with controlled pH and DO along with feeding and a temperature shift at the predicted time of peak cell concentration, the culture conditions should be able to maximise antibody titres from those conditions previously investigated. Previous work with ambr® systems has been reported to accelerate timelines for commercial cell line development as the high-throughput nature of these systems allows for screening of cell lines, process optimizations and design of experiments (DoE's) to be run with significantly reduced costs than those in traditional bench-scale bioreactors (Sandner *et al.*, 2019). In addition to cell line development and screening, ambr® 250 systems have been proven to serve as representative scale-down models for monoclonal antibody production processes at scales >10,000 L and provide reliable estimates of process performance and product quality from bench to pilot scale (Manahan *et al.*, 2019).

For the ambr® 250 experiments, the cell lines D1A-16-8 and D2-1 were each seeded at 0.2×10^6 viable cells/mL into bioreactors 1 and 2, respectively, and remained at >95% viability until day 5 of the run. The D2-1 cells had the best performance in terms

of cell concentration achieved and culture longevity, with a peak cell concentration of 20.67×10^6 viable cells/mL and culture viability above 80% for 13 days. The D1A-16-8 cells reached their peak cell concentration of 18.02×10^6 viable cells/mL on day 5 and had a sharp decline from day 5 onwards with cells harvested on day 9 at 20% viability.

Whilst the growth data for each of these cultures was almost identical until day 5, the online parameter monitoring recorded by the ambr system showed that D1A-16-8 experienced a sharp decrease in pH which required base additions, to a greater degree than those seen in the D2-1 culture. It is unknown if this was just an issue with the fermenter reactor or a cell line and molecule specific impact that cannot be determined from a single run. Data from the D2-1 cell line showed a much better control of culture parameters with smoother pH drops that were able to be gently corrected with base additions and increases in O₂ gas flow which were able to regulate the DO. However, on day 9 there was a large spike in the foam sensor readings which was followed by a slow decline of the culture viability until harvest. These cultures were not controlled with anti-foaming agent and from this data it is possible that D2-1 could have survived longer with addition of anti-foam.

Western blot analysis of supernatant samples collected from daily sampling of each culture vessel showed a steady increase of mAb (indicated by heavy chain) over time for both cell lines, though the signal was visually stronger in those from the D2-1 culture. Interestingly, the heavy chain signal in the D2-1 supernatants was also mainly at the size indicative of fully-formed antibody molecules, whilst the signal present in the supernatants of D1A-16-8 was more spread across varying molecular weights, consistent with individual antibody fragments as well as less intense bands of fully formed antibody. This may reflect the D2 antibody expressed by D2-1 being more stable than the D1 antibody expressed by D1A-16-8 however further studies would be required to confirm this.

Although the results from the ambr® 250 run did not result in the production of higher mAb yields, the system was run under conditions which were estimated to be

appropriate for a CHO-S cell line and had not been tested previously. Further work is therefore required to optimise the process parameters required for culture of the CHO-S cells expressing the anti-dengue antibody in an ambr® 250 system. As described above, the ambr® 250 systems are a staple in commercial cell line development, serving as high-throughput screening tools and reliable scale-down models for large-scale processes. With further runs in the system and a DoE for the process, it is possible the mAb titres for the cell lines described in this chapter could be increased further.

5.3.4 Investigation of Potential Bottlenecks in Antibody Production for the Different Anti-Dengue mAbs

During the development of stable cell pools for each of the five re-designed antibody sequences using the original Den54 sequences, it was discovered that one of the stable pools created with the optimised native dengue design (D5A) was expressing heavy chain intracellularly but unable to secrete the protein. After being unable to produce any D5 antibody after scale up and monoclonal cell line development, further work was carried out to determine if the poor secretion could be attributed to a specific bottleneck in the cells protein production pathway. Such intracellular retention of mAbs has previously been reported by others in DTE mAb molecules (Pettit *et al.*, 2016; Kaneyoshi *et al.*, 2019; Johari *et al.*, 2015).

When compared to stable pools created using the other four re-designed antibody sequences (D1-D4), all of which showed strong extracellular heavy chain signal and very low intracellular material by western blot analysis of the heavy chain, there was significantly more intracellular heavy chain than extracellular in harvested material from D5A. As all five sequences were designed using the same signal sequences and codon-optimised for expression in Chinese hamster cells, this seems to suggest that these can be ruled out as potential limiters on secretion of the D5 antibody. Further investigation of the pools included qPCR to determine and compare mRNA transcript levels across the available cell pools with the levels of antibody expression typically seen in each cell pool. The mRNA HC and LC transcript levels for both D5A

and D5B pools were two of the highest of all the pools, suggesting that transcription of the sequences introduced was not a limitation.

An immunofluorescence co-localisation study of the stable cell pools D1, D3 and D5 was also carried out in order to visualise the presence of heavy chain proteins with reference to the nucleus and endoplasmic reticulum (ER), in order to try and identify any obvious retention of material within the cell as reported by others (Kaneyoshi *et al.*, 2019; Mathias *et al.*, 2018; Le Fourn *et al.*, 2014). Confocal microscopy of fixed and stained cells showed there was low-level heavy chain present in all of the stable cell pools examined, but that there was increased heavy chain-tagged fluorescence in the D5 pool cells. This reflects the data seen from comparisons of supernatants and cell pellet lysates probed for heavy chain via western blotting and is in agreement with other studies suggesting DTE mAbs may be prevented from being secreted and retained intracellularly (Mathias *et al.*, 2018; Kaneyoshi *et al.*, 2019). Close examination of the localisation of the heavy chain-tagged fluorescence in the D1 cell pool showed that very low levels were present surrounding the central nucleus-ER area of the cells, whilst in the D5 cell pool the heavy chain-tagged fluorescence co-localises with the ER. Co-localisation of heavy chain at the site of the ER is strong evidence that the D5 heavy chain sequence is successfully transcribed and translated into protein and subsequently directed to the ER for post-translational folding and modification. However, the apparent build-up of the protein at this location in the cell suggests that the translated protein is either not folded correctly upon arrival to the ER, or is unable to undergo post-translational modification which results in successful trafficking through the secretory pathway.

5.4 Conclusions

In response to the DTE nature of antibody sequences for a novel anti-dengue fever antibody, developed and provided by Thai collaborators, five re-engineered designs of the sequences were created utilising new signal sequences; codon-optimisation for expression in CHO cells; and hybridisation with well-characterised off-patent antibody sequences, trastuzumab and nivolumab. Of the new designs, the four which

were hybridised (D1-D4) were able to be expressed after transfection into CHO-S cells.

After generation of stable cell pools for each set of re-designed sequences, a fed-batch production run was carried out for each and harvested material purified and analysed to determine titre which was <0.1 mg/mL for D1-D4 and D5 continued to not produce a detectable concentration of antibody. To boost titres, monoclonal lineages from each pool were isolated, scaled up and clones were selected with the highest expression were selected to take forward. These clones were cultured in an identical fed-batch production run and material harvested for purification and concentration of any antibody material produced. Titres of the monoclonal cell lines showed improvement from those achieved in the stable pool production runs, but was still very low at <1 mg/mL. In an attempt to further isolate clones from the first round of monoclonal lines to eliminate and polyclonal lines which may have been generated, it was found that none of the second-generation clones could improve upon the titres generated by the first generation of clones.

Using the clone with the best expression of all the cell lines during this work, D2_1, a temperature shift experiment was carried out in small-scale shake flasks to see if titres could be further boosted. The temperature shift condition entailed a reduction in incubator temperature from 37 °C to 32 °C once the peak cell density had been reached and saw improved expression levels over constant temperature of 37 °C throughout at the small-scale. However, when applied to a large-scale culture the same cell line failed to reach the titre achieved from the production run without a temperature shift, though this could be due to issues with cell growth during this production run. Culture of the D2_1 cell line in the ambr250 system bioreactors was successful in keeping cells growing for 13 days and to a high density, but antibody titres from the harvested materials were extremely low at 0.1 mg/mL.

Finally, an investigation into the lack of any antibody production in the supernatant of cells transfected with the D5 antibody sequence design was carried out to determine the bottleneck in protein production from the un-hybridized sequences

could be identified. Examination of differences between intracellular and extracellular extracts; mRNA transcript levels; and a co-localisation study of heavy chain molecules with the nucleus and ER across the cell pools showed that heavy chain sequences are successfully transcribed, translated and directed to the ER. However, a build-up of the molecule at the ER suggests that the protein sequence is either unable to undergo post-translational modification and/or unable to progress through the secretory pathways to exit the cells.

Chapter 6: Discussion

The work in this thesis describes approaches to (1) develop proof-of-concept exosome targeting platforms produced from CHO cells as a potential vaccine plug and play approach and (2) examine the expression of potential anti-dengue monoclonal antibodies and protein engineering strategies to improve the expression of these from CHO cell expression systems. Each of these is discussed in more detail below.

6.1 Exosome Targeting Proof-of-Concept CHO Cell Work

6.1.1 Orientation Effects of Ubiquitin Fusions

The initial work in this thesis looked to confirm that exosomes could be isolated from CHO cell culture supernatants and that specific proteins could be targeted into exosomes. The characterisation of the ubiquitin-fusion proteins expressed and described in Chapter 3 suggested that fusions consisting of an N-terminal fluorescent reporter and C-terminal single ubiquitin orientation resulted in the strongest fluorescence and western blot intensity compared with the other ubiquitin fusions explored. The differences observed between the various orientations of similar sequences is not unexpected. Such variations can result in altered expression and activity of fusion proteins as reported by (Nagasaki *et al.*, 2017) who described how the expression of eGFP-actin or actin-eGFP produced different effects on the cellular morphological and physiological phenotypes of NBT-L2b and U2OS cells. A further study which specifically examined the stability of ubiquitin fusion proteins with respect to ubiquitin degradation pathways (Qian *et al.*, 2002), found that fusion proteins which bear a ubiquitin moiety at their C-terminus are metabolically more stable, maintaining their structure and function whereas other orientations are susceptible to proteasomal degradation.

The improved expression profile of the C-terminal ubiquitin fusion proteins in the proof-of-concept work in comparison to other ubiquitin fusion proteins aligns with the idea of susceptibility to degradation in non-C-terminal ubiquitin fusions. However, of the various ubiquitin-SARS-Cov-2 fusion protein profiles described and investigated in Chapter 4, there was no obvious advantage in terms of expression or exosome targeting due to the orientation of the fusions (C- or N-terminal). It is possible that the nature of the SARS-Cov-2 antigens structure either (1) interferes with the mechanism of action for ubiquitin-mediated degradation, (2) form fusion molecules which neither allow ubiquitin-mediated degradation nor facilitate the antigen targeting into exosomes, or (3) the fusion proteins are unable to be correctly expressed as full-length proteins. Considering the almost uniform banding patterns upon western blot analysis for each ubiquitin-SARS-Cov-2 fusion protein, despite the fact these should be of a range of sizes and origins, it is likely that incorrect folding or expression of the fusions has occurred leading to either similar sized 'core' protein products or aggregates.

6.1.2 Differences are observed between GFP and mCherry ubiquitin fusions

Surprisingly, there were differences observed between the ubiquitin fusions which had identical fusion orientations but differing fluorescent tags. Upon western blot analysis it was observed that Ubi_mCh and mCh_Ubi cells produced exosome populations which were positive for mCherry and of the predicted fusion protein molecular weight. This observation would suggest that fusion of mCherry with a ubiquitin moiety for expression in CHO-S cells leads to the successful targeting of the mCherry into exosome populations. However, during analysis of CHO-S cultures expressing identical ubiquitin fusion configurations with GFP as the reporter protein, GFP was not observed in the exosome isolates at its predicted molecular weight. This may be explained by tendency of GFP to oligomerise as it has a dimeric nature in comparison to mCherry which is monomeric (Chudakov *et al.*, 2010). This is a likely explanation for the difference in GFP band sizes in the cell pellet lysates for GFP_Ubi, GFP_PU and Ubi_GFP. However, the large apparent molecular weight of the GFP species detected in each of the exosome isolates suggests expression of these GFP

fusions results in an aggregated or malformed exosome population in each, possibly due to the oligomerization of GFP during either exosome biogenesis or the sample storage of GFP positive exosome sample conditions.

Though monomeric fluorescent reporter proteins such as mCherry were developed for the mitigation of protein dimerization, aggregation and cytotoxicity observed in traditional fluorescent reporters such as GFP (Kleeman *et al.*, 2018), the use of GFP to label and track exosome populations is widespread and therefore it is unlikely to be the sole cause of exosome aggregation in the GFP-fusion exosome isolates here. Reports into the effects of -80°C storage over time and repeated freeze-thaw cycles on EV samples show reductions in EV concentration and purity, increased particle sizes and size variability with time and increased freeze-thaw cycles (Gelibter *et al.*, 2022). Additionally, storage at -80°C has also shown to lead to the occurrence of EV fusions, evidenced by double positive $\text{GFP}^+\text{-mCherry}^+$ EV populations after the storage of the two separate populations as a heterogeneous mix of single positive EVs (Gelibter *et al.*, 2022). It is possible this phenomenon is a contributing factor to the aggregated populations of the GFP-fusion cultures observed here as they were developed and generated first and the resulting exosome samples stored at -80°C until the mCherry-fusion cultures were prepared and harvested.

6.1.3 Exosome cargo loading favours a CD81-fusion approach in CHO-S cells

Despite the high sequence similarity and shared exosome associations of the tetraspanins CD63 and CD81, they have been shown to have separate roles and bind to different molecules within their exosome affiliations. Whilst CD63 can typically be found in intracellular compartments of endosomal or lysosomal origins and can direct melanosomal proteins into intra-luminal vesicles for exosome biogenesis via ESCRT-independent pathways (Yanez-Mo *et al.*, 2015), CD81 is found in ESCRT-derived exosomes (Dogrammatzis *et al.*, 2021); it is known to traffic CD19 to the Golgi and plasma membrane from the ER, can load Wnt-11 cargo into EVs, and associate with CD4 and CD8 cells for the assembly of immune synapses (Yanez-Mo *et al.*, 2015). These differences are likely the reason that the two are found in varied amounts in

exosome populations when comparing those isolated from different cell types (Yang, 2018) as well as the occurrence of exclusive subpopulations from a single cell type such as is observed in viral infection due to hijacking of the exosome machinery by virions which can highly skew the abundance of CD63+/CD81+ exosomes (Dogrammatzis *et al.*, 2021). It may also explain why the over expression of CD63 in a HEK293 (ExpiHEK293™) cell culture results in a shift in exosome protein compositions with reduced CD81 and CD9 (Silva *et al.*, 2021).

This delicate balance in the biogenesis of exosome pathways which leads to such heterogeneity of exosome populations could mean that the favourability of either a CD63- or CD81-fusion protein approach for exosome cargo loading could be cell-type dependant or susceptible to culture conditions. Considering the successful production and isolation of exosomes using a CD63-mCherry fusion protein expression method by (Silva *et al.*, 2021) in HEK293 cells and other successful attempts to engineer CD63-fusion-based exosomes in other cell types (Stickney *et al.*, 2016; Zheng *et al.*, 2023), it is likely that the poor results observed for the CD63-GFP exosome isolates in Chapter 3 may stem from a low compatibility of this approach with CHO-S exosomes in comparison with CD81-GFP expression. Characterisation work of EVs isolated from CHO cell cultures has been shown to indicate CD81 is expressed in higher abundance for CHO EV populations than CD63 (Belliveau and Papoutsakis, 2022) and might provide an explanation as to why the CD81-GFP fusion protein was better able to target GFP into exosomes. Collectively these data indicate that CD81+ exosomes might be the favoured population for this cell type and hence that CD81 is the better tetraspanin with which to form fusion proteins for CHO-S exosome targeting.

6.2 Generation of Recombinant SARS-CoV-2 Antigen Containing Exosomes

6.2.1 Differences between host and recombinant cell line HIS tag presence suggests the successful targeting of fusion proteins to exosome populations

Western blot analysis of SARS-Cov_2 antigen fusion proteins with anti-HIS probes resulted in a banding pattern in the naïve CHO-S cell pellet lysates despite no introduction of exogenous HIS-tagged coding DNA into these cells. Though poly-histidine sequences are found in proteins expressed in mammalian cell lines, and are reported to cause cross-reactivity of anti-His antibodies with endogenous nuclear proteins (Chilumuri, Markiv and Milton, 2014) and transcription regulators (Mahmood and Xie, 2015), these endogenous sequences have been reported exclusively in human cell lines. However, the bands present in the naïve CHO-S cell lysate western blot samples here could be due to non-specific binding with a CHO-S host cell protein under the conditions used in the western blotting procedure, as has been seen in other experimental work using the same cell banks, antibody and blotting protocol described in this thesis in the laboratory at Kent (J Roobol, personal communication). This could be due to an excess concentration of secondary antibody used, but the 'native' HIS-tag bands were easily distinguishable from the additional bands observed in transfected cell lysates. These additional bands in exosome isolates for the recombinant cell lines strongly suggest that the expression of the fusion proteins resulted in targeting of the proteins into exosome populations.

6.2.2 Spike Subunit 2 Is the Best Targeted Exosome Cargo of the SARS-Cov-2 Antigens

There was a difference in the ability to target the SARS-CoV-2 antigens into exosomes further suggesting that the protein of interest itself has an impact on the ability to target it into exosomes using a fusion protein approach. The presence of the Spike protein S2 domain in the exosome isolates produced from both the ubiquitin- and tetraspanin-fusion protein strategies provides evidence that this antigen has a structure with properties amenable to exosome uptake when fused with these exosome targeting proteins. Natural functions of the spike protein S2 subunit during SARS-Cov-2 infection are reported to include fusion to viral and cell membranes after

proteolytic cleavage events within the protein (Yu *et al.*, 2022; Belouzard, Chu and Whittaker, 2009). It is thought that the initiation of membrane fusion by the S2 subunit is likely due to the presence of a hydrophobic region with negatively charged residues which can disrupt phospholipids (Yu *et al.*, 2022; Madu *et al.*, 2009; Lai *et al.*, 2017; Lai and Freed, 2021). Considering the phospholipid bilayer of exosomes, this would explain the apparent compatibility with multiple exosome uptake strategies which, though varied, each aim to insert proteins of interest through incorporation during exosome biogenesis.

The prerequisite of a proteolytic cleavage event triggered by the binding of the S1 subunit of the SARS-CoV-2 spike protein to ACE2 receptors via the receptor binding domain (RBD) within the subunit to release S2's hydrophobic regions for membrane fusions in nature could explain why the truncated full-length spike (tFLS – lacks the transmembrane domain of the protein) antigen was not able to be targeted into exosomes using either described strategy. The tFLS antigen employed in this work was not only in an uncleaved state but also contained a mutation which was designed to prevent cleavage at the S1/S2 site (Wrapp *et al.*, 2020) and could mean it does not expose the hydrophobic regions contained within the protein in this conformation.

6.2.3 Approaches to Exosome Isolation and Characterisation for An Improved and More Robust Analysis in Future Work

To further investigate the exosome populations derived from the stable cell lines generated in Chapters 3 and 4, isolation and characterisation techniques with a greater ability to distinguish the exact profiles of the exosome populations would be desirable. The isolation and characterisation of exosomes has been reported using a variety of methodologies (Greening *et al.*, 2015b; Zhang *et al.*, 2020; Skrika-Alexopoulos and Smales, 2023; Gurunathan *et al.*, 2019). Whilst there are certainly some methodologies more widely reported throughout the literature for isolation, particularly centrifugation-based methods such as those used in this work, there are more complex and refined methods surfacing which produce better exosome yields, quality and functionality than more traditional methods (discussed below). Alongside

EV isolation methodology developments, analytical characterisation techniques are also being developed and refined, helping provide standard measurements required to define exosome preparations which by their nature are heterogeneous. Such standards were outlined previously in a position statement of the International Society for Extracellular Vesicles (Théry *et al.*, 2018).

The most widely reported methods to isolate exosomes from biological fluids and cell cultures are based upon differential ultracentrifugation, density gradient separation and immunoaffinity capture. Both ultracentrifugation and density gradient methods rely on multiple centrifugation steps to separate vesicles within the distinct size range of exosomes. These approaches require relatively large quantities of starting sample, rely on expensive ultracentrifuge, and have lengthy processing times. With ultracentrifugation alone, there is high potential for contamination from aggregates, soluble factors and lipoproteins (Chen *et al.*, 2019), whilst density gradient methods can give improved yield and quality over simple ultracentrifugation (Gupta *et al.*, 2018). Ultracentrifugation methods are also impractical for large-scale bioprocessing with low yields of intact, 'bioactive' exosomes (Willis, Kourembanas and Mitsialis, 2017) and for their isolation for diagnostics from clinical samples where high-throughput of complex, viscous and small sample sizes is required (Baranyai *et al.*, 2015; Zarovni *et al.*, 2015). For this reason, it was decided to use a commercial kit for isolation of exosomes for the investigations described in this thesis as the higher yield and quality of intact exosomes would allow for an easier detection of the presence of membrane bound proteins on the vesicles. However, due to the presence of polyethylene glycol (PEG) in the commercial kit reagents this unfortunately resulted in a high concentration of PEG in the final exosome isolate preparations and they were unable to be easily examined by liquid chromatography-mass spectrometry (LC-MS) proteomic profiling which can be used to assess exosome sample purity (Patel *et al.*, 2019).

Immunoaffinity capture is a more targeted isolation technique, using an approach in which an antibody complementary to one of the molecules routinely found on the surface of exosomes is immobilised to a probe or bead surface, able to capture

exosomes within a sample by binding exosome surface molecules on contact. This method is able to yield more pure and intact exosome populations from complex samples and can even be designed to target specific exosome subpopulations for capture as well as coupled with diagnostic assays (Zarovni *et al.*, 2015). However, this method of purification is costly and does not provide a platform which could be easily scaled up. Additionally, if applied to an unknown heterogenous sample it can result in subpopulation bias as only exosomes positive for the capture antibody will be isolated. Sequential filtration is a strategy for the isolation of clinical exosomes via a workflow which uses pre-filtration followed by tangential flow filtration and finally low-pressure track-etched membrane filtration (Heinemann *et al.*, 2014). Also, Asymmetrical-Flow Field Flow Fractionation (AF4) has been shown to allow for the separation of particles differing by only a few nanometres in size whilst being coupled to a multi-detection system for simultaneous characterisation and quantification has also been applied (Sitar *et al.*, 2015).

Size-exclusion chromatography (SEC) has also had some success in exosome isolation, however an adapted version reported by (Hong *et al.*, 2016), mini-SEC, reported improved yield and quantities of exosomes. SEC for the isolation of exosomes usually requires pre-processing via differential ultracentrifugation or density gradient centrifugation which are not suitable for processing clinical samples, but mini-SEC uses small-size ion exchange columns capable of recovering intact, biologically active exosomes from blood plasma in quantities sufficient for molecular profiling of their cargo in 30 minutes (Hong *et al.*, 2016). The high-throughput nature of this isolation method coupled with the compatibility of resulting isolates for molecular profiling would make it an ideal method to adopt for further work in developing the recombinant exosome platform described in this thesis.

Techniques for determining the presence of, and characterising, exosomes is often through immunoblotting for known exosome marker proteins coupled with visual confirmation via electron microscopy of vesicles which conform to the defined standards of size and morphology for exosomes. There are multiple databases which catalogue cytosolic and transmembrane proteins commonly found in exosome

populations and include subgroupings for cell-type origin and their subpopulations (Mathivanan and Simpson, 2009; Kalra *et al.*, 2012; Kim *et al.*, 2015). There are some proteins which appear to be universal to exosome morphology and are usually linked with their biogenesis and confirmation of exosome isolation in preparations, some of which were employed as anchor proteins for the production of recombinant proteins in this thesis. Nevertheless, electron microscopy analysis for exosome-like vesicle presence is usually also required as the marker proteins do not provide a definitive analysis regarding purity or quality of isolates.

Both Transmission Electron Microscopy (TEM) and Scanning Electron Microscopy (SEM) are capable of visualising exosomes, but while SEM creates 3D renderings, TEM has stronger resolving power (< 1 nm). Unfortunately, electron microscopy specimens are required to be fixed, dehydrated and examined under vacuum conditions which can alter the size and morphology of the vesicles, though cryo-EM can negate this damage as it does not require staining or fixation and can be carried out at -100°C rather than in a vacuum (Momen-Heravi *et al.*, 2012). Additional analysis via EM imaging includes the use of immuno-gold labelling to bind gold nanoparticles to defined surface molecules to elucidate various exosome subpopulations via receptors or motifs bound to their membrane (Brisson *et al.*, 2017). However, TEM analysis was unavailable to carry out analysis of the exosomes isolated from the cell lines generated here, although others in the laboratory have shown by TEM the presence of exosomes from CHO-S cell culture supernatants using isolation procedures similar to those used in this thesis (Skrika-Alexopoulos and Smales, 2023). The lack of access to TEM combined with the incompatibility of the isolation kits used to purify exosomes from cell culture with mass spectrometry, resulted in somewhat limited characterisation profiles. Further work on this platform would be greatly advanced by immunogold-labelled electron microscopy and LC-MS to determine the efficiency of cargo uptake by the exosomes generated in these cell lines expressing fusion proteins.

High-throughput size analysis was possible using Dynamic Light Scattering (DLS), which is a laser-based spectroscopy method capable of determining particle radii and

size distribution within the range of 1 nm – 6 µm and provides a sensitive, quantitative characterisation of exosome isolates (Khatun *et al.*, 2016). This technology performs better with homogenous sample populations, due to larger vesicles creating a skew in the data, though it is not suitable for measuring the absolute concentration of vesicles present (Khatun *et al.*, 2016). In future work, DLS limitations could be overcome using Nanoparticle Tracking Analysis (NTA) which tracks the motion of each particle in a sample in order to calculate its size, as well as the overall concentration of each particle size subclass within a sample. NTA can identify particles as small as 30 nm, measure the concentration of a sample, track and measure fluorescently labelled particles and has been used to distinguish between disease and non-disease associated vesicles (Malloy, 2012). The tracking of changes in exosome subpopulations is particularly impressive in the context of biomarker exosomes for diagnostics, where it has been shown to successfully identify separate populations and measure changes in their respective concentrations to accurately predict treatment outcomes of exosomes that had been administered in a diabetes insipidus model (Oosthuyzen *et al.*, 2013). The ability to distinguish subpopulations of exosomes strongly suggests it would be incredibly useful for determining the percentage of exosomes in a population isolated from a cell line whereby the protein of interest is targeted successfully into exosomes.

Another analytical tool that could be applied for further exosome characterisation work is tunable Resistive Pulse Sensing (tRPS), a technique provided by the qNano platform (Izon Science Ltd), capable of determining the size and concentration of exosomes within a sample by passing them through a nanopore positioned on a non-conductive membrane and measuring the changes in baseline current which has been applied (Maas, Broekman and de Vrij, 2017). This platform is particularly attractive for exosome characterisation as it is able to give fast, reliable measurement of vesicle size and concentration as well as measuring zeta potential, although it requires sample volumes that are much larger (~40 mL) (Vogel *et al.*, 2016) than were generated in the work described in this thesis.

6.3 Improvement of anti-dengue monoclonal antibody secretory expression from CHO-S cells

6.3.1 Sequence Hybridization of Den54 with Nivolumab Showed the Most Improvement in Expression

Sequence engineering of the novel anti-dengue fever antibody, Den54, and consequent expression in CHO-S cell cultures resulted in varied increases in antibody titres compared with the Den54 original sequences. Of the five re-engineered variants of the molecules designed (D1-D5), it was found that low levels of D5 were expressed but not secreted whilst pools and clones developed from the D2 variant went on to give the highest titres of the five variants. Given the degree of hybridisation in the D1 and D2 molecules, which retained the dengue framework regions and CDRs, with D3 and D4 which retained only the dengue CDRs, it is somewhat surprising that D2 produced the most improved titre. This outcome suggests that the sequences in the framework regions in the original Den54 sequences are not responsible for the secretion bottleneck observed in the D5 transfection data. The higher expression of the D2 variant compared to the D1 could also indicate that the dengue framework regions form structures more compatible with expression and secretion when grafted to an IgG4 based-molecule than an IgG1. In light of the fact that the original Den54 molecule was also an IgG1, this may well be a contributing factor to its poor expression and poor secretion. The fact that material was observed intracellularly but not secreted suggests an issue with the folding or assembly of the original molecule that is, at least partially, addressed upon replacement of the constant regions with alternative constant regions from other well-expressed antibodies (for both light and heavy chain constant regions). Additionally, both the original Den54 molecule and D5 also contained a mutation of the Fc region which was introduced in an attempt to create a neutralising effect for the antibody (Ramadhany *et al.*, 2015). However, it is possible that this mutation caused the generation of a molecule that was incompatible with folding or secretion once the antibody chains were assembled into their final structure. This could be assessed by reversing this mutation.

Isolation of clones through limiting dilutions from each of the stable cell pools generated for each variant resulted in the generation of several cell lines with distinctly different expression profiles which evolved throughout the scale-up process. Initial differences in the expression of clones from each line, despite each being selected for their high expression identified through dot blots, was likely contributed to heavily by the application of cells and supernatant directly to the nitrocellulose membranes. Due to the secretory issues seen in these variants which resulted in the presence of a build-up of antibody in cell lysates, it is likely that the clonal selection via dot blot analysis was susceptible to false positives. For those clones which were selected and taken forward for scale-up, this intracellular bias could explain the drop in expression observed for many clones when shifting to a supernatant-based analysis, most significantly D5 clones. However, it should be noted that scale-up often results in the shift of high-expression clones to exhibiting lower expression or vice-versa during the scale-up phase of cell line development (Porter *et al.*, 2010). This can be attributed to environmental changes, such as culture vessels, media, feeds and process parameters, interacting with the various cellular phenotypes and genotypes in a cell pool, as well as unpredictable stability of transgenes depending on the loci of their integration into the genome (Porter *et al.*, 2010). Overall, clonal selection from cell pools can allow for the selection of clones from original heterogeneous population, generated during transfection due to random integration, which exhibit the highest expression profiles. However, this can be both labour and cost intensive with diminishing returns in the case of difficult-to-express antibodies.

6.3.2 The Secretion Bottleneck of Den54 May Be Due to Fc Engineering Leading to Intra-ER Crystal Aggregate Formation

The data presented in this thesis using western blot, qPCR and immunofluorescent microscopy analysis suggests that the D5 sequences were able to be expressed intracellularly but are bottlenecked at the secretion. Bottlenecking can occur due at

many stages of the protein secretory pathway, including (1) competition for translational machinery, (2) poor translocation to the ER, (3) aggregation of misfolded proteins in the ER due to sequence errors, (4) poor ER processing capacity, (5) an overloaded ER burden from processing complex molecules and post-translational modifications, or (6) the formation of inclusion bodies. Genetic manipulation of the CHO genome via overexpression of lipid modifying genes has been shown to improve secretion of difficult-to-express antibodies by increasing the membrane fluidity of the ER resulting in its expansion and improved processing power (Budge *et al.*, 2020). Examination of the antibody sequences to identify regions which produce structures which exhibit poor folding ability, and subsequent modification of the sequences to create ones which may pass the folding and QC processes employed by the ER have also been successful in alleviation of secretion bottlenecks (Torres and Dickson, 2021). Considering the presence of protein which correspond to intracellular full-sized antibody molecules and the localisation of heavy chain molecules with calnexin, it is possible that the poor secretion of this antibody was not due to errors in the initial stages of protein folding which take place in the ER. It does however give a strong indication that the antibody molecules formed intra-ER crystals, a form of inclusion body, which form when correctly folded IgG molecules and free subunit chains accumulate at the ER and are unable to be degraded or secreted (Torres, Hussain and Dickson, 2023). These crystals have been known to occur in the expression of antibodies which have undergone sequence alterations in their constant regions, including the Fc region, and in cases where alterations are made to switch the IgG class (e.g IgG-1 to IgG-4, or vice versa) (Hasegawa *et al.*, 2014).

6.3.3 Future Approaches in Sequence Optimisation and Cell Line Development to Improve the Expression and Secretion of the anti-dengue mAb in CHO.

As a result of the Identification of the heavy chain constant regions/Fc regions as potential causes for the poor secretion of this antibody, a further sequence engineering investigation, including the reversal of the Fc mutation of Den54 to induce subclass switching, could be carried out to elucidate a molecule compatible

with secretion in a CHO host. Additionally, alongside consideration of the localisation of secretory issues likely originating in the heavy chain Fc region, work to investigate the effectiveness of dual-vector systems with varied ratios of light and heavy chain plasmids rather than a double gene vector approach may yield better results (Schlatter *et al.*, 2005). It has been observed in some recombinant antibody CHO cell lines that transfecting two separate vectors for the light chain and heavy chain with ratio favoured towards light chain concentration can result in improved antibody titres, due to the protein assembly and folding pathways having a more balanced throughput (Schlatter *et al.*, 2005). Other strategies for controlling LC:HC ratios for improved mAb expression include use of a dual-promoter vector system (Carrara *et al.*, 2021), or cleavable linkers such as 2A peptides between the LC and HC genes (Chng *et al.*, 2015), which allow for improved integration during transfection as there are no cells receiving only half of the transgenes required. Furthermore, engineering of the Den54 sequences could include an exploration of multiple signal sequences to enhance secretion of the fully-assembled antibodies after expression. Signal sequence choice is known to have a direct impact on the amount of secretory productivity that can be achieved for antibodies from CHO cells and should also be explored in order to potentially boost titres (Kober, Zehe and Bode, 2013; Haryadi *et al.*, 2015; You *et al.*, 2018; Srila *et al.*, 2022).

Future work to develop a cell line capable of yielding higher titres for this specific antibody could include transfection using a site-directed integration system, capable of targeting the transgenes to specific regions of the CHO cell chromosomes. Examples of systems which could achieve a targeted integration of plasmid include Flp-In™ CHO cells, piggyBac transposon delivery or CRISPR-Cas-based delivery. These approaches combined with a transcriptomic analysis of the CHO genome would allow for integration at identified transcriptionally active sites within the genome and in some, uniform gene copy numbers which would allow for less variability during clone selection and scale-up. Alternatively, UCOE elements might be employed to allow the insertion of transgenes into an area of heterochromatin with greater transcriptional activity (Saunders *et al.*, 2015).

6.4 Conclusions

This work provides evidence that CHO-S cells are a suitable platform for the development of novel approaches for the production of biotherapeutic products. Here data is presented which shows that, using CHO-S as a cell host, engineered exosomes can be isolated which contain targeted proteins of interest. Also presented is an approach for optimisation of difficult-to-express antibodies in the CHO-S cell host via hybridisation with well-expressed molecules to experimentally highlight sequence domains that are problematic. The hybridisation and sequence optimisation of novel anti-dengue antibody, Den54, was able to improve the expression of the DTE mAb and highlight the mutated Fc region as a region causing secretion bottlenecks, possibly due to formation of intra-ER crystals.

Investigation of two targeting strategies, ubiquitin fusion protein and tetraspanin fusion protein expression, showed that both were able to target proteins into the CHO-S exosome populations but that fusion with CD81 had the greatest success, possibly due to the higher abundance of CD81+ exosomes in native CHO-S exosome populations. Further investigation of exosome targeting, testing five SARS-Cov-2 antigens as proteins of interest, showed that targeting proteins into exosomes can also be affected by the target protein with the spike subunit 2 antigen being more amenable to targeting than other proteins and subunits investigated. The outcomes and methodologies used in this thesis highlight the potential for using engineered exosomes as a novel vaccine platform, via the well-characterised CHO host cell line, as well as discussing the limitations that must be overcome to further the technology.

References

- Admyre, C., Johansson, S. M., Paulie, S. and Gabrielsson, S. (2006) 'Direct exosome stimulation of peripheral human T cells detected by ELISPOT', *European Journal of Immunology*, 36(7), pp. 1772-1781.
- Agarwal, A., Fanelli, G., Letizia, M., Tung, S. L., Boardman, D., Lechler, R., Lombardi, G. and Smyth, L. A. (2014) 'Regulatory T cell-derived exosomes: possible therapeutic and diagnostic tools in transplantation', *Frontiers in Immunology*, 5.
- Alied, M., Nguyen, D., Abdul Aziz, J. M., Vinh, D. P. and Huy, N. T. (2023) 'Dengue fever on the rise in Southeast Asia', *Pathog Glob Health*, 117(1), pp. 1-2.
- Anticoli, S., Manfredi, F., Chiozzini, C., Arenaccio, C., Olivetta, E., Ferrantelli, F., Capocéfalo, A., Falcone, E., Ruggieri, A. and Federico, M. (2018) 'An Exosome-Based Vaccine Platform Imparts Cytotoxic T Lymphocyte Immunity Against Viral Antigens', *Biotechnology Journal*, 13(4).
- Attallah, C., Etcheverrigaray, M., Kratje, R. and Oggero, M. (2017) 'A highly efficient modified human serum albumin signal peptide to secrete proteins in cells derived from different mammalian species', *Protein Expr Purif*, 132, pp. 27-33.
- Bai, Z., Cao, Y., Liu, W. and Li, J. (2021) 'The SARS-CoV-2 Nucleocapsid Protein and Its Role in Viral Structure, Biological Functions, and a Potential Target for Drug or Vaccine Mitigation', *Viruses*, 13(6).
- Baiersdörfer, M., Boros, G., Muramatsu, H., Mahiny, A., Vlatkovic, I., Sahin, U. and Karikó, K. (2019) 'A Facile Method for the Removal of dsRNA Contaminant from In Vitro-Transcribed mRNA', *Mol Ther Nucleic Acids*, 15, pp. 26-35.
- Baietti, M. F., Zhang, Z., Mortier, E., Melchior, A., Degeest, G., Geeraerts, A., Ivarsson, Y., Depoortere, F., Coomans, C., Vermeiren, E., Zimmermann, P. and David, G. (2012) 'Syndecan-syntenin-ALIX regulates the biogenesis of exosomes', *Nat Cell Biol*, 14(7), pp. 677-85.
- Baranyai, T., Herczeg, K., Onódi, Z., Voszka, I., Módos, K., Marton, N., Nagy, G., Mäger, I., Wood, M. J., El Andaloussi, S., Pálincás, Z., Kumar, V., Nagy, P., Kittel, Á., Buzás, E. I., Ferdinandy, P. and Giricz, Z. (2015) 'Isolation of Exosomes from Blood Plasma: Qualitative and Quantitative Comparison of Ultracentrifugation and Size Exclusion Chromatography Methods', *PLoS One*, 10(12), pp. e0145686.
- Barnes, L. M., Bentley, C. M. and Dickson, A. J. (2003) 'Stability of protein production from recombinant mammalian cells', *Biotechnol Bioeng*, 81(6), pp. 631-9.
- Beit-Yannai, E., Tabak, S. and Stamer, W. D. (2018) 'Physical exosome:exosome interactions', *J Cell Mol Med*, 22(3), pp. 2001-2006.
- Belliveau, J. and Papoutsakis, E. T. (2022) 'Extracellular vesicles facilitate large-scale dynamic exchange of proteins and RNA among cultured Chinese hamster ovary and human cells', *Biotechnol Bioeng*, 119(5), pp. 1222-1238.
- Belouzard, S., Chu, V. C. and Whittaker, G. R. (2009) 'Activation of the SARS coronavirus spike protein via sequential proteolytic cleavage at two distinct sites', *Proc Natl Acad Sci U S A*, 106(14), pp. 5871-6.
- Bergman, P. J., Camps-Palau, M. A., McKnight, J. A., Leibman, N. F., Craft, D. M., Leung, C., Liao, J., Riviere, I., Sadelain, M., Hohenhaus, A. E., Gregor, P., Houghton, A. N., Perales, M. A. and Wolchok, J. D. (2006) 'Development of a xenogeneic DNA

vaccine program for canine malignant melanoma at the Animal Medical Center', *Vaccine*, 24(21), pp. 4582-5.

Bhatt, S., Gething, P. W., Brady, O. J., Messina, J. P., Farlow, A. W., Moyes, C. L., Drake, J. M., Brownstein, J. S., Hoen, A. G., Sankoh, O., Myers, M. F., George, D. B., Jaenisch, T., Wint, G. R. W., Simmons, C. P., Scott, T. W., Farrar, J. J. and Hay, S. I. (2013) 'The global distribution and burden of dengue', *Nature*, 496(7446), pp. 504-507.

Bliss, C. M., Parsons, A. J., Nachbagauer, R., Hamilton, J. R., Cappuccini, F., Ulaszewska, M., Webber, J. P., Clayton, A., Hill, A. V. S. and Coughlan, L. (2020) 'Targeting Antigen to the Surface of EVs Improves the In Vivo Immunogenicity of Human and Non-human Adenoviral Vaccines in Mice', *Molecular Therapy-Methods & Clinical Development*, 16, pp. 108-125.

Bloom, K., van den Berg, F. and Arbuthnot, P. (2021) 'Self-amplifying RNA vaccines for infectious diseases', *Gene Ther*, 28(3-4), pp. 117-129.

Brisson, A. R., Tan, S., Linares, R., Gounou, C. and Arraud, N. (2017) 'Extracellular vesicles from activated platelets: a semiquantitative cryo-electron microscopy and immuno-gold labeling study', *Platelets*, 28(3), pp. 263-271.

Budge, J. D., Knight, T. J., Povey, J., Roobol, J., Brown, I. R., Singh, G., Dean, A., Turner, S., Jaques, C. M., Young, R. J., Racher, A. J. and Smales, C. M. (2020) 'Engineering of Chinese hamster ovary cell lipid metabolism results in an expanded ER and enhanced recombinant biotherapeutic protein production', *Metab Eng*, 57, pp. 203-216.

Budge, J. D., Roobol, J., Singh, G., Mozzanino, T., Knight, T. J., Povey, J., Dean, A., Turner, S. J., Jaques, C. M., Young, R. J., Racher, A. J. and Smales, C. M. (2021) 'A proline metabolism selection system and its application to the engineering of lipid biosynthesis in Chinese hamster ovary cells', *Metab Eng Commun*, 13, pp. e00179.

Busse, A. and Lüftner, D. (2019) 'What Does the Pipeline Promise about Upcoming Biosimilar Antibodies in Oncology?', *Breast Care (Basel)*, 14(1), pp. 10-16.

Carrara, S. C., Fiebig, D., Bogen, J. P., Grzeschik, J., Hock, B. and Kolmar, H. (2021) 'Recombinant Antibody Production Using a Dual-Promoter Single Plasmid System', *Antibodies (Basel)*, 10(2).

Chae, H., Cho, S., Jeong, M., Kwon, K., Choi, D., Lee, J., Nam, W., Hong, J., Yoon, S. and Hong, H. (2021) 'Improvement of Biophysical Properties and Affinity of a Human Anti-L1CAM Therapeutic Antibody through Antibody Engineering Based on Computational Methods', *Int J Mol Sci*, 22(13).

Chakrabarti, S., Barrow, C. J., Kanwar, R. K., Ramana, V. and Kanwar, J. R. (2016) 'Studies to Prevent Degradation of Recombinant Fc-Fusion Protein Expressed in Mammalian Cell Line and Protein Characterization', *Int J Mol Sci*, 17(6).

Chandrasekera, D., Shah, R., van Hout, I., De Jonge, W., Bunton, R., Parry, D., Davis, P. and Katare, R. (2023) 'Combination of precipitation and size exclusion chromatography as an effective method for exosome like extracellular vesicle isolation from pericardial fluids', *Nanotheranostics*, 7(4), pp. 345-352.

Chaput, N. and Thery, C. (2011) 'Exosomes: immune properties and potential clinical implementations', *Seminars in Immunopathology*, 33(5), pp. 419-440.

Chen, B. Y., Sung, C. W., Chen, C., Cheng, C. M., Lin, D. P., Huang, C. T. and Hsu, M. Y. (2019) 'Advances in exosomes technology', *Clin Chim Acta*, 493, pp. 14-19.

Chen, R. H., Chen, Y. H. and Huang, T. Y. (2019) 'Ubiquitin-mediated regulation of autophagy', *J Biomed Sci*, 26(1), pp. 80.

Cheng, Y. and Schorey, J. S. (2013) 'Exosomes carrying mycobacterial antigens can protect mice against *Mycobacterium tuberculosis* infection', *European Journal of Immunology*, 43(12), pp. 3279-3290.

Cheng, Y. and Schorey, J. S. (2016) 'Targeting soluble proteins to exosomes using a ubiquitin tag', *Biotechnology and Bioengineering*, 113(6), pp. 1315-1324.

Chilumuri, A., Markiv, A. and Milton, N. G. (2014) 'Immunocytochemical staining of endogenous nuclear proteins with the HIS-1 anti-poly-histidine monoclonal antibody: a potential source of error in His-tagged protein detection', *Acta Histochem*, 116(6), pp. 1022-8.

Chng, J., Wang, T., Nian, R., Lau, A., Hoi, K. M., Ho, S. C., Gagnon, P., Bi, X. and Yang, Y. (2015) 'Cleavage efficient 2A peptides for high level monoclonal antibody expression in CHO cells', *MAbs*, 7(2), pp. 403-12.

Chudakov, D. M., Matz, M. V., Lukyanov, S. and Lukyanov, K. A. (2010) 'Fluorescent proteins and their applications in imaging living cells and tissues', *Physiol Rev*, 90(3), pp. 1103-63.

Conigliaro, A., Costa, V., Lo Dico, A., Saieva, L., Buccheri, S., Dieli, F., Manno, M., Raccosta, S., Mancone, C., Tripodi, M., De Leo, G. and Alessandro, R. (2015) 'CD90+liver cancer cells modulate endothelial cell phenotype through the release of exosomes containing H19 lncRNA', *Molecular Cancer*, 14.

Davidson, A. H., Traub-Dargatz, J. L., Rodeheaver, R. M., Ostlund, E. N., Pedersen, D. D., Moorhead, R. G., Stricklin, J. B., Dewell, R. D., Roach, S. D., Long, R. E., Albers, S. J., Callan, R. J. and Salman, M. D. (2005) 'Immunologic responses to West Nile virus in vaccinated and clinically affected horses', *J Am Vet Med Assoc*, 226(2), pp. 240-5.

Dejnirattisai, W., Jumnainsong, A., Onsirisakul, N., Fitton, P., Vasanawathana, S., Limpitikul, W., Puttikhunt, C., Edwards, C., Duangchinda, T., Supasa, S., Chawansuntati, K., Malasit, P., Mongkolsapaya, J. and Screaton, G. (2010) 'Cross-reacting antibodies enhance dengue virus infection in humans', *Science*, 328(5979), pp. 745-8.

Delcayre, A., Estelles, A., Sperinde, J., Roulon, T., Paz, P., Aguilar, B., Villanueva, J., Khine, S. and Le Pecq, J. B. (2005) 'Exosome Display technology: Applications to the development of new diagnostics and therapeutics', *Blood Cells Molecules and Diseases*, 35(2), pp. 158-168.

Di Bonito, P., Chiozzini, C., Arenaccio, C., Anticoli, S., Manfredi, F., Olivetta, E., Ferrantelli, F., Falcone, E., Ruggieri, A. and Federico, M. (2017) 'Antitumor HPV E7-specific CTL activity elicited by in vivo engineered exosomes produced through DNA inoculation', *Int J Nanomedicine*, 12, pp. 4579-4591.

Dogrammatzis, C., Saleh, S., Deighan, C. and Kalamvoki, M. (2021) 'Diverse Populations of Extracellular Vesicles with Opposite Functions during Herpes Simplex Virus 1 Infection', *J Virol*, 95(6).

Donaldson, J. S., Dale, M. P. and Rosser, S. J. (2021) 'Decoupling Growth and Protein Production in CHO Cells: A Targeted Approach', *Front Bioeng Biotechnol*, 9, pp. 658325.

Dorai, H., Corisdeo, S., Ellis, D., Kinney, C., Chomo, M., Hawley-Nelson, P., Moore, G., Betenbaugh, M. J. and Ganguly, S. (2012) 'Early prediction of instability of Chinese hamster ovary cell lines expressing recombinant antibodies and antibody-fusion proteins', *Biotechnol Bioeng*, 109(4), pp. 1016-30.

Dreyer, F. and Baur, A. (2016) 'Biogenesis and Functions of Exosomes and Extracellular Vesicles', *Methods Mol Biol*, 1448, pp. 201-16.

Dyball, L. E. and Smales, C. M. (2022) 'Exosomes: Biogenesis, targeting, characterization and their potential as "Plug & Play" vaccine platforms', *Biotechnol J*, 17(11), pp. e2100646.

Escudier, B., Dorval, T., Chaput, N., Andre, F., Caby, M. P., Novault, S., Flament, C., Leboulaire, C., Borg, C., Amigorena, S., Boccaccio, C., Bonnerot, C., Dhellin, O., Movassagh, M., Piperno, S., Robert, C., Serra, V., Valente, N., Le Pecq, J. B., Spatz, A., Lantz, O., Tursz, T., Angevin, E. and Zitvogel, L. (2005) 'Vaccination of metastatic melanoma patients with autologous dendritic cell (DC) derived-exosomes: results of the first phase I clinical trial', *Journal of Translational Medicine*, 3.

Eusébio, D., Neves, A. R., Costa, D., Biswas, S., Alves, G., Cui, Z. and Sousa, Â. (2021) 'Methods to improve the immunogenicity of plasmid DNA vaccines', *Drug Discov Today*, 26(11), pp. 2575-2592.

Falsey, A. R., Sobieszczyk, M. E., Hirsch, I., Sproule, S., Robb, M. L., Corey, L., Neuzil, K. M., Hahn, W., Hunt, J., Mulligan, M. J., McEvoy, C., DeJesus, E., Hassman, M., Little, S. J., Pahud, B. A., Durbin, A., Pickrell, P., Daar, E. S., Bush, L., Solis, J., Carr, Q. O., Oyedele, T., Buchbinder, S., Cowden, J., Vargas, S. L., Guerreros Benavides, A., Call, R., Keefer, M. C., Kirkpatrick, B. D., Pullman, J., Tong, T., Brewinski Isaacs, M., Benkeser, D., Janes, H. E., Nason, M. C., Green, J. A., Kelly, E. J., Maaske, J., Mueller, N., Shoemaker, K., Takas, T., Marshall, R. P., Pangalos, M. N., Villafana, T. and Gonzalez-Lopez, A. (2021) 'Phase 3 Safety and Efficacy of AZD1222 (ChAdOx1 nCoV-19) Covid-19 Vaccine', *N Engl J Med*, 385(25), pp. 2348-2360.

Fares, J., Kashyap, R. and Zimmermann, P. (2017) 'Syntenin: Key player in cancer exosome biogenesis and uptake?', *Cell Adh Migr*, 11(2), pp. 124-126.

Federico, M. (2012) 'From virus-like particles to engineered exosomes for a new generation of vaccines', *Future Virology*, 7(5), pp. 473-482.

Fernandez-Messina, L., Rodriguez-Galan, A., de Yebenes, V. G., Gutierrez-Vazquez, C., Tenreiro, S., Seabra, M. C., Ramiro, A. R. and Sanchez-Madrid, F. (2020) 'Transfer of extracellular vesicle-microRNA controls germinal center reaction and antibody production', *Embo Reports*, 21(4).

Ferrantelli, F., Manfredi, F., Chiozzini, C., Anticoli, S., Olivetta, E., Arenaccio, C. and Federico, M. (2018) 'DNA Vectors Generating Engineered Exosomes Potential CTL Vaccine Candidates Against AIDS, Hepatitis B, and Tumors', *Molecular Biotechnology*, 60(11), pp. 773-782.

Fox, S. R., Patel, U. A., Yap, M. G. and Wang, D. I. (2004) 'Maximizing interferon-gamma production by Chinese hamster ovary cells through temperature shift optimization: experimental and modeling', *Biotechnol Bioeng*, 85(2), pp. 177-84.

Franzin, R., Netti, G. S., Spadaccino, F., Porta, C., Gesualdo, L., Stallone, G., Castellano, G. and Ranieri, E. (2020) 'The Use of Immune Checkpoint Inhibitors in Oncology and the Occurrence of AKI: Where Do We Stand?', *Front Immunol*, 11, pp. 574271.

Fuenmayor, J., Godia, F. and Cervera, L. (2017) 'Production of virus-like particles for vaccines', *N Biotechnol*, 39(Pt B), pp. 174-180.

Garver, K. A., LaPatra, S. E. and Kurath, G. (2005) 'Efficacy of an infectious hematopoietic necrosis (IHN) virus DNA vaccine in Chinook *Oncorhynchus tshawytscha* and sockeye *O. nerka* salmon', *Dis Aquat Organ*, 64(1), pp. 13-22.

Gelibter, S., Marostica, G., Mandelli, A., Siciliani, S., Podini, P., Finardi, A. and Furlan, R. (2022) 'The impact of storage on extracellular vesicles: A systematic study', *J Extracell Vesicles*, 11(2), pp. e12162.

Gibson, S. J., Bond, N. J., Milne, S., Lewis, A., Sheriff, A., Pettman, G., Pradhan, R., Higazi, D. R. and Hatton, D. (2017) 'N-terminal or signal peptide sequence engineering prevents truncation of human monoclonal antibody light chains', *Biotechnol Bioeng*, 114(9), pp. 1970-1977.

Giri, P. K. and Schorey, J. S. (2008) 'Exosomes Derived from M-Bovis BCG Infected Macrophages Activate Antigen-Specific CD4(+) and CD8(+) T Cells In Vitro and In Vivo', *Plos One*, 3(6).

Gould, S. J., Booth, A. M. and Hildreth, J. E. (2003) 'The Trojan exosome hypothesis', *Proc Natl Acad Sci U S A*, 100(19), pp. 10592-7.

Greening, D. W., Gopal, S. K., Xu, R., Simpson, R. J. and Chen, W. S. (2015a) 'Exosomes and their roles in immune regulation and cancer', *Seminars in Cell & Developmental Biology*, 40, pp. 72-81.

Greening, D. W., Xu, R., Ji, H., Tauro, B. J. and Simpson, R. J. (2015b) 'A protocol for exosome isolation and characterization: evaluation of ultracentrifugation, density-gradient separation, and immunoaffinity capture methods', *Methods Mol Biol*, 1295, pp. 179-209.

Gupta, S., Rawat, S., Arora, V., Kottarath, S. K., Dinda, A. K., Vaishnav, P. K., Nayak, B. and Mohanty, S. (2018) 'An improvised one-step sucrose cushion ultracentrifugation method for exosome isolation from culture supernatants of mesenchymal stem cells', *Stem Cell Research & Therapy*, 9.

Gurunathan, S., Kang, M. H., Jeyaraj, M., Qasim, M. and Kim, J. H. (2019) 'Review of the Isolation, Characterization, Biological Function, and Multifarious Therapeutic Approaches of Exosomes', *Cells*, 8(4).

Gąciarz, A. and Ruddock, L. W. (2017) 'Complementarity determining regions and frameworks contribute to the disulfide bond independent folding of intrinsically stable scFv', *PLoS One*, 12(12), pp. e0189964.

Halstead, S. B., Mahalingam, S., Marovich, M. A., Ubol, S. and Mosser, D. M. (2010) 'Intrinsic antibody-dependent enhancement of microbial infection in macrophages: disease regulation by immune complexes', *Lancet Infect Dis*, 10(10), pp. 712-22.

Han, Q. F., Li, W. J., Hu, K. S., Gao, J., Zhai, W. L., Yang, J. H. and Zhang, S. J. (2022) 'Exosome biogenesis: machinery, regulation, and therapeutic implications in cancer', *Mol Cancer*, 21(1), pp. 207.

Hansel, T. T., Kropshofer, H., Singer, T., Mitchell, J. A. and George, A. J. (2010) 'The safety and side effects of monoclonal antibodies', *Nat Rev Drug Discov*, 9(4), pp. 325-38.

Harding, C., Heuser, J. and Stahl, P. (1983) 'Receptor-mediated endocytosis of transferrin and recycling of the transferrin receptor in rat reticulocytes', *J Cell Biol*, 97(2), pp. 329-39.

Haryadi, R., Ho, S., Kok, Y. J., Pu, H. X., Zheng, L., Pereira, N. A., Li, B., Bi, X., Goh, L. T., Yang, Y. and Song, Z. (2015) 'Optimization of heavy chain and light chain signal peptides for high level expression of therapeutic antibodies in CHO cells', *PLoS One*, 10(2), pp. e0116878.

Hasegawa, H., Forte, C., Barber, I., Turnbaugh, S., Stoops, J., Shen, M. and Lim, A. C. (2014) 'Modulation of in vivo IgG crystallization in the secretory pathway by heavy

chain isotype class switching and N-linked glycosylation', *Biochim Biophys Acta*, 1843(7), pp. 1325-38.

Heinemann, M. L., Illmer, M., Silva, L. P., Hawke, D. H., Recio, A., Vorontsova, M. A., Alt, E. and Vykoukal, J. (2014) 'Benchmark isolation and characterization of functional exosomes by sequential filtration', *Journal of Chromatography A*, 1371, pp. 125-135.

Hessvik, N. P. and Llorente, A. (2018) 'Current knowledge on exosome biogenesis and release', *Cellular and Molecular Life Sciences*, 75(2), pp. 193-208.

Ho, S. C., Koh, E. Y., van Beers, M., Mueller, M., Wan, C., Teo, G., Song, Z., Tong, Y. W., Bardor, M. and Yang, Y. (2013) 'Control of IgG LC:HC ratio in stably transfected CHO cells and study of the impact on expression, aggregation, glycosylation and conformational stability', *J Biotechnol*, 165(3-4), pp. 157-66.

Hong, C. S., Funk, S., Muller, L., Boyiadzis, M. and Whiteside, T. L. (2016) 'Isolation of biologically active and morphologically intact exosomes from plasma of patients with cancer', *Journal of Extracellular Vesicles*, 5.

Hong, Y., Nam, G. H., Koh, E., Jeon, S., Kim, G. B., Jeong, C., Kim, D. H., Yang, Y. and Kim, I. S. (2018) 'Exosome as a Vehicle for Delivery of Membrane Protein Therapeutics, PH20, for Enhanced Tumor Penetration and Antitumor Efficacy', *Advanced Functional Materials*, 28(5).

Hoshan, L., Jiang, R., Moroney, J., Bui, A., Zhang, X., Hang, T. C. and Xu, S. (2019) 'Effective bioreactor pH control using only sparging gases', *Biotechnol Prog*, 35(1), pp. e2743.

Hu, B., Guo, H., Zhou, P. and Shi, Z. L. (2021) 'Characteristics of SARS-CoV-2 and COVID-19', *Nat Rev Microbiol*, 19(3), pp. 141-154.

Hurley, J. H. and Hanson, P. I. (2010) 'Membrane budding and scission by the ESCRT machinery: it's all in the neck', *Nat Rev Mol Cell Biol*, 11(8), pp. 556-66.

Hussain, H., Fisher, D. I., Roth, R. G., Mark Abbott, W., Carballo-Amador, M. A., Warwicker, J. and Dickson, A. J. (2018) 'A protein chimera strategy supports production of a model "difficult-to-express" recombinant target', *FEBS Lett*, 592(14), pp. 2499-2511.

Hübel, K., Kron, F. and Lux, M. P. (2020) 'Biosimilars in oncology: Effects on economy and therapeutic innovations', *Eur J Cancer*, 139, pp. 10-19.

Injampa, S., Muenngern, N., Pipattanaboon, C., Benjathummarak, S., Boonha, K., Hananantachai, H., Wongwit, W., Ramasoota, P. and Pitaksajakul, P. (2017) 'Generation and characterization of cross neutralizing human monoclonal antibody against 4 serotypes of dengue virus without enhancing activity', *PeerJ*, 5, pp. e4021.

Jackson, C. B., Farzan, M., Chen, B. and Choe, H. (2022) 'Mechanisms of SARS-CoV-2 entry into cells', *Nat Rev Mol Cell Biol*, 23(1), pp. 3-20.

Jeppesen, D. K., Fenix, A. M., Franklin, J. L., Higginbotham, J. N., Zhang, Q., Zimmerman, L. J., Liebler, D. C., Ping, J., Liu, Q., Evans, R., Fissell, W. H., Patton, J. G., Rome, L. H., Burnette, D. T. and Coffey, R. J. (2019) 'Reassessment of Exosome Composition', *Cell*, 177(2), pp. 428-445.e18.

Jiang, Y., Yu, K., Zhang, H., Zhang, P., Li, C., Tian, G., Li, Y., Wang, X., Ge, J., Bu, Z. and Chen, H. (2007) 'Enhanced protective efficacy of H5 subtype avian influenza DNA vaccine with codon optimized HA gene in a pCAGGS plasmid vector', *Antiviral Res*, 75(3), pp. 234-41.

Johari, Y. B., Estes, S. D., Alves, C. S., Sinacore, M. S. and James, D. C. (2015) 'Integrated cell and process engineering for improved transient production of a

"difficult-to-express" fusion protein by CHO cells', *Biotechnol Bioeng*, 112(12), pp. 2527-42.

Jones, P. T., Dear, P. H., Foote, J., Neuberger, M. S. and Winter, G. (1986) 'Replacing the complementarity-determining regions in a human antibody with those from a mouse', *Nature*, 321(6069), pp. 522-5.

Kalluri, R. (2016) 'The biology and function of exosomes in cancer', *Journal of Clinical Investigation*, 126(4), pp. 1208-1215.

Kalluri, R. and LeBleu, V. S. (2020) 'The biology, function, and biomedical applications of exosomes', *Science*, 367(6478).

Kalra, H., Simpson, R. J., Ji, H., Aikawa, E., Altevogt, P., Askenase, P., Bond, V. C., Borrás, F. E., Breakefield, X., Budnik, V., Buzas, E., Camussi, G., Clayton, A., Cocucci, E., Falcon-Perez, J. M., Gabriëlsson, S., Gho, Y. S., Gupta, D., Harsha, H. C., Hendrix, A., Hill, A. F., Inal, J. M., Jenster, G., Kramer-Albers, E. M., Lim, S. K., Llorente, A., Lotvall, J., Marcilla, A., Mincheva-Nilsson, L., Nazarenko, I., Nieuwland, R., Hoen, E. N. M., Pandey, A., Patel, T., Piper, M. G., Pluchino, S., Prasad, T. S. K., Rajendran, L., Raposo, G., Record, M., Reid, G. E., Sanchez-Madrid, F., Schiffelers, R. M., Siljander, P., Stensballe, A., Stoorvogel, W., Taylor, D., Thery, C., Valadi, H., van Balkom, B. W. M., Vazquez, J., Vidal, M., Wauben, M. H. M., Yanez-Mo, M., Zoeller, M. and Mathivanan, S. (2012) 'Vesiclepedia: A Compendium for Extracellular Vesicles with Continuous Community Annotation', *Plos Biology*, 10(12).

Kaneyoshi, K., Kuroda, K., Uchiyama, K., Onitsuka, M., Yamano-Adachi, N., Koga, Y. and Omasa, T. (2019) 'Secretion analysis of intracellular "difficult-to-express" immunoglobulin G (IgG) in Chinese hamster ovary (CHO) cells', *Cytotechnology*, 71(1), pp. 305-316.

Kang, M., Ren, M. P., Li, Y., Fu, Y. Q., Deng, M. M. and Li, C. P. (2018) 'Exosome-mediated transfer of lncRNA PART1 induces gefitinib resistance in esophageal squamous cell carcinoma via functioning as a competing endogenous RNA', *Journal of Experimental & Clinical Cancer Research*, 37.

Karikó, K., Muramatsu, H., Ludwig, J. and Weissman, D. (2011) 'Generating the optimal mRNA for therapy: HPLC purification eliminates immune activation and improves translation of nucleoside-modified, protein-encoding mRNA', *Nucleic Acids Res*, 39(21), pp. e142.

Karikó, K., Muramatsu, H., Welsh, F. A., Ludwig, J., Kato, H., Akira, S. and Weissman, D. (2008) 'Incorporation of pseudouridine into mRNA yields superior nonimmunogenic vector with increased translational capacity and biological stability', *Mol Ther*, 16(11), pp. 1833-40.

Karimi, N., Dalirfardouei, R., Dias, T., Lötvall, J. and Lässer, C. (2022) 'Tetraspanins distinguish separate extracellular vesicle subpopulations in human serum and plasma - Contributions of platelet extracellular vesicles in plasma samples', *J Extracell Vesicles*, 11(5), pp. e12213.

Khatun, Z., Bhat, A., Sharma, S. and Sharma, A. (2016) 'Elucidating diversity of exosomes: biophysical and molecular characterization methods', *Nanomedicine*, 11(17), pp. 2359-2377.

Khobragade, A., Bhate, S., Ramaiah, V., Deshpande, S., Giri, K., Phophle, H., Supe, P., Godara, I., Revanna, R., Nagarkar, R., Sanmukhani, J., Dey, A., Rajanathan, T. M. C., Kansagra, K. and Koradia, P. (2022) 'Efficacy, safety, and immunogenicity of the DNA

SARS-CoV-2 vaccine (ZyCoV-D): the interim efficacy results of a phase 3, randomised, double-blind, placebo-controlled study in India', *Lancet*, 399(10332), pp. 1313-1321.

Kim, D. K., Lee, J., Kim, S. R., Choi, D. S., Yoon, Y. J., Kim, J. H., Go, G., Nhung, D., Hong, K., Jang, S. C., Kim, S. H., Park, K. S., Kim, O. Y., Park, H. T., Seo, J. H., Aikawa, E., Baj-Krzyworzeka, M., van Balkom, B. W. M., Belting, M., Blanc, L., Bond, V., Bongiovanni, A., Borrás, F. E., Buee, L., Buzas, E. I., Cheng, L., Clayton, A., Cocucci, E., Dela Cruz, C. S., Desiderio, D. M., Di Vizio, D., Ekstrom, K., Falcon-Perez, J. M., Gardiner, C., Giebel, B., Greening, D. W., Gross, J. C., Gupta, D., Hendrix, A., Hill, A. F., Hill, M. M., Hoen, E. N., Hwang, D. W., Inal, J., Jagannadham, M. V., Jayachandran, M., Jee, Y. K., Jorgensen, M., Kim, K. P., Kim, Y. K., Kislinger, T., Lasser, C., Lee, D. S., Lee, H., van Leeuwen, J., Lener, T., Liu, M. L., Lotvall, J., Marcilla, A., Mathivanan, S., Moller, A., Morhayim, J., Mullier, F., Nazarenko, I., Nieuwland, R., Nunes, D. N., Pang, K., Park, J., Patel, T., Pocsfalvi, G., del Portillo, H., Putz, U., Ramirez, M. I., Rodrigues, M. L., Roh, T. Y., Royo, F., Sahoo, S., Schiffelers, R., Sharma, S., Siljander, P., Simpson, R. J., Soekmadji, C., Stahl, P., Stensballe, A., Stepien, E., Tahara, H., Trummer, A., Valadi, H., Vella, L. J., Wai, S. N., Witwer, K., Yanez-Mo, M., Youn, H., Zeidler, R. and Gho, Y. S. (2015) 'EVpedia: a community web portal for extracellular vesicles research', *Bioinformatics*, 31(6), pp. 933-939.

Kim, M., O'Callaghan, P. M., Droms, K. A. and James, D. C. (2011) 'A mechanistic understanding of production instability in CHO cell lines expressing recombinant monoclonal antibodies', *Biotechnol Bioeng*, 108(10), pp. 2434-46.

Kleeman, B., Olsson, A., Newkold, T., Kofron, M., DeLay, M., Hildeman, D. and Grimes, H. L. (2018) 'A guide to choosing fluorescent protein combinations for flow cytometric analysis based on spectral overlap', *Cytometry A*, 93(5), pp. 556-562.

Kober, L., Zehe, C. and Bode, J. (2013) 'Optimized signal peptides for the development of high expressing CHO cell lines', *Biotechnol Bioeng*, 110(4), pp. 1164-73.

Kowaboot, S., Puangmanee, W., Benjathummarak, S., Boonha, K., Chaisri, U., Ramasoota, P. and Pitaksajakul, P. (2022) 'Characterization of Human Anti-Dengue NS1 Monoclonal Antibodies Derived from Patients Infected with DENV-2', *Jpn J Infect Dis*, 75(1), pp. 24-30.

Kowal, J., Arras, G., Colombo, M., Jouve, M., Morath, J. P., Primdal-Bengtson, B., Dingli, F., Loew, D., Tkach, M. and Théry, C. (2016) 'Proteomic comparison defines novel markers to characterize heterogeneous populations of extracellular vesicle subtypes', *Proc Natl Acad Sci U S A*, 113(8), pp. E968-77.

Kuate, S., Cinatl, J., Doerr, H. W. and Uberla, K. (2007) 'Exosomal vaccines containing the S protein of the SARS coronavirus induce high levels of neutralizing antibodies', *Virology*, 362(1), pp. 26-37.

Köhler, G. and Milstein, C. (1975) 'Continuous cultures of fused cells secreting antibody of predefined specificity', *Nature*, 256(5517), pp. 495-7.

Lai, A. L. and Freed, J. H. (2021) 'SARS-CoV-2 Fusion Peptide has a Greater Membrane Perturbating Effect than SARS-CoV with Highly Specific Dependence on Ca(2)', *J Mol Biol*, 433(10), pp. 166946.

Lai, A. L., Millet, J. K., Daniel, S., Freed, J. H. and Whittaker, G. R. (2017) 'The SARS-CoV Fusion Peptide Forms an Extended Bipartite Fusion Platform that Perturbs Membrane Order in a Calcium-Dependent Manner', *J Mol Biol*, 429(24), pp. 3875-3892.

Lamb, Y. N. (2021) 'BNT162b2 mRNA COVID-19 Vaccine: First Approval', *Drugs*, 81(4), pp. 495-501.

Lao-Gonzalez, T., Bueno-Soler, A., Duran-Hernandez, A., Sosa-Aguiar, K., Hinojosa-Puerta, L. E., Hernandez-Garcia, T., de la Luz-Hernandez, K. R., Palacios-Oliva, J. and Boggiano-Ayo, T. (2021) 'Screening and selection strategy for the establishment of biosimilar to trastuzumab-expressing CHO-K1 cell lines', *AMB Express*, 11(1), pp. 1.

Lasser, C. (2015) 'Exosomes in diagnostic and therapeutic applications: biomarker, vaccine and RNA interference delivery vehicle', *Expert Opinion on Biological Therapy*, 15(1), pp. 103-117.

Lattanzi, L. and Federico, M. (2012) 'A strategy of antigen incorporation into exosomes: Comparing cross-presentation levels of antigens delivered by engineered exosomes and by lentiviral virus-like particles', *Vaccine*, 30(50), pp. 7229-7237.

Le Fourn, V., Girod, P. A., Buceta, M., Regamey, A. and Mermod, N. (2014) 'CHO cell engineering to prevent polypeptide aggregation and improve therapeutic protein secretion', *Metab Eng*, 21, pp. 91-102.

Ledford, H. (2020) 'Moderna COVID vaccine becomes second to get US authorization', *Nature*. England.

Lerner, R. A. (2016) 'Combinatorial antibody libraries: new advances, new immunological insights', *Nat Rev Immunol*, 16(8), pp. 498-508.

Li, J., Lai, S., Gao, G. F. and Shi, W. (2021) 'The emergence, genomic diversity and global spread of SARS-CoV-2', *Nature*, 600(7889), pp. 408-418.

Li, Y. W., Liu, Y., Xiu, F. M., Wang, J. N., Cong, H., He, S. Y., Shi, Y. Y., Wang, X. Y., Li, X. and Zhou, H. Y. (2018) 'Characterization of exosomes derived from *Toxoplasma gondii* and their functions in modulating immune responses', *International Journal of Nanomedicine*, 13, pp. 467-477.

Ling, W. L., Su, C. T., Lua, W. H., Poh, J. J., Ng, Y. L., Wipat, A. and Gan, S. K. (2020) 'Essentially Leading Antibody Production: An Investigation of Amino Acids, Myeloma, and Natural V-Region Signal Peptides in Producing Pertuzumab and Trastuzumab Variants', *Front Immunol*, 11, pp. 604318.

Liu, M. A. (2019) 'A Comparison of Plasmid DNA and mRNA as Vaccine Technologies', *Vaccines (Basel)*, 7(2).

Lonberg, N., Taylor, L. D., Harding, F. A., Trounstein, M., Higgins, K. M., Schramm, S. R., Kuo, C. C., Mashayekh, R., Wymore, K., McCabe, J. G. and et al. (1994) 'Antigen-specific human antibodies from mice comprising four distinct genetic modifications', *Nature*, 368(6474), pp. 856-9.

Lozano-Andrés, E., Libregts, S. F., Toribio, V., Royo, F., Morales, S., López-Martín, S., Valés-Gómez, M., Reyburn, H. T., Falcón-Pérez, J. M., Wauben, M. H., Soto, M. and Yáñez-Mó, M. (2019) 'Tetraspanin-decorated extracellular vesicle-mimetics as a novel adaptable reference material', *J Extracell Vesicles*, 8(1), pp. 1573052.

Lu, R. M., Hwang, Y. C., Liu, I. J., Lee, C. C., Tsai, H. Z., Li, H. J. and Wu, H. C. (2020) 'Development of therapeutic antibodies for the treatment of diseases', *J Biomed Sci*, 27(1), pp. 1.

Lu, Y., Zhou, Q., Han, Q., Wu, P., Zhang, L., Zhu, L., Weaver, D. T., Xu, C. and Zhang, B. (2018) 'Inactivation of deubiquitinase CYLD enhances therapeutic antibody production in Chinese hamster ovary cells', *Appl Microbiol Biotechnol*, 102(14), pp. 6081-6093.

Maas, S. L., Broekman, M. L. and de Vrij, J. (2017) 'Tunable Resistive Pulse Sensing for the Characterization of Extracellular Vesicles', *Methods Mol Biol*, 1545, pp. 21-33.

Madu, I. G., Roth, S. L., Belouzard, S. and Whittaker, G. R. (2009) 'Characterization of a highly conserved domain within the severe acute respiratory syndrome coronavirus spike protein S2 domain with characteristics of a viral fusion peptide', *J Virol*, 83(15), pp. 7411-21.

Mahboob, T., Ismail, A. A., Shah, M. R., Rahmatullah, M., Paul, A. K., Pereira, M. L., Wiart, C., Wilairatana, P., Rajagopal, M., Dolma, K. G. and Nissapatorn, V. (2023) 'Development of SARS-CoV-2 Vaccine: Challenges and Prospects', *Diseases*, 11(2).

Mahmood, N. and Xie, J. (2015) 'An endogenous 'non-specific' protein detected by a His-tag antibody is human transcription regulator YY1', *Data Brief*, 2, pp. 52-5.

Malloy, A. (2012) 'Exosome and Microvesicle Characterization', *Genetic Engineering & Biotechnology News*, 32(7), pp. 34-35.

Manahan, M., Nelson, M., Cacciatore, J. J., Weng, J., Xu, S. and Pollard, J. (2019) 'Scale-down model qualification of ambr[®] 250 high-throughput mini-bioreactor system for two commercial-scale mAb processes', *Biotechnol Prog*, 35(6), pp. e2870.

Marichal-Gallardo, P. A. and Alvarez, M. M. (2012) 'State-of-the-art in downstream processing of monoclonal antibodies: process trends in design and validation', *Biotechnol Prog*, 28(4), pp. 899-916.

Marx, N., Eisenhut, P., Weinguny, M., Klanert, G. and Borth, N. (2022) 'How to train your cell - Towards controlling phenotypes by harnessing the epigenome of Chinese hamster ovary production cell lines', *Biotechnol Adv*, 56, pp. 107924.

Mashouri, L., Yousefi, H., Aref, A. R., Ahadi, A. M., Molaei, F. and Alahari, S. K. (2019) 'Exosomes: composition, biogenesis, and mechanisms in cancer metastasis and drug resistance', *Mol Cancer*, 18(1), pp. 75.

Mason, M., Sweeney, B., Cain, K., Stephens, P. and Sharfstein, S. T. (2014) 'Reduced Culture Temperature Differentially Affects Expression and Biophysical Properties of Monoclonal Antibody Variants', *Antibodies (Basel)*, 3(3), pp. 253-271.

Mathias, S., Fischer, S., Handrick, R., Fieder, J., Schulz, P., Bradl, H., Gorr, I., Gamer, M. and Otte, K. (2018) 'Visualisation of intracellular production bottlenecks in suspension-adapted CHO cells producing complex biopharmaceuticals using fluorescence microscopy', *J Biotechnol*, 271, pp. 47-55.

Mathias, S., Wippermann, A., Raab, N., Zeh, N., Handrick, R., Gorr, I., Schulz, P., Fischer, S., Gamer, M. and Otte, K. (2020) 'Unraveling what makes a monoclonal antibody difficult-to-express: From intracellular accumulation to incomplete folding and degradation via ERAD', *Biotechnol Bioeng*, 117(1), pp. 5-16.

Mathieu, M., Martin-Jaular, L., Lavie, G. and Thery, C. (2019) 'Specificities of secretion and uptake of exosomes and other extracellular vesicles for cell-to-cell communication', *Nature Cell Biology*, 21(1), pp. 9-17.

Mathivanan, S. and Simpson, R. J. (2009) 'ExoCarta: A compendium of exosomal proteins and RNA', *Proteomics*, 9(21), pp. 4997-5000.

McHugh, K. P., Xu, J., Aron, K. L., Borys, M. C. and Li, Z. J. (2020) 'Effective temperature shift strategy development and scale confirmation for simultaneous optimization of protein productivity and quality in Chinese hamster ovary cells', *Biotechnol Prog*, 36(3), pp. e2959.

Meyer, C., Losacco, J., Stickney, Z., Li, L., Marriott, G. and Lu, B. (2017) 'Pseudotyping exosomes for enhanced protein delivery in mammalian cells', *Int J Nanomedicine*, 12, pp. 3153-3170.

Mohsen, M. O., Zha, L., Cabral-Miranda, G. and Bachmann, M. F. (2017) 'Major findings and recent advances in virus-like particle (VLP)-based vaccines', *Semin Immunol*, 34, pp. 123-132.

Momen-Heravi, F., Balaj, L., Alian, S., Tigges, J., Toxavidis, V., Ericsson, M., Distel, R. J., Ivanov, A. R., Skog, J. and Kuo, W. P. (2012) 'Alternative methods for characterization of extracellular vesicles', *Frontiers in Physiology*, 3.

Montaner-Tarbes, S., Borrás, F. E., Montoya, M., Fraile, L. and del Portillo, H. A. (2016) 'Serum-derived exosomes from non-viremic animals previously exposed to the porcine respiratory and reproductive virus contain antigenic viral proteins', *Veterinary Research*, 47.

Montecalvo, A., Larregina, A. T., Shufesky, W. J., Stolz, D. B., Sullivan, M. L. G., Karlsson, J. M., Baty, C. J., Gibson, G. A., Erdos, G., Wang, Z. L., Milosevic, J., Tkacheva, O. A., Divito, S. J., Jordan, R., Lyons-Weiler, J., Watkins, S. C. and Morelli, A. E. (2012) 'Mechanism of transfer of functional microRNAs between mouse dendritic cells via exosomes', *Blood*, 119(3), pp. 756-766.

Montecalvo, A., Shufesky, W. J., Stolz, D. B., Sullivan, M. G., Wang, Z. L., Divito, S. J., Papworth, G. D., Watkins, S. C., Robbins, P. D., Larregina, A. T. and Morelli, A. E. (2008) 'Exosomes as a short-range mechanism to spread alloantigen between dendritic cells during T cell allorecognition', *Journal of Immunology*, 180(5), pp. 3081-3090.

Moreira, E. D., Jr., Kitchin, N., Xu, X., Dychter, S. S., Lockhart, S., Gurtman, A., Perez, J. L., Zerbini, C., Dever, M. E., Jennings, T. W., Brandon, D. M., Cannon, K. D., Koren, M. J., Denham, D. S., Berhe, M., Fitz-Patrick, D., Hammitt, L. L., Klein, N. P., Nell, H., Keep, G., Wang, X., Koury, K., Swanson, K. A., Cooper, D., Lu, C., Türeci, Ö., Lagkadinou, E., Tresnan, D. B., Dormitzer, P. R., Şahin, U., Gruber, W. C. and Jansen, K. U. (2022) 'Safety and Efficacy of a Third Dose of BNT162b2 Covid-19 Vaccine', *N Engl J Med*, 386(20), pp. 1910-1921.

Morse, M. A., Garst, J., Osada, T., Khan, S., Hobeika, A., Clay, T. M., Valente, N., Shreeniwas, R., Sutton, M. A., Delcayre, A., Hsu, D. H., Le Pecq, J. B. and Lyerly, H. K. (2005) 'A phase I study of dexosome immunotherapy in patients with advanced non-small cell lung cancer', *Journal of Translational Medicine*, 3.

Nagano, R. and Masuda, K. (2014) 'Establishment of a signal peptide with cross-species compatibility for functional antibody expression in both *Escherichia coli* and Chinese hamster ovary cells', *Biochem Biophys Res Commun*, 447(4), pp. 655-9.

Nagasaki, A., S, T. K., Yumoto, T., Imaizumi, M., Yamagishi, A., Kim, H., Nakamura, C. and T, Q. P. U. (2017) 'The Position of the GFP Tag on Actin Affects the Filament Formation in Mammalian Cells', *Cell Struct Funct*, 42(2), pp. 131-140.

Nanaware, N., Banerjee, A., Mullick Bagchi, S., Bagchi, P. and Mukherjee, A. (2021) 'Dengue Virus Infection: A Tale of Viral Exploitations and Host Responses', *Viruses*, 13(10).

Nathanson, N. and Langmuir, A. D. (1963) 'THE CUTTER INCIDENT. POLIOMYELITIS FOLLOWING FORMALDEHYDE- INACTIVATED POLIOVIRUS VACCINATION IN THE UNITED STATES DURING THE SPRING OF 1955. I. BACKGROUND', *Am J Hyg*, 78, pp. 16-28.

Nguyen, D. G., Booth, A., Gould, S. J. and Hildreth, J. E. (2003) 'Evidence that HIV budding in primary macrophages occurs through the exosome release pathway', *J Biol Chem*, 278(52), pp. 52347-54.

Nguyen, L. N., Baumann, M., Dhiman, H., Marx, N., Schmieder, V., Hussein, M., Eisenhut, P., Hernandez, I., Koehn, J. and Borth, N. (2019) 'Novel Promoters Derived from Chinese Hamster Ovary Cells via In Silico and In Vitro Analysis', *Biotechnol J*, 14(11), pp. e1900125.

Nguyen, L. N., Novak, N., Baumann, M., Koehn, J. and Borth, N. (2020) 'Bioinformatic Identification of Chinese Hamster Ovary (CHO) Cold-Shock Genes and Biological Evidence of their Cold-Inducible Promoters', *Biotechnol J*, 15(3), pp. e1900359.

Nichols, P., Li, L., Kumar, S., Buck, P. M., Singh, S. K., Goswami, S., Balthazor, B., Conley, T. R., Sek, D. and Allen, M. J. (2015) 'Rational design of viscosity reducing mutants of a monoclonal antibody: hydrophobic versus electrostatic inter-molecular interactions', *MAbs*, 7(1), pp. 212-30.

Obi, J. O., Gutiérrez-Barbosa, H., Chua, J. V. and Deredge, D. J. (2021) 'Current Trends and Limitations in Dengue Antiviral Research', *Trop Med Infect Dis*, 6(4).

Ohtake, F., Tsuchiya, H., Saeki, Y. and Tanaka, K. (2018) 'K63 ubiquitylation triggers proteasomal degradation by seeding branched ubiquitin chains', *Proc Natl Acad Sci U S A*, 115(7), pp. E1401-e1408.

Oosthuyzen, W., Sime, N. E. L., Ivy, J. R., Turtle, E. J., Street, J. M., Pound, J., Bath, L. E., Webb, D. J., Gregory, C. D., Bailey, M. A. and Dear, J. W. (2013) 'Quantification of human urinary exosomes by nanoparticle tracking analysis', *Journal of Physiology-London*, 591(23), pp. 5833-5842.

Osteikoetxea, X., Silva, A., Lázaro-Ibáñez, E., Salmond, N., Shatnyeva, O., Stein, J., Schick, J., Wren, S., Lindgren, J., Firth, M., Madsen, A., Mayr, L. M., Overman, R., Davies, R. and Dekker, N. (2022) 'Engineered Cas9 extracellular vesicles as a novel gene editing tool', *J Extracell Vesicles*, 11(5), pp. e12225.

Owji, H., Nezafat, N., Negahdaripour, M., Hajiebrahimi, A. and Ghasemi, Y. (2018) 'A comprehensive review of signal peptides: Structure, roles, and applications', *Eur J Cell Biol*, 97(6), pp. 422-441.

Pan, B. T. and Johnstone, R. M. (1983) 'Fate of the transferrin receptor during maturation of sheep reticulocytes in vitro: selective externalization of the receptor', *Cell*, 33(3), pp. 967-78.

Pardi, N., Hogan, M. J. and Weissman, D. (2020) 'Recent advances in mRNA vaccine technology', *Curr Opin Immunol*, 65, pp. 14-20.

Pardi, N., Tuyishime, S., Muramatsu, H., Kariko, K., Mui, B. L., Tam, Y. K., Madden, T. D., Hope, M. J. and Weissman, D. (2015) 'Expression kinetics of nucleoside-modified mRNA delivered in lipid nanoparticles to mice by various routes', *J Control Release*, 217, pp. 345-51.

Park, P. W. (2018) 'Isolation and functional analysis of syndecans', in Mechem, R.P. (ed.) *Methods in Extracellular Matrix Biology Methods in Cell Biology*. San Diego: Elsevier Academic Press Inc, pp. 317-333.

Parray, H. A., Shukla, S., Samal, S., Shrivastava, T., Ahmed, S., Sharma, C. and Kumar, R. (2020) 'Hybridoma technology a versatile method for isolation of monoclonal antibodies, its applicability across species, limitations, advancement and future perspectives', *Int Immunopharmacol*, 85, pp. 106639.

Patel, G. K., Khan, M. A., Zubair, H., Srivastava, S. K., Khushman, M., Singh, S. and Singh, A. P. (2019) 'Comparative analysis of exosome isolation methods using culture supernatant for optimum yield, purity and downstream applications', *Sci Rep*, 9(1), pp. 5335.

Patel, N. A., Anderson, C. R., Terkildsen, S. E., Davis, R. C., Pack, L. D., Bhargava, S. and Clarke, H. R. G. (2018) 'Antibody expression stability in CHO clonally derived cell lines and their subclones: Role of methylation in phenotypic and epigenetic heterogeneity', *Biotechnol Prog*, 34(3), pp. 635-649.

Patel, Y. D., Brown, A. J., Zhu, J., Rosignoli, G., Gibson, S. J., Hatton, D. and James, D. C. (2021) 'Control of Multigene Expression Stoichiometry in Mammalian Cells Using Synthetic Promoters', *ACS Synth Biol*, 10(5), pp. 1155-1165.

Pegtel, D. M., Cosmopoulos, K., Thorley-Lawson, D. A., van Eijndhoven, M. A. J., Hopmans, E. S., Lindenberg, J. L., de Gruijl, T. D., Wurdinger, T. and Middeldorp, J. M. (2010) 'Functional delivery of viral miRNAs via exosomes', *Proceedings of the National Academy of Sciences of the United States of America*, 107(14), pp. 6328-6333.

Pegtel, D. M. and Gould, S. J. (2019) 'Exosomes', *Annu Rev Biochem*, 88, pp. 487-514.

Peng, L., Yu, X., Li, C., Cai, Y., Chen, Y., He, Y., Yang, J., Jin, J. and Li, H. (2016) 'Enhanced recombinant factor VII expression in Chinese hamster ovary cells by optimizing signal peptides and fed-batch medium', *Bioengineered*, 7(3), pp. 189-97.

Perez-Hernandez, D., Gutierrez-Vazquez, C., Jorge, I., Lopez-Martin, S., Ursa, A., Sanchez-Madrid, F., Vazquez, J. and Yanez-Mo, M. (2013) 'The Intracellular Interactome of Tetraspanin-enriched Microdomains Reveals Their Function as Sorting Machineries toward Exosomes', *Journal of Biological Chemistry*, 288(17), pp. 11649-11661.

Pettit, D. K., Rogers, R. S., Arthur, K., Brodsky, Y., Clark, R. H., Crowell, C., Ennis, J., Gillespie, A., Gillespie, R., Livingston, B., Nalbandian, E., Pace, D., Smidt, P., Pauly, M., Timmons, K., Trentalange, M., Whaley, K. J., Zeitlin, L. and Thomas, J. N. (2016) 'CHO cell production and sequence improvement in the 13C6FR1 anti-Ebola antibody', *MAbs*, 8(2), pp. 347-57.

Pilbrough, W., Munro, T. P. and Gray, P. (2009) 'Intraclonal protein expression heterogeneity in recombinant CHO cells', *PLoS One*, 4(12), pp. e8432.

Pintado Silva, J. and Fernandez-Sesma, A. (2023) 'Challenges on the development of a dengue vaccine: a comprehensive review of the state of the art', *J Gen Virol*, 104(3).

Plotkin, S. (2014) 'History of vaccination', *Proc Natl Acad Sci USA*, 111(34), pp. 12283-7.

Podda, A., De Luca, E. C., Contu, B., Furlan, R., Maida, A., Moiraghi, A., Stramare, D., Titone, L., Uxa, F., Di Pisa, F., Peppoloni, S. and et al. (1994) 'Comparative study of a whole-cell pertussis vaccine and a recombinant acellular pertussis vaccine. The Italian Multicenter Group for the Study of Recombinant Acellular Pertussis Vaccine', *J Pediatr*, 124(6), pp. 921-6.

Polack, F. P., Thomas, S. J., Kitchin, N., Absalon, J., Gurtman, A., Lockhart, S., Perez, J. L., Pérez Marc, G., Moreira, E. D., Zerbini, C., Bailey, R., Swanson, K. A., Roychoudhury, S., Koury, K., Li, P., Kalina, W. V., Cooper, D., Frenck, R. W., Jr., Hammitt, L. L., Türeci, Ö., Nell, H., Schaefer, A., Ünal, S., Tresnan, D. B., Mather, S., Dormitzer, P. R., Şahin, U., Jansen, K. U. and Gruber, W. C. (2020) 'Safety and Efficacy of the BNT162b2 mRNA Covid-19 Vaccine', *N Engl J Med*, 383(27), pp. 2603-2615.

Pollard, A. J. and Bijker, E. M. (2021) 'A guide to vaccinology: from basic principles to new developments', *Nat Rev Immunol*, 21(2), pp. 83-100.

Porter, A. J., Racher, A. J., Preziosi, R. and Dickson, A. J. (2010) 'Strategies for selecting recombinant CHO cell lines for cGMP manufacturing: improving the efficiency of cell line generation', *Biotechnol Prog*, 26(5), pp. 1455-64.

Priola, J. J., Calzadilla, N., Baumann, M., Borth, N., Tate, C. G. and Betenbaugh, M. J. (2016) 'High-throughput screening and selection of mammalian cells for enhanced protein production', *Biotechnol J*, 11(7), pp. 853-65.

Qian, C., Liu, X., Xu, Q., Wang, Z., Chen, J., Li, T., Zheng, Q., Yu, H., Gu, Y., Li, S. and Xia, N. (2020) 'Recent Progress on the Versatility of Virus-Like Particles', *Vaccines (Basel)*, 8(1).

Qian, S. B., Ott, D. E., Schubert, U., Bennink, J. R. and Yewdell, J. W. (2002) 'Fusion proteins with COOH-terminal ubiquitin are stable and maintain dual functionality in vivo', *J Biol Chem*, 277(41), pp. 38818-26.

Raab, N., Mathias, S., Alt, K., Handrick, R., Fischer, S., Schmieder, V., Jadhav, V., Borth, N. and Otte, K. (2019) 'CRISPR/Cas9-Mediated Knockout of MicroRNA-744 Improves Antibody Titer of CHO Production Cell Lines', *Biotechnol J*, 14(5), pp. e1800477.

Rajan, A., Kim, C., Heery, C. R., Guha, U. and Gulley, J. L. (2016) 'Nivolumab, anti-programmed death-1 (PD-1) monoclonal antibody immunotherapy: Role in advanced cancers', *Hum Vaccin Immunother*, 12(9), pp. 2219-31.

Ramadhany, R., Hirai, I., Sasaki, T., Ono, K., Ramasoota, P., Ikuta, K. and Kurosu, T. (2015) 'Antibody with an engineered Fc region as a therapeutic agent against dengue virus infection', *Antiviral Res*, 124, pp. 61-8.

Ramezani, A., Mahmoudi Maymand, E., Yazdanpanah-Samani, M., Hosseini, A., Toghraie, F. S. and Ghaderi, A. (2017) 'Improving Pertuzumab production by gene optimization and proper signal peptide selection', *Protein Expr Purif*, 135, pp. 24-32.

Reinhart, D., Damjanovic, L., Kaisermayer, C., Sommeregger, W., Gili, A., Gasselhuber, B., Castan, A., Mayrhofer, P., Grünwald-Gruber, C. and Kunert, R. (2019) 'Bioprocessing of Recombinant CHO-K1, CHO-DG44, and CHO-S: CHO Expression Hosts Favor Either mAb Production or Biomass Synthesis', *Biotechnol J*, 14(3), pp. e1700686.

Robertson, D. (1998) 'Genentech's anticancer Mab expected by November', *Nat Biotechnol*, 16(7), pp. 615.

Rodrigues, M., Fan, J., Lyon, C., Wan, M. H. and Hu, Y. (2018) 'Role of Extracellular Vesicles in Viral and Bacterial Infections: Pathogenesis, Diagnostics, and Therapeutics', *Theranostics*, 8(10), pp. 2709-2721.

Romanova, N. and Noll, T. (2018) 'Engineered and Natural Promoters and Chromatin-Modifying Elements for Recombinant Protein Expression in CHO Cells', *Biotechnol J*, 13(3), pp. e1700232.

Roucourt, B., Meeussen, S., Bao, J., Zimmermann, P. and David, G. (2015) 'Heparanase activates the syndecan-syntenin-ALIX exosome pathway', *Cell Research*, 25(4), pp. 412-428.

Roy, S. K. and Bhattacharjee, S. (2021) 'Dengue virus: epidemiology, biology, and disease aetiology', *Can J Microbiol*, 67(10), pp. 687-702.

Rugo, H. S., Pennella, E. J., Gopalakrishnan, U., Hernandez-Bronchud, M., Herson, J., Koch, H. F., Loganathan, S., Deodhar, S., Marwah, A., Manikhas, A., Bondarenko, I., Mukhametshina, G., Nemsadze, G., Parra, J. D., Abesamis-Tiambeng, M. L. T.,

Baramidze, K., Akewanlop, C., Vynnychenko, I., Sriuranpong, V., Mamillapalli, G., Roy, S., Yanez Ruiz, E. P., Barve, A., Fuentes-Albuero, A. and Waller, C. F. (2021) 'Final overall survival analysis of the phase 3 HERITAGE study demonstrates equivalence of trastuzumab-dkst to trastuzumab in HER2-positive metastatic breast cancer', *Breast Cancer Res Treat*, 188(2), pp. 369-377.

Salzberger, B., Buder, F., Lampl, B., Ehrenstein, B., Hitzenbichler, F., Holzmann, T., Schmidt, B. and Hanses, F. (2021) 'Epidemiology of SARS-CoV-2', *Infection*, 49(2), pp. 233-239.

Sandner, V., Pybus, L. P., McCreath, G. and Glassey, J. (2019) 'Scale-Down Model Development in ambr systems: An Industrial Perspective', *Biotechnol J*, 14(4), pp. e1700766.

Santos, J. C., Lima, N. D., Sarian, L. O., Matheu, A., Ribeiro, M. L. and Derchain, S. F. M. (2018) 'Exosome-mediated breast cancer chemoresistance via miR-155 transfer', *Scientific Reports*, 8.

Saunders, F., Sweeney, B., Antoniou, M. N., Stephens, P. and Cain, K. (2015) 'Chromatin function modifying elements in an industrial antibody production platform--comparison of UCOE, MAR, STAR and cHS4 elements', *PLoS One*, 10(4), pp. e0120096.

Schlatter, S., Stansfield, S. H., Dinnis, D. M., Racher, A. J., Birch, J. R. and James, D. C. (2005) 'On the optimal ratio of heavy to light chain genes for efficient recombinant antibody production by CHO cells', *Biotechnol Prog*, 21(1), pp. 122-33.

Setthapramote, C., Sasaki, T., Puiprom, O., Limkittikul, K., Pitaksajjakul, P., Pipattanaboon, C., Sasayama, M., Leuangwutiwong, P., Phumratanaprapin, W., Chamnachanan, S., Kusolsuk, T., Jittmittraphap, A., Asai, A., Arias, J. F., Hirai, I., Kuhara, M., Okuno, Y., Kurosu, T., Ramasoota, P. and Ikuta, K. (2012) 'Human monoclonal antibodies to neutralize all dengue virus serotypes using lymphocytes from patients at acute phase of the secondary infection', *Biochem Biophys Res Commun*, 423(4), pp. 867-72.

Seyfizadeh, N., Borzouisileh, S., Elahimanesh, F., Hosseini, V. and Nouri, M. (2019) 'Exosome-mediated therapeutic delivery: A new horizon for human neurodegenerative disorders' treatment (with a focus on siRNA delivery improvement)', *Process Biochemistry*, 85, pp. 164-174.

Shenoda, B. B. and Ajit, S. K. (2016) 'Modulation of Immune Responses by Exosomes Derived from Antigen-Presenting Cells', *Clinical Medicine Insights- Pathology*, 9, pp. 1-8.

Shimbo, K., Miyaki, S., Ishitobi, H., Kato, Y., Kubo, T., Shimose, S. and Ochi, M. (2014) 'Exosome-formed synthetic microRNA-143 is transferred to osteosarcoma cells and inhibits their migration', *Biochemical and Biophysical Research Communications*, 445(2), pp. 381-387.

Shukla, R., Ramasamy, V., Shanmugam, R. K., Ahuja, R. and Khanna, N. (2020) 'Antibody-Dependent Enhancement: A Challenge for Developing a Safe Dengue Vaccine', *Front Cell Infect Microbiol*, 10, pp. 572681.

Silva, A. M., Lázaro-Ibáñez, E., Gunnarsson, A., Dhande, A., Daaboul, G., Peacock, B., Osteikoetxea, X., Salmond, N., Friis, K. P., Shatnyeva, O. and Dekker, N. (2021) 'Quantification of protein cargo loading into engineered extracellular vesicles at single-vesicle and single-molecule resolution', *J Extracell Vesicles*, 10(10), pp. e12130.

Sitar, S., Kejzar, A., Pahovnik, D., Kogej, K., Tusek-Znidaric, M., Lenassi, M. and Zagar, E. (2015) 'Size Characterization and Quantification of Exosomes by Asymmetrical-Flow Field-Flow Fractionation', *Analytical Chemistry*, 87(18), pp. 9225-9233.

Skrika-Alexopoulos, E. and Smales, C. M. (2023) 'Isolation and characterisation of exosomes from Chinese hamster ovary (CHO) cells', *Biotechnol Lett*, 45(4), pp. 425-437.

Skryabin, G. O., Komelkov, A. V., Savelyeva, E. E. and Tchevkina, E. M. (2020) 'Lipid Rafts in Exosome Biogenesis', *Biochemistry (Mosc)*, 85(2), pp. 177-191.

Smith, G. P. (1985) 'Filamentous fusion phage: novel expression vectors that display cloned antigens on the virion surface', *Science*, 228(4705), pp. 1315-7.

Smith, S. A., de Alwis, A. R., Kose, N., Jadi, R. S., de Silva, A. M. and Crowe, J. E., Jr. (2014) 'Isolation of dengue virus-specific memory B cells with live virus antigen from human subjects following natural infection reveals the presence of diverse novel functional groups of antibody clones', *J Virol*, 88(21), pp. 12233-41.

Sobieszczyk, M. E., Maaske, J., Falsey, A. R., Sproule, S., Robb, M. L., Frenck, R. W., Jr., Tieu, H. V., Mayer, K. H., Corey, L., Neuzil, K. M., Tong, T., Brewinski Isaacs, M., Janes, H., Bansal, H., Edwards, L. M., Green, J. A., Kelly, E. J., Shoemaker, K., Takas, T., White, T., Bhuyan, P., Villafana, T. and Hirsch, A. I. (2022) 'Durability of protection and immunogenicity of AZD1222 (ChAdOx1 nCoV-19) COVID-19 vaccine over 6 months', *J Clin Invest*, 132(18).

Sootichote, R., Puangmanee, W., Benjathummarak, S., Kowaboot, S., Yamanaka, A., Boonnak, K., Ampawong, S., Chatchen, S., Ramasoota, P. and Pitaksajjakul, P. (2023) 'Potential Protective Effect of Dengue NS1 Human Monoclonal Antibodies against Dengue and Zika Virus Infections', *Biomedicines*, 11(1).

Srila, W., Baumann, M., Borth, N. and Yamabhai, M. (2022) 'Codon and signal peptide optimization for therapeutic antibody production from Chinese hamster ovary (CHO) cell', *Biochem Biophys Res Commun*, 622, pp. 157-162.

Steć, A., Targońska, M., Karkosińska, E., Słowik, M., Płoska, A., Kalinowski, L., Wielgomas, B., Waleron, K., Jasiński, J. and Dziomba, S. (2023) 'Protein overproduction alters exosome secretion in Chinese hamster ovary cells', *Anal Bioanal Chem*.

Stickney, Z., Losacco, J., McDevitt, S., Zhang, Z. and Lu, B. (2016) 'Development of exosome surface display technology in living human cells', *Biochem Biophys Res Commun*, 472(1), pp. 53-9.

Synoground, B. F., McGraw, C. E., Elliott, K. S., Leuze, C., Roth, J. R., Harcum, S. W. and Sandoval, N. R. (2021) 'Transient ammonia stress on Chinese hamster ovary (CHO) cells yield alterations to alanine metabolism and IgG glycosylation profiles', *Biotechnol J*, 16(7), pp. e2100098.

Takahashi, A., Okada, R., Nagao, K., Kawamata, Y., Hanyu, A., Yoshimoto, S., Takasugi, M., Watanabe, S., Kanemaki, M. T., Obuse, C. and Hara, E. (2017) 'Exosomes maintain cellular homeostasis by excreting harmful DNA from cells', *Nature Communications*, 8.

Tejwani, V., Chaudhari, M., Rai, T. and Sharfstein, S. T. (2021) 'High-throughput and automation advances for accelerating single-cell cloning, monoclonality and early phase clone screening steps in mammalian cell line development for biologics production', *Biotechnol Prog*, 37(6), pp. e3208.

Thacker, E. L., Holtkamp, D. J., Khan, A. S., Brown, P. A. and Draghia-Akli, R. (2006) 'Plasmid-mediated growth hormone-releasing hormone efficacy in reducing disease associated with *Mycoplasma hyopneumoniae* and porcine reproductive and respiratory syndrome virus infection', *J Anim Sci*, 84(3), pp. 733-42.

They, C., Ostrowski, M. and Segura, E. (2009) 'Membrane vesicles as conveyors of immune responses', *Nature Reviews Immunology*, 9(8), pp. 581-593.

Thomas, S. J., Moreira, E. D., Jr., Kitchin, N., Absalon, J., Gurtman, A., Lockhart, S., Perez, J. L., Pérez Marc, G., Polack, F. P., Zerbini, C., Bailey, R., Swanson, K. A., Xu, X., Roychoudhury, S., Koury, K., Bouguermouh, S., Kalina, W. V., Cooper, D., Frenck, R. W., Jr., Hammitt, L. L., Türeci, Ö., Nell, H., Schaefer, A., Ünal, S., Yang, Q., Liberator, P., Tresnan, D. B., Mather, S., Dormitzer, P. R., Şahin, U., Gruber, W. C. and Jansen, K. U. (2021) 'Safety and Efficacy of the BNT162b2 mRNA Covid-19 Vaccine through 6 Months', *N Engl J Med*, 385(19), pp. 1761-1773.

Théry, C. and Witwer, K. W. and Aikawa, E. and Alcaraz, M. J. and Anderson, J. D. and Andriantsitohaina, R. and Antoniou, A. and Arab, T. and Archer, F. and Atkin-Smith, G. K. and Ayre, D. C. and Bach, J. M. and Bachurski, D. and Baharvand, H. and Balaj, L. and Baldacchino, S. and Bauer, N. N. and Baxter, A. A. and Bebawy, M. and Beckham, C. and Bedina Zavec, A. and Benmoussa, A. and Berardi, A. C. and Bergese, P. and Bielska, E. and Blenkiron, C. and Bobis-Wozowicz, S. and Boilard, E. and Boireau, W. and Bongiovanni, A. and Borràs, F. E. and Bosch, S. and Boulanger, C. M. and Breakefield, X. and Breglio, A. M. and Brennan, M. and Brigstock, D. R. and Brisson, A. and Broekman, M. L. and Bromberg, J. F. and Bryl-Górecka, P. and Buch, S. and Buck, A. H. and Burger, D. and Busatto, S. and Buschmann, D. and Bussolati, B. and Buzás, E. I. and Byrd, J. B. and Camussi, G. and Carter, D. R. and Caruso, S. and Chamley, L. W. and Chang, Y. T. and Chen, C. and Chen, S. and Cheng, L. and Chin, A. R. and Clayton, A. and Clerici, S. P. and Cocks, A. and Cocucci, E. and Coffey, R. J. and Cordeiro-da-Silva, A. and Couch, Y. and Coumans, F. A. and Coyle, B. and Crescitelli, R. and Criado, M. F. and D'Souza-Schorey, C. and Das, S. and Datta Chaudhuri, A. and de Candia, P. and De Santana, E. F. and De Wever, O. and Del Portillo, H. A. and Demaret, T. and Deville, S. and Devitt, A. and Dhondt, B. and Di Vizio, D. and Dieterich, L. C. and Dolo, V. and Dominguez Rubio, A. P. and Dominici, M. and Dourado, M. R. and Driedonks, T. A. and Duarte, F. V. and Duncan, H. M. and Eichenberger, R. M. and Ekström, K. and El Andaloussi, S. and Elie-Caille, C. and Erdbrügger, U. and Falcón-Pérez, J. M. and Fatima, F. and Fish, J. E. and Flores-Bellver, M. and Försonits, A. and Frelet-Barrand, A. and Fricke, F. and Fuhrmann, G. and Gabrielsson, S. and Gámez-Valero, A. and Gardiner, C. and Gärtner, K. and Gaudin, R. and Gho, Y. S. and Giebel, B. and Gilbert, C. and Gimona, M. and Giusti, I. and Goberdhan, D. C. and Görgens, A. and Gorski, S. M. and Greening, D. W. and Gross, J. C. and Gualerzi, A. and Gupta, G. N. and Gustafson, D. and Handberg, A. and Haraszti, R. A. and Harrison, P. and Hegyesi, H. and Hendrix, A. and Hill, A. F. and Hochberg, F. H. and Hoffmann, K. F. and Holder, B. and Holthofer, H. and Hosseinkhani, B. and Hu, G. and Huang, Y. and Huber, V. and Hunt, S. and Ibrahim, A. G. and Ikezu, T. and Inal, J. M. and Isin, M. and Ivanova, A. and Jackson, H. K. and Jacobsen, S. and Jay, S. M. and Jayachandran, M. and Jenster, G. and Jiang, L. and Johnson, S. M. and Jones, J. C. and Jong, A. and Jovanovic-Taliman, T. and Jung, S. and Kalluri, R. and Kano, S. I. and Kaur, S. and Kawamura, Y. and Keller, E. T. and Khamari, D. and Khomyakova, E. and Khvorova, A. and Kierulf, P. and Kim, K. P. and

Kislinger, T. and Klingeborn, M. and Klinke, D. J., 2nd and Kornek, M. and Kosanović, M. M. and Kovács Á, F. and Krämer-Albers, E. M. and Krasemann, S. and Krause, M. and Kurochkin, I. V. and Kusuma, G. D. and Kuypers, S. and Laitinen, S. and Langevin, S. M. and Languino, L. R. and Lannigan, J. and Lässer, C. and Laurent, L. C. and Lavieu, G. and Lázaro-Ibáñez, E. and Le Lay, S. and Lee, M. S. and Lee, Y. X. F. and Lemos, D. S. and Lenassi, M. and Leszczynska, A. and Li, I. T. and Liao, K. and Libregts, S. F. and Ligeti, E. and Lim, R. and Lim, S. K. and Linē, A. and Linnemannstöns, K. and Llorente, A. and Lombard, C. A. and Lorenowicz, M. J. and Lörincz Á, M. and Lötval, J. and Lovett, J. and Lowry, M. C. and Loyer, X. and Lu, Q. and Lukomska, B. and Lunavat, T. R. and Maas, S. L. and Malhi, H. and Marcilla, A. and Mariani, J. and Mariscal, J. and Martens-Uzunova, E. S. and Martin-Jaular, L. and Martinez, M. C. and Martins, V. R. and Mathieu, M. and Mathivanan, S. and Maugeri, M. and McGinnis, L. K. and McVey, M. J. and Meckes, D. G., Jr. and Meehan, K. L. and Mertens, I. and Minciocchi, V. R. and Möller, A. and Møller Jørgensen, M. and Morales-Kastresana, A. and Morhayim, J. and Mullier, F. and Muraca, M. and Musante, L. and Mussack, V. and Muth, D. C. and Myburgh, K. H. and Najrana, T. and Nawaz, M. and Nazarenko, I. and Nejsun, P. and Neri, C. and Neri, T. and Nieuwland, R. and Nimrichter, L. and Nolan, J. P. and Nolte-'t Hoen, E. N. and Noren Hooten, N. and O'Driscoll, L. and O'Grady, T. and O'Loghlen, A. and Ochiya, T. and Olivier, M. and Ortiz, A. and Ortiz, L. A. and Osteikoetxea, X. and Østergaard, O. and Ostrowski, M. and Park, J. and Pegtel, D. M. and Peinado, H. and Perut, F. and Pfaffl, M. W. and Phinney, D. G. and Pieters, B. C. and Pink, R. C. and Pisetsky, D. S. and Pogge von Strandmann, E. and Polakovicova, I. and Poon, I. K. and Powell, B. H. and Prada, I. and Pulliam, L. and Quesenberry, P. and Radeghieri, A. and Raffai, R. L. and Raimondo, S. and Rak, J. and Ramirez, M. I. and Raposo, G. and Rayyan, M. S. and Regev-Rudzki, N. and Ricklefs, F. L. and Robbins, P. D. and Roberts, D. D. and Rodrigues, S. C. and Rohde, E. and Rome, S. and Rouschop, K. M. and Rughetti, A. and Russell, A. E. and Saá, P. and Sahoo, S. and Salas-Huenuleo, E. and Sánchez, C. and Saugstad, J. A. and Saul, M. J. and Schiffelers, R. M. and Schneider, R. and Schøyen, T. H. and Scott, A. and Shahaj, E. and Sharma, S. and Shatnyeva, O. and Shekari, F. and Shelke, G. V. and Shetty, A. K. and Shiba, K. and Siljander, P. R. and Silva, A. M. and Skowronek, A. and Snyder, O. L., 2nd and Soares, R. P. and Sódar, B. W. and Soekmadji, C. and Sotillo, J. and Stahl, P. D. and Stoorvogel, W. and Stott, S. L. and Strasser, E. F. and Swift, S. and Tahara, H. and Tewari, M. and Timms, K. and Tiwari, S. and Tixeira, R. and Tkach, M. and Toh, W. S. and Tomasini, R. and Torrecilhas, A. C. and Tosar, J. P. and Toxavidis, V. and Urbanelli, L. and Vader, P. and van Balkom, B. W. and van der Grein, S. G. and Van Deun, J. and van Herwijnen, M. J. and Van Keuren-Jensen, K. and van Niel, G. and van Royen, M. E. and van Wijnen, A. J. and Vasconcelos, M. H. and Vechetti, I. J., Jr. and Veit, T. D. and Vella, L. J. and Velot, É. and Verweij, F. J. and Vestad, B. and Viñas, J. L. and Visnovitz, T. and Vukman, K. V. and Wahlgren, J. and Watson, D. C. and Wauben, M. H. and Weaver, A. and Webber, J. P. and Weber, V. and Wehman, A. M. and Weiss, D. J. and Welsh, J. A. and Wendt, S. and Wheelock, A. M. and Wiener, Z. and Witte, L. and Wolfram, J. and Xagorari, A. and Xander, P. and Xu, J. and Yan, X. and Yáñez-Mó, M. and Yin, H. and Yuana, Y. and Zappulli, V. and Zarubova, J. and Žekas, V. and Zhang, J. Y. and Zhao, Z. and Zheng, L. and Zheutlin, A. R. and Zickler, A. M. and Zimmermann, P. and Zivkovic, A. M. and Zocco, D. and Zuba-Surma, E. K. (2018) 'Minimal information for studies of extracellular vesicles 2018 (MISEV2018): a position statement of the

International Society for Extracellular Vesicles and update of the MISEV2014 guidelines', *J Extracell Vesicles*, 7(1), pp. 1535750.

Torres, M., Akhtar, S., McKenzie, E. A. and Dickson, A. J. (2021) 'Temperature Down-Shift Modifies Expression of UPR-/ERAD-Related Genes and Enhances Production of a Chimeric Fusion Protein in CHO Cells', *Biotechnol J*, 16(2), pp. e2000081.

Torres, M. and Dickson, A. J. (2021) 'Overexpression of transcription factor BLIMP1/prdm1 leads to growth inhibition and enhanced secretory capacity in Chinese hamster ovary cells', *Metab Eng*, 67, pp. 237-249.

Torres, M., Hussain, H. and Dickson, A. J. (2023) 'The secretory pathway - the key for unlocking the potential of Chinese hamster ovary cell factories for manufacturing therapeutic proteins', *Crit Rev Biotechnol*, 43(4), pp. 628-645.

Torres-Flores, J. M., Reyes-Sandoval, A. and Salazar, M. I. (2022) 'Dengue Vaccines: An Update', *BioDrugs*, 36(3), pp. 325-336.

Torres-Obreque, K. M., Meneguetti, G. P., Muso-Cachumba, J. J., Feitosa, V. A., Santos, J., Ventura, S. P. M. and Rangel-Yagui, C. O. (2021) 'Building better biobetters: From fundamentals to industrial application', *Drug Discov Today*.

Trajkovic, K., Hsu, C., Chiantia, S., Rajendran, L., Wenzel, D., Wieland, F., Schwille, P., Brügger, B. and Simons, M. (2008) 'Ceramide triggers budding of exosome vesicles into multivesicular endosomes', *Science*, 319(5867), pp. 1244-7.

Tsai, W. Y., Durbin, A., Tsai, J. J., Hsieh, S. C., Whitehead, S. and Wang, W. K. (2015) 'Complexity of Neutralizing Antibodies against Multiple Dengue Virus Serotypes after Heterotypic Immunization and Secondary Infection Revealed by In-Depth Analysis of Cross-Reactive Antibodies', *J Virol*, 89(14), pp. 7348-62.

Valadi, H., Ekstrom, K., Bossios, A., Sjostrand, M., Lee, J. J. and Lotvall, J. O. (2007) 'Exosome-mediated transfer of mRNAs and microRNAs is a novel mechanism of genetic exchange between cells', *Nature Cell Biology*, 9(6), pp. 654-U72.

van der Kant, R., Karow-Zwick, A. R., Van Durme, J., Blech, M., Gallardo, R., Seeliger, D., Aßfalg, K., Baatsen, P., Compennolle, G., Gils, A., Studts, J. M., Schulz, P., Garidel, P., Schymkowitz, J. and Rousseau, F. (2017) 'Prediction and Reduction of the Aggregation of Monoclonal Antibodies', *J Mol Biol*, 429(8), pp. 1244-1261.

van Niel, G., D'Angelo, G. and Raposo, G. (2018) 'Shedding light on the cell biology of extracellular vesicles', *Nat Rev Mol Cell Biol*, 19(4), pp. 213-228.

Veith, N., Ziehr, H., MacLeod, R. A. and Reamon-Buettner, S. M. (2016) 'Mechanisms underlying epigenetic and transcriptional heterogeneity in Chinese hamster ovary (CHO) cell lines', *BMC Biotechnol*, 16, pp. 6.

Velugula-Yellela, S. R., Kohnhorst, C., Powers, D. N., Trunfio, N., Faustino, A., Angart, P., Berilla, E., Faison, T. and Agarabi, C. (2018) 'Use of High-Throughput Automated Microbioreactor System for Production of Model IgG1 in CHO Cells', *J Vis Exp*, (139).

Vogel, R., Coumans, F. A., Maltesen, R. G., Böing, A. N., Bonnington, K. E., Broekman, M. L., Broom, M. F., Buzás, E. I., Christiansen, G., Hajji, N., Kristensen, S. R., Kuehn, M. J., Lund, S. M., Maas, S. L., Nieuwland, R., Osteikoetxea, X., Schnoor, R., Scicluna, B. J., Shambrook, M., de Vrij, J., Mann, S. I., Hill, A. F. and Pedersen, S. (2016) 'A standardized method to determine the concentration of extracellular vesicles using tunable resistive pulse sensing', *J Extracell Vesicles*, 5, pp. 31242.

Voysey, M., Clemens, S. A. C., Madhi, S. A., Weckx, L. Y., Folegatti, P. M., Aley, P. K., Angus, B., Baillie, V. L., Barnabas, S. L., Bhorat, Q. E., Bibi, S., Briner, C., Cicconi, P., Collins, A. M., Colin-Jones, R., Cutland, C. L., Darton, T. C., Dheda, K., Duncan, C. J. A.,

Emary, K. R. W., Ewer, K. J., Fairlie, L., Faust, S. N., Feng, S., Ferreira, D. M., Finn, A., Goodman, A. L., Green, C. M., Green, C. A., Heath, P. T., Hill, C., Hill, H., Hirsch, I., Hodgson, S. H. C., Izu, A., Jackson, S., Jenkin, D., Joe, C. C. D., Kerridge, S., Koen, A., Kwatra, G., Lazarus, R., Lawrie, A. M., Lelliott, A., Libri, V., Lillie, P. J., Mallory, R., Mendes, A. V. A., Milan, E. P., Minassian, A. M., McGregor, A., Morrison, H., Mujadidi, Y. F., Nana, A., O'Reilly, P. J., Padayachee, S. D., Pittella, A., Plested, E., Pollock, K. M., Ramasamy, M. N., Rhead, S., Schwarzbald, A. V., Singh, N., Smith, A., Song, R., Snape, M. D., Sprinz, E., Sutherland, R. K., Tarrant, R., Thomson, E. C., Török, M. E., Toshner, M., Turner, D. P. J., Vekemans, J., Villafana, T. L., Watson, M. E. E., Williams, C. J., Douglas, A. D., Hill, A. V. S., Lambe, T., Gilbert, S. C. and Pollard, A. J. (2021) 'Safety and efficacy of the ChAdOx1 nCoV-19 vaccine (AZD1222) against SARS-CoV-2: an interim analysis of four randomised controlled trials in Brazil, South Africa, and the UK', *Lancet*, 397(10269), pp. 99-111.

Walker, J. D., Maier, C. L. and Pober, J. S. (2009) 'Cytomegalovirus-Infected Human Endothelial Cells Can Stimulate Allogeneic CD4(+) Memory T Cells by Releasing Antigenic Exosomes', *Journal of Immunology*, 182(3), pp. 1548-1559.

Wang, J., Teng, Y., Zhao, G., Li, F., Hou, A., Sun, B., Kong, W., Gao, F., Cai, L. and Jiang, C. (2019) 'Exosome-Mediated Delivery of Inducible miR-423-5p Enhances Resistance of MRC-5 Cells to Rabies Virus Infection', *Int J Mol Sci*, 20(7).

Wang, J. J., Yao, Y. L., Chen, X. M., Wu, J. H., Gu, T. and Tang, X. (2018) 'Host derived exosomes-pathogens interactions: Potential functions of exosomes in pathogen infection', *Biomedicine & Pharmacotherapy*, 108, pp. 1451-1459.

WHO (2022) *Coronavirus Disease (COVID-19): Vaccines*. [https://www.who.int/news-room/questions-and-answers/item/coronavirus-disease-\(covid-19\)-vaccines](https://www.who.int/news-room/questions-and-answers/item/coronavirus-disease-(covid-19)-vaccines): World Health Organization. Available at: [https://www.who.int/news-room/questions-and-answers/item/coronavirus-disease-\(covid-19\)-vaccines](https://www.who.int/news-room/questions-and-answers/item/coronavirus-disease-(covid-19)-vaccines) (Accessed: 30th April 2023 2023).

WHO (2023) *Dengue and Severe Dengue*. <https://www.who.int/news-room/fact-sheets/detail/dengue-and-severe-dengue>: WHO. Available at: <https://www.who.int/news-room/fact-sheets/detail/dengue-and-severe-dengue> (Accessed: 23/04/23 2023).

Willis, G. R., Kourembanas, S. and Mitsialis, S. A. (2017) 'Toward Exosome-Based Therapeutics: Isolation, Heterogeneity, and Fit-for-Purpose Potency', *Frontiers in Cardiovascular Medicine*, 4.

Wohlenberg, O. J., Kortmann, C., Meyer, K. V., Schellenberg, J., Dahlmann, K., Bahnemann, J., Scheper, T. and Solle, D. (2022) 'Optimization of a mAb production process with regard to robustness and product quality using quality by design principles', *Eng Life Sci*, 22(7), pp. 484-494.

Wolf, P. (1967) 'The nature and significance of platelet products in human plasma', *Br J Haematol*, 13(3), pp. 269-88.

Wolfers, J., Lozier, A., Raposo, G., Regnault, A., Thery, C., Masurier, C., Flament, C., Pouzieux, S., Faure, F., Tursz, T., Angevin, E., Amigorena, S. and Zitvogel, L. (2001) 'Tumor-derived exosomes are a source of shared tumor rejection antigens for CTL cross-priming', *Nature Medicine*, 7(3), pp. 297-303.

Wrapp, D., Wang, N., Corbett, K. S., Goldsmith, J. A., Hsieh, C. L., Abiona, O., Graham, B. S. and McLellan, J. S. (2020) 'Cryo-EM structure of the 2019-nCoV spike in the prefusion conformation', *Science*, 367(6483), pp. 1260-1263.

Xu, Y., Wang, D., Mason, B., Rossomando, T., Li, N., Liu, D., Cheung, J. K., Xu, W., Raghava, S., Katiyar, A., Nowak, C., Xiang, T., Dong, D. D., Sun, J., Beck, A. and Liu, H. (2019) 'Structure, heterogeneity and developability assessment of therapeutic antibodies', *MABs*, 11(2), pp. 239-264.

Yanez-Mo, M., Siljander, P. R. M., Andreu, Z., Zavec, A. B., Borrás, F. E., Buzas, E. I., Buzas, K., Casal, E., Cappello, F., Carvalho, J., Colas, E., Cordeiro-da Silva, A., Fais, S., Falcon-Perez, J. M., Ghobrial, I. M., Giebel, B., Gimona, M., Graner, M., Gursel, I., Gursel, M., Heegaard, N. H. H., Hendrix, A., Kierulf, P., Kokubun, K., Kosanovic, M., Kralj-Iglic, V., Kramer-Albers, E. M., Laitinen, S., Lasser, C., Lener, T., Ligeti, E., Line, A., Lipps, G., Llorente, A., Lotvall, J., Mancek-Keber, M., Marcilla, A., Mittelbrunn, M., Nazarenko, I., Nolte-t' Hoen, E. N. M., Nyman, T. A., O'Driscoll, L., Olivan, M., Oliveira, C., Pallinger, E., del Portillo, H. A., Reventos, J., Rigau, M., Rohde, E., Sammar, M., Sanchez-Madrid, F., Santarem, N., Schallmoser, K., Ostendorf, M. S., Stoorvogel, W., Stukelj, R., Van der Grein, S. G., Vasconcelos, M. H., Wauben, M. H. M. and De Wever, O. (2015) 'Biological properties of extracellular vesicles and their physiological functions', *Journal of Extracellular Vesicles*, 4.

Yang, H. and Rao, Z. (2021) 'Structural biology of SARS-CoV-2 and implications for therapeutic development', *Nat Rev Microbiol*, 19(11), pp. 685-700.

Yang, Y., Hong, Y., Cho, Kim, G.B. & Kim, I. (2018) 'Extracellular vesicles as a platform for membrane-associated therapeutic protein delivery', *Journal of Extracellular Vesicles*, (1), pp. 1440131.

You, M., Yang, Y., Zhong, C., Chen, F., Wang, X., Jia, T., Chen, Y., Zhou, B., Mi, Q., Zhao, Q., An, Z., Luo, W. and Xia, N. (2018) 'Efficient mAb production in CHO cells with optimized signal peptide, codon, and UTR', *Appl Microbiol Biotechnol*, 102(14), pp. 5953-5964.

Yu, S., Zheng, X., Zhou, B., Li, J., Chen, M., Deng, R., Wong, G., Lavillette, D. and Meng, G. (2022) 'SARS-CoV-2 spike engagement of ACE2 primes S2' site cleavage and fusion initiation', *Proc Natl Acad Sci U S A*, 119(1).

Zarovni, N., Corrado, A., Guazzi, P., Zocco, D., Lari, E., Radano, G., Muhhina, J., Fondelli, C., Gavrilova, J. and Chiesi, A. (2015) 'Integrated isolation and quantitative analysis of exosome shuttled proteins and nucleic acids using immunocapture approaches', *Methods*, 87, pp. 46-58.

Zhang, H., Freitas, D., Kim, H. S., Fabijanic, K., Li, Z., Chen, H., Mark, M. T., Molina, H., Martin, A. B., Bojmar, L., Fang, J., Rampersaud, S., Hoshino, A., Matei, I., Kenific, C. M., Nakajima, M., Mutvei, A. P., Sansone, P., Buehring, W., Wang, H., Jimenez, J. P., Cohen-Gould, L., Paknejad, N., Brendel, M., Manova-Todorova, K., Magalhães, A., Ferreira, J. A., Osório, H., Silva, A. M., Massey, A., Cubillos-Ruiz, J. R., Galletti, G., Giannakakou, P., Cuervo, A. M., Blenis, J., Schwartz, R., Brady, M. S., Peinado, H., Bromberg, J., Matsui, H., Reis, C. A. and Lyden, D. (2018) 'Identification of distinct nanoparticles and subsets of extracellular vesicles by asymmetric flow field-flow fractionation', *Nat Cell Biol*, 20(3), pp. 332-343.

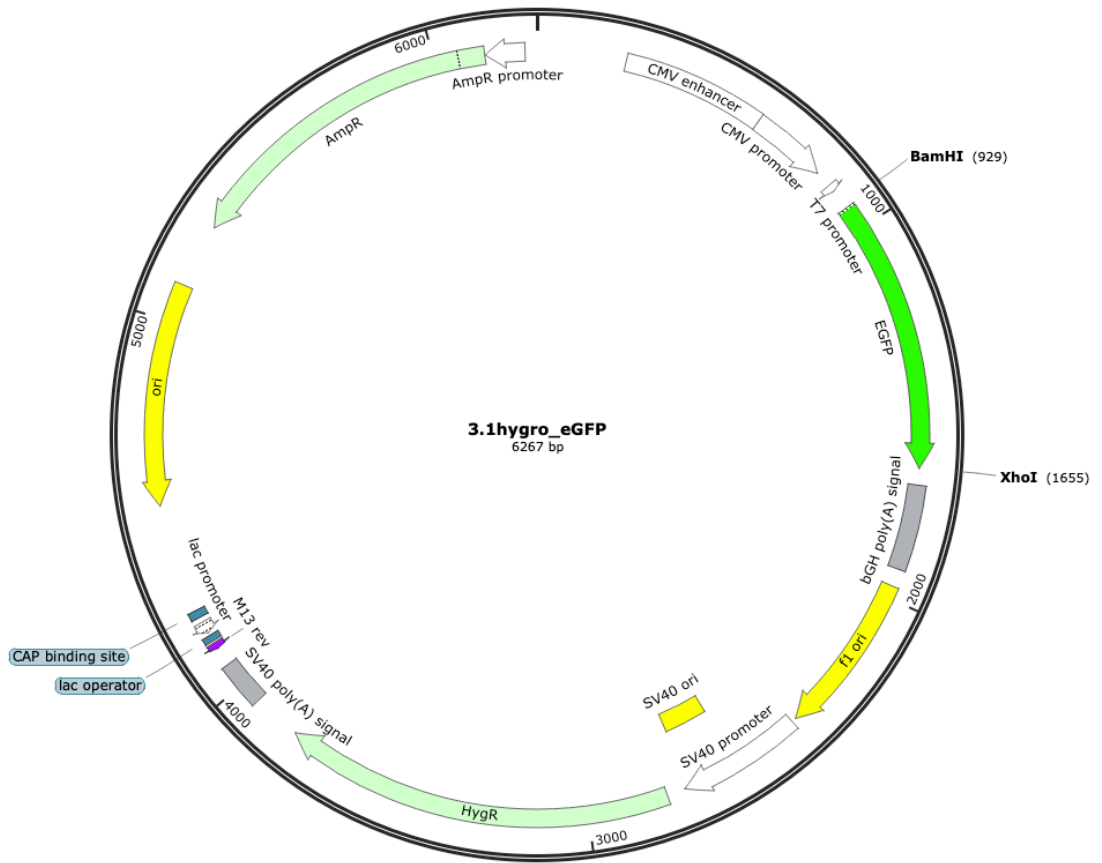
Zhang, H. and Lyden, D. (2019) 'Asymmetric-flow field-flow fractionation technology for exosome and small extracellular vesicle separation and characterization', *Nat Protoc*, 14(4), pp. 1027-1053.

Zhang, J. H., Shan, L. L., Liang, F., Du, C. Y. and Li, J. J. (2022) 'Strategies and Considerations for Improving Recombinant Antibody Production and Quality in Chinese Hamster Ovary Cells', *Front Bioeng Biotechnol*, 10, pp. 856049.

- Zhang, Y., Bi, J., Huang, J., Tang, Y., Du, S. and Li, P. (2020) 'Exosome: A Review of Its Classification, Isolation Techniques, Storage, Diagnostic and Targeted Therapy Applications', *Int J Nanomedicine*, 15, pp. 6917-6934.
- Zheng, B. J., Zhou, J. M. and Wang, H. (2020) 'Host microRNAs and exosomes that modulate influenza virus infection', *Virus Research*, 279.
- Zheng, W., Rädler, J., Sork, H., Niu, Z., Roudi, S., Bost, J. P., Görgens, A., Zhao, Y., Mamand, D. R., Liang, X., Wiklander, O. P. B., Lehto, T., Gupta, D., Nordin, J. Z. and El Andaloussi, S. (2023) 'Identification of scaffold proteins for improved endogenous engineering of extracellular vesicles', *Nat Commun*, 14(1), pp. 4734.
- Zhou, Q., Zhang, Y., Lu, X., Wang, C., Pei, X., Lu, Y., Cao, C., Xu, C. and Zhang, B. (2021) 'Stable overexpression of mutated PTEN in Chinese hamster ovary cells enhances their performance and therapeutic antibody production', *Biotechnol J*, 16(9), pp. e2000623.
- Zitvogel, L., Regnault, A., Lozier, A., Wolfers, J., Flament, C., Tenza, D., Ricciardi-Castagnoli, P., Raposo, G. and Amigorena, S. (1998) 'Eradication of established murine tumors using a novel cell-free vaccine: dendritic cell-derived exosomes', *Nature Medicine*, 4(5), pp. 594-600.

Appendix

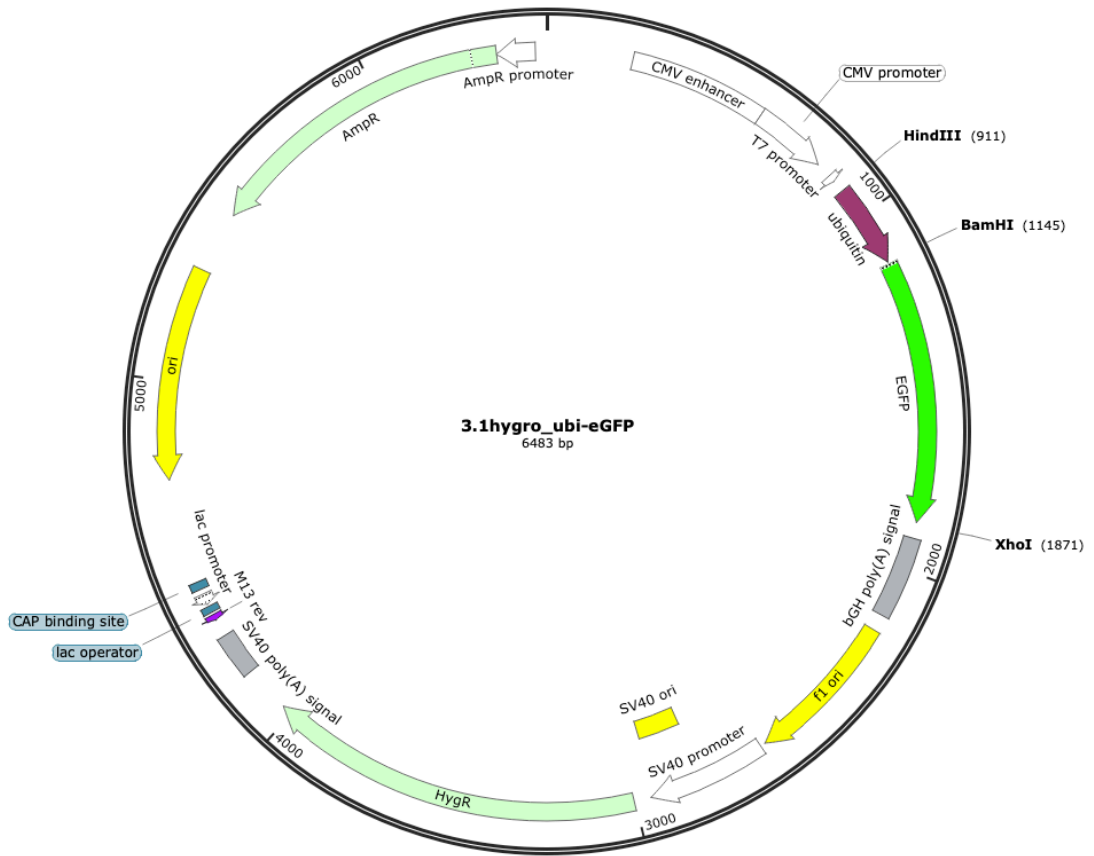
Vector Maps



Construct Name: GFP (only)

Gene(s) Inserted: GFP

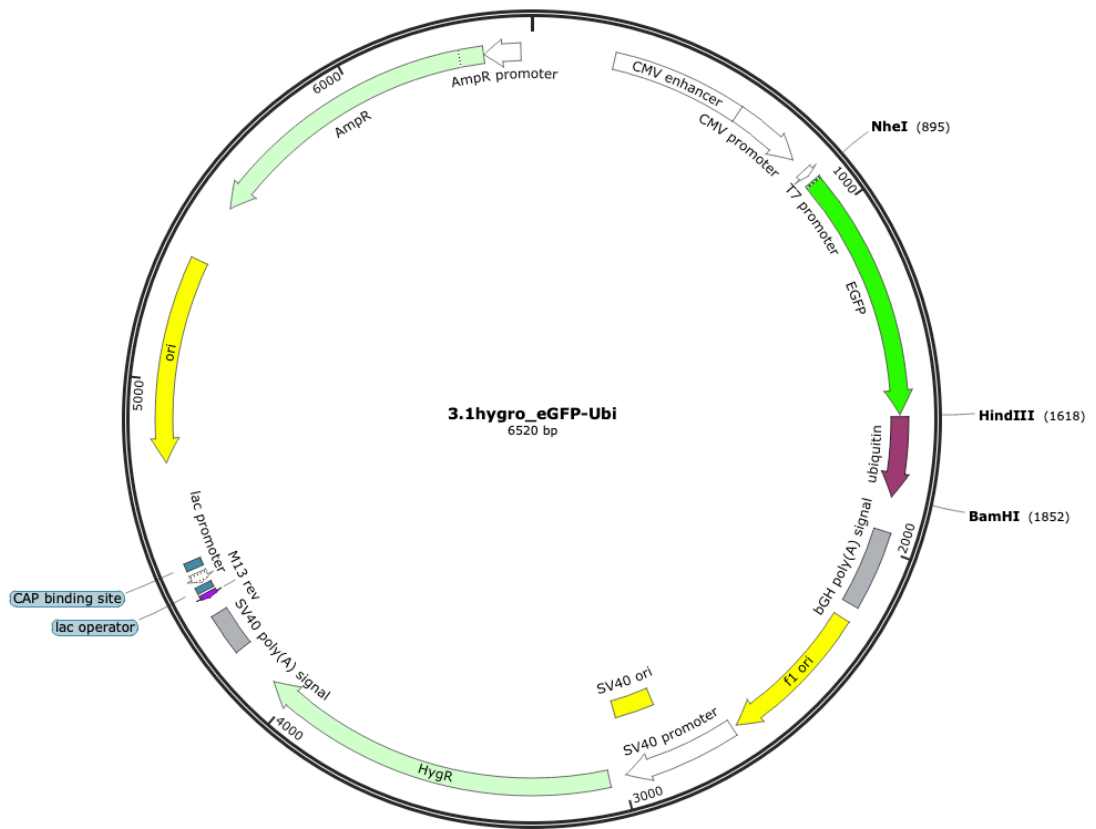
Restriction Site Insertion Points: BamHI, XhoI



Construct Name: Ubi_GFP

Gene(s) Inserted: Ubiquitin, GFP

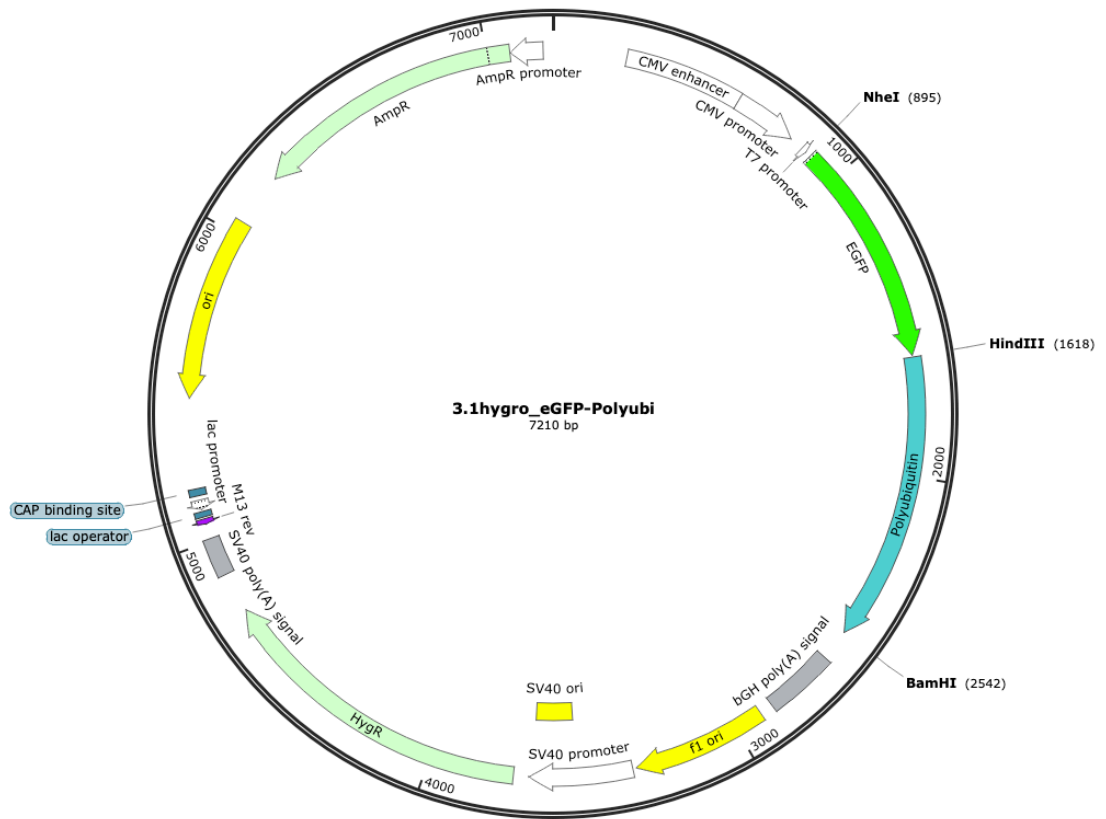
Restriction Site Insertion Points: HindIII, BamHI, XhoI



Construct Name: GFP_Ubi

Gene(s) Inserted: Ubiquitin, GFP

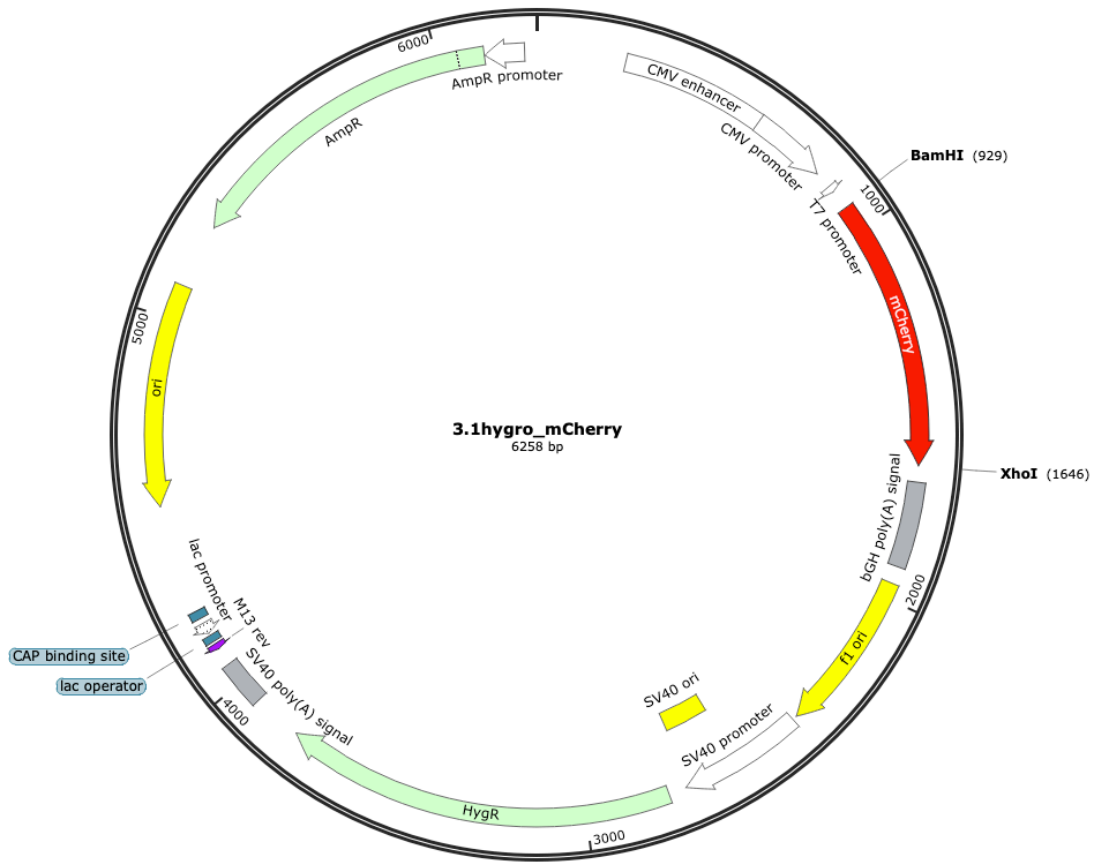
Restriction Site Insertion Points: NheI, HindIII, BamHI



Construct Name: GFP_PolyUbi

Gene(s) Inserted: Polyubiquitin, GFP

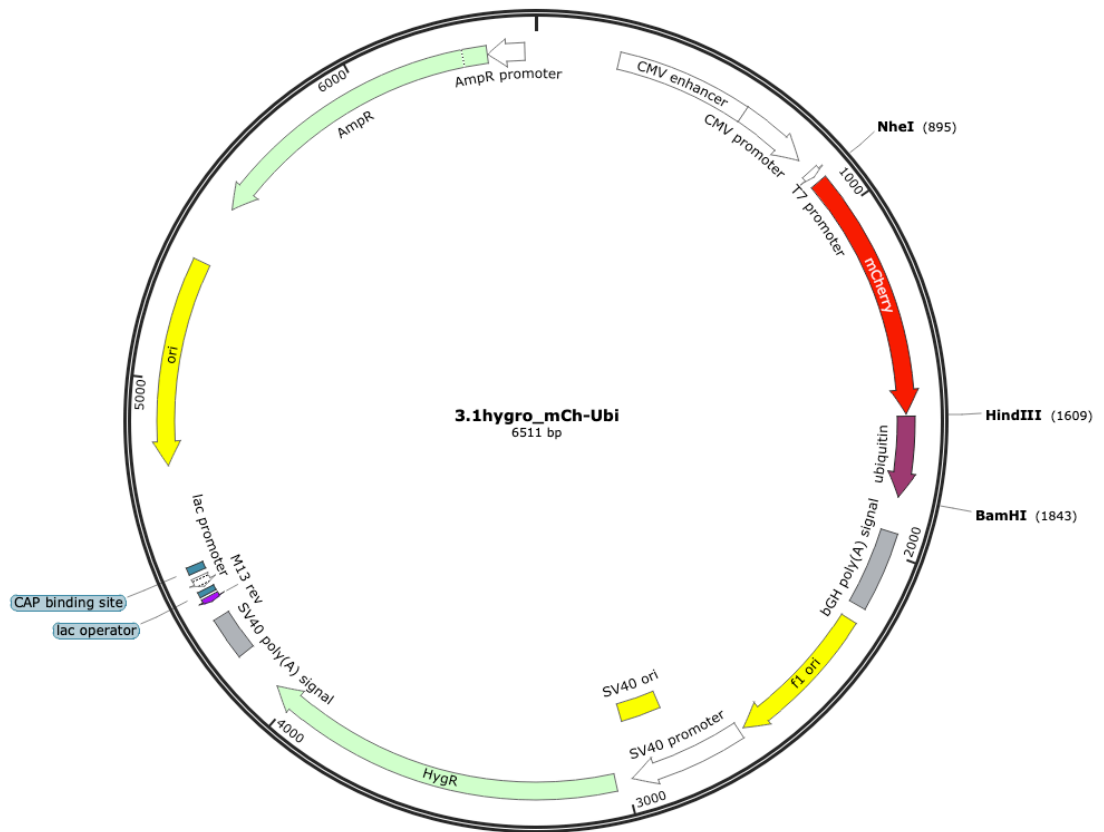
Restriction Site Insertion Points: NheI, HindIII, BamHI



Construct Name: mCherry (only)

Gene(s) Inserted: mCherry

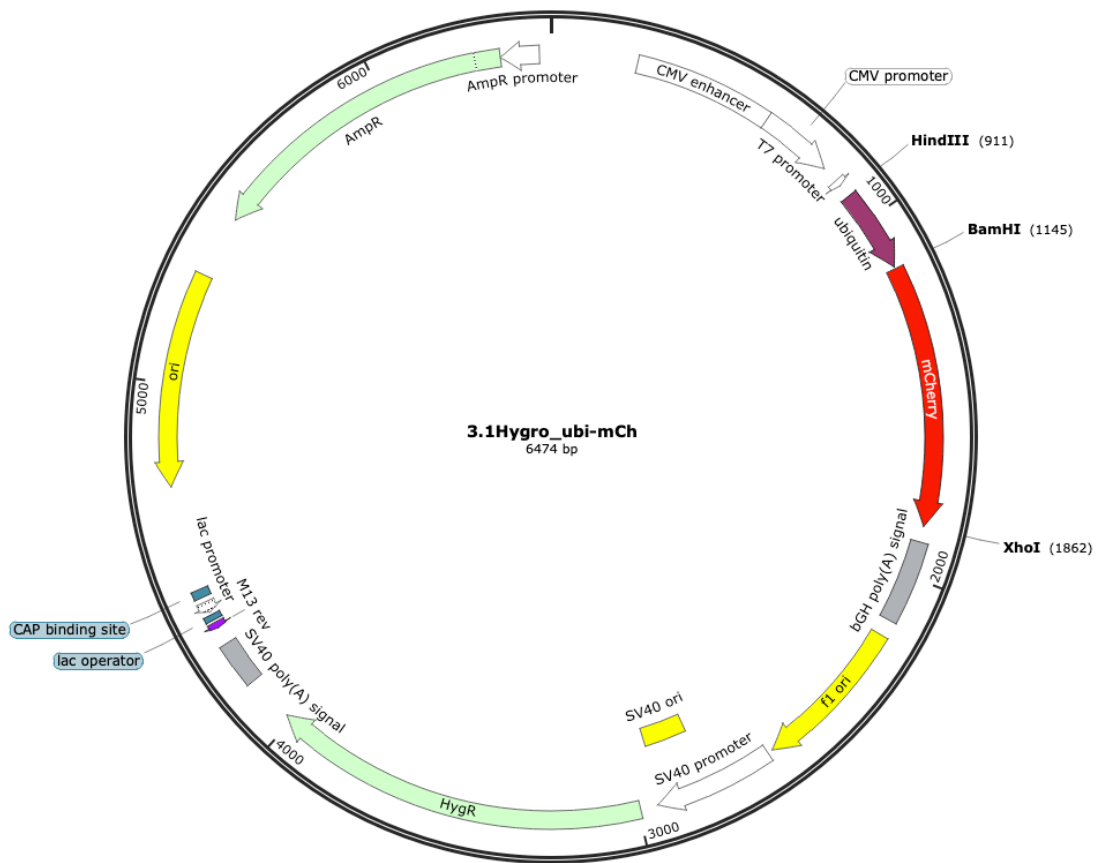
Restriction Site Insertion Points: BamHI, XhoI



Construct Name: mCh_Ubi

Gene(s) Inserted: Ubiquitin, mCherry

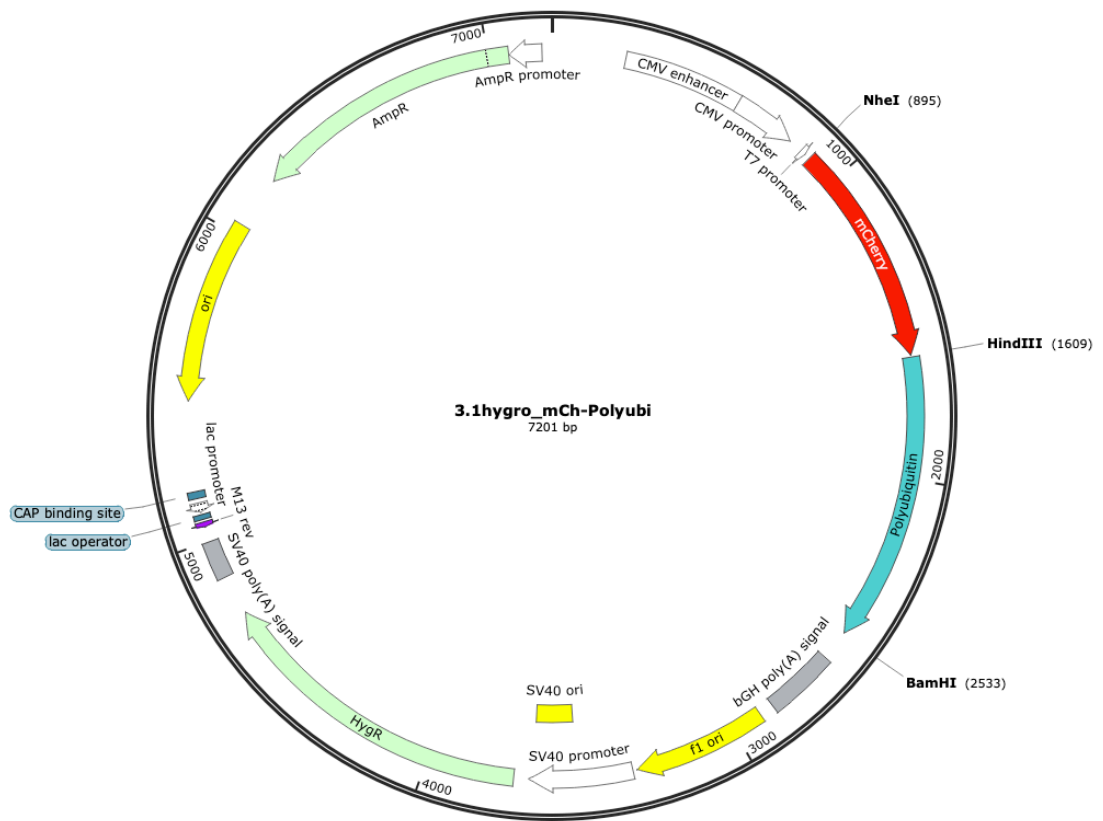
Restriction Site Insertion Points: NheI, HindIII, BamHI



Construct Name: Ubi_mCh

Gene(s) Inserted: Ubiquitin, mCherry

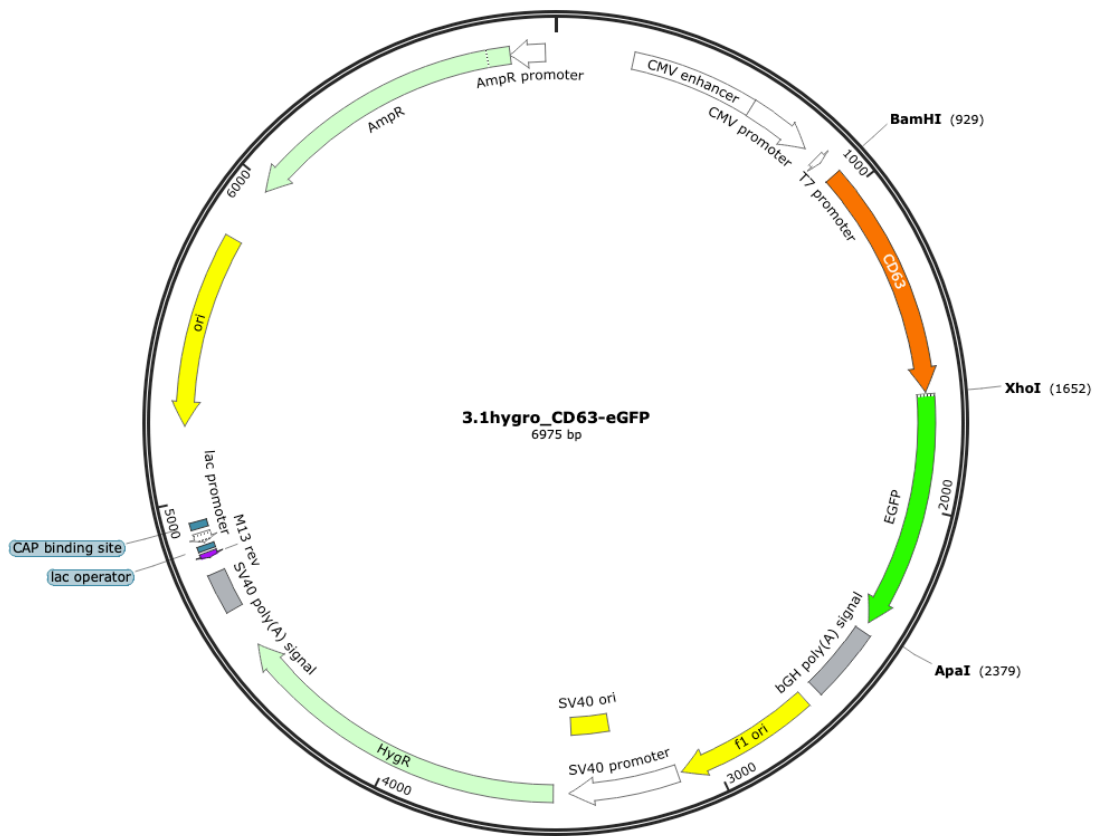
Restriction Site Insertion Points: HindIII, BamHI, XhoI



Construct Name: mCh_PolyUbi

Gene(s) Inserted: Polyubiquitin, mCherry

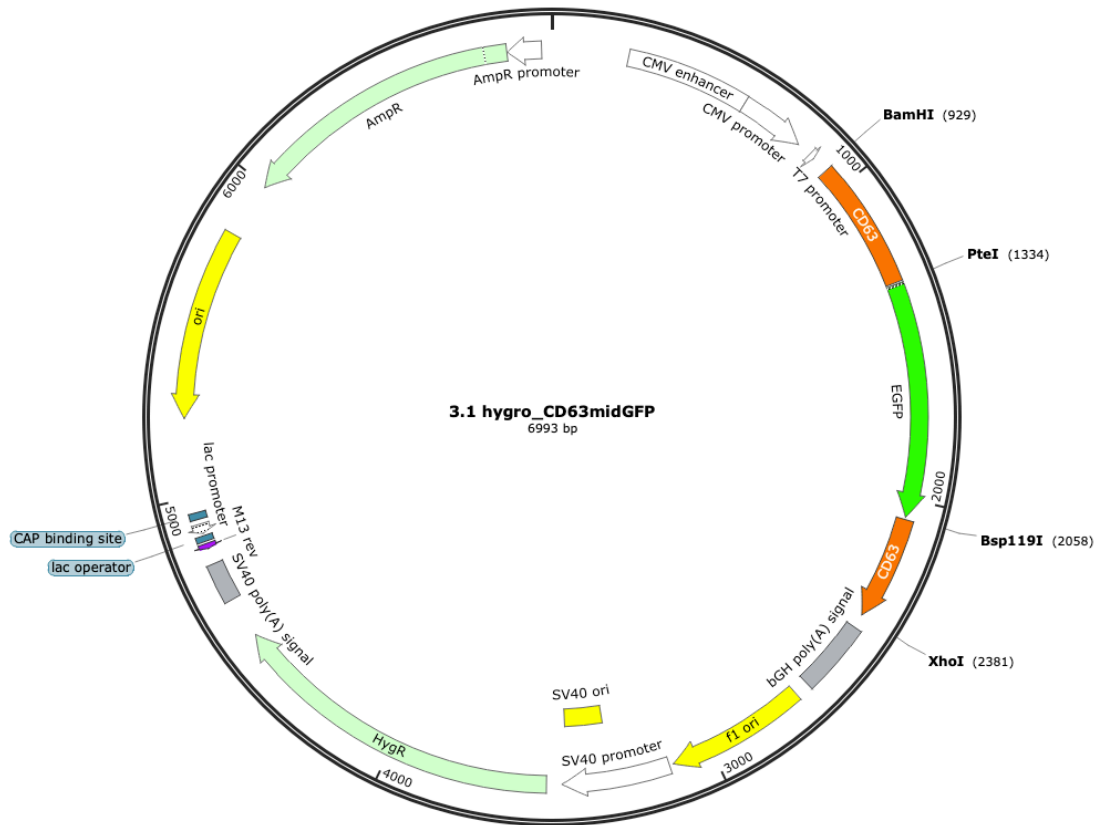
Restriction Site Insertion Points: NheI, HindIII, BamHI



Construct Name: CD63_GFP

Gene(s) Inserted: CD63, GFP

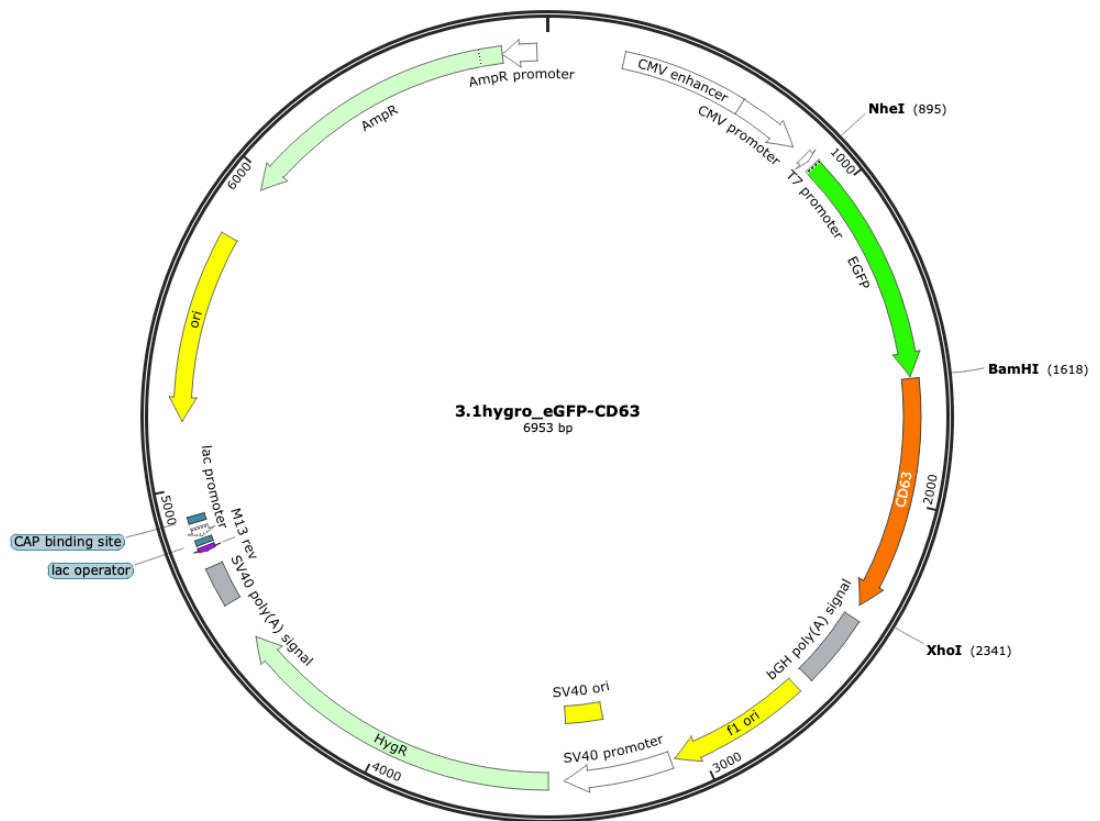
Restriction Site Insertion Points: BamHI, XhoI, ApaI



Construct Name: CD63midGFP

Gene(s) Inserted: CD63, GFP

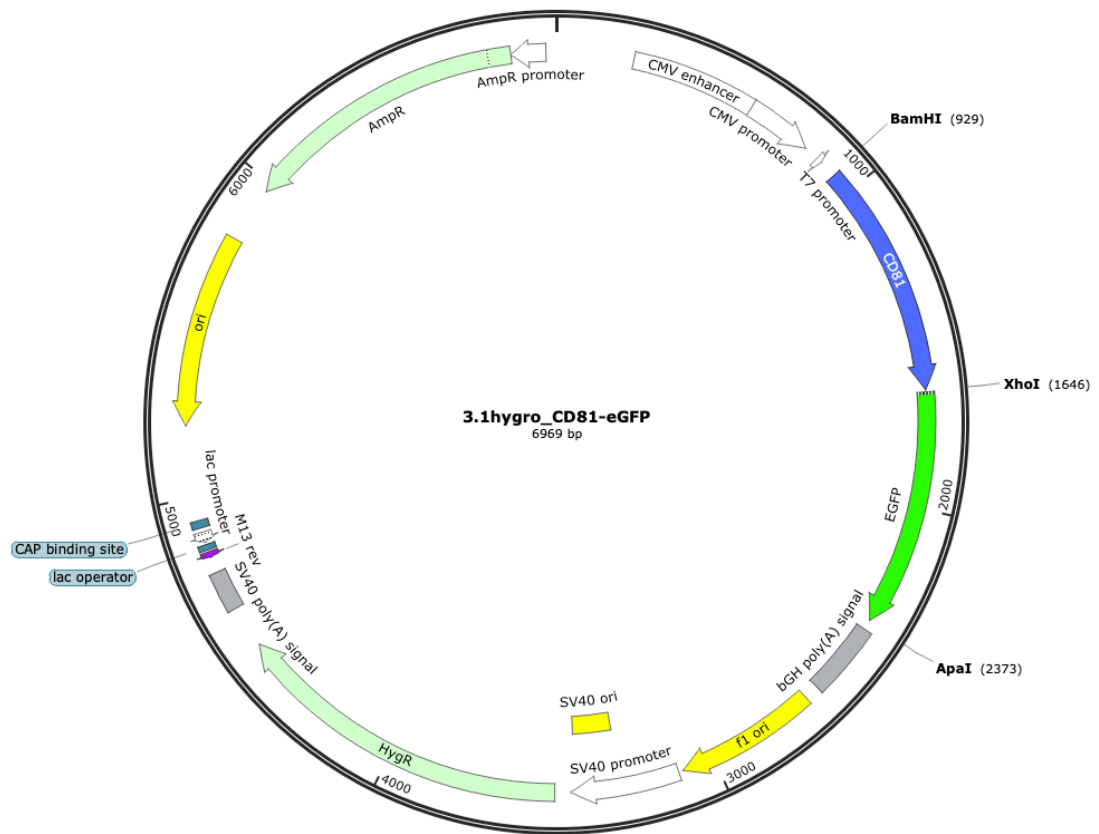
Restriction Site Insertion Points: BamHI, PteI, Bsp119I, XhoI



Construct Name: GFP_CD63

Gene(s) Inserted: CD63, GFP

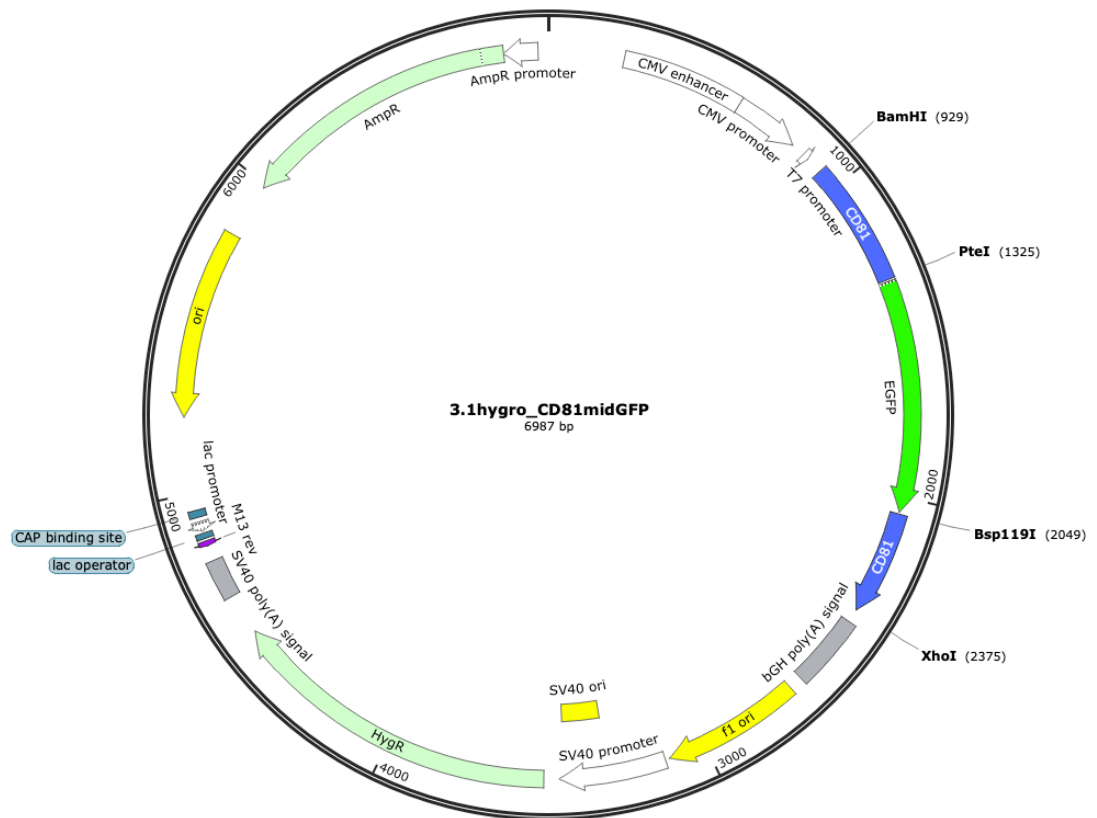
Restriction Site Insertion Points: NheI, BamHI, XhoI



Construct Name: CD81_GFP

Gene(s) Inserted: CD81, GFP

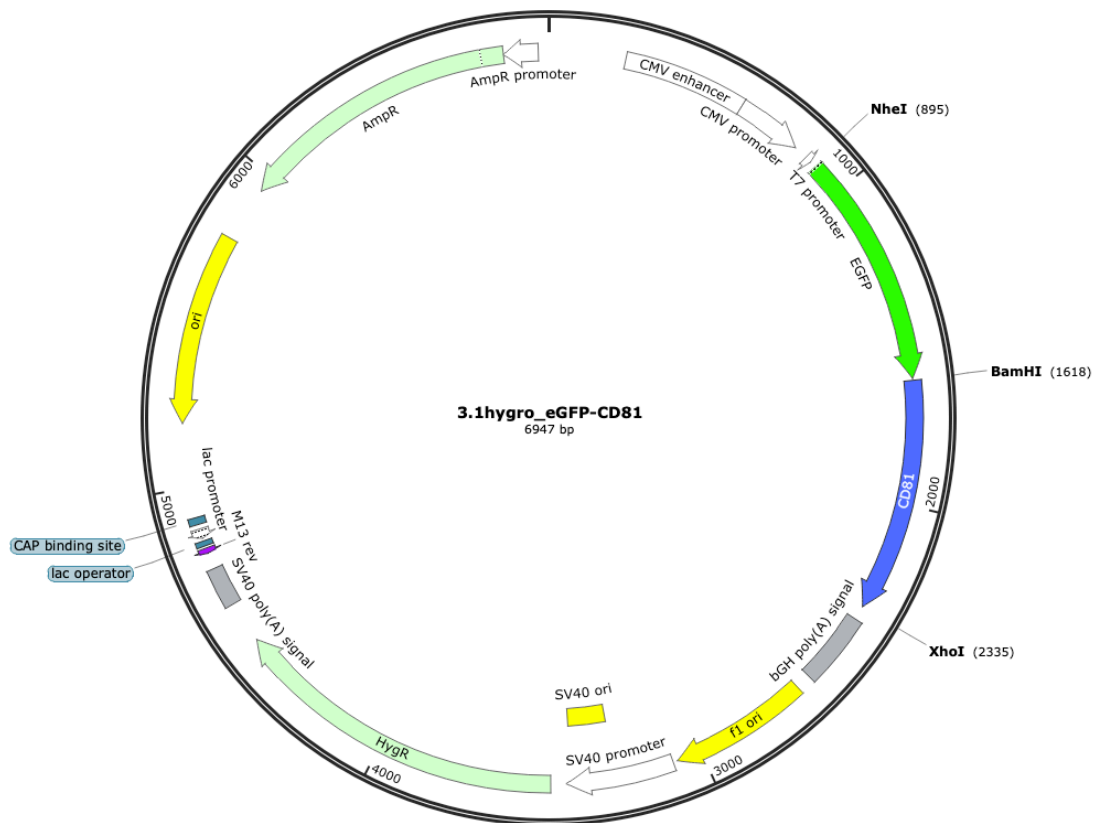
Restriction Site Insertion Points: BamHI, XhoI, ApaI



Construct Name: CD81midGFP

Gene(s) Inserted: CD81, GFP

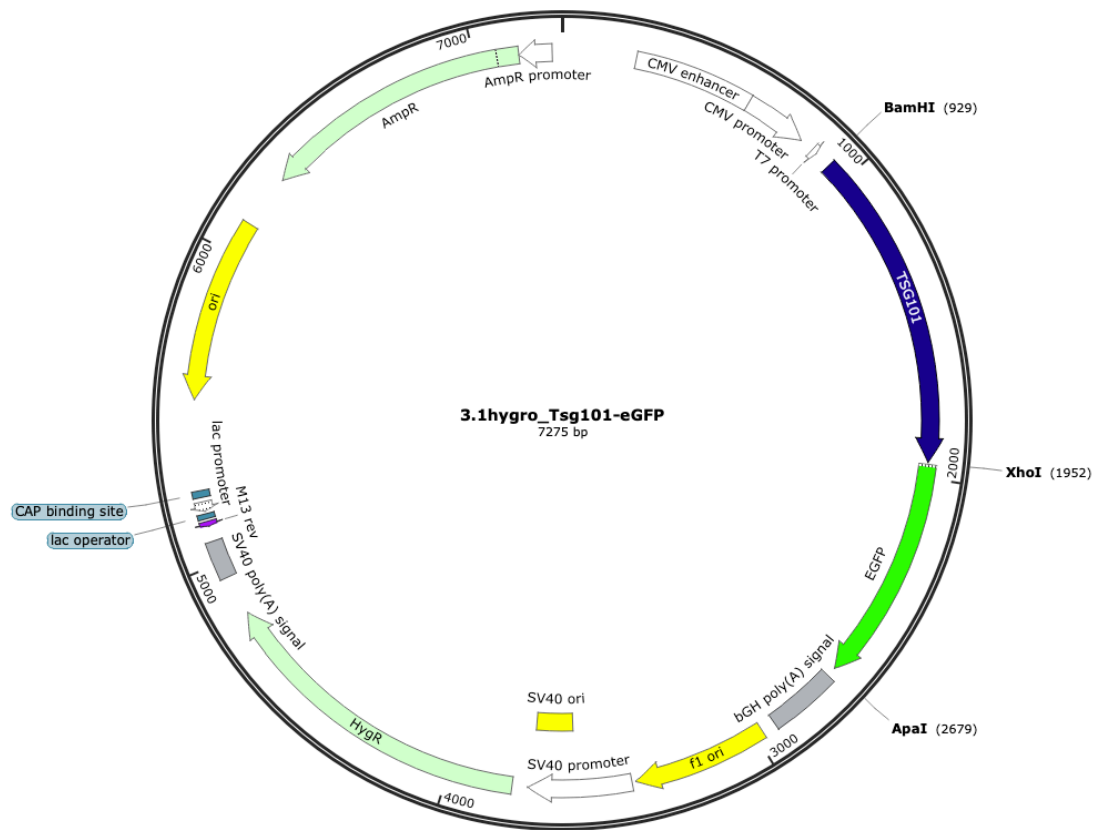
Restriction Site Insertion Points: BamHI, PteI, Bsp119I, XhoI



Construct Name: GFP_CD81

Gene(s) Inserted: CD81, GFP

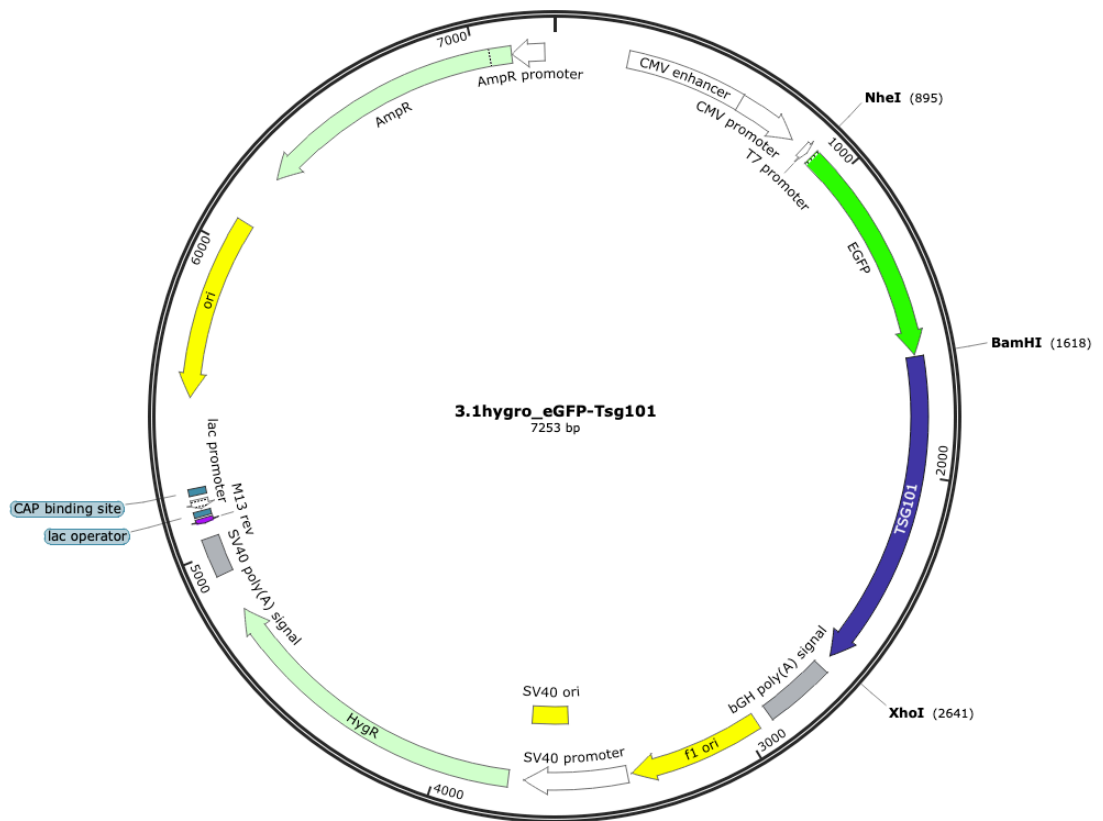
Restriction Site Insertion Points: NheI, BamHI, XhoI



Construct Name: Tsg101_GFP

Gene(s) Inserted: Tsg101, GFP

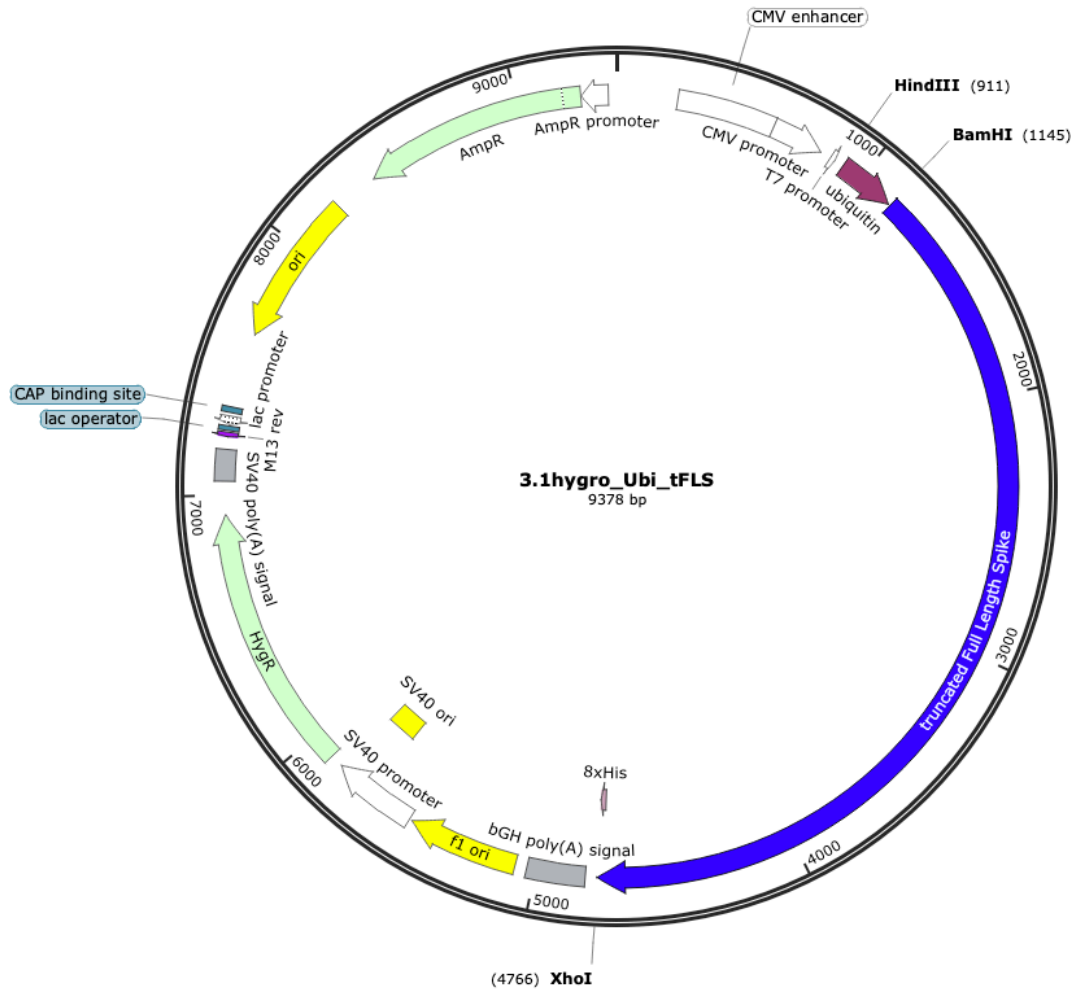
Restriction Site Insertion Points: BamHI, XhoI, ApaI



Construct Name: GFP_Tsg101

Gene(s) Inserted: Tsg101, GFP

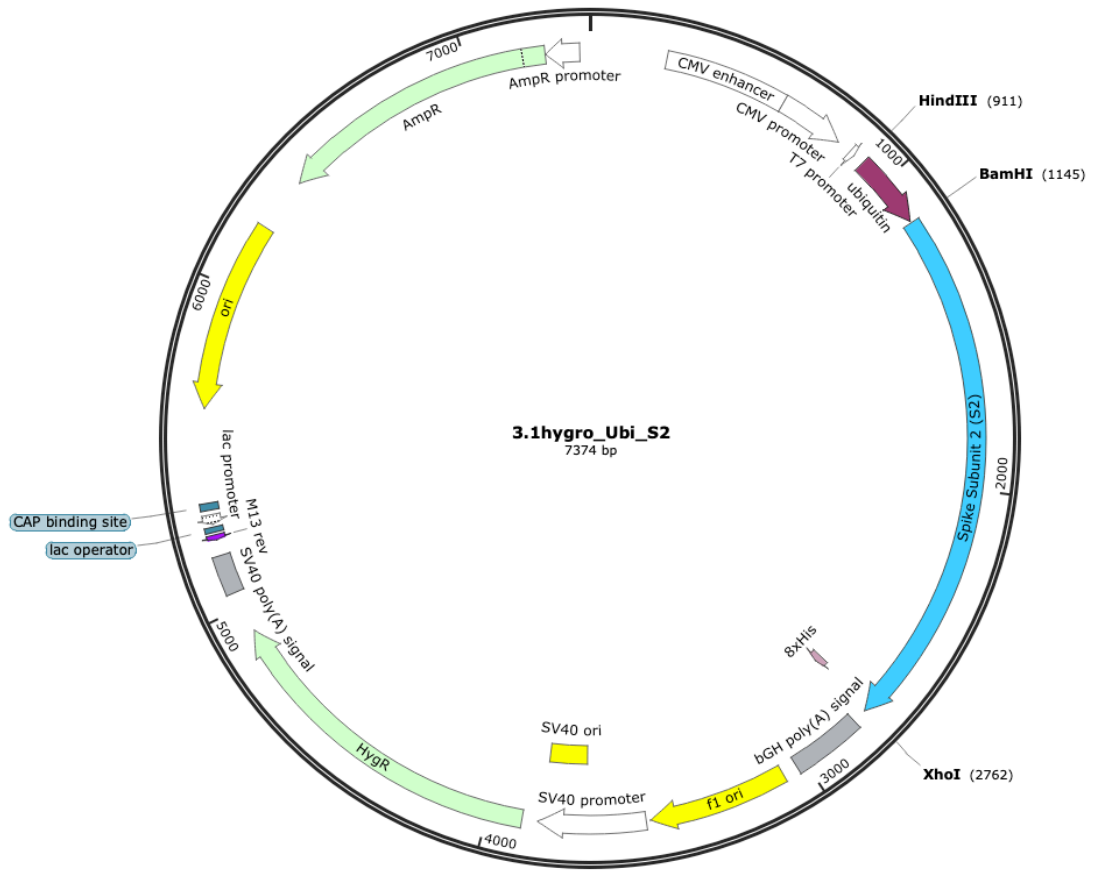
Restriction Site Insertion Points: NheI, BamHI, XhoI



Construct Name: Ubi_tFLS

Gene(s) Inserted: Ubiquitin, truncated Full Length Spike (tFLS)

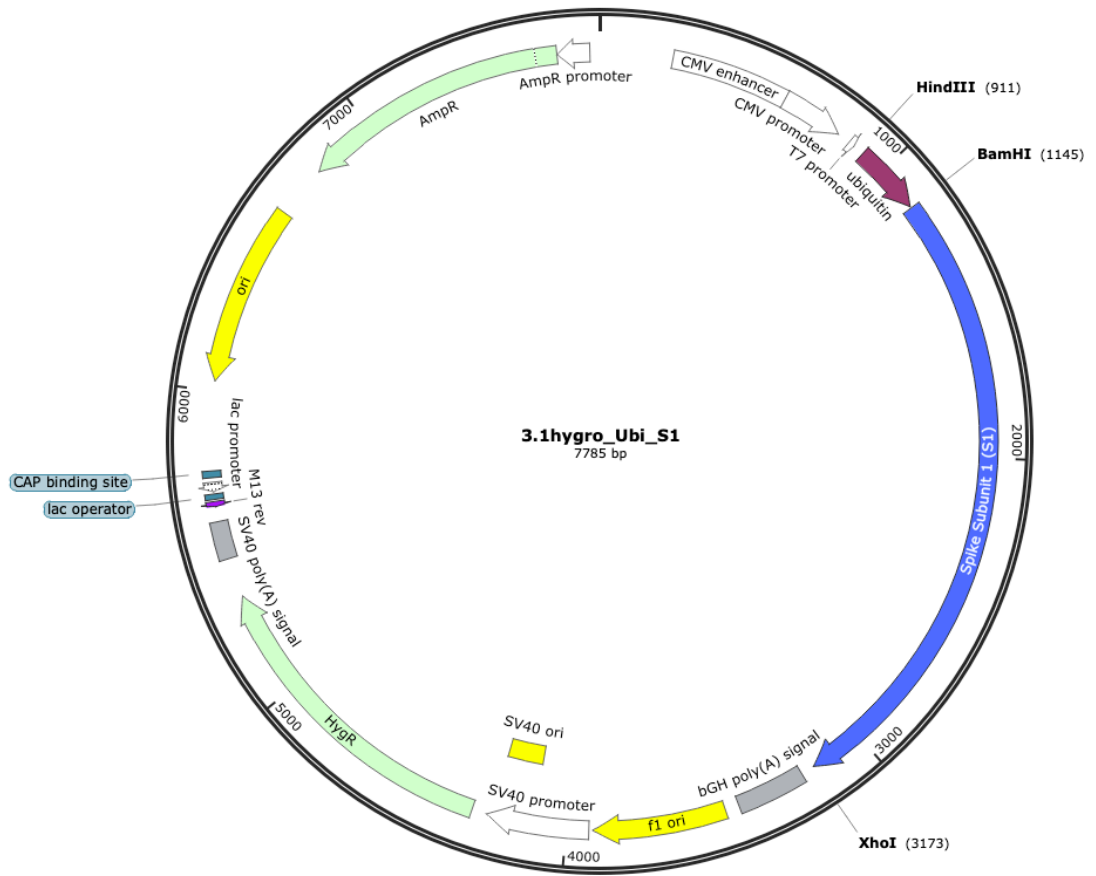
Restriction Site Insertion Points: HindIII, BamHI, XhoI



Construct Name: Ubi_S1

Gene(s) Inserted: Ubiquitin, Spike Subunit 1 (S1)

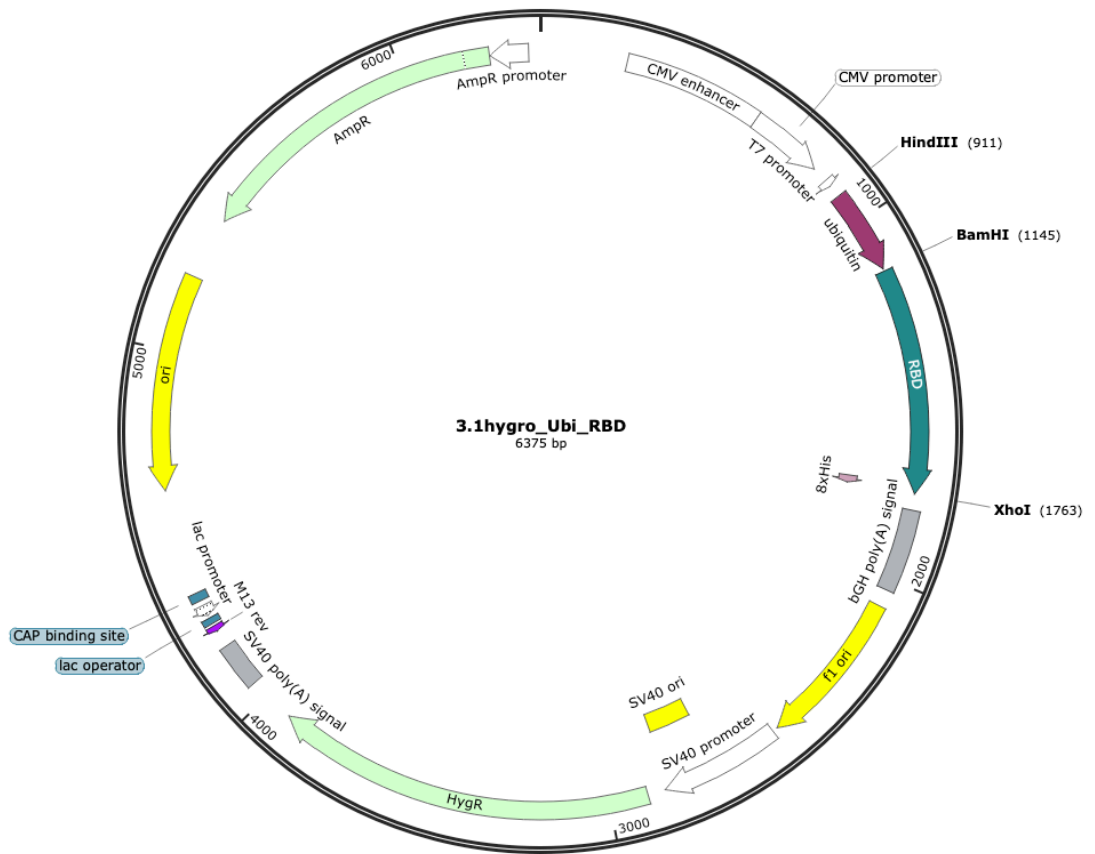
Restriction Site Insertion Points: HindIII, BamHI, XhoI



Construct Name: Ubi_S2

Gene(s) Inserted: Ubiquitin, Spike Subunit 2 (S2)

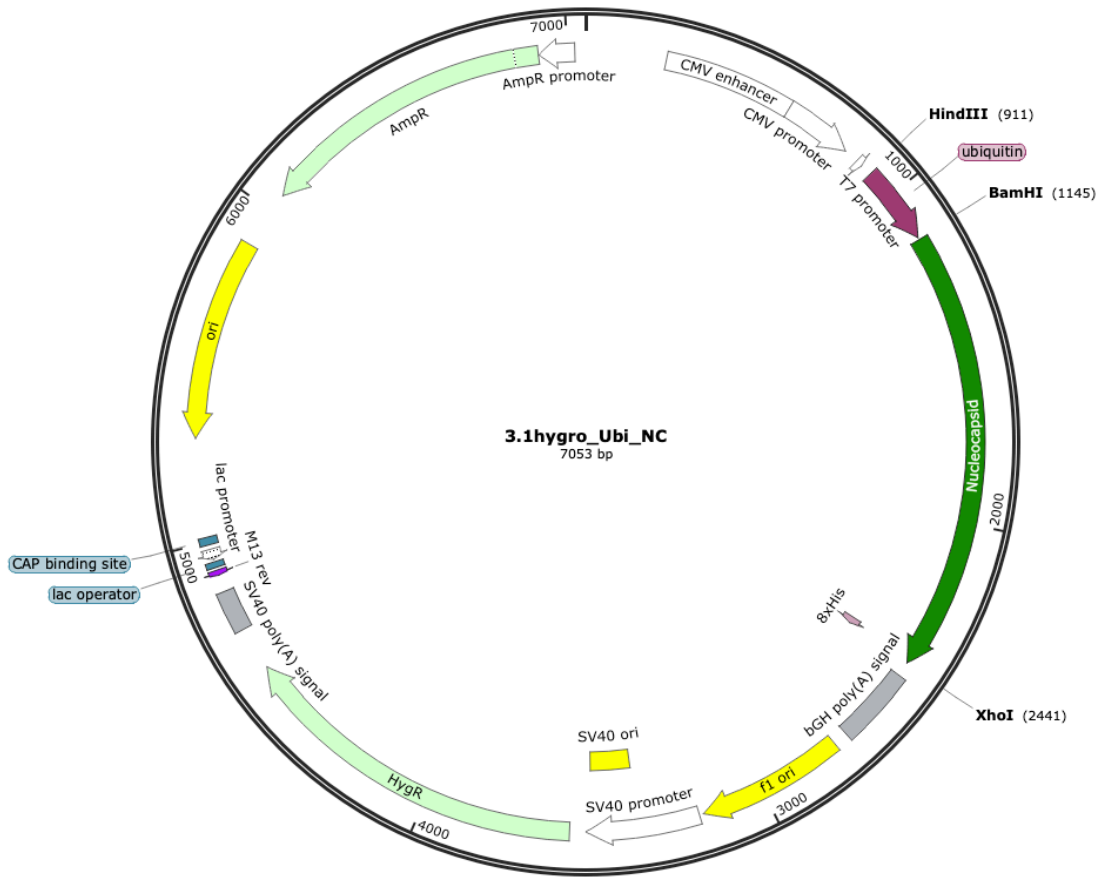
Restriction Site Insertion Points: HindIII, BamHI, XhoI



Construct Name: Ubi_RBD

Gene(s) Inserted: Ubiquitin, Receptor Binding Domain (RBD)

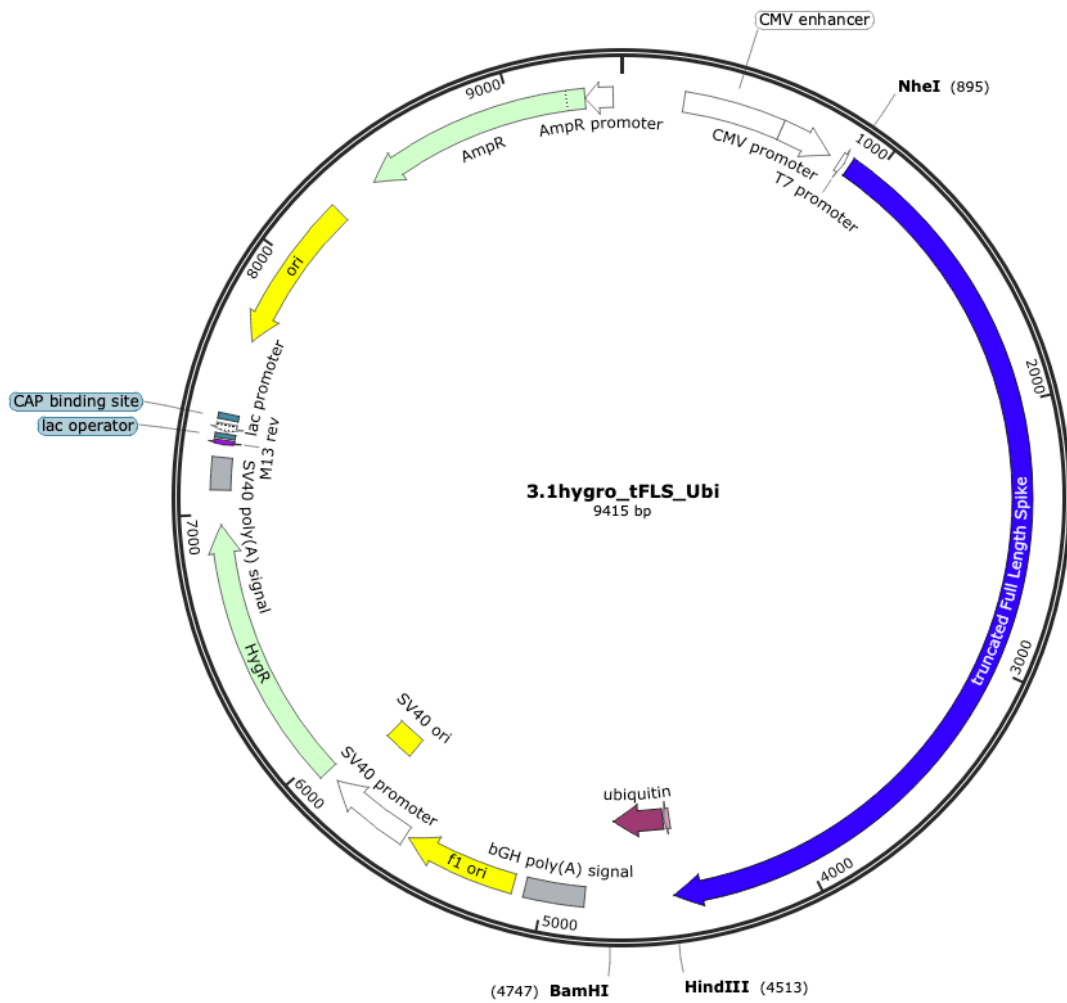
Restriction Site Insertion Points: HindIII, BamHI, XhoI



Construct Name: Ubi_NC

Gene(s) Inserted: Ubiquitin, Nucleocapsid (NC)

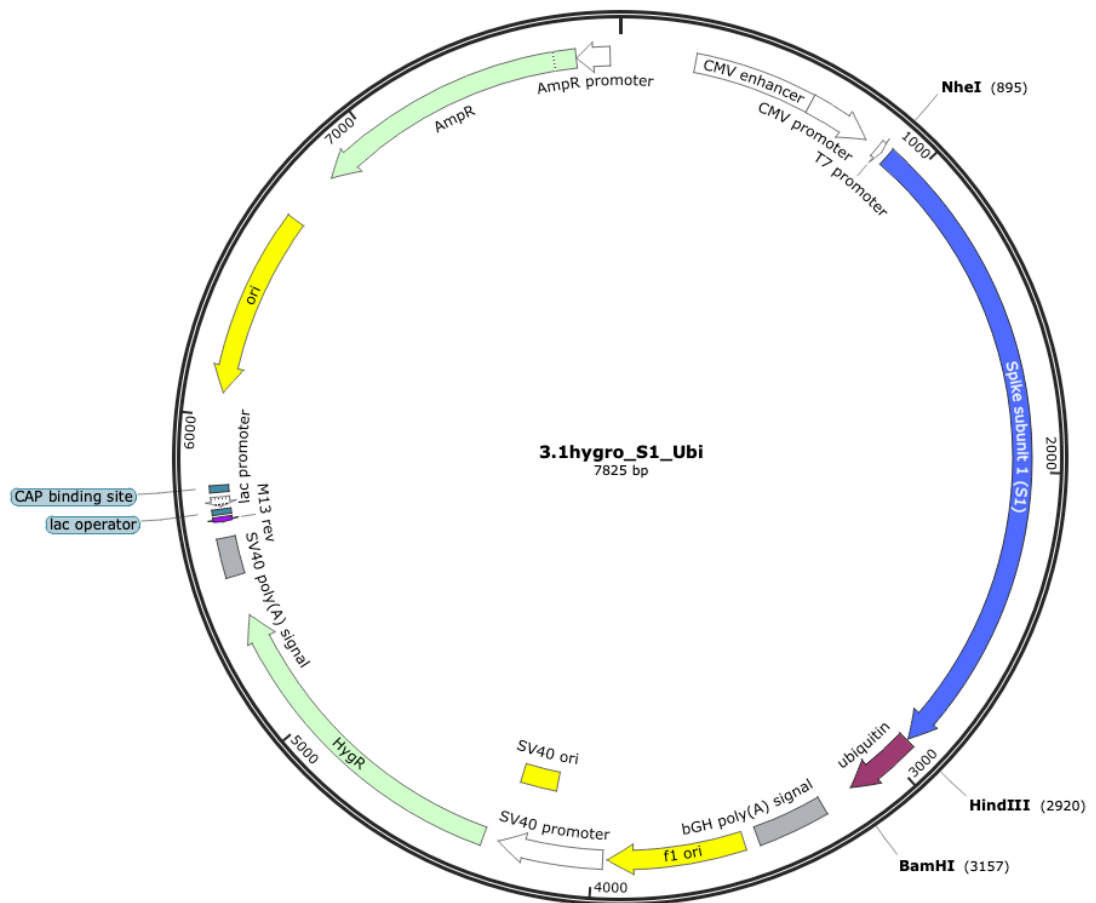
Restriction Site Insertion Points: HindIII, BamHI, XhoI



Construct Name: tFLS_Ubi

Gene(s) Inserted: Ubiquitin, truncated Full Length Spike (tFLS)

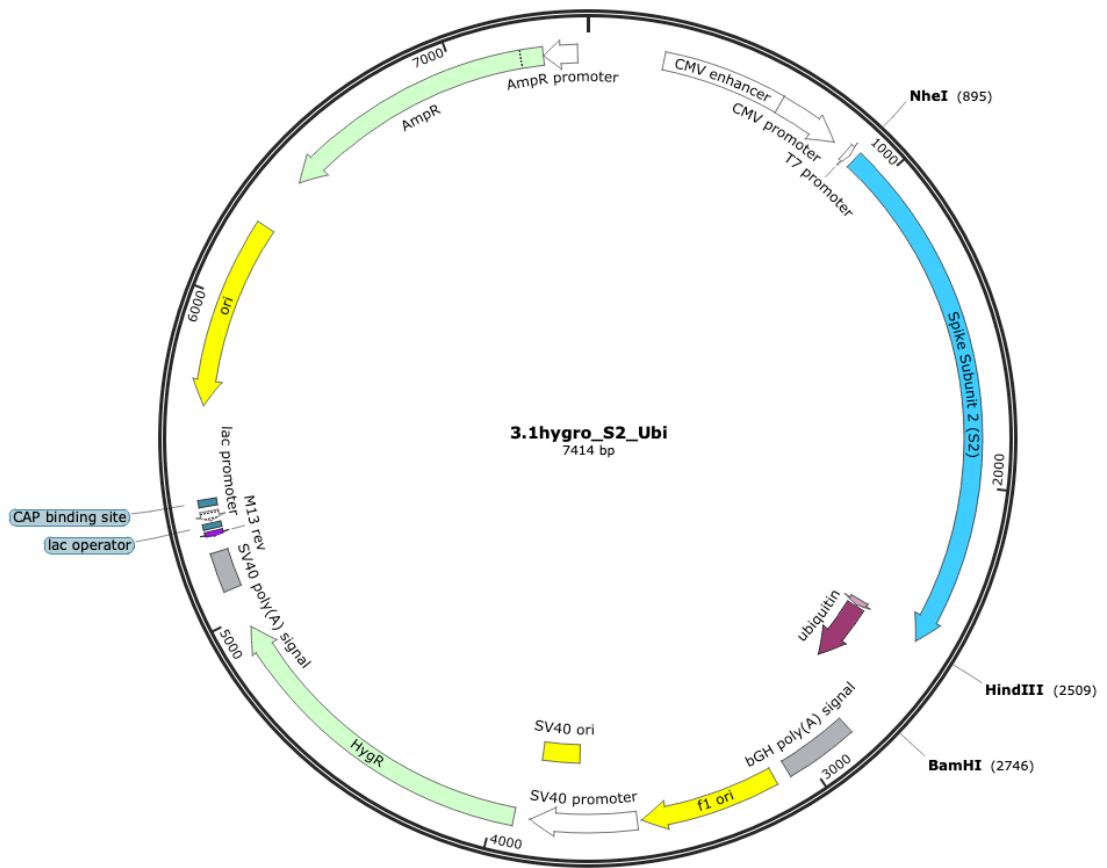
Restriction Site Insertion Points: NheI, HindIII, BamHI



Construct Name: S1_Ubi

Gene(s) Inserted: Spike Subunit 1 (S1), Ubiquitin

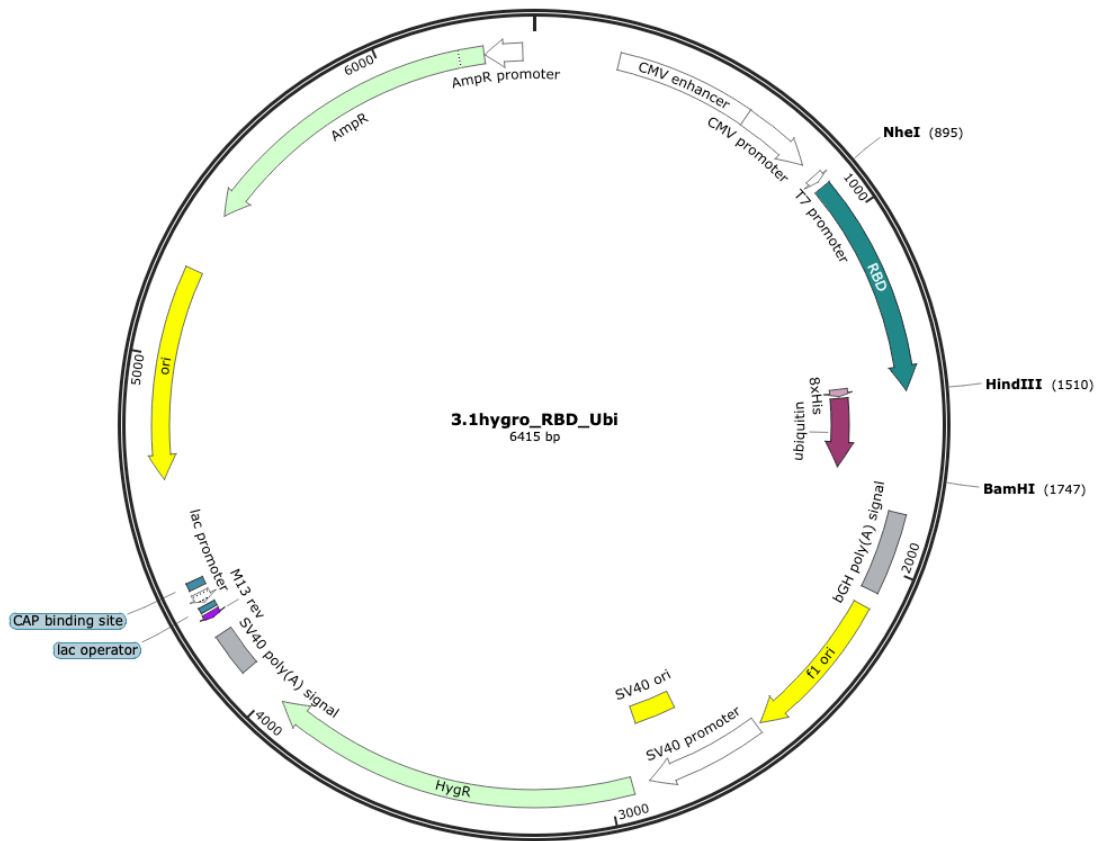
Restriction Site Insertion Points: NheI, HindIII, BamHI



Construct Name: S2_Ubi

Gene(s) Inserted: Ubiquitin, Spike Subunit 2 (S2)

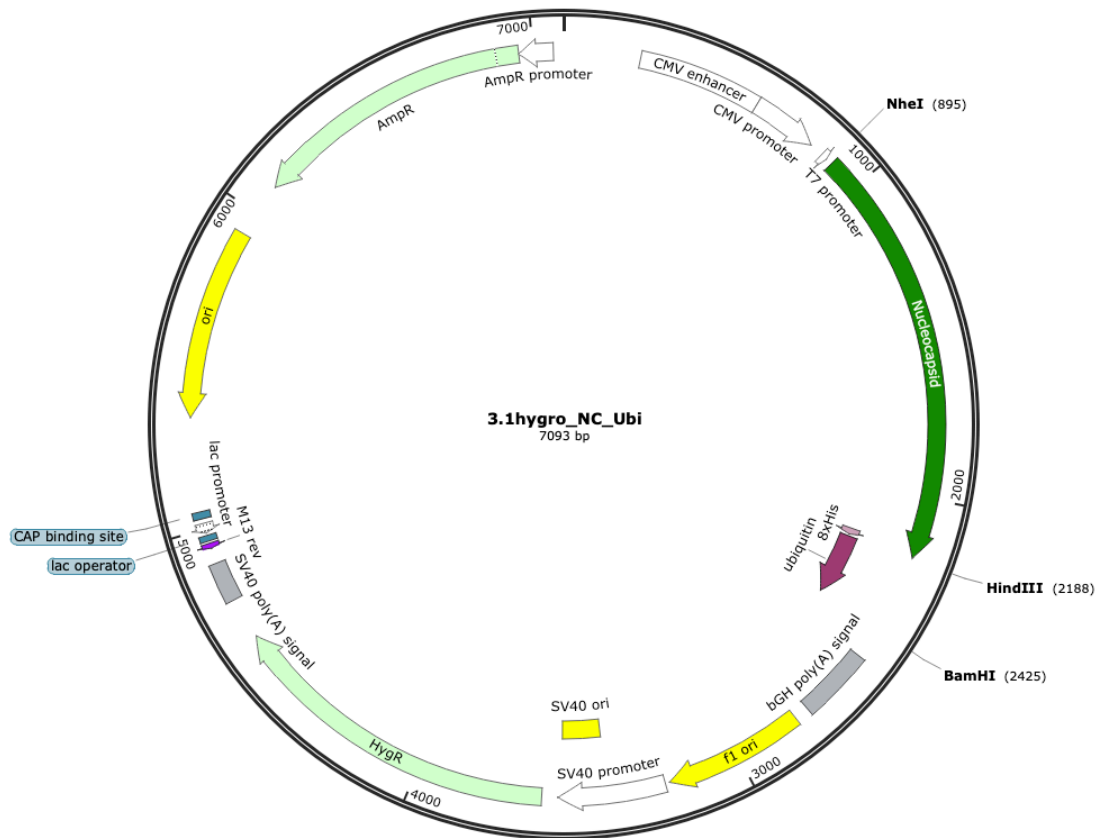
Restriction Site Insertion Points: NheI, HindIII, BamHI



Construct Name: RBD_Ubi

Gene(s) Inserted: Ubiquitin, Receptor Binding Domain (RBD)

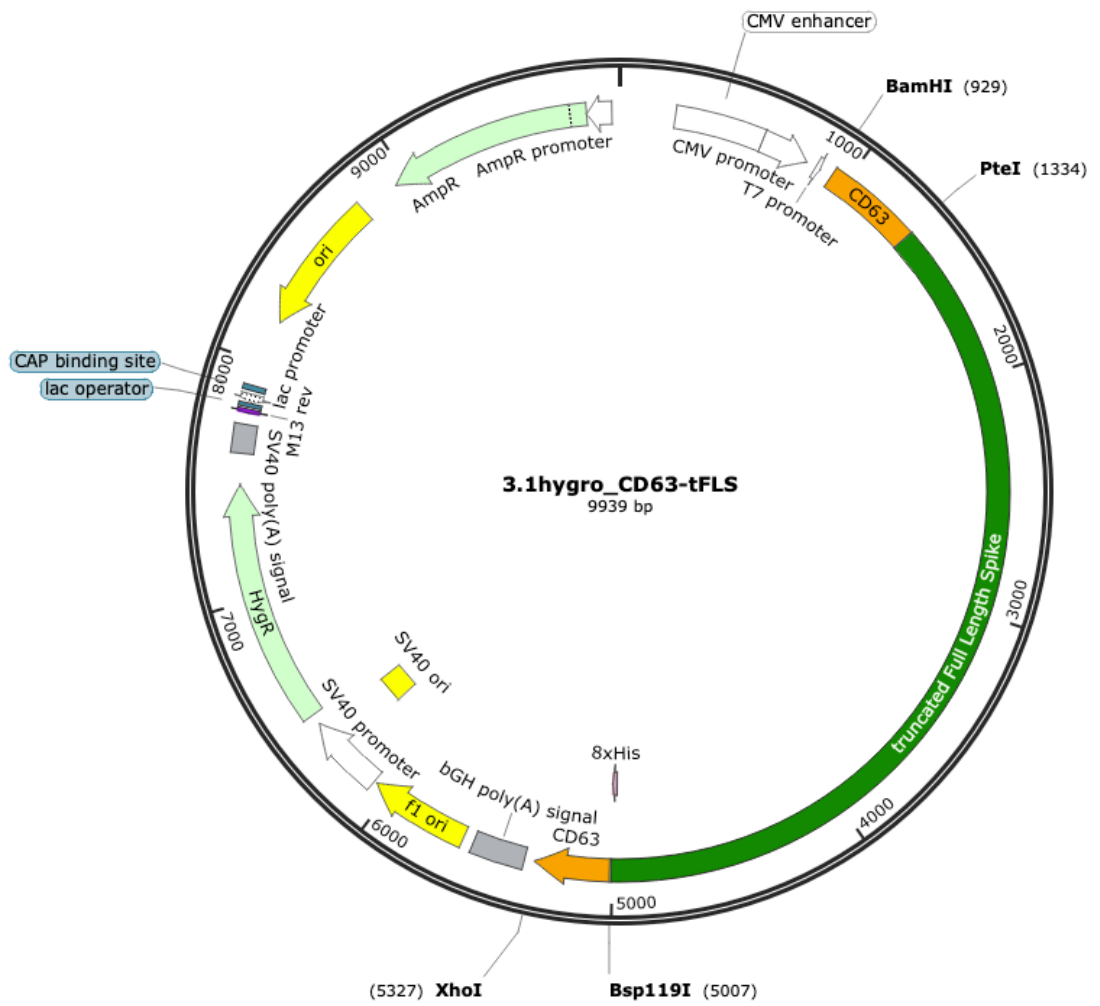
Restriction Site Insertion Points: NheI, HindIII, BamHI



Construct Name: NC_Ubi

Gene(s) Inserted: Ubiquitin, Nucleocapsid (NC)

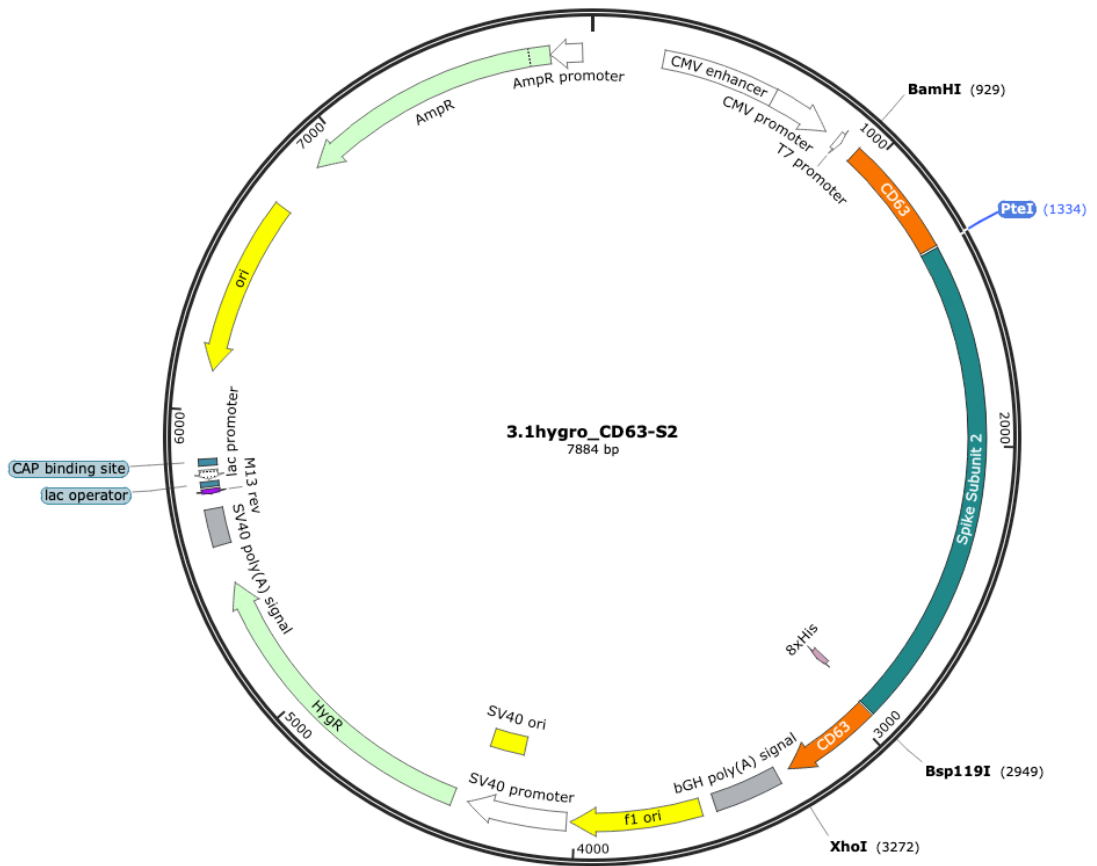
Restriction Site Insertion Points: NheI, HindIII, BamHI



Construct Name: CD63_tFLS

Gene(s) Inserted: CD63, truncated Full Length Spike

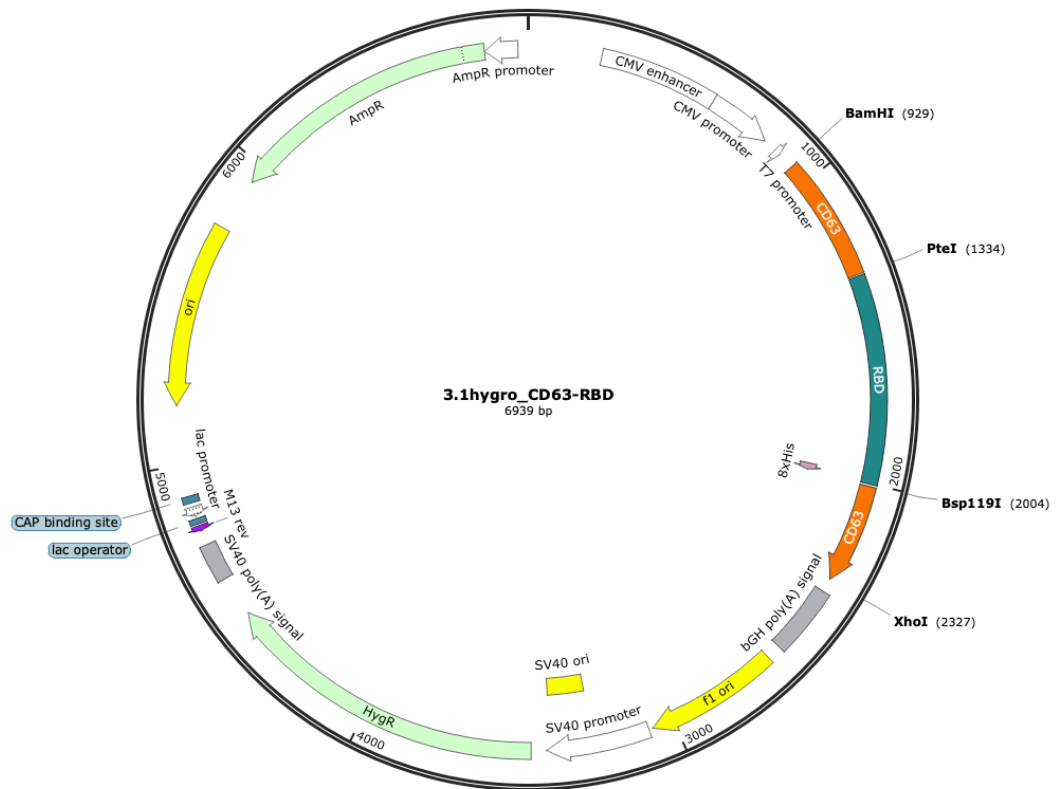
Restriction Site Insertion Points: BamHI, PteI, Bsp119I, XhoI



Construct Name: CD63_S2

Gene(s) Inserted: CD63, Spike Subunit 2 (S2)

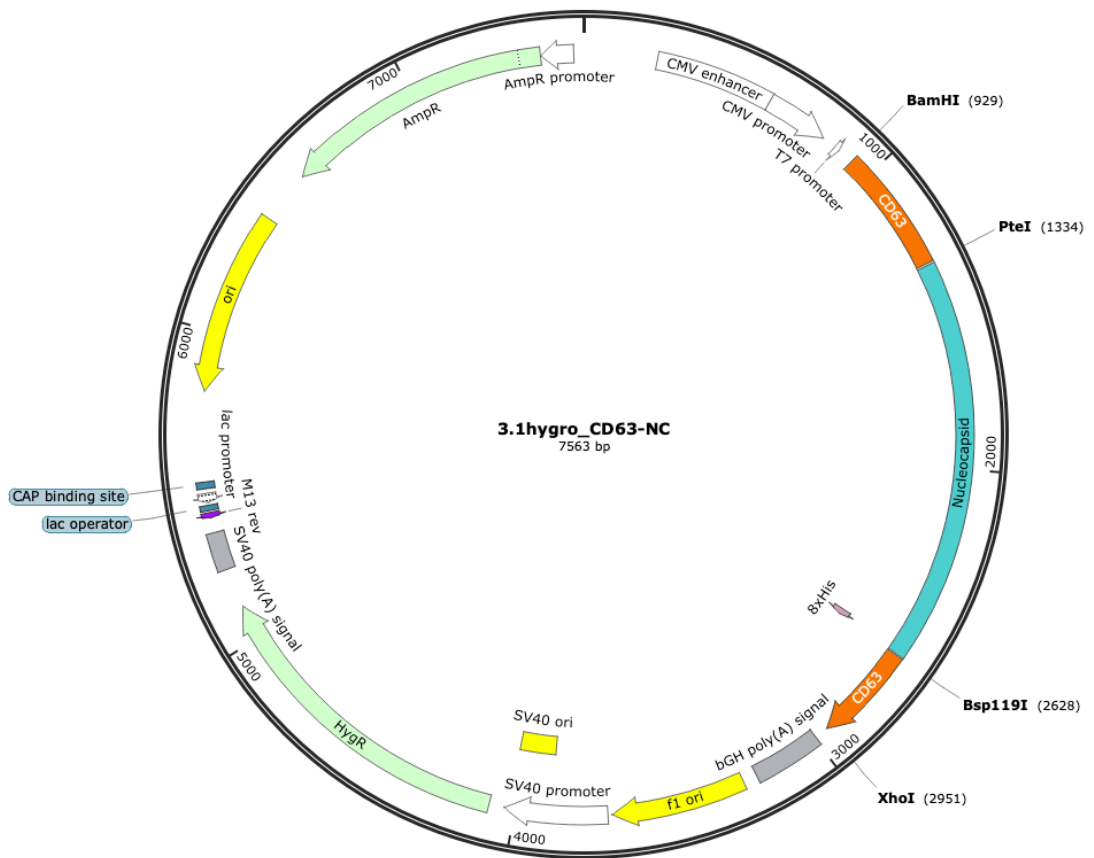
Restriction Site Insertion Points: BamHI, PteI, Bsp119I, XhoI



Construct Name: CD63_RBD

Gene(s) Inserted: CD63, Receptor Binding Domain (RBD)

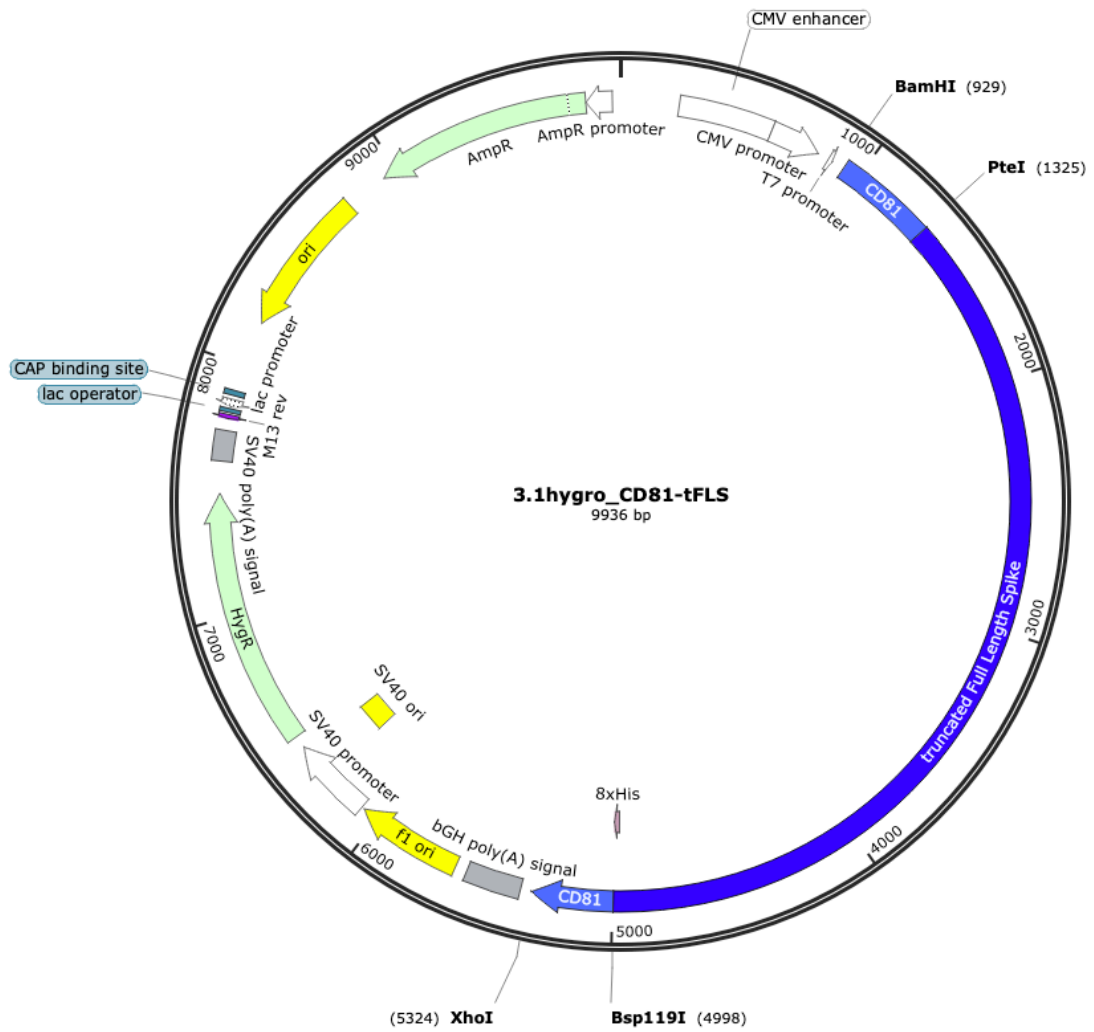
Restriction Site Insertion Points: BamHI, PteI, Bsp119I, XhoI



Construct Name: CD63_NC

Gene(s) Inserted: CD63, Nucleocapsid (NC)

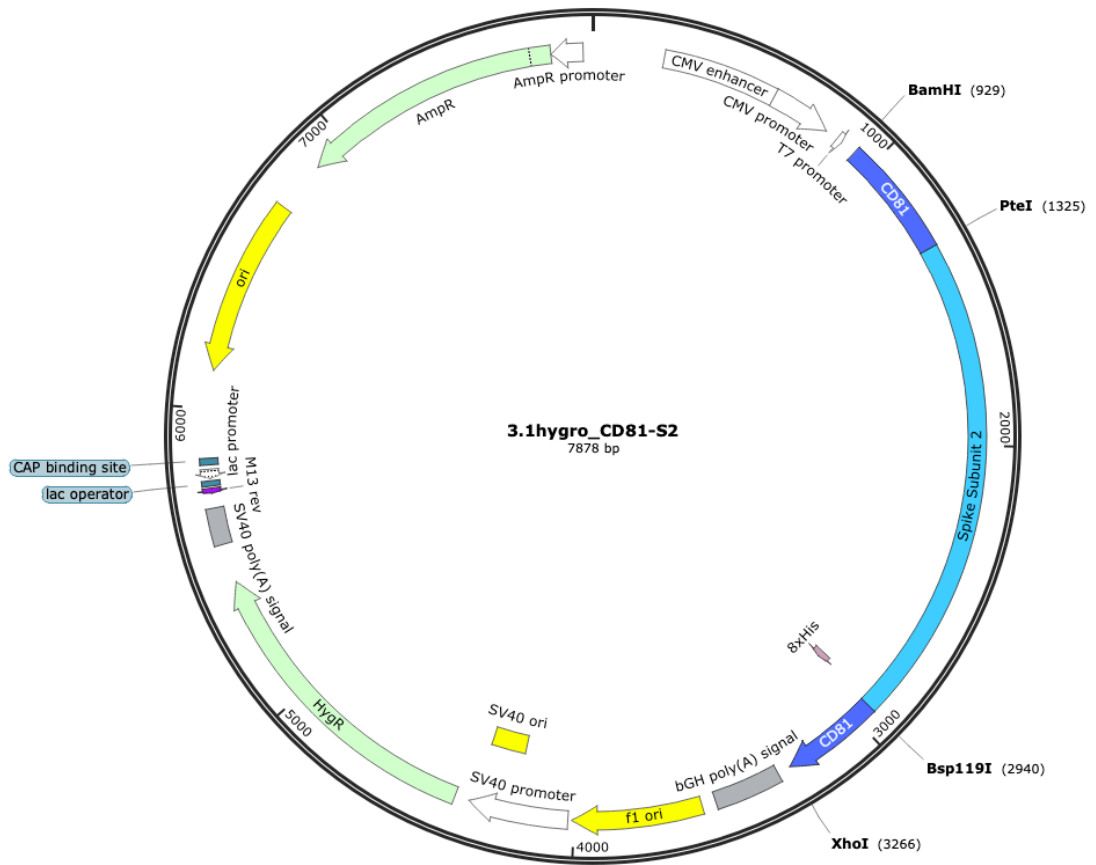
Restriction Site Insertion Points: BamHI, PteI, Bsp119I, XhoI



Construct Name: CD81_tFLS

Gene(s) Inserted: CD81, truncated Full Length Spike

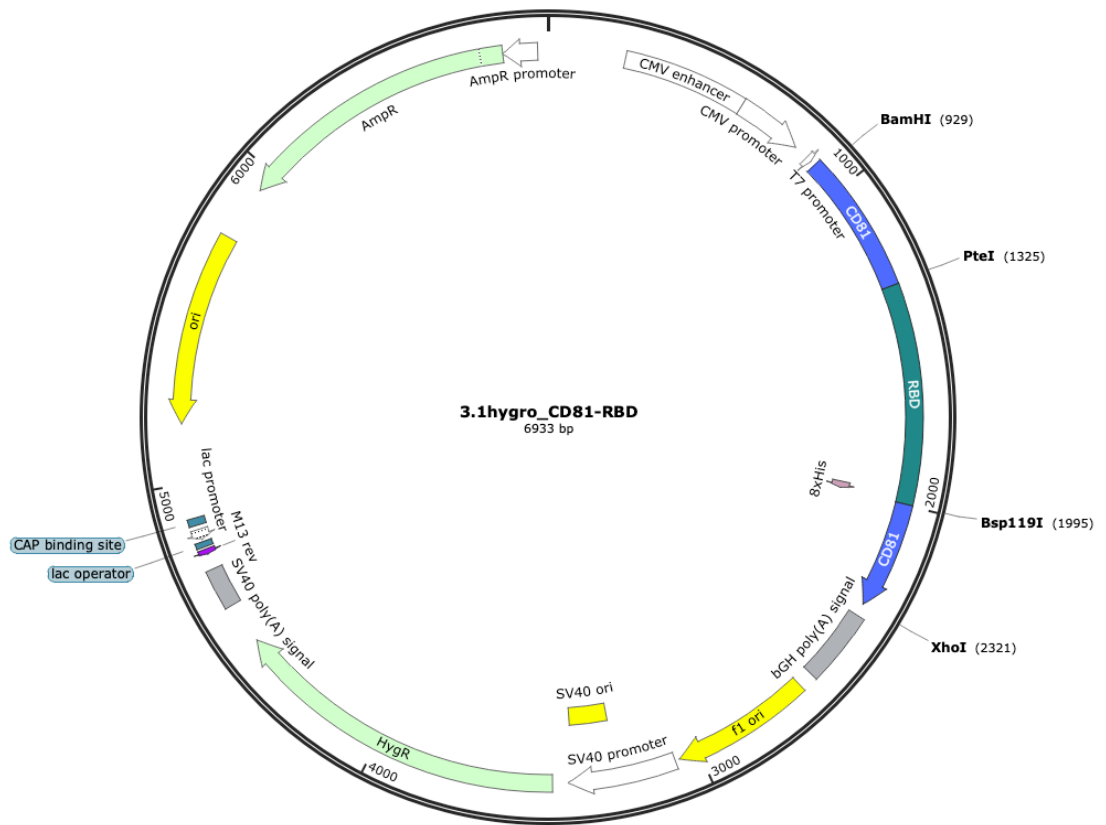
Restriction Site Insertion Points: BamHI, PteI, Bsp119I, XhoI



Construct Name: CD81_S2

Gene(s) Inserted: CD81, Spike Subunit 2 (S2)

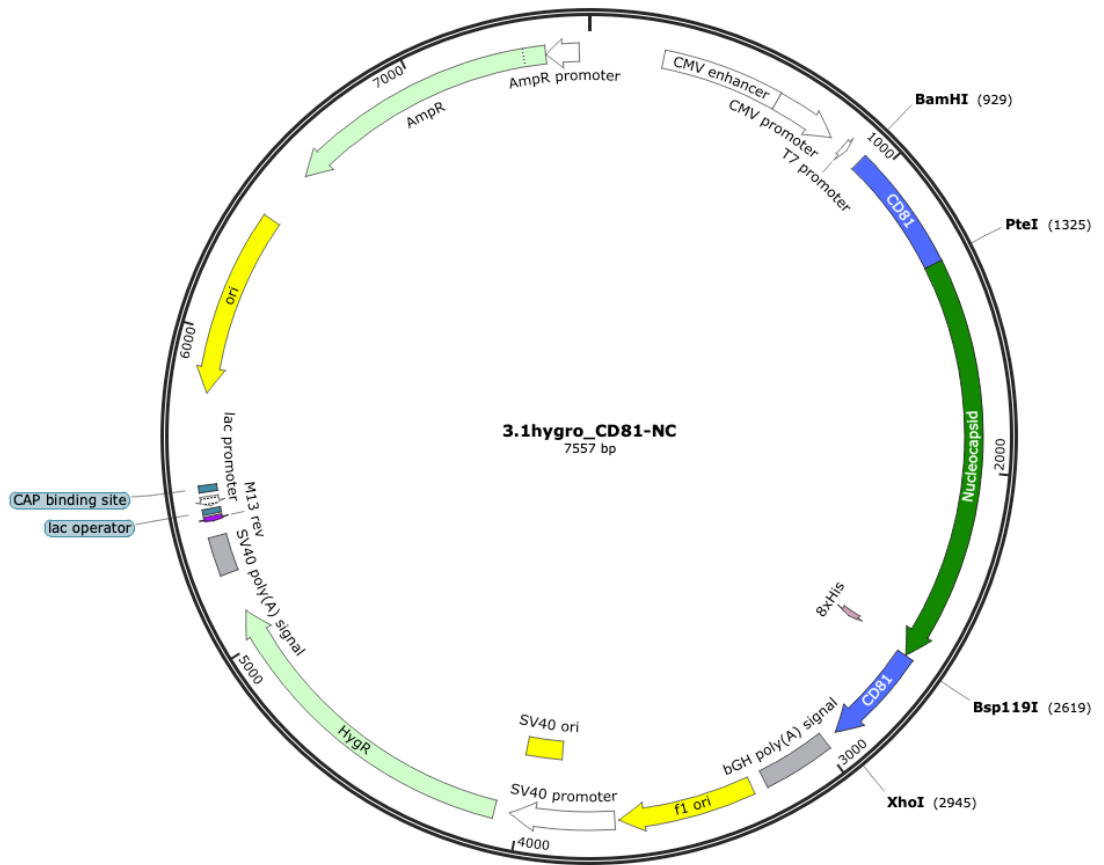
Restriction Site Insertion Points: BamHI, PteI, Bsp119I, XhoI



Construct Name: CD81_RBD

Gene(s) Inserted: CD81, Receptor Binding Domain (RBD)

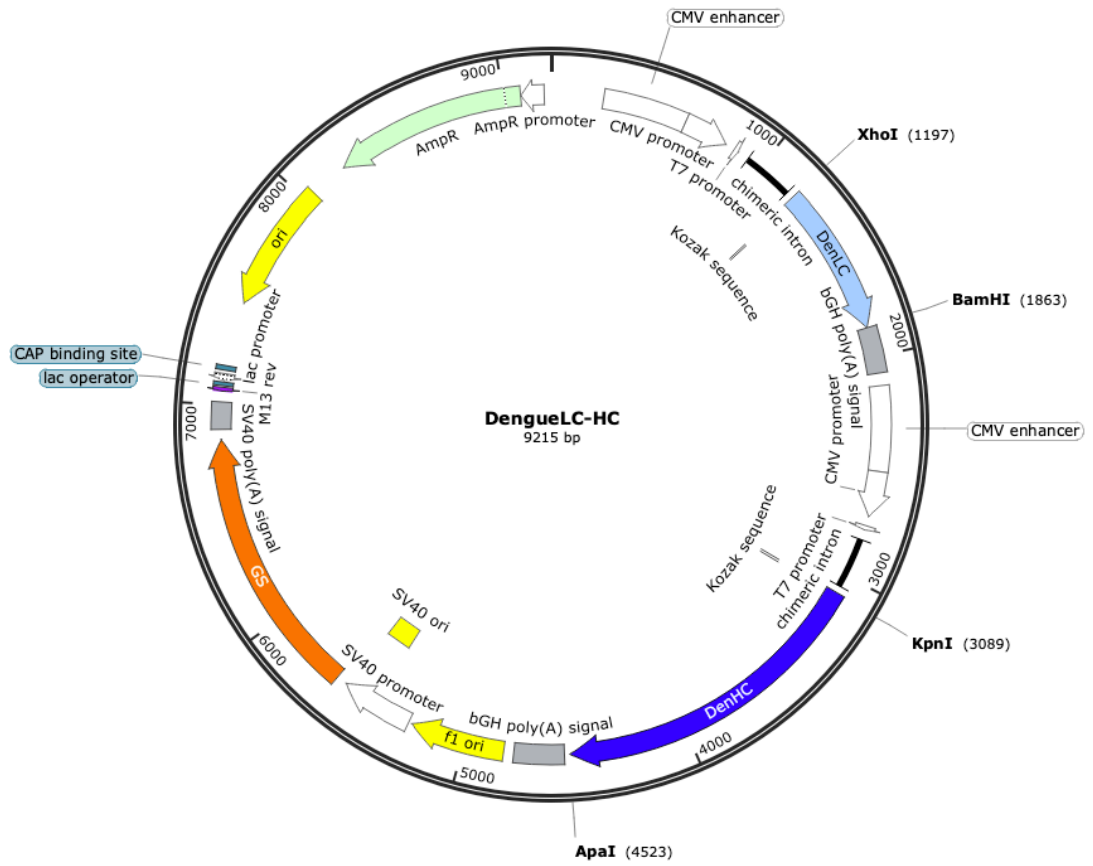
Restriction Site Insertion Points: BamHI, PteI, Bsp119I, XhoI



Construct Name: CD81_NC

Gene(s) Inserted: CD81, Nucleocapsid (NC)

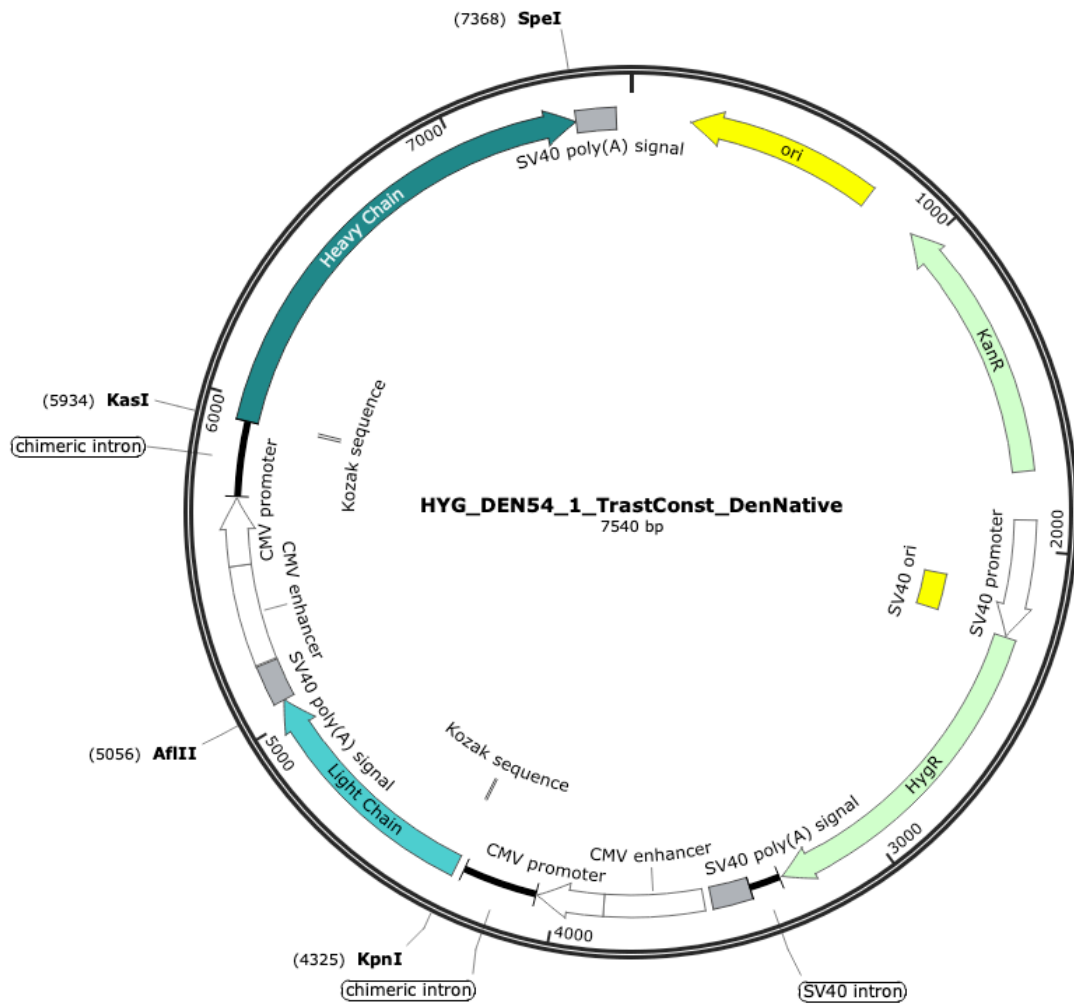
Restriction Site Insertion Points: BamHI, PteI, Bsp119I, XhoI



Construct Name: Den54 (native)

Gene(s) Inserted: Den54 native Light Chain, Den54 native Heavy Chain

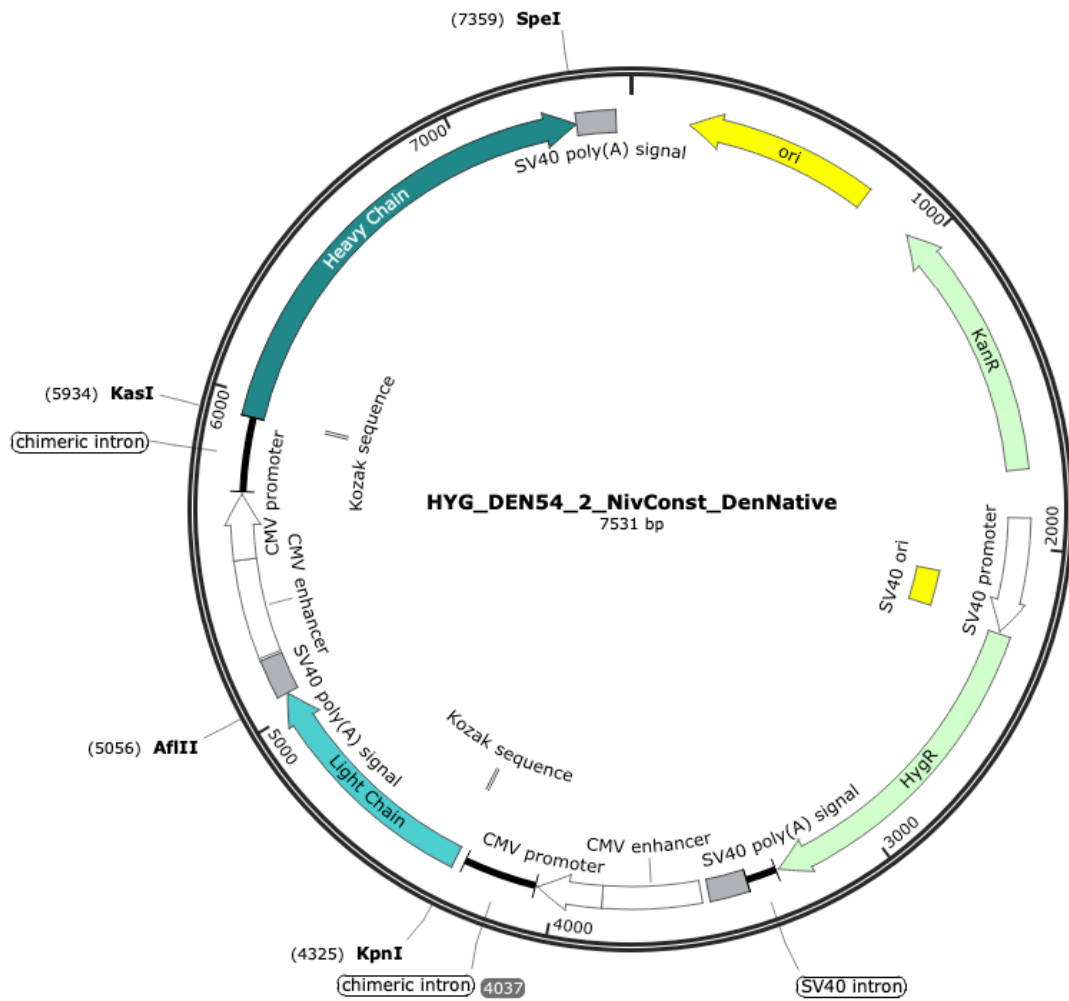
Restriction Site Insertion Points: XhoI, BamHI, KpnI, ApaI



Construct Name: Den1

Gene(s) Inserted: Den54_LC1/2, Den54_HC1

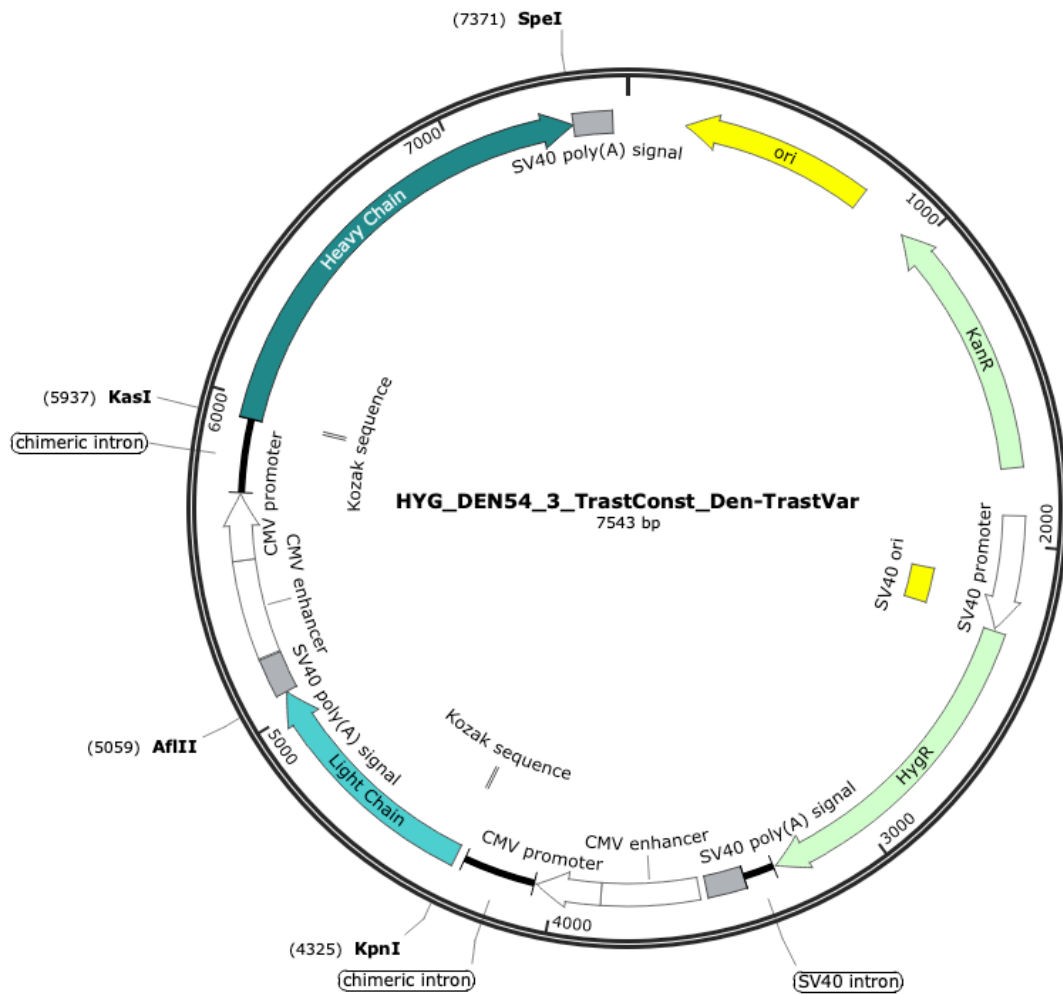
Restriction Site Insertion Points: KpnI, AflII, KasI, SpeI



Construct Name: Den2

Gene(s) Inserted: Den54_LC1/2, Den54_HC2

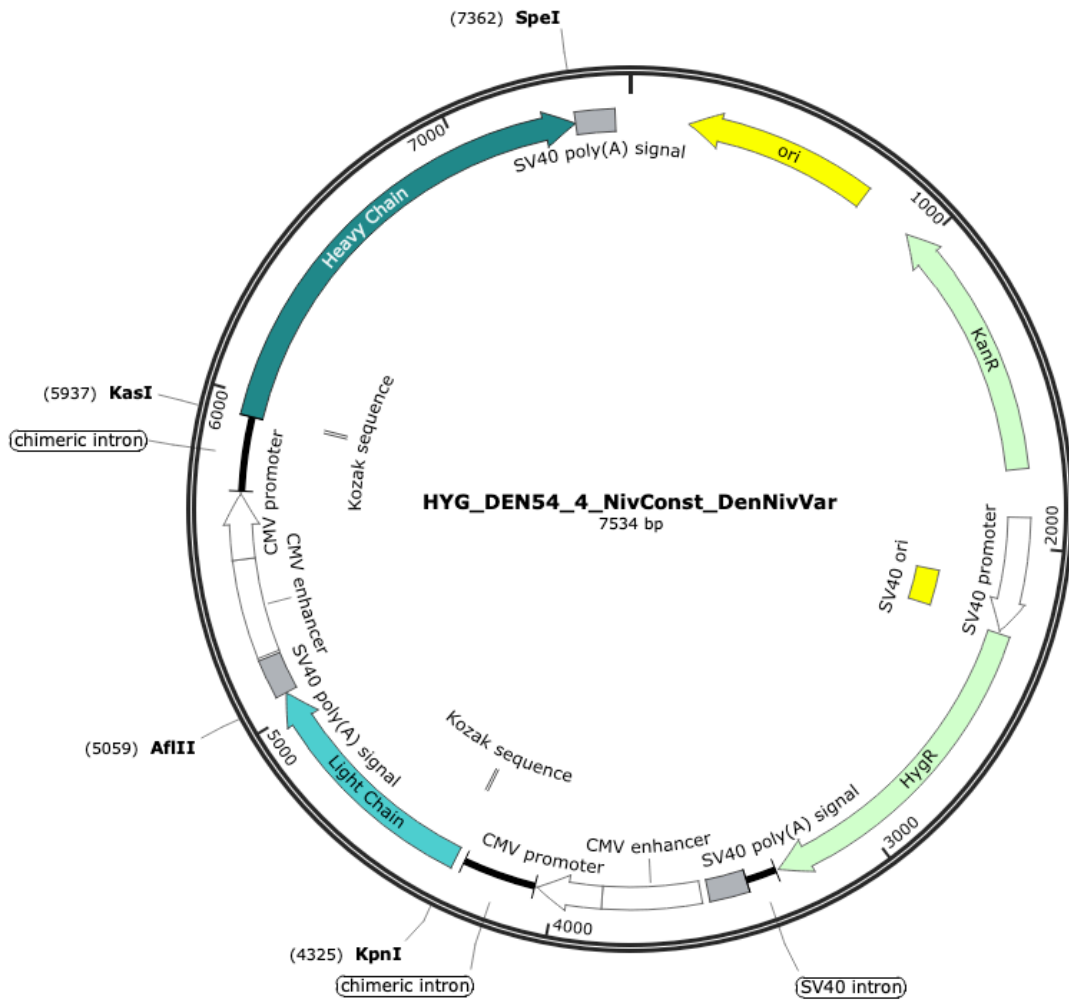
Restriction Site Insertion Points: KpnI, AflII, KasI, SpeI



Construct Name: Den3

Gene(s) Inserted: Den54_LC3, Den54_HC3

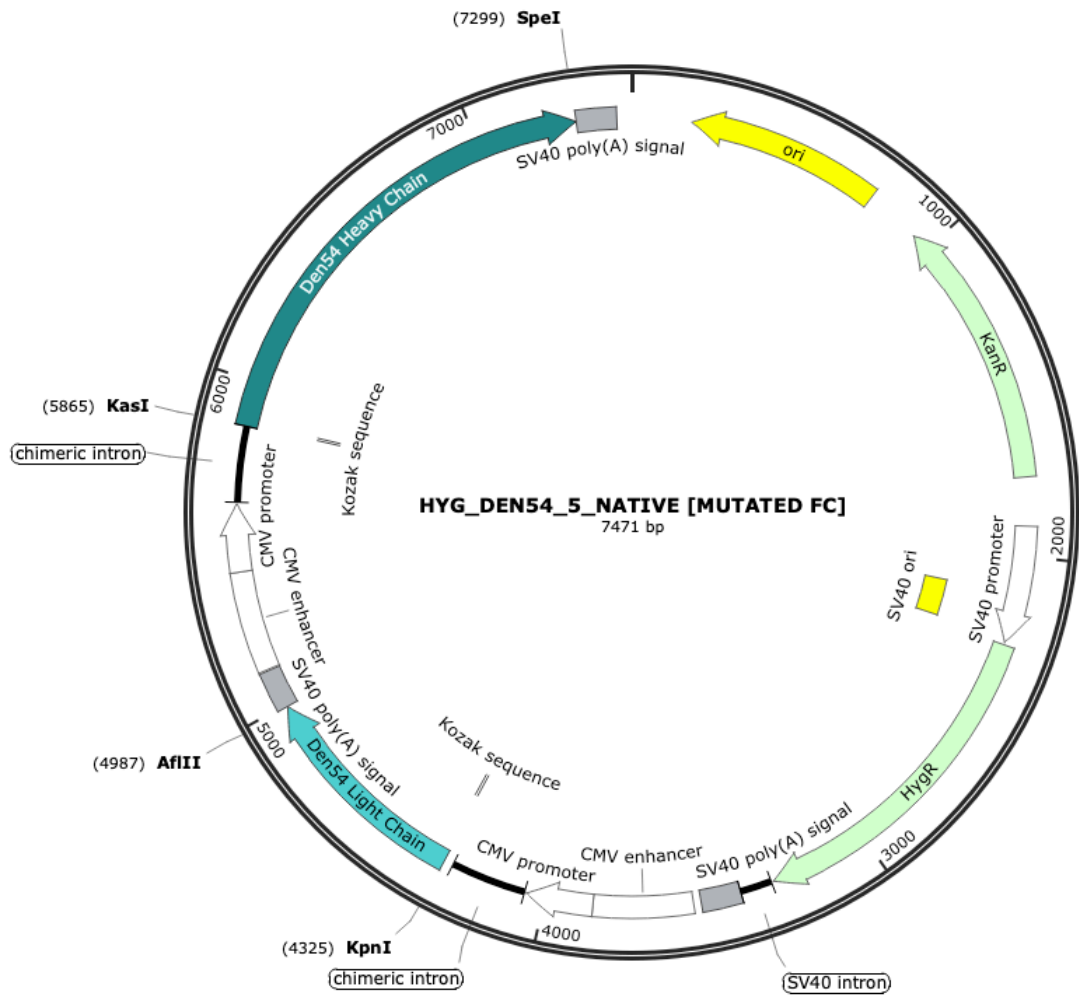
Restriction Site Insertion Points: KpnI, AflII, KasI, SpeI



Construct Name: Den4

Gene(s) Inserted: Den54_LC4, Den54_HC4

Restriction Site Insertion Points: KpnI, AflII, KasI, SpeI



Construct Name: Den5

Gene(s) Inserted: Den54_LC5, Den54_HC5

Restriction Site Insertion Points: KpnI, AflII, KasI, SpeI

Gene Sequences

>GFP

ATGGTGAGCAAGGGCGAGGAGCTGTTCACCGGGTGGTGCCCATCCTGGTTCGAGCTGGA
CGGCGACGTAAACGGCCACAAGTTCAGCGTGTCCGGCGAGGGCGAGGGCGATGCCACCT
ACGGCAAGCTGACCCTGAAGTTCATCTGCACCACCGGCAAGCTGCCCGTGCCCTGGCCCAC
CCTCGTGACCACCTGACCTACGGCGTGCAGTGCTTCAGCCGCTACCCCGACCACATGAAG
CAGCACGACTTCTTCAAGTCCGCCATGCCC GAAGGCTACGTCCAGGAGCGCACCATCTTCT
TCAAGGACGACGGCAACTACAAGACCCGCGCCGAGGTGAAGTTCGAGGGCGACACCCTG
GTGAACCGCATCGAGCTGAAGGGCATCGACTTCAAGGAGGACGGCAACATCCTGGGGCA
CAAGCTGGAGTACA ACTACAACAGCCACAACGTCTATATCATGGCCGACAAGCAGAAGAA
CGGCATCAAGGTGAACTTCAAGATCCGCCACAACATCGAGGACGGCAGCGTGCAGCTCGC
CGACCACTACCAGCAGAACACCCCATCGGCGACGGCCCCGTGCTGCTGCCCGACAACCA
CTACCTGAGCACCCAGTCCGCCCTGAGCAAAGACCCCAACGAGAAGCGCGATCACATGGT
CCTGCTGGAGTTCGTGACCGCCGCCGGGATCACTCTCGGCATGGACGAGCTGTACAAG

>mCherry

ATGGTGAGCAAGGGCGAGGAGGATAACATGGCCATCATCAAGGAGTTCATGCGCTTCAA
GGTGCACATGGAGGGCTCCGTGAACGGCCACGAGTTCGAGATCGAGGGCGAGGGCGAG
GGCCGCCCTACGAGGGCACCCAGACCGCCAAGCTGAAGGTGACCAAGGGTGGCCCCCT
GCCCTTCGCTGGGACATCCTGTCCCCTCAGTTCATGTACGGCTCCAAGGCCTACGTGAAG
CACCCGCCGACATCCCCGACTACTTGAAGCTGTCCTTCCCCGAGGGCTTCAAGTGGGAGC
GCGTGATGAACTTCGAGGACGGCGGCGTGGTGACCGTGACCCAGGACTCCTCCCTGCAG
GACGGCGAGTTCATCTACAAGGTGAAGCTGCGCGGCACCAACTTCCCCTCCGACGGCCCC
GTAATGCAGAAGAAGACCATGGGCTGGGAGGCCTCCTCCGAGCGGATGTACCCGAGGA
CGGCGCCCTGAAGGGCGAGATCAAGCAGAGGCTGAAGCTGAAGGACGGCGGCCACTAC
GACGCTGAGGTCAAGACCACCTACAAGGCCAAGAAGCCCGTGCAGCTGCCCGGCGCCTAC
AACGTCAACATCAAGTTGGACATCACCTCCCACAACGAGGACTACCCATCGTGGAACAGT
ACGAACGCGCCGAGGGCCGCCACTCCACCGCGGCATGGACGAGCTGTACAAGTAG

>Ubiquitin

ATGCAAATCTTCGTGAAGACCCTGACCGGCAAGACCATCACCTAGAGGTGGAACCCAGT
GACACCATCGAGAATGTCAAGGCCAAGATCCAGGATAAGGAGGGCATCCCCCGACCA
GCAGCGACTCATCTTTGCCGGCAAGCAGCTGGAAGATGGCCGCACTCTTTCTGATTACAAC
ATCCAGAAAGAGTCCACCCTGCACCTGGTCCTCCGCCTCAGGGGTGGC

>Polyubiquitin

ATGCAAATCTTCGTGAAGACCCTGACCGGCAAGACCATCACCTAGAGGTGGAACCCAGT
GACACCATCGAGAATGTCAAGGCCAAGATCCAGGATAAGGAGGGCATCCCCCGACCA
GCAGCGACTCATCTTTGCCGGCAAGCAGCTGGAAGATGGCCGCACTCTTTCTGATTACAAC
ATCCAGAAAGAGTCCACCCTGCACCTGGTCCTCCGCCTCAGGGGTGGCATGCAGATTTTCG
TGAAGACCCTGACCGGCAAGACCATCACCTAGAGGTGGAACCCAGTGACACCATCGAGA
ATGTCAAGGCCAAGATCCAGGATAAGGAGGGCATCCCCCGACCAGCAGCGACTCATCT
TTGCCGGCAAGCAGCTGGAAGATGGCCGCACTCTTTCTGATTACAACATCCAGAAAGAGT
CCACCCTGCACCTGGTCCTCCGCCTCAGGGGTGGCATGCAGATTTTCGTGAAGACCCTGAC
CGGCAAGACCATCACCTAGAGGTGGAACCCAGTGACACCATCGAGAATGTCAAGGCCAA
GATCCAGGATAAGGAGGGCATCCCCCGACCAGCAGCGACTCATCTTTGCCGGCAAGCA
GCTGGAAGATGGCCGCACTCTTTCTGATTACAACATCCAGAAAGAGTCCACCCTGCACCTG
GTCCTCCGCCTCAGGGGTGGCATGCAGATTTTCGTGAAGACCCTGACCGGCAAGACCATC
ACCCTAGAGGTGGAACCCAGTGACACCATCGAGAATGTCAAGGCCAAGATCCAGGATAA
GGAGGGCATCCCCCGACCAGCAGCGACTCATCTTTGCCGGCAAGCAGCTGGAAGATGG
CCGCACTCTTTCTGATTACAACATCCAGAAAGAGTCCACCCTGCACCTGGTCCTCCGCCTCA
GGGGTGGCTATTAA

>CD63

ATGGCGGTGGAAGGAGGAATGAAGTGTGTCAAGTTTCTGCTCTACGTTCTCCTGCTGGCC
TTTTGCGCCTGTGCAGTGGCATTGATTGCCATTGGTGTAGCAGTTCAGGTTGTTTTGAATC
AGACCATCACCCGTGAGACTACGCCTGGCTCCCTGTTGCCTGTGGTCATCATTGCAGTGGG
CGCCTTCTTCTCCTGGTAGCCTTTGTGGGCTGCTGTGGGGCCTGCAAGGAGAACTACTGT
CTTATGATTACATTTGCCATCTTCTGTCTTATCATGCTAGTGGAGGTGGCTGTAGCCAT
TGCCGGCTATGTGTTTAGAGACAAGGTGAAGTCAGAGTTTAATAAGA ACTCCGGCAGCA
GATGCAAAATTACCTTAAAGACAACAAGACGGCCTTAGTTCTGGACGGATGGCAGAAGGA
ATTTGAGTGCTGTGGAGCTAACA ACTACACAGATTGGGAGAACATCACTGGTATGCCTAA

GGACCGAGTCCCTGATTCTGCTGCATCAACATCACTGTGGGCTGTGGAATTGATTTCAAG
GAAAACAAGATCCATACTCAGGGCTGCGTGGAGAATATAGGGGTCTGGCTGAGGAAGAA
TGTATTGCTGGTGGCTGCAGCAGCCCTGGGCATTGCTTTTGTGGAGATCCTGGGAATTATC
TTCTCTTGCTGTCTGGTGAAAAGTATCCGAAGTGGCTATGAAGTAATGTAG

>CD81

ATGGGGGTGGAGGGCTGCACCAAATGCATCAAATACCTGCTCTTCGTTTTCAATTCATCT
TCTGGCTGGCTGGAGGTGTGATCCTAGGTGTGGCTCTGTGGTTACGCCATGACCCACAGA
CCACCAGCCTGCTCTATCTGGAATTAGGAGACAGACCAGCACCCAGCACCTTCTATGTGGG
CATCTACATTCTCATTGCTGTGGGAGCTGTGATGATGTTTGTGGGCTTCTGGGGTGCTAT
GGGGCCATCCAAGAGTCCCAGTGCCTGCTGGGGACGTTCTTCACCTGCCTTGTGATCCTGT
TTGCCTGTGAGGTGGCTGCTGGCATCTGGGGCTTCGTAAACAAAGACCAGATCGCCAAGG
ATGTGAAGCAGTTCTATGATCAAGCCCTTCAACAGGCTGTGGTGGATGACGATGCCAATA
ATGCCAAGGCTGTGGTGAAGACCTCCATGAGACGCTCAACTGCTGTGGCTCCAACGCACT
GACCGCACTGACCACCTCTGTGCTGAAGAACAGCCTGTGTCCCTCAGGCACCAACATATTC
AACTCCTTGATGAAGGAGGATTGCCATCAGAAAATCGATGAGCTCTTTTCTGGGAAGCTGT
ACCTCATTGGTATTGCGGCCATCGTGGTAGCTGTCATCATGATCTTCGAGATGATTCTGAG
CATGGTGTGCTGTGGCATCCGGAACAGCTCCGTGTACTGA

>Tsg101

>CD63 (with inserted mid-gene restriction sites)

TATGGATCCATGGCGGTGGAAGGAGGAATGAAGTGTGTCAAGTTTCTGCTCTACGTTCTC
CTGCTGGCCTTTTGCCTGTGCAGTGGCATTGATTGCCATTGGTGTAGCAGTTCAGGTTG
TTTTGAATCAGACCATCACCCGTGAGACTACGCCTGGCTCCCTGTTGCCTGTGGTCATCATT
GCAGTGGGCGCCTTCTCCTCCTGGTAGCCTTTGTGGGCTGCTGTGGGGCCTGCAAGGAG
AACTACTGTCTTATGATTACATTTGCCATCTCCTGTCTCTTATCATGCTAGTGGAGGTGGC
TGTAGCCATTGCCGGCTATGTGTTTAGAGACAAGGTGAAGTCAGAGTTTAATAAGAACTTC
CGGCAGCAGATGCAAAATTACCTTAAAGACAACAAGACGGCCGCGCGGTAAGGGAGT
AGCTTTCGAATTAGTTCTGGACGGATGGCAGAAGGAATTTGAGTGTGCTGTGGAGCTAACAA
CTACACAGATTGGGAGAACATCACTGGTATGCCTAAGGACCGAGTCCCTGATTCCTGCTGC

ATCAACATCACTGTGGGCTGTGGAATTGATTTCAAGGAAAACAAGATCCATACTCAGGGCT
GCGTGGAGAATATAGGGGTCTGGCTGAGGAAGAATGTATTGCTGGTGGCTGCAGCAGCC
CTGGGCATTGCTTTTGTGGAGATCCTGGGAATTATCTTCTCTTGCTGTCTGGTGAAAAGTAT
CCGAAGTGGCTATGAAGTAATGTAGCTCGAGTAT

>CD81 (with inserted mid-gene restriction sites)

TATGGATCCATGGGGGTGGAGGGCTGCACCAAATGCATCAAATACCTGCTCTTCGTTTTCA
ATTTTCATCTTCTGGCTGGCTGGAGGTGTGATCCTAGGTGTGGCTCTGTGGTTACGCCATGA
CCCACAGACCACCAGCCTGCTCTATCTGGAATTAGGAGACAGACCAGCACCCAGCACCTTC
TATGTGGGCATCTACATTCTATTGCTGTGGGAGCTGTGATGATGTTTGTGGGCTTCCTGG
GGTGCTATGGGGCCATCCAAGAGTCCCAGTGCCTGCTGGGGACGTTCTTCACCTGCCTTGT
GATCCTGTTTGCCTGTGAGGTGGCTGCTGGCATCTGGGGCTTCGTAAACAAAGACCAGAT
CGCCAAGGATGTGAAGCAGTTCTATGATCAAGCCGCGCGGTAAGGGAGTAGCTTTTCGA
ACTTCAACAGGCTGTGGTGGATGACGATGCCAATAATGCCAAGGCTGTGGTGAAGACCTT
CCATGAGACGCTCAACTGCTGTGGCTCCAACGCACTGACCGCACTGACCACCTCTGTGCTG
AAGAACAGCCTGTGTCCCTCAGGCACCAACATATTCAACTCCTTGATGAAGGAGGATTGCC
ATCAGAAAATCGATGAGCTCTTTTCTGGGAAGCTGTACCTCATTGGTATTGCGGCCATCGT
GGTAGCTGTCATCATGATCTTCGAGATGATTCTGAGCATGGTGCTGTGCTGTGGCATCCGG
AACAGCTCCGTGTACTIONACTCGAGTAT

>tFLS

ATGGTGAATCTGACCACCAGAACACAGCTGCCTCCAGCCTACACCAACAGCTTCACCAGAG
GCGTGTACTACCCCGACAAGGTGTTCCGGTCCTCCGTGCTGCATTCTACCCAGGATCTGTT
CCTGCCTTTCTTCAGCAACGTGACCTGGTTCACGCCATCCATGTGTCTGGCACCAACGGC
ACCAAGAGATTCGACAACCCCGTGCTGCCTTTCAACGACGGGGTGTACTTTGCCTCCACCG
AGAAGTCCAACATCATCAGAGGCTGGATCTTCGGCACCACACTGGACAGCAAGACCCAGA
GCCTGCTGATCGTGAACAACGCCACCAACGTGGTCATCAAAGTGTGCGAGTTCCAGTTCTG
CAACGACCCCTTCTGGGCGTCTACTACCACAAGAACAACAAGTCTGGATGGAATCCGA
GTTCCGGGTGTACTIONACTCCGCCAACACTIONACTGCACCTTCGAGTACGTGTCCCAGCCTTTCTGA
TGACCTGGAAGGCAAGCAGGGCAACTTCAAGAACCTGCGCGAGTTCGTGTTCAAGAACA
TCGACGGCTACTTCAAATCTACTCCAAGCACACCCCTATCAACCTCGTGCGGGATCTGCCT
CAGGGCTTCTCTGCTCTGGAACCCCTGGTGGATCTGCCATCGGCATCAACATCACCCGGT

TTCAGACCCTGCTGGCCCTGCACCGGTCTTATTTGACCCCTGGCGACTCCTCTTCTGGCTGG
ACTGCTGGTGCTGCCGCTTACTACGTGGGCTACCTGCAGCCTAGAACCTTCTGCTGAAGT
ACAACGAGAATGGCACCATCACCGACGCCGTGGACTGTGCTCTTGACCCTCTGTCCGAGAC
AAAGTGACCCTGAAGTCCTTACCGTGGAAAAGGGCATCTACCAGACCTCCAACCTCCGG
GTGCAGCCCACCGAGTCTATCGTGCGGTTCCCTAACATCACCAACCTGTGTCCTTTCCGGC
AGGTGTTCAATGCCACCAGATTCGCTCTGTGTACGCCTGGAACCGGAAGCGGATCTCTAA
CTGCGTGGCCGACTACAGCGTGCTGTACAACCTCCGCCTCCTTACGACCTTCAAGTGCTAC
GGCGTGTCCCCTACCAAGCTGAACGACCTGTGCTTCACAAACGTGTACGCCGACTCCTTCG
TGATCCGGGGAGATGAAGTGCGGCAGATCGCTCCTGGACAGACCGGCAAGATCGCCGAT
TACAACATAAGCTGCCCAGACTTCACCGGCTGTGTGATCGCTTGGAACTCCAACAACC
TGGACTCCAAAGTCGGCGGCAACTACAACCTGTACCGGCTGTTCCGGAAGTCTAACCT
GAAGCCTTTCGAGCGGGACATCTCCACCGAAATCTACCAGGCTGGCAGCACCCCTTGCAAC
GGCGTGAAGGCTTCAACTGCTACTTCCACTGCAGTCCTACGGCTTTCAGCCCACCAATG
GCGTGGGCTATCAGCCCTATAGAGTGGTGGTGCTGTCTTCGAGCTGCTGCATGCTCCTGC
TACCGTGTGCGGCCCTAAGAAATCCACCAATCTGGTCAAGAACAATGCGTGAACCTCAAC
TTCAACGGCCTGACCGGCACAGGCGTGCTGACAGAGTCCAACAAGAAGTTCCTGCCATTC
CAGCAGTTCGGCCGGATATCGCCGATACCACAGACGCCGTCAGAGATCCCCAGACACTG
GAAATCCTGGACATCACCCCTTGTTCTTCGGCGGAGTGTCTGTGATCACCCCAGGCACCA
ACACCTTAACCAGGTGGCCGTGCTGTATCAGGACGTGAACTGTACCGAGGTGCCCGTGG
CTATCCATGCCGATCAGCTGACCCCTACATGGCGCGTGTACTCCACCGGCTCCAACGTGTT
CCAGACAAGAGCTGGCTGTCTGATCGGCGCTGAGCACGTGAACAATTCCTACGAGTGCGA
CATCCCCATCGGAGCCGGAATCTGCGCCTTTATCAGACCCAGACCAACTCTCCTGGCTCC
GCCTCTTCTGTGGCCAGCCAGTCTATCATTGCTTACACCATGAGCCTGGGCGCCGAGA
CTGTGGCCTACAGCAACAACCTCTATCGCTATCCCCACCAACTTCACCATCTCCGTGACAACC
GAGATCCTGCCTGTGTCCATGACCAAGACCAGCGTGGACTGCACCATGTACATCTGCGGC
GACTCTACCGAGTGTCCAACCTGCTGCTGCAGTACGGCTCCTTCTGCACCCAGCTGAATA
GAGCCCTGACCGGAATCGCCGTGGAACAGGACAAGAACACCCAAGAGGTGTTCCGCCAA
GTGAAGCAAATCTACAAGACCCCTCCTATCAAGGACTTCGGCGGCTTCAATTTCTCCAGA
TTCTGCCCGATCCTAGCAAGCCCTCCAAGCGGTCTTTCATCGAGGACCTGCTGTTCAACAA
AGTGACACTGGCCGACGCCGGCTTCATCAAGCAGTATGGCGATTGCCTGGGCGACATTGC
CGCCAGGGATCTGATCTGTGCCAGAAGTTTAAACGGACTGACAGTGTGCCTCCTCTGCTG
ACCGATGAGATGATCGCCCAGTACACCTCCGCACTGCTGGCTGGCACAATCACCTCTGGAT

GGACATTTGGCGCTGGCGCCGCTCTGCAGATCCCTTTCGCTATGCAGATGGCCTACCGGTT
CAACGGCATCGGCGTGACCCAGAATGTGCTGTACGAGAACCAGAAGCTGATCGCCAACCA
GTTCAACAGCGCCATCGGAAAGATCCAGGACAGCCTGTCCAGCACCGCTTCTGCCCTGGG
AAAGCTGCAGGATGTGGTCAACCAGAACGCTCAGGCCCTGAACACCCTGGTCAAGCAGCT
GTCCTCTAACTTCGGCGCCATCTCCTCTGTGCTGAACGATATCCTGAGCCGGCTGGACCCTC
CTGAGGCTGAGGTGCAGATCGACAGACTGATCACCGGCAGACTGCAGAGCCTCCAGACCT
ATGTGACCCAGCAGCTGATCAGAGCCGCCGAGATTAGAGCCTCTGCCAATCTGGCCGCCA
CCAAGATGTCTGAGTGTGTGCTGGGCCAGTCCAAGAGAGTGGACTTTTGGCGCAAGGGCT
ACCACCTGATGAGCTTCCCTCAGTCTGCTCCTCACGGCGTGGTGTTCCTGCACGTGACATAC
GTGCCCCTCAAGAGAAGAAGTTTACCACCGCTCCTGCCATCTGCCACGACGGCAAGGCTC
ACTTTCTAGAGAAGGCGTGTTTCGTGTCTAACGGCACCCATTGGTTCGTGACACAGCGGAA
CTTCTACGAGCCCCAGATCATCACCACCGACAACACCTTTGTGTCCGGCAACTGCGACGTC
GTGATCGGAATTGTGAACAATACCGTGTACGACCCTCTGCAGCCCAGCTGGACTCCTTCA
AAGAGGAACTGGACAAGTACTTTAAGAACCACACAAGCCCCGACGTGGACCTGGGAGAC
ATCTCTGGCATCAACGCCTCCGTGGTCAACATCCAGAAAGAGATCGACCGGCTGAACGAG
GTGGCCAAGAATCTGAACGAGTCCCTGATCGACCTGCAAGAACTGGGGAAGTACGAGCA
GTCTAGACACCACCACCATCACCATCATCACTGA

>S1

ATGGGCGTGCACTCCGTGAATCTGACCACCAGAACACAGCTGCCTCCAGCCTACACCAACA
GCTTACCAGAGGCGTGTACTACCCCGACAAGGTGTTCCGGTCCTCCGTGCTGCATTCTAC
CCAGGATCTGTTCTGCCTTTCTTACGCAACGTGACCTGGTTCCACGCCATCCATGTGTCTG
GCACCAACGGCACCAAGAGATTCGACAACCCCGTGTGCCTTTCAACGACGGGGTGTACT
TTGCCTCCACCGAGAAGTCCAACATCATCAGAGGCTGGATCTTCGGCACCACTGGACAG
CAAGACCCAGAGCCTGCTGATCGTGAACAACGCCACCAACGTGGTCATCAAAGTGTGCGA
GTTCCAGTTCTGCAACGACCCCTTCCCTGGGCGTCTACTACCACAAGAACAACAAGTCTGG
ATGGAATCCGAGTTCGGGTGTACTCCTCCGCCAACAACTGCACCTTCGAGTACGTGTCCC
AGCCTTTCCTGATGGACCTGGAAGGCAAGCAGGGCAACTTCAAGAACCTGCGCGAGTTCCG
TGTTCAAGAACATCGACGGCTACTTCAAATCTACTCCAAGCACACCCTATCAACCTCGTG
CGGGATCTGCCTCAGGGCTTCTCTGCTCTGGAACCCCTGGTGGATCTGCCATCGGCATCA
ACATCACCCGGTTTCAGACCCTGCTGGCCCTGCACCGGTCTTATTTGACCCCTGGCGACTCC
TCTTCTGGCTGGACTGCTGGTGTGCTGCCGCTTACTACGTGGGCTACCTGCAGCCTAGAACCT

TCCTGCTGAAGTACAACGAGAATGGCACCATCACCGACGCCGTGGACTGTGCTCTTGACCC
TCTGTCCGAGACAAAGTGCACCCTGAAGTCCTTACCCTGGAAAAGGGCATCTACCAGAC
CTCCAACCTCCGGGTGCAGCCCACCGAGTCTATCGTGCGGTTCCCTAACATCACCAACCTGT
GTCCTTTCGGCGAGGTGTTCAATGCCACCAGATTGCGCTCTGTGTACGCCTGGAACCGGAA
GCGGATCTCTAACTGCGTGGCCGACTACAGCGTGCTGTACAACCTCCGCCTCCTTCAGCACC
TTCAAGTGCTACGGCGTGTCCTACCAAGCTGAACGACCTGTGCTTCACAAACGTGTACG
CCGACTCCTTCGTGATCCGGGGAGATGAAGTGCGGCAGATCGCTCCTGGACAGACCGGCA
AGATCGCCGATTACAACCTACAAGCTGCCCGACGACTTACCCTGGTGTGTGATCGCTTGAA
CTCCAACAACCTGGACTCCAAAGTCGGCGGCAACTACAACCTACCTGTACCGGCTGTTCCGG
AAGTCTAACCTGAAGCCTTTCGAGCGGGACATCTCCACCGAAATCTACCAGGCTGGCAGC
ACCCCTTGCAACGGCGTGGAAGGCTTCAACTGCTACTTCCCACTGCAGTCTACGGCTTTC
AGCCACCAATGGCGTGGGCTATCAGCCCTATAGAGTGGTGGTGTGCTGCTCCTTCGAGCTGC
TGCATGCTCCTGCTACCGTGTGCGGCCCTAAGAAATCCACCAATCTGGTCAAGAACAATG
CGTGAACCTTCAACTTCAACGGCCTGACCGGCACAGGCGTGCTGACAGAGTCCAACAAGAA
GTTCTGCCATTCCAGCAGTTCGGCCGGGATATCGCCGATACCACAGACGCCGTCAGAGAT
CCCAGACTGGAATCCTGGACATCACCCCTTGTTCCTTCGGCGGAGTGTCTGTGATCA
CCCAGGCACCAACACCTCTAACCAGGTGGCCGTGCTGTATCAGGACGTGAACTGTACCG
AGGTGCCCGTGGCTATCCATGCCGATCAGCTGACCCCTACATGGCGCGTGTACTCCACCGG
CTCCAACGTGTTCCAGACAAGAGCTGGCTGTCTGATCGGCGTGAGCACGTGAACAATTCC
TACGAGTGCGACATCCCCATCGGAGCCGGAATCTGCGCCTCTTATCAGACCCAGACCAACT
CTCCTGGCTCCCACCACCACCATCACCATCATCACTGA

>S2

ATGGCCTCTTCTGTGGCCAGCCAGTCTATCATTGCTTACACCATGAGCCTGGGCGCCGAGA
ACTCTGTGGCCTACAGCAACAACCTCTATCGCTATCCCCACCAACTTCACCATCTCCGTGACA
ACCGAGATCCTGCCTGTGTCCATGACCAAGACCAGCGTGGACTGCACCATGTACATCTGCG
GCGACTCTACCGAGTGTCCAACCTGCTGCTGCAGTACGGCTCCTTCTGCACCCAGCTGAA
TAGAGCCCTGACCGGAATCGCCGTGGAACAGGACAAGAACACCCAAGAGGTGTTCGCCC
AAGTGAAGCAAATCTACAAGACCCCTCCTATCAAGGACTTCGGCGGCTTCAATTTCTCCCA
GATTCTGCCCGATCCTAGCAAGCCCTCAAGCGGTCTTTCATCGAGGACCTGCTGTTCAAC
AAAGTGACACTGGCCGACCGGCTTCATCAAGCAGTATGGCGATTGCCTGGGCGACATT
GCCGCCAGGGATCTGATCTGTGCCAGAAGTTTAAACGGACTGACAGTGCTGCCTCCTCTGC

TGACCGATGAGATGATCGCCCAGTACACCTCCGCACTGCTGGCTGGCACAATCACCTCTGG
ATGGACATTTGGCGCTGGCGCCGCTCTGCAGATCCCTTTCGCTATGCAGATGGCCTACCG
TTCAACGGCATCGGCGTGACCCAGAATGTGCTGTACGAGAACCAGAAGCTGATCGCCAAC
CAGTTCAACAGCGCCATCGGAAAGATCCAGGACAGCCTGTCCAGCACCGCTTCTGCCCTG
GGAAAGCTGCAGGATGTGGTCAACCAGAACGCTCAGGCCCTGAACACCCTGGTCAAGCA
GCTGTCCTCTAACTTCGGCGCCATCTCCTCTGTGCTGAACGATATCCTGAGCCGGCTGGAC
CCTCTGAGGCTGAGGTGCAGATCGACAGACTGATCACCGGCAGACTGCAGAGCCTCCAG
ACCTATGTGACCCAGCAGCTGATCAGAGCCGCCGAGATTAGAGCCTCTGCCAATCTGGCC
GCCACCAAGATGTCTGAGTGTGTGCTGGGCCAGTCCAAGAGAGTGGACTTTTTCGGCAAG
GGCTACCACCTGATGAGCTTCCCTCAGTCTGCTCCTCACGGCGTGGTGTCTGCACGTGA
CATACGTGCCCGCTCAAGAGAAGAAGTTTACCACCGCTCCTGCCATCTGCCACGACGGCAA
GGCTCACTTTCCTAGAGAAGGCGTGTTTCGTGTCTAACGGCACCCATTGGTTCGTGACACAG
CGAACTTCTACGAGCCCCAGATCATCACCACCGACAACACCTTTGTGTCCGGCAACTGCG
ACGTCGTGATCGGAATTGTGAACAATACCGTGTACGACCCTCTGCAGCCCGAGCTGGACTC
CTTCAAAGAGGAACTGGACAAGTACTTTAAGAACCACACAAGCCCCGACGTGGACCTGGG
AGACATCTCTGGCATCAACGCCTCCGTGGTCAACATCCAGAAAGAGATCGACCGGCTGAA
CGAGGTGGCCAAGAATCTGAACGAGTCCCTGATCGACCTGCAAGAACTGGGGAAGTACG
AGCAGTCTAGACACCACCACCATCACCATCATCACTGA

>RBD

ATGCCCAATATCACCAACCTGTGTCCTTTCGGCGAGGTGTTCAACGCCACCAGATTCGCCTC
TGTGTACGCCTGGAACCGGAAGCGGATCTCTAACTGCGTGGCCGACTACTCCGTGCTGTA
CAACTCCGCCTCCTTCAGCACCTTCAAGTGCTACGGCGTGTCCCCTACCAAGCTGAACGAC
CTGTGCTTACCAACGTGTACGCCGACTCCTTCGTGATCAGAGGCGACGAAGTGCGGCAG
ATCGTCTCTGGACAGACCGGCAAGATCGCCGACTACAACACTACAAGCTGCCCGACGACTC
ACCGGCTGTGTGATCGCTTGGAACCTCAACAACCTGGACTCCAAAGTCGGCGGCAACTAC
AATTACCTGTACCGGCTGTTCCGGAAGTCCAACCTGAAGCCTTTCGAGCGGGACATCTCCA
CCGAAATCTACCAGGCTGGCAGCACCCCTTGCAATGGCGTGGAAAGGCTTCAACTGCTACTT
CCCACTGCAGTCTACGGCTTCCAGCCTACAAACGGCGTGGGCTACCAGCCTTACAGAGTG
GTGGTGTGTCCTTCGAGCTGCTGCACGCTCCCTCTAGACACCACCATCATCACCATCACCA
CTGA

>NC

ATGTCGACAACGGCCCTCAGAACCAGAGAAACGCCCTCGGATCACCTTTGGCGGCCCT
AGTGATTCCACCGGCTCTAACCAGAACGGCGAGAGAAGCGGGCTCGGTCTAACAGAG
AAGGCCTCAGGGCCTGCCTAACACACCGCCTCTTGTTTACCGCTCTGACCCAGCACGGC
AAAGAGGACCTGAAGTTCCCTAGAGGACAGGGCGTGCCCATCAACACCAACTCTAGCCCT
GACGACCAGATCGGCTACTACAGACGGGCCACCAGAAGAATCAGAGGCGGGACGGCAA
GATGAAGGACCTGTCTCCTCGGTGGTACTTCTACTACCTCGGCACCGGACCAGAGGCTGG
ATTGCCTTATGGCGCCAACAAGGACGGCATCATCTGGGTTGCAACAGAGGGCGCTCTGAA
CACCCCTAAGGACCACATCGGCACCCGGAATCCTGCCAACAAATGCCGCTATTGTGCTGCAG
CTGCCACAGGGCACAACCCTGCCTAAGGGCTTTTACGCTGAGGGAAGCAGAGGCGGATCT
CAGGCCTCTTCCAGATCCAGCTCTCGGTCCAGAACTCCAGCCGGAATTCTACCCCTGGCT
CCTCTCGGGGAACCTCTCCTGCTAGAATGGCTGGCAATGGCGGAGATGCTGCTCTGGCTCT
GCTGCTGCTGGACAGACTGAACCAGCTGGAATCCAAGATGTCCGGCAAGGGCCAGCAGC
AACAGGGACAGACCGTGACCAAGAAGTCTGCCGCCGAGGCCTCCAAGAAGCCTAGACAG
AAGAGAACCGCCACCAAGGCCTACAACGTGACCCAGGCCTTTGGCAGAAGAGGCCCAGA
ACAGACCCAGGGCAACTTCGGCGATCAAGAGCTGATCAGACAGGGCACCGACTACAAGC
ACTGGCCTCAGATCGCCCAGTTTGCCCTTCTGCCTCTGCCTTCTTCGGCATGTCCCGGATC
GGCATGGAAGTGACCCCATCTGGCACCTGGCTGACCTATAACGGCGCCATCAAGCTGGAC
GACAAGGACCCCAACTTCAAGGACCAAGTGATCCTGCTGAACAAGCACATCGACGCCTAC
AAGACCTTTCCACCTACCGAGCCTAAGAAGGACAAGAAGAAGAAGGCCGACGAGACACA
GGCCCTGCCTCAGAGACAGAAAAAGCAGCAGACAGTGACCCTGCTGCCTGCCGCTGACCT
GGACGATTTCTCCAAGCAGCTCCAGCAGTCCATGTCTCCGCCGATTCTACCCAGGCTTCTA
GACACCACCATCATCACCATCACCCTGA

>Den54_HC

GTACCGCCACCATGGACTGGACTTGGAGAATCCTGTTTCGTGGTGGCTGCTGCTACCGGCG
TGCAGTCTCAGTTTCAAGTTGGTTTCAAGTCCGGCGCTGAAGTGAAGAAACCCGCCTCTCTGT
GAAGGTGTCCTGCAAGGCTTCTGGCGGCACCTTTGGAACCTACGCCATCTCCTGGGTCCGA
CAGGCTCCTGGCAAAGGCTTGGAAATGGATGGGCGGCATCATCCCTCTGTACAAGCAGTCC
ACCTACGCTCAGAAATTCGGGGCAGAGTGACCATCACCGCCGACGAGTCTACCAACACC
GCCTACATGGAAGTGAACGGCCTGAGCCTGGAAGATAACCGCCGTGTTCTACTGCGCTACCC
TGATTGCTGTGGCCGGCTCTGAAGGCGCTGGCTCTTTTGATATCTGGGGCCAGGGCACCA

TGGTCACCGTGTCTCTGCTTCTACCAAGGGACCCAGCGTGTTCCCTCTGGCTCCTTCCAGC
AAGTCTACCTCCGGTGGAACAGCTGCTCTGGGCTGCCTGGTCAAGGACTACTTTCCTGAGC
CAGTGACCGTGTCTTGGAACCTCCGGCGCTCTGACATCTGGCGTGACACCTTTCCAGCTGT
GCTGCAGTCTCCGGCCTGACTCTCTGTCCTCTGTCGTGACCGTGCCTTCCAGCTCTCTGG
GAACCCAGACCTACATCTGCAATGTGAACCACAAGCCTGGCAACACCAAGGTGGACAAGA
AGGACGAGCCCAAGTCTGCGACAAGACCCACACATGTCCTCCATGGCCTGCTCCAGAACT
GCTCGGAGGCCCTTCCGTGTTCTGTTTCTCCAAAGCCTAAGGACACCCTGATGATCTCTC
GGACCCCTGAAGTGACCTGCGTGGTGGTGGATGTGTCTCACGAGGACCCAGAAGTGAAG
TTCAACTGGAACGTGGACGGCGTGGAAGTGCAACAACGCCAAGACCAAGCCTAGAGAGGA
ACAGTACCAGAGCACCTACAGAGTGGTGTCCGTGCTGACCGTGTGACCCAGGATTGGAT
GAACGGCAAAGAGTACAAGTGCAAGGTGTCCAACAAGGCCCTGCCTGCTCCTATCGAAAA
GACCATCTCCAAGGCCAAGGGCCAGCCTAGGGAACCCAGGTTTACACCTTGCCTCCATCT
CGGGACGAGCTGACCAAGAACCAGGTGCCCTGACCTGTCTCGTGAAGGGCTTCTACCCC
TCCGATATCGCCGTGGAATGGGAGTCTAATGGCCAGCCTGAGAACAACCTACAAGACCACA
CCTCCTGTGCTGGACTCCGACGGCTCATTCTTCTGTACTCCAAGCTGACAGTGGACAAGT
CCAGATGGCAGCAGGGCAACGTGTTCTCCTGCTCCGTGATGCACGAGGCCCTGCACAATC
ACTACACACAGAAGTCCCTGTCTCTGTCCCCTGGCAAGTGAGGGCC

>Den54_LC

TCGAGGCCACCATGGCTTGGGCTCCTCTGCTGCTGACACTGCTGACTCAGGATACCGGCTC
CTGGGCTCAGTCTGCTTTGACCCAGCCTGCTTCCGTGTCTGGCTCTCCCGGCCAGTCTATCA
CCATCTCTTGTACCGGCACCTCTGGCGACGTCGGCGGAGATTCTCTGGTGTCTGGTATCA
GCAGCACCCCTGGCAAGGCCCTAAGCTGATCATCTACGAGGACCACAAGCGGCCTTCCGG
CGTGTCTCTAGATTCTTCGGCTCCAAGTCCGGCAACGCCGCCTCTCTGACAATTAGCGGA
CTGCAGGCTGAGGACGAGGCCGACTACTACTGCTGCTCCTACGCCATCTCTTCCGTGCGGG
TTTTGTTTGGCGGAGGCACCAAAGTGACCGTGTGGGACAACCTAAGGCCGCTCCTACCG
TGACACTGTTCCCTCCATCCTCCGAAGAACTGCAGGCCAACAAGGCTACCCTCGTGTGCCT
GATCTCCGACTTCTATCCTGGCGCTGTGACCGTGGCCTGGAAGGCTGATAGTTCTCCTGTG
AAGGCCGGCGTGGAACCACCACACCTTCCAAGCAGTCCAACAACAAATACGCCGCCAGC
TCCTACCTGTCTCTGACCCCTGAACAGTGGAAGTCCCACAGATCCTACAGCTGCTGAGGAT
C

>Den_LC1/2

GTACCGCCACCATGGACATGAGAGTGCCTGCTCAGCTGCTGGGACTGCTGCTGTTGTGGT
TGTCTGGCGCTAGATGCCAGAGCGCCTTGACACAGCCTGCCTCTGTGTCTGGATCTCCCGG
CCAGTCCATCACCATCTTGTACCGGAACCTCTGGCGACGTCGGCGGAGATTCTCTGGTG
TCCTGGTATCAGCAGCACCTGGCAAGGCCCTAAGCTGATCATCTACGAGGACCACAAG
CGGCCTCCGGCGTGTCTCTAGATTCTTCGGCTCCAAGTCGGCAACGCCGCTCTCTGA
CAATTAGCGGACTGCAGGCTGAGGACGAGGCCGACTACTACTGCTGCTCCTACGCCATCTC
TTCCGTGCGGGTTTTGTTTGGCGGAGGCACCAAAGTGACCGTGCTGGGACAACCAGCTGC
TCCCTCCGTGTTTCATCTTCCCACCTTCCGACGAGCAGCTGAAGTCTGGCACAGCCTCTGTCTG
TGTGCCTGCTGAACAATTCTACCCTCGGGAAGCCAAGGTGCAGTGGAAAGGTGGACAATG
CCCTGCAGAGCGGCAACTCCCAAGAGTCTGTGACCGAGCAGGACTCCAAGGACAGCACCT
ACAGCCTGTCCTCCACACTGACCCTGTCCAAGGCCGATTACGAGAAGCACAAGGTGTACG
CCTGCGAAGTGACCCATCAGGGCCTGTCTAGCCCTGTGACCAAGTCTTTCAACCGGGGCG
AGTGCTGACTTAA

>Den_HC1

GCGCCGCCACCATGGATTGGACTTGGAGATTCTGTTCGTGGTGGCCGCTGCTACAGGCG
TGCAGTCTCAGGTTAGCTGGTTCAGTCTGGCGCTGAAGTGAAGAAACCCGCCTCCTCCGT
GAAGGTGTCTGCAAAGCTTCTGGCGGCACCTTCGGAACCTACGCCATCTTGGGTCCGA
CAGGCTCCTGGCAAAGGCCTGGAATGGATGGGCGGAATCATCCCTCTGTACAAGCAGTCC
ACCTACGCTCAGAAATTCCGGGGCAGAGTGACCATCACCGCCGACGAGTCTACCAACACC
GCCTACATGGAAGTGAACGGCCTGAGCCTGGAAGATACCGCCGTGTTCTACTGCGCTACCC
TGATCGCTGTGGCCGGATCTGAAGGCGCTGGCTCTTTTGATATCTGGGGCCAGGGCACCA
TGGTACCCTGTCCTCTGCTTCTACCAAGGGACCCAGCGTGTTCCTCTGGCTCCTTCCAGC
AAGTCTACCTCCGGTGGAAACAGCTGCTCTGGGCTGCCTGGTCAAGGACTACTTTCCTGAGC
CAGTGACCGTGTCTTGGAACTCCGGCGCTCTGACATCTGGCGTGACACCTTTCCAGCTGT
GCTGCAGTCTCCGGCCTGACTCTCTGTCTCTGTCTGACCGTGCCTTCCAGCTCTCTGG
GAACCCAGACCTACATCTGCAATGTGAACCACAAGCCTTCCAACACCAAGGTGGACAAGA
AGGTGGAACCCAAGTCTGCGACAAGACCCACACCTGTCTCCATGTCTGCTCCAGAACT
GCTCGGCGGACCTTCCGTGTTCTGTTTCTCCAAAGCCTAAGGACACCCTGATGATCTCTC
GGACCCCTGAAGTGACCTGCGTGGTGGTGGATGTGTCTCACGAGGATCCCGAAGTGAAGT
TCAATTGGTACGTGGACGGCGTGGAAAGTGACAACGCCAAGACCAAGCCTAGAGAGGAA

CAGTACA ACTCCACCTACAGAGTGGTGTCCGTGCTGACCGTGCTGCACCAGGATTGGCTG
AACGGCAAAGAGTACAAGTGCAAGGTGTCCAACAAGGCCCTGCCTGCTCCTATCGAAAAG
ACCATCAGCAAGGCCAAGGGCCAGCCTAGGGAACCCAGGTTTACACCCTGCCTCCAAGC
CGGGAAGAGATGACCAAGAACCAGGTGTCCCTGACCTGCCTCGTGAAGGGCTTCTACCCT
TCCGATATCGCCGTGGAATGGGAGAGCAATGGCCAGCCTGAGAACA ACTACAAGACAACC
CCTCCTGTGCTGGACTCCGACGGCTCATTCTTCTGTACTCCAAGCTGACAGTGGACAAGT
CCAGATGGCAGCAGGGCAACGTGTTCTCCTGCTCCGTGATGCACGAGGCCCTGCACAATC
ACTACACCCAGAAGTCCCTGTCTCTGTCCCCTGGCAAGTGA ACTAG

>Den_HC2

GCGCCGCCACCATGGATTGGACTTGGAGATTCTGTTCGTGGTGGCCGCTGCTACAGGCG
TGCAGTCTCAGGTT CAGCTGGTTCAGTCTGGCGCTGAAGTGAAGAAACCCGCCTCCTCCGT
GAAGGTGCTCCTGCAAAGCTTCTGGCGGCACCTTCGGAACCTACGCCATCTTTGGGTCCGA
CAGGCTCCTGGCAAAGGCCTGGAATGGATGGGCGGAATCATCCCTCTGTACAAGCAGTCC
ACCTACGCTCAGAAATTCCGGGGCAGAGTGACCATCACCGCCGACGAGTCTACCAACACC
GCCTACATGGA ACTGAACGGCCTGAGCCTGGAAGATACCGCCGTGTTCTACTGCGTACCC
TGATCGCTGTGGCCGGATCTGAAGGCGCTGGCTCTTTTGATATCTGGGGCCAGGGCACCA
TGGTCACCGTGTCTCTGCTTCTACCAAGGGACCCAGCGTGTTCCCTCTGGCTCCTTGCTCC
AGATCCACCTCCGAGTCTACAGCTGCTCTGGGCTGCCTGGTCAAGGACTACTTTCCTGAGC
CAGTGACCGTGTCTTGGA ACTCCGGCGCTCTGACATCTGGCGTGACACCTTTCCAGCTGT
GCTGCAGTCTCCGGCCTGACTCTCTGTCTCTGTCTGACCGTGCTTCTCTAGCCTGG
GCACCAAGACCTACACCTGTAATGTGGACCACAAGCCTTCCAACACCAAGGTGGACAAGC
GCGTGGAATCTAAGTACGGCCCTCCTTGTCTCCATGTCTGCTCCAGAGTTTCTCGGGCG
ACCCTCCGTGTTCTGTTTCTCCAAAGCCTAAGGACACCCTGATGATCTCTCGGACCCCTG
AAGTGACCTGCGTGGTGGTGGATGTGTCCAAGAGGATCCCGAGGTGCAGTTCAATTGGT
ACGTGGACGGCGTGGAAGTGACAACGCCAAGACCAAGCCTAGAGAGGAACAGTTCAAC
TCCACCTACAGAGTGGTGTCCGTGCTGACCGTGCTGCACCAGGATTGGCTGAACGGCAA
GAGTACAAGTGCAAGGTGTCCAACAAGGGCCTGCCTTCCAGCATCGAAAAGACCATCAGC
AAGGCCAAGGGCCAGCCTAGGGAACCCAGGTTTACACCCTGCCTCCAAGCCAAGAGGAA
ATGACCAAGAACCAGGTGTCCCTGACCTGCCTCGTGAAGGGCTTCTACCCTTCCGATATCG
CCGTGGAATGGGAGAGCAATGGCCAGCCTGAGAACA ACTACAAGACAACCCCTCCTGTGC
TGGACTCCGACGGCAGCTTCTTCTGTATTCCCGCCTGACCGTGGACAAGTCCAGATGGCA

AGAGGGCAACGTGTTCTCCTGCTCCGTGATGCACGAGGCCCTGCACAATCACTACACCCAG
AAGTCCCTGTCTCTGTCCCTGGGCAAGTGAAGTGA

>Den_LC3

GTACCGCCACCATGGACATGAGAGTGCCTGCTCAGCTGCTGGGACTGCTGCTGTTGTGGT
TGTCTGGCGCTAGATGCGACATCCAGATGACCCAGTCTCCATCCTCTCTGTCCGCCTCTGTG
GGCGACAGAGTGACCATCACCTGTACCGGAACATCTGGCGACGTCGGCGGAGACTCTCTG
GTGTCTTGGTATCAGCAGAAGCCCGCAAGGCCCTAAGCTGCTGATCTACGAGGACCAC
AAGAGGCCTTCCGGCGTGCCCTCTAGATTCTCCGGCTCTAGATCTGGCACCGACTTTACCC
TGACAATCTCCAGCCTGCAGCCTGAGGACTTCGCCACCTACTACTGCTGCTCCTACGCCATC
TCTTCCGTGCGGGTGTGTTTGGCCAGGGCACCAAGGTGGAAATCAAGCGGACAGTGGCC
GCTCCTTCCGTGTTTCATCTTCCCACCTTCCGACGAGCAGCTGAAGTCCGGCACAGCTTCTGT
CGTGTGCCTGCTGAACAACCTTCTACCCTCGGGAAGCCAAGGTGCAGTGGAAAGGTGGACAA
TGCCCTGCAGTCCGGCAACTCCCAAGAGTCTGTGACCGAGCAGGACTCCAAGGACAGCAC
CTACAGCCTGTCTCCACACTGACCCTGTCCAAGGCCGACTACGAGAAGCACAAGGTGTAC
GCCTGCGAAGTGACCCATCAGGGCCTGTCTAGCCCTGTGACCAAGTCTTTCAACCGGGGC
GAGTGCTGACTTAA

>Den_HC3

GCGCCGCCACCATGGATTGGACTTGGAGATTCTGTTTCGTGGTGGCCGCTGCTACAGGCG
TGCAGTCTGAAGTGCAGCTGGTGGAAATCTGGCGGAGGATTGGTTCAGCCTGGCGGCTCTC
TGAGACTGTCTTGTGCCGCTCTGGCTTCAACATCAAGACCTACGCCATCTCCTGGGTCCG
ACAGGCTCCTGGCAAAGGACTGGAATGGGTGGCCGGAATCATCCCTCTGTACAAGCAGTC
CACCTACGCTCAGAAGTTCCGGGGCAGATTACCATCTCCGCCGACACCTTAAGAACACC
GCCTACCTGCAGATGAACTCCCTGAGAGCCGAGGACACCGCCGTGTACTIONACTGCTCTAGAC
TGATCGCCGTGGCCGGCTCTGAAGGCGCTGGCTCTTTTGATATCTGGGGCCAGGGCACCC
TGGTCACCGTTTCTTCCGCTTCTACCAAGGGACCCAGCGTGTCCCTCTGGCTCCTTCCAGC
AAGTCTACCTCTGGCGGAACAGCTGCTCTGGGCTGCCTGGTCAAGGACTACTTTCCTGAGC
CTGTGACCGTGTCTGGAACCTCTGGCGCTCTGACATCTGGCGTGCACACCTTTCCAGCTGT
GCTGCAGTCTCCGGCCTGTACTIONACTGCTCTGTCTGCTGACCGTGCCTTCCAGCTCTCTGG
GAACCCAGACCTACATCTGCAATGTGAACCACAAGCCTTCCAACACCAAGGTGGACAAGA
AGGTGGAACCCAAGTCCTGCGACAAGACCCACACCTGTCTCCATGTCTGCTCCAGAAGT

GCTCGGCGGACCTTCCGTGTTCTGTTTCCTCCAAAGCCTAAGGACACCCTGATGATCTCTC
GGACCCCTGAAGTGACCTGCGTGGTGGTGGATGTGTCTCACGAGGATCCCGAAGTGAAGT
TCAATTGGTACGTGGACGGCGTGGAAGTGCACAACGCCAAGACCAAGCCTAGAGAGGAA
CAGTACAACCTCCACCTACAGAGTGGTGTCCGTGCTGACCGTGCTGCACCAGGATTGGCTG
AACGGCAAAGAGTACAAGTGCAAGGTGTCCAACAAGGCCCTGCCTGCTCCTATCGAAAAG
ACCATCAGCAAGGCCAAGGGCCAGCCTAGGGAACCCAGGTTTACACCCTGCCTCCAAGC
CGGGAAGAGATGACCAAGAACCAGGTGTCCCTGACCTGCCTCGTGAAGGGCTTCTACCCT
TCCGATATCGCTGTGGAATGGGAGAGCAACGGCCAGCCTGAGAACAACCTACAAGACAACC
CCTCCTGTGCTGGACTCCGACGGCTCATTCTTCTGTACTCCAAGCTGACAGTGGACAAGT
CCAGATGGCAGCAGGGCAACGTGTTCTCTGCTCCGTGATGCACGAGGCCCTGCACAATC
ACTACACCCAGAAGTCCCTGTCTCTGTCCCCTGGCAAGTGAAGTGA

>Den_LC4

GTACCGCCACCATGGACATGAGAGTGCCTGCTCAGCTGCTGGGACTGCTGCTGTTGTGGT
TGTCTGGCGCTAGATGCGAGATCGTGCTGACCCAGTCTCCTGCCACACTGTCACTGTCTCC
AGGCGAGAGAGCTACCCTGTCTTGTACCGAACATCTGGCGACGTCGGCGGCGATTCTCT
GGTGTCTTGGTATCAGCAGAAGCCCGGCCAGGCTCCTAGACTGCTGATCTACGAGGACCA
CAAGCGGCCCTCTGGCATCCCTGCTAGATTTTCCGGCTCTGGCTCTGGCACCGACTTTACCC
TGACCATCTCCAGCCTGGAACCTGAGGACTTCGCCGTGTACTACTGCTGCTCCTACGCCAT
CTCTTCCGTGCGGGTGTGTTTGGCCAGGGCACCAAGGTGGAATCAAGCGGACAGTGGC
CGCTCCTTCCGTGTTTCATCTTCCCACCTTCCGACGAGCAGCTGAAGTCCGGCACAGCTTCTG
TCGTGTGCCTGCTGAACAACCTTCTACCCTCGGGAAGCCAAGGTGCAGTGAAGGTGGACA
ATGCCCTGCAGTCCGGCAACTCCCAAGAGTCTGTGACCGAGCAGGACTCCAAGGACAGCA
CCTACAGCCTGTCTCCACACTGACCCTGTCCAAGGCCGACTACGAGAAGCACAAGGTGTA
CGCCTGCGAAGTGACCCATCAGGGCCTGTCTAGCCCTGTGACCAAGTCTTTCAACCGGGG
CGAGTGCTGACTTAA

>Den_HC4

GCGCCGCCACCATGGAATTTGGACTGTCTTGGGTGTTCTGGTGGCCCTGTTTAGAGGCGT
GCAGTGTGAGGTGCAGCTGGTGGAAATCTGGTGGCGGAGTTGTGCAGCCTGGCAGATCTCT
GAGACTGGACTGCAAGGCCTCCGGCATCACCTTCTCTACCTACGCCATCTCCTGGGTCCGA
CAGGCTCCTGGCAAAGGACTGGAATGGGTGGCCGGAATCATCCCTCTGTACAAGCAGTCC

ACCTACGCTCAGAAGTTCCGGGGCAGATTACCATCAGCCGGGACAACCTCCAAGAACACC
CTGTTTCTGCAGATGAACTCCCTGAGAGCCGAGGACACCGCCGTGTACTATTGCGCTACAC
TGATCGCCGTGGCCGGCTCTGAAGGCGCTGGCTCTTTTGATATCTGGGGCCAGGGCACCC
TGGTCACCGTTTCTTCCGCTTCTACCAAGGGACCCAGCGTGTCCCTCTGGCTCCTTGCTCC
AGATCCACCTCCGAGTCTACAGCTGCTCTGGGCTGCCTGGTCAAGGACTACTTTCCTGAGC
CTGTGACCGTGTCTGGAACCTCTGGCGCTCTGACATCTGGCGTGCACACCTTTCAGCTGT
GCTGCAGTCTCCGGCCTGTACTCTGTCTCTGTCTGACCGTGCCTTCTCTAGCCTGG
GCACCAAGACCTACACCTGTAATGTGGACCACAAGCCTTCCAACACCAAGGTGGACAAGC
GCGTGGAATCTAAGTACGGCCCTCCTTGTCTCCATGTCCTGCTCCAGAGTTTCTCGGCGG
ACCCTCCGTGTTCTGTTTCTCCAAAGCCTAAGGACACCCTGATGATCTCTCGGACCCCTG
AAGTGACCTGCGTGGTGGTGGATGTGTCCAAGAGGATCCCGAGGTGCAGTTCAATTGGT
ACGTGGACGGCGTGGAAGTGCACAACGCCAAGACCAAGCCTAGAGAGGAACAGTTCAAC
TCCACCTACAGAGTGGTGTCCGTGCTGACCGTGTCTGCACCAGGATTGGCTGAACGGCAA
GAGTACAAGTGCAAGGTGTCCAACAAGGGCCTGCCTTCCAGCATCGAAAAGACCATCTCC
AAGGCCAAGGGCCAGCCTAGGGAACCCAGGTTTACACCCTGCCTCCAAGCCAAGAGGAA
ATGACCAAGAACCAGGTGTCCCTGACCTGCCTCGTGAAGGGCTTCTACCCTCCGATATCG
CTGTGGAATGGGAGAGCAACGGCCAGCCTGAGAACAACCTACAAGACAACCCCTCCTGTGC
TGGACTCCGACGGCAGCTTCTTCTGTATTCTCGCCTGACCGTGGACAAGTCCAGATGGCA
AGAGGGCAACGTGTTCTCCTGCTCCGTGATGCACGAGGCCCTGCACAATCACTACACCCAG
AAGTCCCTGTCTCTGTCCCTGGGCAAGTGAAGTGA

>Den_LC5

GTACCGCCACCATGGCTTGGGCTCTGCTGCTGCTGACACTGCTGACCCAGGATACCGGATC
TTGGGCCAGTCTGCTCTGACCCAGCCTGCTTCTGTGTCTGGCTCTCCCGGCCAGTCCATCA
CCATCTCTTGTACCGGAACCTCTGGCGACGTCGGCGGAGATTCTCTGGTGTCTGCTGATCA
GCAGCACCCCTGGCAAGGCCCTAAGCTGATCATCTACGAGGACCACAAGCGGCCTTCCGG
CGTGTCTCTAGATTCTTCGGCTCCAAGTCCGGCAACGCCGCCTCTCTGACAATTAGCGGA
CTGCAGGCTGAGGACGAGGCCGACTACTACTGCTGCTCCTACGCCATCTTCCGTGCGGG
TTTTGTTTGGCGGAGGCACCAAAGTGACCGTGTCTGGGACAACCTAAGGCCGCTCCTTCCGT
GACACTGTTCCCTCCATCCTCCGAAGAAGTGCAGGCCAACAAGGCTACCCTCGTGTGCCTG
ATCTCCGACTTCTATCCTGGCGCTGTGACCGTGGCCTGGAAGGCTGATAGTTCTCCTGTGA

AGGCCGGCGTGGAACCACCACACCTTCCAAGCAGTCCAACAACAAATACGCCGCCAGCT
CCTACCTGTCTCTGACCCCTGAACAGTGGGAGTCCCACCGTCTACTCTTGCTAACTTAA

>Den_HC5

GCGCCGCCACCATGGATTGGACTTGGCGGATTCTGTTCGTGGTGGCTGCTGCTACAGGCG
TGCAGTCTCAGGTTAGCTGGTTCAGTCTGGCGCTGAAGTGAAGAAACCCGCCTCCTCCGT
GAAGGTGTCCTGCAAAGCTTCTGGCGGCACCTTCGGAACCTACGCCATCTTTGGGTCCGA
CAGGCTCCTGGCAAAGGCCTGGAATGGATGGGCGGAATCATCCCTCTGTACAAGCAGTCC
ACCTACGCTCAGAAATTCCGGGGCAGAGTGACCATCACCGCCGACGAGTCTACCAACACC
GCCTACATGGAAGTGAACGGCCTGAGCCTGGAAGATACCGCCGTGTTCTACTGCGCTACCC
TGATCGCTGTGGCCGGATCTGAAGGCGCTGGCTCTTTTGATATCTGGGGCCAGGGCACCA
TGGTCACCGTGTCTCTGCTTCTACCAAGGGACCCAGCGTGTTCCCTCTGGCTCCTTCCAGC
AAGTCTACCTCCGGTGGAACAGCTGCTCTGGGCTGCCTGGTCAAGGACTACTTTCCTGAGC
CAGTGACCGTGTCTTGGAAGTCCGGCGCTCTGACATCTGGCGTGACACCTTTCCAGCTGT
GCTGCAGTCTCCGGCCTGACTCTCTGTCCTCTGTCGTGACCGTGCCTTCCAGCTCTCTGG
GAACCCAGACCTACATCTGCAATGTGAACCACAAGCCTTCCAACACCAAGGTGGACAAGA
AGGTGGAACCCAAGTCTGCGACAAGACCCACACCTGTCTCCATGTCTGCTCCAGAACT
GCTCGGCGGACCTTCCGTGTTCTGTTTCTCCAAGCCTAAGGACACCCTGATGATCTCTC
GGACCCCTGAAGTGACCTGCGTGGTGGTGGATGTGTCTCACGAGGATCCCGAAGTGAAGT
TCAATTGGTACGTGGACGGCGTGGAAAGTGCACAACGCCAAGACCAAGCCTAGAGAGGAA
CAGTACAACCTCACCTACAGAGTGGTGTCCGTGCTGACCGTGCCTGACCAGGATTGGCTG
AACGGCAAAGAGTACAAGTGAAGGTGTCCAACAAGGCCCTGCCTGCTCCTATCGAAAAG
ACCATCTCCAAGGCCAAGGGCCAGCCTAGGGAACCCAGGTTTACACCTTGCCTCCATCTC
GGGACGAGCTGACCAAGAACCAGGTGTCCCTGACCTGTCTCGTGAAGGGCTTCTACCCCT
CCGATATCGCCGTGGAATGGGAGTCTAATGGCCAGCCTGAGAACAACACTACAAGACAACCC
CTCCTGTGCTGGACTCCGACGGCTCATTCTTCTGTAAGCTGACAGTGGACAAGTC
CAGATGGCAGCAGGGCAACGTGTTCTCCTGCTCCGTGATGCACGAGGCCCTGCACAATCA
CTACACCCAGAAGTCCCTGTCTCTGTCCCCTGGCAAGTGAAGTGAAGTGAAGTGAAGTGAAGT